# MATHEMATICAL MODELLING OF RAYLEIGH WAVE FIELDS INCORPORATING MICROSTRUCTURAL AND RESONATOR EFFECTS

Ph.D. Thesis

 $\begin{array}{c} \text{By} \\ \textbf{MANASA BHAT} \end{array}$ 



# DEPARTMENT OF MATHEMATICS INDIAN INSTITUTE OF TECHNOLOGY INDORE APRIL 2025

# MATHEMATICAL MODELLING OF RAYLEIGH WAVE FIELDS INCORPORATING MICROSTRUCTURAL AND RESONATOR EFFECTS

#### A THESIS

Submitted in partial fulfillment of the requirements for the award of the degree

of

#### DOCTOR OF PHILOSOPHY

by MANASA BHAT



# DEPARTMENT OF MATHEMATICS INDIAN INSTITUTE OF TECHNOLOGY INDORE APRIL 2025



#### INDIAN INSTITUTE OF TECHNOLOGY INDORE

I hereby certify that the work which is being presented in the thesis entitled MATHEMATICAL MODELLING OF RAYLEIGH WAVE FIELDS INCORPORATING MICROSTRUCTURAL AND RESONATOR EFFECTS in the partial fulfillment of the requirements for the award of the degree of DOCTOR OF PHILOSOPHY and submitted in the DEPARTMENT OF MATHEMATICS, Indian Institute of Technology Indore, is an authentic record of my own work carried out during the time period from May 2021 to April 2025 under the supervision of Dr. Santanu Manna, Associate Professor, Department of Mathematics, Indian Institute of Technology Indore.

The matter presented in this thesis has not been submitted by me for the award of any other degree of this or any other institute.

Signature of the student with date
(Manasa Bhat)

\_\_\_\_\_

This is to certify that the above statement made by the candidate is correct to the best of my knowledge.

27/06/2025 Signature of Thesis Supervisor with date

(Dr. Santanu Manna)

-----

Manasa Bhat has successfully given her Ph.D. Oral Examination held on 27/06/2025

27/06/2025

Signature of Thesis Supervisor with date

(Dr. Santanu Manna)

#### ACKNOWLEDGEMENTS

The completion of this thesis has been both an academic challenge and a deeply transformative personal and philosophical journey. Each step, each completed section, brought with it a quiet, heartfelt satisfaction. This thesis marks the closing chapter of my doctoral journey, a long and winding road that opened countless doors. This discipline of gratitude is the explicit effort to acknowledge people who made this tenure easier with words of encouragement, motivation, guidance and intellectually satisfying support. The joy of this achievement is strongly tied to their contributions, and to not express my deepest appreciation would leave this feeling incomplete.

Above all, this journey would not have been possible without the blessings of God—the source of knowledge and wisdom—whose grace and mercy guided me throughout my studies. My deepest gratitude goes to my parents, who nurtured my curiosity and supported my educational endeavours from the very beginning. Their continuous support and belief in my academic pursuits have been instrumental in my success. A special thanks to my brother, Dr. Gautham who despite working with actual patients, still had the patience to listen to me complain about my research.

I am profoundly grateful for the enduring support of my supervisor, Dr. Santanu Manna, whose steadfast belief in my capabilities and academic potential encouraged me to persevere even during my lowest moments. He had the remarkable ability to know when to challenge us to reach our limits and when to let us pause and breathe, making this journey at times intense and at times truly enjoyable. His mentorship has been invaluable, not only in navigating my doctoral journey, but also in preparing me for the demands of a successful professional career. I am thankful to my PSPC committee members, Prof. Sandeep Chaudhary and Dr. Sanjeev Singh for their time and consideration throughout this journey. I also thank Head of the Department for their support. And I appreciate the helpful resources and assistance from the faculty and office staff of the Department of Mathematics, IIT Indore. During my research visit to the UK, I had the privilege of collaborating with Professor Julius Kaplunov and Dr. Danila Prikazchikov of Keele University, UK. I am immensely grateful for their online guidance, in-person expertise, and collaborative spirit, all of which were essential in the production of our joint paper. I also wish to express my sincere appreciation to the Prime Minister's Research Fellowship (PMRF), Government of India, for their financial assistance, (under ID no: 2101707)

encompassing both fellowship and contingency funds. This support was instrumental in allowing me to pursue my research without financial concerns.

Further, I am thankful to Indian Institute of Technology Indore for its state-of-the-art facilities and the conducive research environment that fostered my academic growth. Also, I extend my appreciation to the Applied Mathematics and Geomechanics Lab, Department of Mathematics, IIT Indore, for their provision of the requisite research facilities and computational systems, which significantly aided my research. I am deeply grateful to my lab senior and friend, Dr. Dipendu Pramanik, for his timely comic relief, stress-relieving banter and unwavering encouragement. The late-night research discussions and countless chai talks with my labmates, Dr. Dipendu Pramanik and Mr. Rahul Som, provided not only valuable research insights but also enriching life and philosophical perspectives. The enriching discussions and consistent support from my junior labmates, Mr. Manish Chakraborty and Mr. Deepak, as well as the alumni of the AMG lab, especially Ms. Tanisha Kumari, Mr. Nikhil and Ms. Mansi made this research journey both enjoyable and successful. I acknowledge the contributions of my friends, like Dr. Anuradha Kumari, Mr. Aniruddh Deshmukh, Mr. Debdeep Roy, Mr. Sajin Vincent, Ms. Sheetal Wankhede, Ms. Shubhi Bansal and other colleagues in and outside the department, whose creation of a supportive environment was instrumental in the successful navigation of my doctoral journey. Their encouragement and shared experiences were invaluable.

Last but not the least, I acknowledge my fiancé, Mr. Siddharth Bhat, whose presence, though arriving late in this journey, offered invaluable emotional support by understanding and consistently lending a patient ear throughout its highs and lows.

### **DEDICATION**

To my Pappa and Amma

#### **SYNOPSIS**

Applied mathematics plays a crucial role in investigating Rayleigh waves, a fundamental class of surface waves, by enabling analysis and modelling of their propagation in complex media. This necessitates the application of sophisticated mathematical frameworks, which mainly involves the rigorous study of wave propagation theory, the formulation of the problem using partial differential equations, and the application of diverse mathematical tools to derive the solution. Specifically, this research focuses on the mathematical modelling of Rayleigh wave generation, propagation and control, emphasizing the development and application of analytical, asymptotic and numerical techniques to solve complex mathematical problems arising from these geophysical phenomena. This approach allows for a purely mathematical investigation of wave behavior, together with a mechanical interpretation to some extent, and contributes to the advancement of mathematical methodologies applicable to a range of wave-based problems.

The thesis, entitled 'MATHEMATICAL MODELLING OF RAYLEIGH WAVE FIELDS INCORPORATING MICROSTRUCTURAL AND RESONATOR EFFECTS', investigates the mathematical modelling, analysis, and control of Rayleigh wave fields within the frameworks of classical and small-scale elasticity theories. Addressing initial and boundary value problems, this research explores Rayleigh wave propagation in various complex media, including small-scale elastic behaviors in nonlocal micropolar continuum and nonlinear metasurfaces. Key aspects of the study include (a) the development and modification of existing classical elasticity conditions to derive refined boundary and interface conditions for nonlocal micropolar structures (b) the incorporation of viscoelastic effects (c) the investigation of wave propagation in microstructured layered media, and (d) the analysis of Rayleigh wave scattering and control along metasurfaces. This investigation aims to bridge theoretical gaps in nonlocal and micropolar elasticity theories while highlighting potential applications in seismic wave mitigation and advanced material design.

A fundamental branch of continuum mechanics is the classical theory of elasticity, which plays a crucial role in studying the mechanical behavior of these waves in various structures. This offers a foundational framework for describing the behavior of deformable solids, assuming small and reversible deformations. However, it has significant limitations,

including neglecting microstructural effects (e.g., cracks, inclusions) and predicting infinite stress at crack tips, which is physically unrealistic. To overcome these limitations, generalized continuum frameworks like Eringen's nonlocal elasticity [59] and micropolar elasticity [51] theories have been developed that incorporate intrinsic length scales and microstructural effects. These advanced theories enhance seismic exploration by improving subsurface characterization, refining resolution, and providing reliable predictions for applications like hydrocarbon exploration and earthquake hazard assessment.

While recent Rayleigh wave studies utilize nonlocal models, inconsistencies in boundary conditions have been observed, limiting their applicability. Specifically, discrepancies between differential and integral formulations, as demonstrated by Kaplunov et al. [204], highlight the inadequacy of traditional nonlocal boundary conditions. To address this, modified models and refined boundary conditions, derived using asymptotic techniques to account for boundary layer effects, are necessary. However, relying solely on nonlocal elasticity may not fully capture the behavior of materials with complex, intricate microstructures, necessitating further investigation.

Furthermore, recent technological advancements have driven the development of nanoand micro-materials. Accurately capturing size-dependent effects and dispersion phenomena within these materials necessitates the consideration of microstructural effects. This
in turn, requires modelling wave propagation within the framework of nonlocal micropolar
solids. A significant gap in the current literature pertains to the formulation of suitable
boundary conditions for nonlocal micropolar solids. Furthermore, the derivation of appropriate boundary conditions for 'layered' structures under the framework of nonlocal and
micropolar elasticity remains an open challenge. This thesis addresses these critical
issues by developing a refined model that incorporates the effects of boundary layers in a nonlocal micropolar medium. This involves deriving refined
boundary and interface conditions for obtaining corrected dispersion relations
that effectively capture the influence of boundary layer effects.

While understanding Rayleigh wave propagation in various elastic environments offers valuable insight into their natural behavior, controlling these waves broadens the scope for practical applications, facilitating the design of safer, more efficient, and innovative systems. Metasurfaces, a class of artificially engineered surfaces comprising subwavelength-scale structures, offer a promising technique for achieving such control. These structures

can manipulate wavefronts in diverse ways, providing precise control over Rayleigh wave propagation. By carefully tailoring the geometry and properties of these metasurfaces, researchers can achieve phenomena like wave focusing, steering, and cloaking, unlocking new possibilities in seismic hazard mitigation, enhanced sensing, and advanced wave-based technologies.

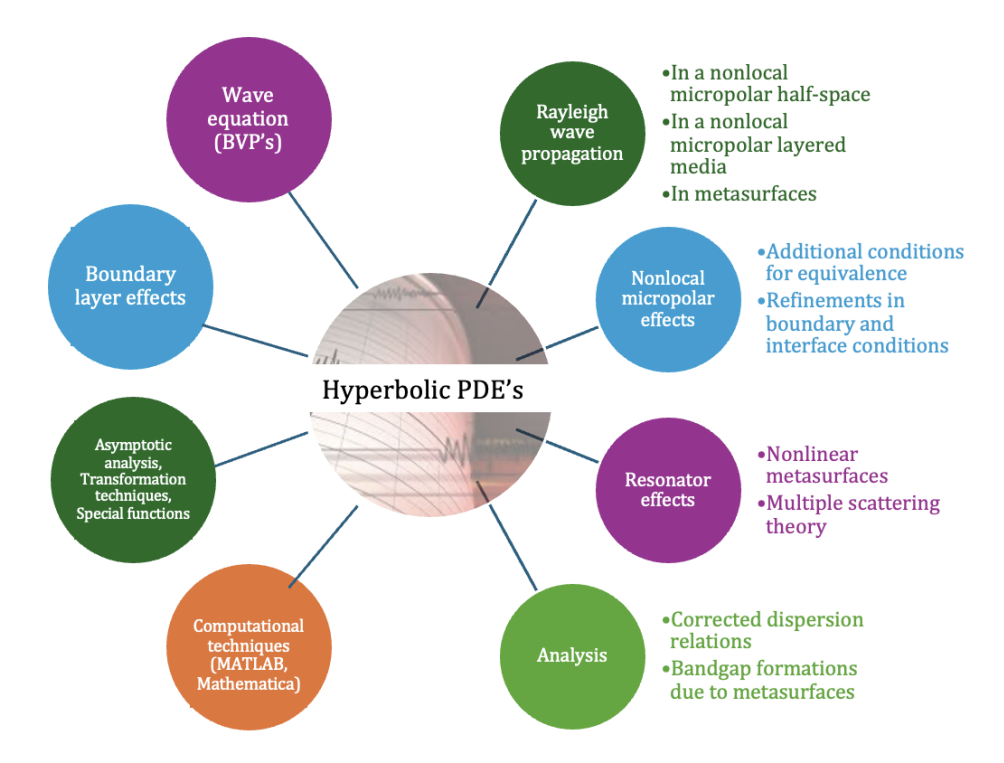
Despite the growing interest in structural protection against seismic events, the combined influence of multiple physical phenomena on Rayleigh wave propagation along metasurfaces remains largely unexplored. This thesis investigates novel strategies for controlling and manipulating Rayleigh waves within the framework of small-scale elasticity, considering some crucial phenomena to enhance structural protection. Furthermore, while most geomechanics problems are traditionally formulated as boundary value problems, this thesis introduces a novel approach by initially defining an initial value problem for Rayleigh wave propagation. This framework subsequently evolves into a boundary value problem, offering new insights into the dynamics of wave propagation in complex geological media.

The primary research objectives of this thesis are:

- Developing refined boundary conditions within the framework of nonlocal micropolar mechanics for accurate wave propagation modelling and further analyzing the characteristics of multiple Rayleigh wave modes in nonlocal micropolar viscoelastic media, as an application.
- Extending the derivation of refined boundary and interface conditions for nonlocal micropolar elasticity problems to model wave propagation in layered media.
- Investigating Rayleigh wave control and scattering mechanisms using nonlinear metasurfaces and advanced resonance phenomena.
- modelling the generation and propagation of Rayleigh waves due to interior sources and surface loading within an elastic media.

The methodology employed in this thesis involves a combination of analytical and numerical techniques to address the various challenges associated with Rayleigh wave propagation in nonlocal micropolar continua and metasurfaces. Initially, the classical theories of elasticity are extended using nonlocal and micropolar elasticity frameworks to account for size-dependent effects and microstructural influences. Asymptotic analysis is utilized to derive refined boundary conditions that effectively capture the impact of

nonlocal boundary layer effects on wave propagation. For wave control and scattering in metasurfaces, the properties of subwavelength-scale structures are studied and multiple scattering theory is employed to obtain the displacement solutions. Numerical simulations using MATLAB and/or Mathematica are conducted to visualize the dispersion curves for Rayleigh waves, which provide insights into phase velocities and wave interactions with complex media. Additionally, the Laplace transformation technique is applied to solve initial value problem, which subsequently evolve into boundary value problems, providing a novel perspective on wave propagation dynamics in elastic environments. A visualization to the research framework and methodology employed in the thesis is provided below:



This thesis is organized into six chapters, each dedicated to a specific set of research objectives, outlining the motivations behind the study, highlighting novel contributions, and detailing the mathematical methodologies employed in the analysis. The summary of each chapter is presented below.

Chapter 1 provides a comprehensive introduction, a thorough literature review, and the preliminaries essential for establishing the context of the research problems presented in this thesis. It begins with an introduction to Rayleigh waves, followed by an overview of metasurfaces and relevant mathematical techniques. Furthermore, a brief overview of classical elasticity theory, its limitations, and the evolution of generalized continuum

theories, such as nonlocal elasticity and micropolar elasticity, is provided, along with a review of the current state-of-the-art research in these areas.

Chapter 2 investigates Rayleigh wave propagation in nonlocal micropolar media, considering the combined effects of nonlocality and micro-rotation. This chapter focuses on refining the boundary value problem to ensure equivalence between the differential and integral formulations of nonlocal micropolar elasticity. This chapter is further divided into two subchapters as follows:

- Subchapter 2.1 derives refined boundary conditions for Rayleigh wave propagation in a nonlocal micropolar semi-infinite medium using asymptotic analysis while also demonstrating the failure of traditional boundary conditions.
- Subchapter 2.2 utilizes the derived refined boundary conditions to analyze wave propagation in nonlocal micropolar viscoelastic media. The analysis includes examining particle paths, identifying different wave modes (nonlocal, micropolar, viscoelastic), and investigating their dependence on material parameters. Graphical representations are provided to visualize these behaviors.

Chapter 3 extends the derivation of refined boundary and interface conditions to address wave propagation in layered structures. Recognizing the need for refined interfacial conditions, which have been largely unexplored in both nonlocal elasticity and nonlocal micropolar elasticity, this chapter investigates the following:

- Subchapter 3.1 focuses on deriving refined boundary and interface conditions for Rayleigh wave propagation in layered media within the framework of nonlocal elasticity. Asymptotic techniques are employed to account for nonlocal boundary and interfacial layers, leading to the derivation of first-order corrected dispersion relations for Rayleigh waves.
- Subchapter 3.2 extends the analysis to nonlocal micropolar elasticity. Refined boundary and interface conditions, incorporating modifications to couple stress and force stress conditions, are derived to account for boundary and interfacial layer effects. The propagation of Rayleigh waves in a nonlocal micropolar layered structure is then investigated as an application of these refined conditions.

Chapter 4 focuses on controlling Rayleigh wave vibrations using artificially engineered metasurfaces. The chapter explores the influence of nonlinearity and small-scale effects

within the metasurface, investigating the formation of bandgaps that prohibit the propagation of Rayleigh waves at specific frequencies.

- Subchapter 4.1 introduces a novel metasurface design comprising an array of dual spring-mass resonators situated on a nonlocal host substrate. This subchapter combines nonlocal elasticity, nonlinearity, and double resonance concepts to analyze Rayleigh wave dispersion relations.
- Subchapter 4.2 investigates the control of Rayleigh waves generated by an interior source using a nonlinear metasurface. Multiple scattering theory is employed to account for wave scattering by the resonators. Subsequently, dispersion analysis is conducted by extracting the Rayleigh wave contribution from the total wave fields.

Chapter 5 investigates the generation of Rayleigh waves by considering both initial and boundary value problems. Transformation techniques are employed to model both the interior and the surface source effectively.

- Subchapter 5.1 models the generation of Rayleigh waves due to an interior source using an initial value problem. Laplace transforms are employed to model the interior source, and an asymptotic hyperbolic-elliptic model is utilized to obtain the asymptotic solution. The results from the asymptotic and exact solutions for both surface and bulk wave fields are compared and analyzed.
- Subchapter 5.2 focuses on the generation of Rayleigh waves in a micropolar medium subjected to seismic surface loading. Hankel transforms are applied to obtain the solution, and a matrix approach is employed to extend the analysis to layered media.

Chapter 6 presents a discussion of the essential results obtained in the thesis, along with potential avenues for future research and development.

The key findings of the thesis include:

- The derivation of refined boundary and interface conditions within the frameworks of nonlocal elasticity and nonlocal micropolar elasticity, addressing the critical issue of the equivalence between differential and integral formulations.
- The derivation of corrected dispersion relations clearly demonstrates the dependence of the propagation of different wave modes on material parameters and high-lights the influence of small-scale effects.

- The demonstration of Rayleigh wave vibration control through the design of novel nonlinear metasurfaces, resulting in the formation of bandgaps that restrict wave propagation at specific frequencies.
- The accurate prediction of Rayleigh wave propagation induced by interior initial conditions using an asymptotic hyperbolic-elliptic model while also highlighting the limitations of this model in predicting bulk wave fields.

In brief, this thesis significantly advances the mathematical and theoretical understanding of Rayleigh wave propagation in various media, encompassing nonlocal micropolar continuum and engineered metasurfaces. By addressing critical gaps in boundary conditions and exploring novel wave control strategies, this research bridges classical and small-scale elasticity frameworks. The findings offer valuable insights into wave dynamics with implications for seismic hazard mitigation and advanced technologies, laying a strong foundation for future research in wave propagation and control.

#### LIST OF PUBLICATIONS

#### List of Published/Communicated Research Papers from the Thesis

- Bhat, M., & Manna, S. (2025). A novel approach to modelling nonlocal surface waves: refinements in boundary and interface conditions. *IMA Journal of Applied Mathematics* (Oxford Academic), hxaf007. DOI: 10.1093/imamat/hxaf007. IF: 1.4.
- 2. **Bhat, M.**, & Manna, S. (2025). Refining boundary value problems in non-local micropolar mechanics. *Zeitschrift für angewandte Mathematik und Physik* (Springer), 76(1), 28. DOI: 10.1007/s00033-024-02407-4. IF: 1.7.
- 3. **Bhat, M.**, & Manna, S. (2025). Refined conditions for nonlocal micropolar wave propagation in layered media. *Mathematics and Mechanics of Solids* (SAGE). 10812865251336257. DOI: 10.1177/10812865251336257 IF: 1.7.
- 4. Bhat, M., & Manna, S. (2024). On different modes of Rayleigh wave fields in a micropolar nonlocal viscoelastic medium. ZAMM-Journal of Applied Mathematics and Mechanics/Zeitschrift für Angewandte Mathematik und Mechanik (Wiley), e202400604. DOI: 10.1002/zamm.202400604. IF: 2.3.
- 5. **Bhat, M.**, Manna, S., & Alkinidri, M. (2024). Rayleigh wave fields in a multilayered micropolar media. *International Journal of Geomechanics* (ASCE Library), 24(4), 04024026. DOI: 10.1061/IJGNAI.GMENG-8725. IF: 3.3.
- 6. Bhat, M., & Manna, S. (2024). Hybrid Rayleigh wave along a nonlocal nonlinear metasurface with two-degree-of-freedom spring-mass resonators. European Journal of Mechanics-A/Solids (Elsevier), 104, 105214. DOI: 10.1016/j.euromechsol.2023.105214. IF: 4.4.
- 7. **Bhat, M.**, & Manna, S. (2025). Interior source-induced Rayleigh waves and its multiple scattering formulation in a nonlinear metasurface. (Submitted to the journal).
- 8. **Bhat, M.**, Manna, S., Kaplunov, J., & Prikazchikov, D. (2025). Rayleigh waves induced by interior initial conditions. (Ready to submit).

#### List of Published Research Papers Other Than the Thesis

- 9. Manna, S., Deepak, D., & **Bhat**, **M.** (2025). Rayleigh wave propagation in micropolar layered media with perfect and slip interfaces. *Journal of Elasticity* (Springer), 157(3), 1-25. IF: 1.8.
- 10. Manna, S., & **Bhat**, **M.** (2022). Love wave fields in a non-local elastic model with reinforced and inhomogeneous media. *Soil Dynamics and Earthquake Engineering* (Elsevier), 161, 107388. DOI: 10.1016/j.soildyn.2022.107388. IF: 4.2.
- 11. Bhat, M., & Manna, S. (2023). Behavior of love-wave fields due to the reinforcement, porosity distributions, non-local elasticity and irregular boundary surfaces. *International Journal of Applied Mechanics* (World Scientific Publishing), 15(06), 2350042. DOI: 10.1142/S1758825123500424. IF: 2.9.

# TABLE OF CONTENTS

LIST	F FIGURESx	xiii
LIST	F TABLESx	xix
NOM	NCLATUREx	xxi
Chap	r 1 Introduction and Preliminaries	1
1.1	introduction	3
1.2	Literature review	10
1.3	Preliminaries	15
Chap	r 2 Rayleigh Wave Propagation in Nonlocal Micropolar Semi-	
	infinite Medium	41
2.1	Derivation of refined boundary conditions on the surface of a nonlocal mi-	
	cropolar semi-infinite medium	43
2.2	Application in a nonlocal micropolar viscoelastic medium	61
Chap	Rayleigh Wave Propagation in Nonlocal Micropolar Layered	
	Medium	91
3.1	Derivation of refined boundary and interface conditions in a nonlocal layered	
	media with an application	93
3.2	Extension to nonlocal micropolar elasticity with an application	111
Chap	r 4 Rayleigh Wave Propagation and Control by Metasurfaces	131
4.1	Nonlinear metasurface with dual spring-mass resonators	133
4.2	A multiple scattering formulation in a nonlinear metasurface	149
Chap	7 5 Rayleigh Waves Generation and Propagation due to External	
	Sources	171
5.1	nterior initial value problem in a semi-infinite medium	173

5.2	Surface boundary value problem in a multi-layered micropolar media	. 189
Chapt	ter 6 Concluding Remarks and Future Directions	209
6.1	Summary and concluding remarks	. 211
6.2	Future directions	. 214
APPI	ENDICES	215
REFF	ERENCES	219

# LIST OF FIGURES

1.1.1	Structure of the thesis	7
1.3.1	Rayleigh waves in an elastic semi-infinite medium	16
1.3.2	Variation of $R(y)$ with $y$ for $\Gamma = \frac{1}{\sqrt{3}}$	19
2.1.1	Corrected phase velocity curves for one of the modes corresponding to elastic counterpart	57
2.1.2	Corrected phase velocity curves for micropolar dispersive mode for different values of $l=\frac{a^2}{j}$	58
2.1.3	Variation of the sensitivity of phase velocity $c$ with respect to nonlocal elastic parameter $\epsilon$ as a function of (a) micropolarity parameter $d$ (or $\delta$ ) (b) Poisson's ratio $\nu$	<b>5</b> 9
2.1.4	Variation of the sensitivity of phase velocity $c$ with respect to micropolar parameter $d(\text{or }\delta)$ as a function of (a) nonlocal elastic parameter $\epsilon$ (b) Poisson's ratio $\nu$	60
2.2.1	(a) Geometry of the model (b) A unit micropolar cell displaying force stresses and couple stresses	61
2.2.2	Variation of phase velocity $(v)$ with the material parameter $\left(\frac{\kappa}{\mu}\right)$ for different values of $\epsilon$ in an incompressible solid semi-infinite medium	71
2.2.3	Normalized (a) displacement components $(U_i)$ (b) stress components $(P_i)$ versus dimensionless depth $\left(\frac{z}{\Lambda}\right)$ for a quasi-elastic mode of Rayleigh waves in an incompressible solid	
2.2.4	Variation of critical $\delta a_c$ with material parameter $d$ for different $\epsilon$	<b>7</b> 3
2.2.5	Variation of phase velocity $v$ with material parameter $\epsilon$ for different $\epsilon$	74

2.2.6	Normalized (a) displacement components $(U_i)$ (b) stress components $(P_i)$ versus dimensionless depth $\left(\frac{z}{\Lambda}\right)$ for a viscoelastic mode of Rayleigh waves
	in an incompressible solid
2.2.7	Nature of roots $c$ for different values of $\epsilon$ and $d$
2.2.8	Variation of phase velocity of Rayleigh waves, $v$ in a quasi-elastic mode
220	with material parameter $\frac{\kappa}{\mu}$ for different values of $\epsilon$
2.2.9	Variation of critical $\delta a_c$ with material parameter $d$ for different $\epsilon \dots 81$
2.2.10	Variation of phase velocity $v$ with material parameter $\frac{\kappa}{\mu}$ for different $\epsilon$ 82
2.2.11	Normalized (a) displacement components $(U_i)$ (b) stress components $(P_i)$ versus dimensionless depth $\left(\frac{z}{\Lambda}\right)$ for a quasi-elastic mode of Rayleigh waves in a Poisson solid
2.2.12	Regions indicating the range of values of $\epsilon$ and $d$ for the possible number of viscoelastic modes
2.2.13	Variation of values of $\delta a_c$ with the material parameter $d$ in the Region III (where one viscoelastic mode may propagate)
2.2.14	Variation of phase velocity, $v$ with the material parameter $\frac{\kappa}{\mu}$ in the Region III (where one viscoelastic mode may propagate)
2.2.15	Variation of values of $\delta a_c$ with the material parameter $d$ in the Region IV (where two viscoelastic modes may propagate)
2.2.16	Variation of phase velocity, $v$ with the material parameter $\frac{\kappa}{\mu_o}$ in the Region IV (where two viscoelastic modes may propagate)
2.2.17	Normalized (a) displacement components $(U_i)$ (b) stress components $(P_i)$ versus dimensionless depth $\left(\frac{z}{\Lambda}\right)$ for a viscoelastic mode of Rayleigh waves in an incompressible solid
3.1.1	Geometry of the problem
3.1.2	Dispersion curves for nonlocal elastic Rayleigh waves in an isotropic layered medium
3.2.1	Geometry of the problem11

3.2.2	Comparision of Rayleigh wave dispersion curves under the influence of micropolarity and nonlocality in a layered medium
3.2.3	Dispersion curves of nonlocal micropolar Rayleigh waves for different values of micropolar ratio $d^{(2)}$
3.2.4	Variation of dimensionless phase velocity against Poisson's ratio of the semi-infinite medium $\nu^{(1)}$
3.2.5	Dispersion curves of a new micropolar surface wave for different values of $l^{(2)}$
3.2.6	Comparision of nonlocal dispersion curves of Rayleigh waves in a micropolar half-space via different approaches
4.1.1	Schematics of the proposed model (a) design of metasurface (b) a resonant unit cell
4.1.2	Dispersion curves for three different configurations in spring-mass systems.  (a) Linear resonators ( $\nu = 0$ ) (b) Soft nonlinear resonators ( $\nu = -1$ ) (c)  Hard nonlinear resonators ( $\nu = +1$ )
4.1.3	Effect of relative amplitude input on dispersion curves in a soft nonlinear spring. (a) Dispersion curves showing spectral bandgaps (b) Variation of relative amplitude input with dimensionless frequency
4.1.4	Effect of relative amplitude input on dispersion curves in a hard nonlinear spring. (a) Dispersion curves showing spectral bandgaps (b) Variation of relative amplitude input with dimensionless frequency
4.1.5	Dispersion curves showing the effect of linear stiffness $(k/\omega_R)$ of the spring on the spectral bandgaps of (a) soft nonlinear spring-mass systems (b) hard nonlinear spring-mass systems
4.1.6	Dispersion curves showing the effect of nonlocal elastic parameter ( $\epsilon$ ) of the substrate on the spectral bandgaps of (a) soft nonlinear spring-mass systems (b) hard nonlinear spring-mass systems
4.1.7	Dispersion curves showing the effect of material parameter $(\gamma)$ of the substrate property on the spectral bandgaps of (a) soft nonlinear springmass systems (b) hard nonlinear spring-mass systems

4.2.1	Description of the metasurface model
4.2.2	Transmittance $ A_R $ versus dimensionless frequency in a single resonator scenario
4.2.3	Transmittance $ A_R $ versus dimensionless frequency $\frac{\omega}{\omega_{R1}}$ in a pair of resonators scenario
4.2.4	Effect of number of resonators on the transmittance $ A_R $ versus dimensionless frequency $\frac{\omega}{\omega_{R1}}$ curve
4.2.5	Effect of nonlinearity on frequency bandgaps in the dispersion curve 168
4.2.6	Dispersion curves showing the variation of dimensionless wavenumber $\bar{k}$ with dimensionless frequency $\bar{\omega}$
5.1.1	Geometry of the problem
5.1.2	Choice of contour paths and branch cuts for the integral encountered in asymptotic model of Rayleigh waves
5.1.3	Choice of contour paths and branch cuts for the integral encountered in exact solution for Rayleigh waves
5.1.4	Comparison of total wave behavior at a larger time for both asymptotic and exact methods at dimensionless depth (a) $\chi = 0$ (b) $\chi = 10186$
5.2.1	Geometry of the problem
5.2.2	Variation of normalised displacement components $(U)$ of Rayleigh wave fields produced due to case 1 with $r$ -direction for $z=0,\ldots,203$
5.2.3	Variation of normalised displacement components $(U)$ of Rayleigh wave fields produced due to case 1 with $z$ -direction for $r=0,\ldots,204$
5.2.4	Variation of normalised displacement components $(U)$ of Rayleigh wave fields produced due to case 2 with $r$ -direction for $z=0,\ldots,204$
5.2.5	Variation of normalised displacement components $(U)$ of Rayleigh wave fields produced due to case 2 with $z$ -direction for $r=0,\ldots,205$
5.2.6	Surface plot showing the variation of normalized displacement components of Rayleigh wave fields with dimensionless $r-$ and $z-$ direction for case 1206

5.2.7	Surface plot showing the variation of normalized displacement components
	of Rayleigh wave fields with dimensionless $r-$ and $z-$ direction for case 1206
5.2.8	Surface plot showing the variation of normalized displacement components
	of Rayleigh wave fields with dimensionless $r-$ and $z-$ direction for case 2207
5.2.9	Surface plot showing the variation of normalized displacement components
	of Rayleigh wave fields with dimensionless $r-$ and $z-$ direction for case 2207

# LIST OF TABLES

2.2.1	Conditions for which the real roots satisfy the exact dispersion relation.	<b>7</b> 9
4.1.1	Values of some normalized paramteres	143
4.2.1	Values of the mechanical parameters used in the study	162
5.2.1	Values of parameters used in the study	202

#### NOMENCLATURE

 $\omega$  Angular frequency

 $u_n$  Displacement components

 $\epsilon$  Dimensionless nonlocal parameter

 $\phi, \psi$  Displacement potentials

 $\varkappa_f$  Fast variable

ℵ Internal characteristic length

 $k_1$  Linear stiffness of the spring

 $\Lambda, \mu$  Lamé constants

 $\Pi_{mn}$  Local couple stress components

 $\sigma_{mn}$  Local force stress components

 $\rho$  Mass volume density

j Micro-inertia

 $\kappa, \alpha, \beta, \gamma$  Micropolar constants

d Micropolar ratio of  $\kappa$  and  $\mu$ 

 $\Phi_n$  Microrotation components

 $\pi_{mn}$  Nonocal couple stress components

 $k_3$  Nonlinear stiffness of the spring

 $\tau_{mn}$  Nonlocal force stress components

 $\nu$  Poisson's ratio

 $\omega_R$  Resonator frequency

 $\Gamma$  Ratio of transverse velocity  $(c_T)$  and longitudinal velocity  $(c_L)$ 

 $\varkappa_s$  Slow variable

 $A_R$  Transmission ratio

k Wave number

c Wave velocity

 $\lambda$  Wavelength

### CHAPTER 1

Introduction and Preliminaries

#### 1.1 Introduction

Wave propagation in solids [1,2], which forms the foundation of elastodynamics, is governed by the transfer of sharply exerted, localized disturbances from one part of the body to other parts. Although this field is deeply mathematical, it has strong practical relevance and has inspired the formulation of numerous abstract problems. Mathematical frameworks not only offer profound insights into wave phenomena but also complement experimental studies, which provide invaluable information about the properties of various solids, such as the earth, pure metallic crystals, and other materials. For instance, waves are deliberately introduced into the earth to detect oil and gas reservoirs [3–6] and to study its internal structure [7,9]. Similarly, material properties are examined by analyzing transmitted waves, and elastic waves propagating through the human body serve as powerful tools for medical diagnosis and therapy [10–13].

One fascinating phenomenon in elastodynamics is the emergence of Rayleigh wave—a surface wave that propagates along the free surface of an elastic continuum with minimal disturbance to the underlying bulk material. Discovered by Lord Rayleigh [14], these waves exhibit a combination of longitudinal (horizontal) and transverse (vertical) motions. While the horizontal displacement components align with the direction of wave propagation, the vertical components penetrate into the medium. Rayleigh waves play a crucial role in various fields, including the study of wave dispersion, vibration, and bending in solid structures. They have found widespread applications in diverse areas such as material characterization [15–18], geophysical exploration [19–21], acoustic microscopy [22–25], and nondestructive evaluation [26–29].

Furthermore, nanomaterials, renowned for their exceptional thermal, mechanical, and electrical properties, are finding increasing applications in structures like nanobeams [30–33], nanoplates [34–38], and nanoshells [39–42]. While molecular dynamics (MD) simulations [43] can investigate the mechanical behavior of these materials, they are computationally expensive for large systems. Continuum models, which treat nanostructures as elastic solids, provide a more computationally efficient alternative. However, accurately capturing the scale-dependent behavior of nanomaterials necessitates modifications to the classical elasticity theory.

Classical elasticity theory [44, 45] is a well-established macroscale model that effectively describes the behavior of conventional materials. It assumes that stress at a material point depends solely on the local strain, with deformation described by a displacement vector and symmetric stress tensors. This approach aligns well with experimental observations for materials like steel and concrete under moderate stresses. However, this localized approach fails to account for the small-scale effects crucial at micro- and nanoscales. At these scales, intermolecular and interatomic forces, like van der Waals forces, become significant, requiring the incorporation of size effects into theoretical models. Moreover, classical elasticity theory faces limitations in addressing problems involving asymmetric stresses, significant stress gradients, or dynamic phenomena like high-frequency vibrations and short wavelengths, where the microstructure of the material strongly influences deformation.

To address these limitations, various modified continuum theories have been proposed, including couple-stress theories [46–48], micromorphic elasticity theory [49], micropolar elasticity theory [51, 52], nonlocal elasticity theories [53, 54], higher-order strain-gradient theories [55–57], and atomistic-continuum theories [58]. Nonlocal elasticity theory, pioneered by Eringen and Edelen [59], addresses this limitation by acknowledging the nonlocality of stresses. This theory assumes that stress at a given point is influenced by the strain field throughout the entire domain. For homogeneous, isotropic materials, this leads to a set of integro-partial differential equations governing the displacement field. While solving these equations can be challenging, specific kernel choices can reduce them to singular partial differential equations. Notably, these kernels have shown excellent agreement with experimental observations across various length scales, from the microto the macroscale. Furthermore, nonlocal elasticity theory exhibits desirable limiting behaviors: it converges to classical elasticity theory in the long-wave limit and asymptotically approaches atomic lattice dynamics theory in the short-wave limit (as cited in Eringen [60]). This nonlocal approach introduces an internal characteristic length scale into the constitutive equations, enabling a more accurate description of the mechanical behavior of nanomaterials. Consequently, nonlocal elasticity provides a robust theoretical framework for studying wave propagation and other mechanical responses in micro- and nanoscale materials.

Micropolar elasticity [51], on the other hand, extends classical elasticity by incorporating an independent rotation vector in addition to a displacement vector, thereby allowing material particles to undergo microrotation without macrodisplacement. Surface elements exhibit both force and couple stresses, leading to nonsymmetric stress and couple-stress tensors. These tensors are linked to nonsymmetric strain and curvature tensors, capturing size effects critical at the microstructural scale. This theory explains phenomena like higher strength in materials with smaller grain sizes, the strengthening effect of finer dispersed particles in metals, and the increased bending and torsional strength of thin structures. It also addresses the emergence of new wave types in granular materials, polycrystalline structures, and reinforced media, providing a robust framework to model the microstructural effects that classical elasticity cannot capture.

The combination of micropolar and nonlocal effects within a single framework, termed nonlocal micropolar elasticity, provides a powerful tool for analyzing the behavior of complex materials across various length scales, from micro- to nanoscale. Initially developed by Eringen [61], this theory has undergone significant advancements and now finds significant applications in the design and analysis of advanced materials and structures, including those encountered in micro- and nano-electromechanical systems, biomechanics, and geomechanics.

A major challenge in nonlocal elastic models is the dependence of the integration domains in constitutive relations on the distance from the boundary. This leads to boundary layers with localized non-homogeneous stress and strain fields [62]. Despite widespread belief in the equivalence of integral and differential non-local formulations, the validity of differential equations derived from the original integral form remains unverified, particularly for bounded domains. The integral form, considered "strongly nonlocal" due to its reliance on all neighboring points, is challenging to solve. However, the reduction to differential form can be inaccurate, especially when dealing with bounded domains. In such cases, the differential model becomes ill-posed and inaccurate without additional constitutive boundary conditions. This highlights the critical need for refined boundary conditions in non-local models to ensure accurate and consistent predictions. We address this research gap in the context of various elasticity theories in the current thesis.

Elasticity theories provide a foundation for understanding wave propagation in continuous media. However, to manipulate and control seismic wave phenomena beyond

the limitations of natural materials, the concept of seismic metasurfaces has emerged. These artificially engineered interfaces, characterized by subwavelength features, offer unprecedented control over wave transmission, reflection, and refraction, enabling novel wave-guiding [63] and energy harvesting applications [64–66]. This development aligns with the growing need for innovative seismic mitigation strategies, driven by the desire to reduce structural damage and ensure safety. Metamaterials [67], first introduced in 1999, are synthetic composites with engineered structures that exhibit properties not found in naturally occurring materials. Originally developed for optics [68] and electromagnetism [69], these concepts have been extended to acoustic and elastic media, enabling the creation of materials with unconventional properties. While initially focused on bulk materials, the development of metasurfaces has allowed for precise control over surface wave propagation, including seismic waves.

More recently, seismic metamaterials have gained attention for their potential to mitigate Rayleigh waves, which carry significant elastic energy along the Earth's surface. By introducing sub-wavelength resonators or inclusions into the ground, researchers have created structured media that can alter local wave propagation characteristics. When arranged along the soil surface as "metabarriers" [70,71] or "seismic metasurfaces," these resonators can impede surface wave propagation by inducing band gaps around their natural frequencies, effectively reducing wave amplitudes. Engineered periodic structures like these offer unique wave filtering and guiding capabilities, enabling effects such as negative refraction [72, 73] and acoustic invisibility [74, 75]. These properties have been applied across various scales, from microscale optics to geophysical seismic wave mitigation, offering new pathways for controlling wave behavior.

In addition to exploring the propagation and control of elastic waves within the framework of various elasticity theories, including the manipulation of Rayleigh waves using metasurfaces, researchers have recognized the critical need to investigate the mechanisms that initiate these surface waves. Rayleigh waves can arise from a variety of sources [76–78]. Their generation can be modeled using two primary approaches: (a) as an initial value problem, where initial interior conditions, such as initial displacements or velocities, trigger the propagation of elastic waves that evolve into surface Rayleigh waves; and (b) as a boundary value problem, where surface disturbances, such as earthquakes [79], explosions [80–82], and human activities like pile driving [83, 84], generate

seismic energy that propagates through the subsurface and excites Rayleigh waves. Understanding the generation mechanisms of these waves is also crucial for accurate modeling and effective mitigation strategies.

# Structure of the thesis

The structure of this thesis is detailed in the following schematic diagram:

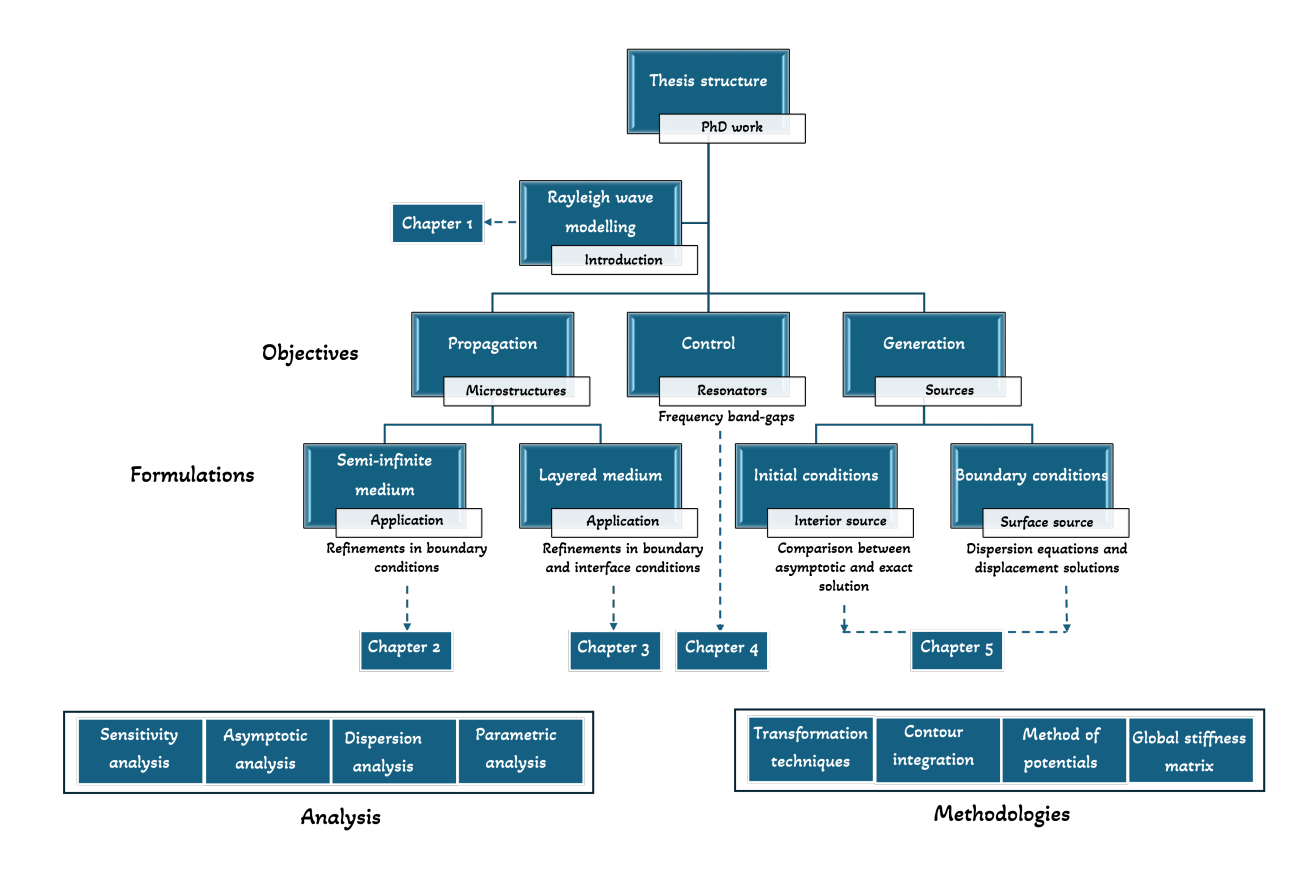


Figure 1.1.1: Structure of the thesis

# Motivation for the thesis

The study of Rayleigh wave propagation has profound implications in both theoretical and applied geophysics, particularly in seismic wave analysis and material characterization. Understanding these waves is critical for assessing the mechanical behavior of geological structures and engineered materials. However, classical elasticity theory, which has traditionally been used to model Rayleigh waves, has inherent limitations when applied to materials with microstructural complexities and nonlocal interactions. These limitations necessitate the development of more refined mathematical frameworks that incorporate

microstructural effects, nonlocality, and size-dependent phenomena. This thesis is motivated by the need to address these theoretical gaps and to provide more accurate and applicable models for Rayleigh wave propagation in complex media.

One of the primary motivations for this study is the inadequacy of classical elasticity in capturing nonlocal effects and microstructural interactions in wave propagation. The introduction of nonlocal elasticity and micropolar elasticity theories has opened new avenues for accurately modeling these effects. However, inconsistencies in the formulation of boundary conditions, particularly in nonlocal micropolar elasticity, have hindered their practical applicability. Addressing these inconsistencies by deriving refined boundary conditions is a central goal of this thesis.

The work of Kaplunov et al. [204] demonstrated that traditional nonlocal boundary conditions fail to correctly account for boundary layer effects in semi-infinite media, leading to discrepancies between differential and integral formulations of nonlocal elasticity. This underscores the necessity of employing asymptotic techniques to capture these effects systematically. Furthermore, when microstructural rotations are considered, as in micropolar elasticity, an additional condition arises in formulating the appropriate boundary conditions. This thesis extends existing nonlocal elasticity frameworks by incorporating micropolar effects and refining boundary and interface conditions for accurate wave propagation modeling in both semi-infinite and layered structures.

Another motivation stems from the rapid advancements in metasurfaces and their potential for controlling Rayleigh wave propagation. Metasurfaces, composed of subwavelength-scale engineered resonating structures, enable unprecedented control over wave phenomena such as wave steering, cloaking, and dispersion modulation. However, current studies predominantly focus on classical elasticity-based metasurfaces, neglecting the influence of nonlocal elasticity effects. This thesis aims to bridge this gap by integrating nonlocal elasticity with metasurface design to achieve enhanced wave control mechanisms, which could have significant applications in seismic hazard mitigation and wave-based engineering technologies.

Additionally, the traditional approach to geomechanical problems has largely been confined to boundary value formulations, neglecting the potential insights gained from initial value problems. This thesis introduces a novel approach by modeling Rayleigh wave generation as an initial value problem, which subsequently evolves into a boundary value

formulation. This shift in perspective provides new insights into wave excitation mechanisms, particularly for initial interior/boundary surface sources within elastic/micropolar media, and allows for a more comprehensive understanding of seismic wave propagation dynamics.

In summary, this thesis is motivated by the need to refine mathematical models of Rayleigh wave propagation to incorporate nonlocal and micropolar effects, develop refined boundary and interface conditions, explore advanced wave control strategies using metasurfaces, and introduce novel initial value problem formulations for wave generation. These contributions aim to bridge critical theoretical gaps and provide practical advancements for seismic wave analysis, material characterization, and wave-based engineering applications.

# 1.2 Literature review

Rayleigh waves exhibit a dual nature near the surface, prompting the development of an asymptotic model to capture this behavior. Kaplunov et al. [85] pioneered this effort with deriving the first hyperbolic-elliptic model. Subsequent research, including multiscale perturbation schemes by Kaplunov et al. [86], extended this approach to describe various types of waves, such as Rayleigh, interfacial, and edge waves [87]. Asymptotic models have been derived for surface waves in diverse media, including incompressible [88] and compressible [89] elastic half-spaces. Recent advancements include models for anisotropic media [90], planes with cubic symmetry [91], and refined models with second-order corrections [92]. These models have been applied to various problems, including mixed boundary value problems (see, Erbas et al. [93]). Additionally, transient motions and dynamic responses of half-planes subjected to moving loads have been studied by Kaplunov [94] and revisited using asymptotic models (see, Kaplunov et al. [95]).

Classical elasticity theory predicts that Rayleigh waves propagating in an elastic half-space are nondispersive. Several researchers have investigated this topic extensively [96–98] However, observations of phonon dispersion experiments, as detailed in the work of Brockhouse et al. [99], Harrison [100], and Wallis [101], have demonstrated a strong dependence of phase velocity on wavelength, particularly in the short-wavelength regime. This discrepancy, along with other phenomena such as surface tension, surface energy, and the presence of optical branches in the dispersion curve, cannot be adequately explained within the framework of classical elasticity.

The limitations of classical elasticity theories have necessitated the development of generalized models of continuum mechanics. These advancements, dating back to Voigt's work in 1887 [102], involve modeling the material as a collection of independently moving and/or deforming particles. Voigt [102] incorporated the effects of moment-based stresses, known as couple stresses, in addition to the classical force stresses, generalizing the symmetric classical theory of elasticity. Building upon Voigt's work, the Cosserat brothers extended the concept by introducing the notion of microrotations - independent rotations within the material. This led to the development of the Cosserat theory (Cosserat and Cosserat, [103]), which assumes that a material is composed of rigid particles with independent rotational degrees of freedom. A defining characteristic of this

theory is the presence of surface and body couples acting independently of surface and body forces. The highly general nonlinear Cosserat theory was later refined and developed in more restricted settings by other researchers [48–50,104–106]. In othe words, this theory received a considerable attention from the researchers and as a result higher-order continuum theories have been developed.

Theories addressing size-dependent behavior can be broadly classified into three categories: strain gradient theories, microcontinuum theories, and nonlocal elasticity theories. The strain gradient theories encompasses several models, including the couple stress theory [46,107–111], the first and second strain gradient theories [47,112], the modified couple stress theory [113], and the modified strain gradient theory [114]. A defining feature of strain gradient theories is the inclusion of both strain and strain gradients in the strain energy density, which introduces material length scale parameters to account for size effects.

Microcontinuum theories [115, 116] encompass a family of models, including micropolar, micromorphic, and microstretch theories. Among these, micropolar theory represents the simplest framework, characterized by a three additional degrees of freedom. Eringen [51] is recognized for extending the Cosserat theory to incorporate body microinertia effects and renaming it as the micropolar theory of elasticity. In his works (Eringen [51], [117], [118]), he further developed both the micropolar and microstretch theories for linear and nonlinear elasticity. Today, the linear theory is commonly referred to as the linear theory of micropolar, Cosserat, or asymmetric elasticity. References on linear micropolar elasticity theory can be found in [119–123]. Nowacki and Olszak [124] presented a general report on the development of micropolar elasticity elasticity. Readers are also encouraged to refer to the survey paper by Hassanpour and Heppler [125] for a comprehensive overview of micropolar moduli and a detailed comparison of the notations used in various formulations of micropolar theory. Notably, the couple-stress theory is also known as the Cosserat theory with constrained rotations or, more briefly, the constrained Cosserat theory. Further, Eringen introduced micromorphic theory [126, 127] to account for the influence of microstructure within a macroscopic framework. A key distinction lies in the fact that micromorphic elasticity allows for more complex micro-deformations, encompassing both rotation and internal strains, whereas micropolar elasticity is limited to considering only micro-rotations. The micromorphic theory is a generalized continuum model that can be simplified to the micropolar and microstretch theory [128]. In recent years, several simplified versions of the general micromorphic theory have been developed (refer, Shaat [129]; Barbagallo et al. [130]; Romano et al. [131]; Neff et al. [132]). They enable the exploration of material dispersion characteristics (refer, Kunin [133–135] Trovalusci and Pau, [136]; Shaat [137]), facilitate multiscale modeling (see, Shaat [129]; Trovalusci [138]), and describe the physical microstructures of materials (see, Capriz [139]; Gurtin and Podio-Guidugli [140]).

Nonlocal field theories can be considered a general class of material models. While all microcontinuum theories implicitly exhibit nonlocal behavior [134,141–143], with nonlocal effects often represented by gradients of microdeformations or kinetic coupling constants between different degrees of freedom, explicit nonlocal models have been developed to explicitly visualize these effects. These models utilize convolution-type constitutive equations, incorporating a nonlocal parameter that is dependent on material properties, molecular structure, and internal characteristic length [144]. It is important to note that the modeling of nonlocal effects, whether through implicit or explicit methods, requires careful consideration of various factors.

The foundation of nonlocal elasticity was laid by Kroner [145], who introduced a model to incorporate the long-range effects of cohesive forces between particles. This theory was later further developed by Edelen [146, 147], Eringen [148, 149] and improved by Eringen and Edelen [59], Eringen et al. [150,151]. The strong form of nonlocal elasticity, involving integrals over the entire domain, has received comparatively less attention due to the inherent complexity of obtaining the solutions. Hence, only limited researchers [152–157] have attempted to explore the solutions to these integral equations. To address the challenges associated with the integral form of nonlocal elasticity, Eringen proposed a differential formulation [60] for a specific choice of the nonlocal moduli. This differential form, often referred to as the weak form of nonlocal elasticity, has garnered significant attention due to its relative ease of implementation. Consequently, it has been widely adopted by researchers for analyzing various structures, including elastic media [158–166], beams [167–172], plates [173–178], and shells [40,179–183]. Several comprehensive reviews and books have also been published on the theoretical foundations and applications of nonlocal mechanics in nanostructures, see Arash and Wang [184], Rafii-Tabar et al. [185], Askari et al. [186], Srinivasa and Reddy [187], Behera and Chakraverty [188], Shaat et

al. [189] Gopalakrishnan and Narendar [190]. Further, unified approaches have been developed to combine nonlocal elasticity with other theories, such as nonlocal micropolar elasticity [61], nonlocal thermoelasticity [191], nonlocal piezoelectricity [192], and nonlocal electromagnetic solids [193] etc. It is worth mentioning that the highly cited work in Eringen [60] and subsequent studies on nonlocal elasticity have not explicitly verified whether the solutions of the differential equations satisfy the original integral formulations. Recent research efforts have addressed this gap by developing refined nonlocal theories.

Nonlocal elasticity models often exhibit a reduction in effective stiffness, leading to lower natural frequencies and increased deflections [194]. However, observed behavior can vary, with instances of stiffening [195–197] or negligible differences compared to classical models [198], highlighting discrepancies between integral and differential models. These inconsistencies arise primarily from the limitations of differential formulations, which often neglect the critical role of boundary conditions. To address these inconsistencies, several approaches have been proposed (see, Tuna and Kirca [199], Shaat et al. [200], Koutsoumaris et al. [201]). A significant advancement in addressing these inconsistencies is the development of refined boundary conditions. These conditions, often derived through asymptotic methods, incorporate additional terms or derivatives of field variables to ensure compatibility with nonlocal constitutive equations. For instance, Chebakov et al. [202] reduced the nonlocal problem in a half-space to an equivalent classical formulation with a localized near-surface inhomogeneity, capturing the effect through effective boundary conditions. Moreover, this refined theory has been extended for two-dimensional nonlocal elastic plates [203], incorporating first-order corrections to account for boundary layer effects. This approach has been extended to various wave propagation scenarios, including Rayleigh waves [204], anti-plane waves [205] and other wave types [206, 207], through asymptotic formulations.

In recent decades, controlling wave propagation using metamaterials and metasurfaces has garnered significant attention across applied physics, mechanics, and civil engineering. Prior to the emergence of metasurfaces, wave control relied heavily on phononic crystals [208,209], which utilize Bragg scattering to create frequency bandgaps [210,211]. However, the effectiveness of phononic crystals diminishes at low frequencies due to the requirement of impractically large structures [212] to accommodate long wavelengths. A ground-breaking work by Liu et al. [213] introduced the concept of locally resonant (LR) units,

enabling the creation of bandgaps in structures much smaller than the wavelength. This innovation, termed 'metamaterials', offers significant advantages over phononic crystals, particularly in controlling low-frequency vibrations due to their compact and lightweight nature. Inspired by this pioneering work, a diverse range of metamaterials have been explored, including those incorporating spring-mass systems [214, 215], rods [216, 217], beams [218–221], and plates [222–224].

Controlling elastic surface waves using resonant arrays, often termed "seismic metasurfaces", has emerged as a significant area of research. The seismic metamaterials have been identified into four major catagories as described in Brûlé et al. [225] (a) Seismic soil-metamaterials consisting of artificially structured soils made up of rigid inclusions (Achaoui et al. [226]) or cyllindrical boreholes (Brûlé et al. [227])(b) Buried massresonators [228–230] consisting of damped resonators buried inside the soil (c) Abovesurface resonators (see, Columbi et al. [231,232], Palermo et al. [233], Colquitt et al. [234]), typically forest of trees, consisting of sub-wavelength structures arranged on the top of elastic half-space (d) Auxetic materials [235], buried inside the soil and characterized by materials with negative Poisson's ratio (e) Other dissipative structures, such as gyrobeams [236], incorporated into the structure to be protected. Through careful design, these metasurfaces can manipulate the dispersive nature of surface waves, enabling functionalities such as wave trapping, waveguiding, and the creation of spectral bandgaps [237]. Recent decades have witnessed a surge in research on metasurface designs, encompassing various methodologies such as incorporating nonlinearity in spring-mass systems (see, Lou et al. [238–240], Palermo et al. [241], Carneiro et al. [242]), exploring multi-physics phenomena in Pu et al. [243], utilizing tunable inertial amplifiers [244–247], and investigating wave propagation along metasurfaces in stratified media (in Zeng et al. [248]).

# 1.3 Preliminaries

In this section, a concise overview of the constitutive relations and governing equations are presented for classical, nonlocal, micropolar, and nonlocal micropolar elasticity theories. Subsequently, an investigation into the propagation of Rayleigh waves is conducted within the context of classical and nonlocal elasticity theories. This also includes a brief explanation on the refined boundary conditions developed for wave propagation within a nonlocal elastic semi-infinite medium.

### 1.3.1 Classical elasticity theory

This theory focuses on a specific class of continua called *linear elastic solids* possessing the unique characteristics of recovering its original shape and size once the forces causing deformation are removed. The fundamental relationship governing the behavior of these linear solids undergoing infinitesimal deformations is described by *Hooke's Law*. The generalized form of Hooke's Law, proposed by Cauchy expresses the linear relationship between stress and strain components for a more complex material as follows:

$$\sigma_{mn} = \mathcal{C}_{mnpq} \epsilon_{pq}, \quad m, n, p, q = 1, 2, 3, \tag{1.3.1}$$

where  $\sigma_{mn}$  and  $\epsilon_{mn}$  are the components of second-order stress tensor and Cauchy's strain tensor, respectively. And  $\mathcal{C}_{mnpq}$  are the components of a fourth-order tensor namely elasticity tensor.

The strain components  $\epsilon_{mn}$  are related to the components  $u_m$  of the displacement vector  $\mathbf{u}$  along the respective  $x_m$ -direction by,

$$\varepsilon_{mn} = \frac{1}{2} \left( \frac{\partial u_m}{\partial x_n} + \frac{\partial u_n}{\partial x_m} \right). \tag{1.3.2}$$

It has been shown in [249] that for a homogeneous linear isotropic elastic solid, the generalized Hooke's law takes the form,

$$\sigma_{mn} = \Lambda \delta_{mn} \epsilon_{kk} + 2\mu \epsilon_{mn}. \tag{1.3.3}$$

Here  $\Lambda$  and  $\mu$  are called Lamé moduli and  $\delta_{mn}$  is the well-known Kronecker delta.

Furthermore, it is important to note that within the classical elasticity framework, the strain tensor is symmetric ( $\varepsilon_{mn} = \varepsilon_{nm}$ ). This symmetry directly implies the symmetricity of the stress tensor ( $\sigma_{mn} = \sigma_{nm}$ ). Alternatively, the symmetry of the stress tensor can

be readily derived by using the principle of conservation of angular momentum, see Heinbockel [250].

From the principle of conservation of linear momentum, the equations governing the motion of an elastic body are given by,

$$\sigma_{mn,m} + F_n = \rho u_{n,tt}, \ m, n = 1, 2, 3,$$
 (1.3.4)

where Einstein summation convention [250] is used. Here  $F_n$  denotes the body force per unit volume,  $\rho$  denotes the mass volume density and  $u_{n,tt}$  denotes the acceleration of the body. Also, the comma in the subscript denotes the derivative with respect to the corresponding variable.

### 1.3.1.1 Classical Rayleigh wave secular equation

Here, we derive the classical secular equation for the propagation of a time harmonic Rayleigh wave in a homogeneous, linear isotropic elastic semi-infinite medium with a stress-free boundary.

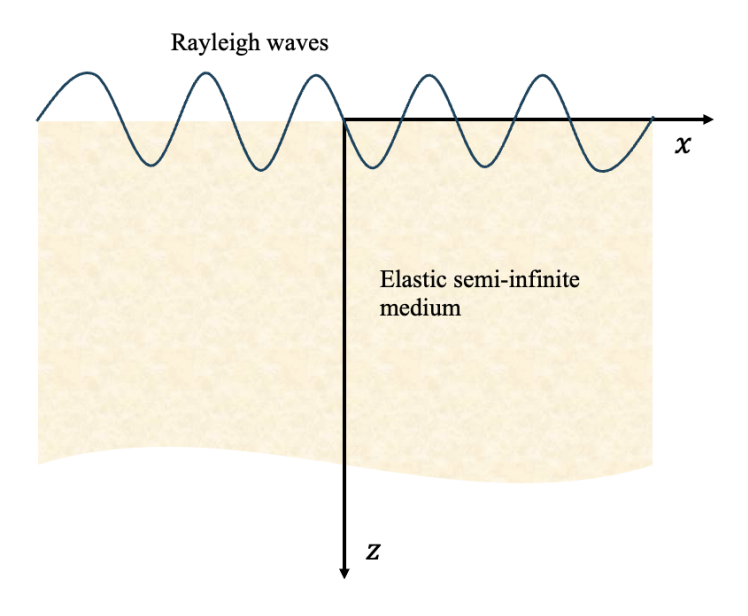


Figure 1.3.1: Rayleigh waves in an elastic semi-infinite medium

Consider a linearly isotropic medium occupying the region,

$$\mathcal{R} = \{(x, y, z) \mid | -\infty < x, y < \infty, \ 0 \le z < \infty \},$$

having stress-free boundary and Rayleigh wave propagating in x-direction along xz-plane with the z-axis pointing vertically downwards as in Figure 1.3.1. The displacement field

is represented by  $\mathbf{u} = (u_1, 0, u_3)$ .

Substituting the constitutive equations in Eq. (1.3.3) in the governing equations of motion in Eq. (1.3.4) gives

$$\mu u_{mm} + (\Lambda + \mu) u_{m,mn} - \rho u_{n,tt} = 0, \ m, n = 1, 3.$$
 (1.3.5)

Decomposing the displacement vector  $\mathbf{u}$  according to the Helmholtz theorem, we can express it as the sum of the gradient of a scalar potential  $\phi$  and curl of a vector potential  $\boldsymbol{\psi} = (\psi_1, \psi, \psi_3)$  as,

$$\mathbf{u} = \nabla \phi + \nabla \times \boldsymbol{\psi},\tag{1.3.6}$$

with the constraint  $\nabla \cdot \boldsymbol{\psi} = 0$ .

This decouples the system of equations in Eq. (1.3.5) into,

$$\nabla^2 \phi - \frac{1}{c_L^2} \phi_{,tt} = 0, \qquad \qquad \nabla^2 \psi - \frac{1}{c_T^2} \psi_{,tt} = 0, \qquad (1.3.7)$$

where  $c_L = \sqrt{\frac{\Lambda + 2\mu}{\rho}}$  and  $c_T = \sqrt{\frac{\mu}{\rho}}$  are the longitudinal and transverse wave velocities, respectively.

In terms of potentials, the components of the stress tensor in z-direction are given by,

$$\sigma_{31} = \mu \left( \frac{\partial^2 \phi}{\partial x \partial z} + \frac{\partial^2 \psi}{\partial x^2} - \frac{\partial^2 \psi}{\partial z^2} \right),$$

$$\sigma_{32} = 0,$$

$$\sigma_{33} = \Lambda \frac{\partial^2 \phi}{\partial x^2} + (\Lambda + 2\mu) \frac{\partial^2 \phi}{\partial z^2} + 2\mu \frac{\partial^2 \psi}{\partial x \partial z}.$$

$$(1.3.8)$$

To investigate Rayleigh wave propagation, we seek displacement potential solutions in the form of travelling harmonic waves,

$$(\phi, \psi) = (A e^{-kr_1 z}, B e^{-kr_2 z}) e^{i(kx - \omega t)},$$
 (1.3.9)

where  $k = \frac{\omega}{c}$  is the wavenumber,  $\omega$  is the angular frequency, c is the wave velocity, and  $r_1$ ,  $r_2$  are attenuation factors to be determined. We require that the real parts of  $r_1$  and  $r_2$  are positive (i.e.,  $\Re(r_1) > 0$ ,  $\Re(r_2) > 0$ ) to ensure the decay of the Rayleigh wave field as  $z \to \infty$ .

Substituting these potential solutions given in Eq. (1.3.9) into the governing wave equations in Eq. (1.3.7) yields expressions for the attenuation factors as,

$$r_1 = \sqrt{1 - \frac{c^2}{c_L^2}}, \ r_2 = \sqrt{1 - \frac{c^2}{c_T^2}}.$$

Since the problem is investigated within a stress-free boundary conditions, we must have at the boundary z = 0,

$$\sigma_{31} = 0 \text{ and } \sigma_{33} = 0$$
 (1.3.10)

As a result, the stresses associated with the displacement potentials in Eq. (1.3.9) can be easily calculated using Eq. (1.3.8). This gives a system of equation in A and B as,

$$-2i\mu r_1 A - \mu (1 + r_2^2) B = 0, 
[-\Lambda + (\Lambda + 2\mu) r_1^2] A - 2i\mu r_2 B = 0.$$
(1.3.11)

In order to ensure a non-zero displacement field  $(\mathbf{u})$ , the coefficients A and B cannot both be zero. This necessitates the system of equations in Eqs. (1.3.11) to possess a non-trivial solution. A necessary and sufficient condition for the existence of a non-trivial solution is that the determinant of the coefficient matrix vanishes. Thus, a simplified version yields

$$\begin{vmatrix} 2ir_1 & \left(2 - \frac{c^2}{c_T^2}\right) \\ \left(2 - \frac{c^2}{c_T^2}\right) & -2ir_2 \end{vmatrix} = 0. \tag{1.3.12}$$

In other words, we have

$$\left(2 - \frac{c^2}{c_T^2}\right)^2 - 4\sqrt{1 - \frac{c^2}{c_L^2}}\sqrt{1 - \frac{c^2}{c_T^2}} = 0.$$
(1.3.13)

This represents the well-known classical Rayleigh wave secular equation [14], which is clearly non-dispersive.

Let us represent the Rayleigh wave equation as,

$$R(y) = (2 - y)^{2} - 4\sqrt{1 - \frac{y}{\Gamma^{-2}}}\sqrt{1 - y} = 0,$$
(1.3.14)

where  $y = \frac{c^2}{c_T^2}$ , and  $\Gamma = \frac{c_T}{c_L} < 1$ . We now proceed to investigate the uniqueness of the solution to the equation in Eq. (1.3.14).

Observe that, R(0) = 0, R(1) = 1, R'(0) < 0 and also,

$$R''(y) = \frac{(\Gamma^{-2} - 1)^2 \sqrt{1 - \frac{y}{\Gamma^{-2}}}}{(1 - y)^{3/2} (y - \Gamma^{-2})^2} + 2 > 0, \text{ for } 0 < y < 1,$$

indicating that the function R(y) is concave upwards in the interval 0 < y < 1. These conditions ensures the existence and uniqueness of the solution, say  $c = c_R$  with  $c_R < c_2$ 

(as y < 1) to the Rayleigh wave secular equation in Eq. (1.3.14). Now, on squaring Eq. (1.3.14), a cubic equation in y can be obtained as

$$y^{3} - 8y^{2} + \left(24 - \frac{16}{\Gamma^{-2}}\right)y - 16\left(1 - \frac{1}{\Gamma^{-2}}\right) = 0.$$
 (1.3.15)

As a limiting case when  $\Lambda = \mu$ , we get  $\Gamma = \frac{1}{\sqrt{3}}$ . This reduces Eq. (1.3.15) as

$$y^3 - 8y^2 + \frac{56}{3}y - \frac{32}{3} = 0. ag{1.3.16}$$

This equation has roots at y=4,  $\frac{2}{3}(3\pm\sqrt{3})$ . The only admissible root, being less than 1 is  $y=\frac{2}{3}(3-\sqrt{3})=0.8453$ . This suggests that Rayleigh wave propagates with the velocity  $c_R=0.8453\,c_2$  when  $\Gamma=\frac{1}{\sqrt{3}}$  for the medium. A variation of R(y) with y is plotted in Figure 1.3.2 to visualize the Rayleigh wave root for a fixed  $\Gamma=\frac{1}{\sqrt{3}}$ .

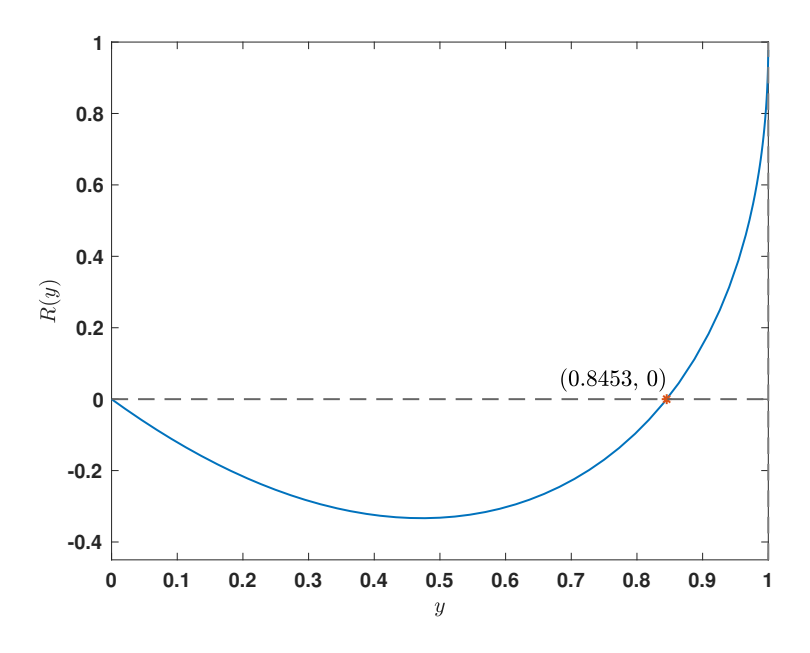


Figure 1.3.2: Variation of R(y) with y for  $\Gamma = \frac{1}{\sqrt{3}}$ 

The pioneering work on the existence and uniqueness of the solution was conducted by Sobolev [251], with subsequent contributions from Babich and Kiselev [252]. Notably, research by Barnett and Lothe [253] and Kamotskii and Kiselev [254] has extended these findings to anisotropic materials.

# 1.3.2 Asymptotic hyperbolic-elliptic model for Rayleigh waves

This section provides an overview of the derivation of the asymptotic hyperbolicelliptic model for near-surface wavefields generated by surface stresses. For a more indepth analysis, readers are referred to the works of Kaplunov and Kossovich [85], Kaplunov et al. [86], and Kaplunov and Prikazchikov [87].

The derivation is based on a perturbation analysis of the self-similar solutions for the homogeneous surface wave in the slow-time domain. This approach ultimately reveals a dual nature of Rayleigh waves, characterized by hyperbolic equations governing their behavior on the surface and elliptic equations describing their behavior in the interior of the medium.

Consider a plane strain problem given in Eq. (1.3.7) involving the propagation of surface Rayleigh waves in a homogeneous, linear, isotropic elastic medium that occupies the region  $\mathcal{R}$ . The problem is subjected to the boundary conditions along the surface z=0 as

$$\sigma_{31} = -P_1(x, t) \text{ and } \sigma_{33} = -P_2(x, t).$$
 (1.3.17)

Now, we perturb the problem defined in Eq. (1.3.7) by introducing a slow-time variable,  $\tau = \epsilon t$ , where  $\epsilon \ll 1$  is a perturbation parameter denoting the small deviation of phase velocity from the Rayleigh waves. This approach, inspired by the work of Friedlander [255] and Chadwick [256] on self-similar solutions for stress-free boundary value problems in the variable  $\xi = x - c_R t$ , allows us to investigate the influence of surface loading on the propagation of Rayleigh waves.

In terms of new variables, the governing equations given in Eq. (1.3.7) transforms into,

$$\frac{\partial^2 \phi}{\partial z^2} + \left(1 - \frac{c_R^2}{c_1^2}\right) \frac{\partial^2 \phi}{\partial \xi^2} + \frac{2\epsilon c_R}{c_1^2} \frac{\partial^2 \phi}{\partial \tau \partial \xi} - \frac{\epsilon^2}{c_1^2} \frac{\partial^2 \phi}{\partial \tau^2} = 0, 
\frac{\partial^2 \psi}{\partial z^2} + \left(1 - \frac{c_R^2}{c_1^2}\right) \frac{\partial^2 \psi}{\partial \xi^2} + \frac{2\epsilon c_R}{c_2^2} \frac{\partial^2 \phi}{\partial \tau \partial \xi} - \frac{\epsilon^2}{c_2^2} \frac{\partial^2 \phi}{\partial \tau^2} = 0,$$
(1.3.18)

and the corresponding boundary conditions are rewritten as,

$$\left(\frac{\partial^2 \phi}{\partial \xi \partial z} + \frac{\partial^2 \psi}{\partial \xi^2} - \frac{\partial^2 \psi}{\partial z^2}\right) = -\frac{P_1}{\mu}, 
(\Gamma^{-2} - 2) \frac{\partial^2 \phi}{\partial x^2} + \Gamma^{-2} \frac{\partial^2 \phi}{\partial z^2} + 2 \frac{\partial^2 \psi}{\partial x \partial z} = -\frac{P_2}{\mu},$$
(1.3.19)

where  $\Gamma = \frac{c_T}{c_L}$ .

Expanding the potentials in asymptotic series of the form,

$$\phi(\xi, z, \tau) = \frac{1}{\epsilon} \left[ \phi^{(0)}(\xi, z, \tau) + \epsilon \phi^{(1)}(\xi, z, \tau) + \cdots \right], 
\psi(\xi, z, \tau) = \frac{1}{\epsilon} \left[ \psi^{(0)}(\xi, z, \tau) + \epsilon \psi^{(1)}(\xi, z, \tau) + \cdots \right].$$
(1.3.20)

By substituting Eq. (1.3.20) into Eq. (1.3.18) and retaining only the leading-order terms, we obtain a set of elliptic equations of the following form,

$$\frac{\partial^2 \phi^{(0)}}{\partial z^2} + \alpha_L^2 \frac{\partial^2 \phi^{(0)}}{\partial \xi^2} = 0, 
\frac{\partial^2 \psi^{(0)}}{\partial z^2} + \alpha_T^2 \frac{\partial^2 \psi^{(0)}}{\partial \xi^2} = 0,$$
(1.3.21)

where 
$$\alpha_L = \sqrt{1 - \frac{c_R^2}{c_L^2}}$$
 and  $\alpha_T = \sqrt{1 - \frac{c_R^2}{c_T^2}}$ .

Based on the works of Friedlander [255] and Chadwick [256], the plane harmonic wave functions that satisfies wave equations in Eq. (1.3.21) can be expressed as

$$\phi^{(0)} = \phi^{(0)}(\xi, \alpha_L z, \tau), \qquad \psi^{(0)} = \psi^{(0)}(\xi, \alpha_T z, \tau). \tag{1.3.22}$$

Computing the first-order terms in Eq. (1.3.18) yields a set of heterogeneous equations,

$$\frac{\partial^2 \phi^{(1)}}{\partial z^2} + \alpha_L^2 \frac{\partial^2 \phi^{(1)}}{\partial \xi^2} = -2 \left[ \frac{1 - \alpha_L^2}{c_R} \right] \frac{\partial^2 \phi^{(0)}}{\partial \xi \partial \tau}, 
\frac{\partial^2 \psi^{(1)}}{\partial z^2} + \alpha_T^2 \frac{\partial^2 \psi^{(1)}}{\partial \xi^2} = -2 \left[ \frac{1 - \alpha_T^2}{c_R} \right] \frac{\partial^2 \psi^{(0)}}{\partial \xi \partial \tau}.$$
(1.3.23)

It can be readily observed that the set of equations presented in Eq. (1.3.23) admits solutions of the form,

$$\phi^{(1)} = \phi^{(1,0)} + z\phi^{(1,1)}, \qquad \psi^{(1)} = \psi^{(1,0)} + z\psi^{(1,1)}, \qquad (1.3.24)$$

where  $\phi^{(1,0)}$  and  $\phi^{(1,1)}$  are the harmonic functions of  $(\xi, \alpha_L z, \tau)$ , while  $\psi^{(1,0)}$  and  $\psi^{(1,1)}$  are the harmonic functions of  $(\xi, \alpha_T z, \tau)$ .

Further, substituting the solutions of the form in Eq. (1.3.24) into Eqs. (1.3.23), we obtain,

$$\frac{\partial \phi^{(1,1)}}{\partial z} + \left[ \frac{1 - \alpha_L^2}{c_R} \right] \frac{\partial^2 \phi^{(0)}}{\partial \xi \, \partial \tau} = 0, \qquad \frac{\partial \psi^{(1,1)}}{\partial z} + \left[ \frac{1 - \alpha_L^2}{c_R} \right] \frac{\partial^2 \psi^{(0)}}{\partial \xi \, \partial \tau} = 0. \tag{1.3.25}$$

These equations on further reduction using Cauchy-Riemann inequalities gives the values,

$$\phi^{(1,1)} = -\left[\frac{1-\alpha_L^2}{c_R \alpha_L}\right] \frac{\partial \phi_c^{(0)}}{\partial \tau}, \qquad \psi^{(1,1)} = -\left[\frac{1-\alpha_T^2}{c_R \alpha_T}\right] \frac{\partial \psi_c^{(0)}}{\partial \tau}, \tag{1.3.26}$$

where the subscript c in the potentials denote their corresponding conjugates.

As a result, the two-term expansion of the wave potentials as written in Eq. (1.3.20) becomes,

$$\phi = \frac{1}{\epsilon} \left[ \phi^{(0)} + \epsilon \left[ \phi^{(1,0)} - z \left( \frac{1 - \alpha_L^2}{c_R \alpha_L} \right) \frac{\partial \phi_c^{(0)}}{\partial \tau} \right] + \cdots \right],$$

$$\psi = \frac{1}{\epsilon} \left[ \psi^{(0)} + \epsilon \left[ \psi^{(1,0)} - z \left( \frac{1 - \alpha_T^2}{c_R \alpha_T} \right) \frac{\partial \phi_c^{(0)}}{\partial \tau} \right] + \cdots \right].$$

$$(1.3.27)$$

Case 1: In case of a <u>normal load</u>, i.e., when  $P_1 = 0$ ,  $P_2 \neq 0$ , the substitution of Eq. (1.3.7) into Eq. (1.3.19) gives at the leading order expressions,

$$\begin{bmatrix}
-2\alpha_L \frac{\partial^2 \phi_c^{(0)}}{\partial \xi^2} + (1 + \alpha_T^2) \frac{\partial^2 \psi^{(0)}}{\partial \xi^2} \end{bmatrix} \Big|_{z=0} = 0, 
\begin{bmatrix}
-(1 + \alpha_T^2) \frac{\partial^2 \phi^{(0)}}{\partial \xi^2} - 2\alpha_T \frac{\partial^2 \psi_c^{(0)}}{\partial \xi^2} \end{bmatrix} \Big|_{z=0} = 0.$$
(1.3.28)

By taking the conjugate of Eq. (1.3.28), it becomes evident that the leading-order system possesses a non-trivial solution if and only if,

$$(1 + \alpha_T^2)^2 - 4\alpha_L \,\alpha_T = 0. \tag{1.3.29}$$

This condition is precisely the well-known Rayleigh wave secular equation, as previously encountered in Eq. (1.3.14).

Also, from Eq. (1.3.28)(a), we can write

$$\frac{\partial \psi^{(0)}}{\partial \xi} \bigg|_{z=0} = -\frac{2}{1+\alpha_T^2} \frac{\partial \phi^{(0)}}{\partial z} \quad \text{or} \quad \psi^{(0)} \bigg|_{z=0} = \frac{2\alpha_L}{1+\alpha_T^2} \phi_c^{(0)} \bigg|_{z=0}. \tag{1.3.30}$$

Either of the above equations denote the boundary conditions for the potential  $\psi^{(0)}$ .

Further, at the next-order, we have the expressions,

$$\begin{bmatrix}
2\frac{\partial^{2}\phi^{(1,0)}}{\partial\xi\partial z} + (1+\alpha_{T}^{2})\frac{\partial^{2}\psi^{(1,0)}}{\partial\xi^{2}} - 2\frac{1-\alpha_{L}^{2}}{\alpha_{L}}\frac{\partial^{2}\phi_{c}^{(0)}}{\partial\xi\partial \tau} + 2\frac{1-\alpha_{T}^{2}}{\alpha_{T}}\frac{\partial^{2}\psi_{c}^{(0)}}{\partial\xi\partial \tau}
\end{bmatrix}\Big|_{z=0} = 0, 
\begin{bmatrix}
(1+\alpha_{T}^{2})\frac{\partial^{2}\phi^{(1,0)}}{\partial\xi^{2}} - 2\frac{\partial^{2}\psi^{(1,0)}}{\partial\xi\partial z} + 2\frac{1-\alpha_{T}^{2}}{\alpha_{L}}\frac{\partial^{2}\phi_{c}^{(0)}}{\partial z\partial \tau} + 2\frac{1-\alpha_{T}^{2}}{\alpha_{T}}\frac{\partial^{2}\psi_{c}^{(0)}}{\partial z\partial \tau}
\end{bmatrix}\Big|_{z=0} = 0, 
(1.3.31)$$

Further Eq. (1.3.31)(a) can be rearranged and reduced using Eq. (1.3.30) to obtain the expression for the derivative of  $\psi^{(1,0)}$  as,

$$\frac{\partial \psi^{(1,0)}}{\partial \xi} \bigg|_{z=0} = \frac{2}{1+\alpha_T^2} \left[ \frac{1}{c_R} \left( \frac{1-\alpha_L^2}{\alpha_L} - 2\alpha_L \frac{1-\alpha_T^2}{1+\alpha_T^2} \right) \frac{\partial \phi_c^{(0)}}{\partial \tau} + \alpha_L \frac{\partial \phi_c^{(1,0)}}{\partial \xi} \right] \bigg|_{z=0}.$$
(1.3.32)

After rigorous calculation, Eq. (1.3.31)(b) can be simplified by using Eqs. (1.3.32) and (1.3.29) to obtain,

$$-\frac{4B}{c_R (1 + \alpha_T^2)} \frac{\partial^2 \phi^{(0)}}{\partial \xi \, \partial \tau} \bigg|_{z=0} = \frac{P_2}{\mu}, \tag{1.3.33}$$

where

$$B = \frac{\alpha_L}{\alpha_T} \left( 1 - \alpha_T^2 \right) + \frac{\alpha_T}{\alpha_L} \left( 1 - \alpha_L^2 \right) - 1 + \alpha_T^4.$$

On expressing the approximate solution,  $\phi = \frac{1}{\epsilon}\phi^{(0)}$ , Eq. (1.3.33) can be rewritten as,

$$\left[ \frac{2\epsilon}{c_R} \frac{\partial^2 \phi}{\partial \xi \, \partial \tau} \right] \bigg|_{z=0} = -\frac{1 + \alpha_T^2}{2\mu B} P_2. \tag{1.3.34}$$

Changing into original variables, Eq. (1.3.34) transforms into,

$$\left[\frac{\partial^2}{\partial x^2} - \frac{1}{c_R^2} \frac{\partial^2}{\partial t^2}\right] \phi(x, 0, t) = -\frac{1 + \alpha_T^2}{2\mu B} P_2. \tag{1.3.35}$$

And the relation between potentials given in Eq. (1.3.30) in terms of original variables can be written as,

$$\frac{\partial \psi}{\partial x}\Big|_{z=0} = -\frac{2}{1+\alpha_T^2} \frac{\partial \phi}{\partial z} \quad \text{or} \quad \psi\Big|_{z=0} = \frac{2\alpha_L}{1+\alpha_T^2} \phi_c\Big|_{z=0}.$$
(1.3.36)

Here  $\phi_c$  is mathematically equivalent to the Hilbert transform of  $\phi$  (cf. Kaplunov et al. [86]).

Furthermore, within the interior of the semi-infinite medium, the elliptic equations derived in Eq. (1.3.21) can be reformulated in terms of the original variables as follows,

$$\frac{\partial^2 \phi}{\partial z^2} + \alpha_L^2 \frac{\partial^2 \phi}{\partial x^2} = 0, \qquad \frac{\partial^2 \psi}{\partial z^2} + \alpha_T^2 \frac{\partial^2 \psi}{\partial x^2} = 0. \tag{1.3.37}$$

The hyperbolic equation for  $\phi$  in Eq. (1.3.35) can be transformed into an equation for the horizontal displacement  $u_1$ , which is given by

$$\left(\frac{\partial^2}{\partial x^2} - \frac{1}{c_R^2} \frac{\partial^2}{\partial t^2}\right) u_1(x, 0, t) = -\frac{1 - \alpha_T^4}{4\mu B} \frac{\partial P_2}{\partial x}.$$
 (1.3.38)

Case 2: In case of the <u>tangential load</u>, i.e., when  $P_1 \neq 0$ ,  $P_2 = 0$ , similar analysis can be carried out which eventually leads to the following hyperbolic equation at the surface,

$$\left[\frac{\partial^2}{\partial x^2} - \frac{1}{c_R^2} \frac{\partial^2}{\partial t^2}\right] \psi(x, 0, t) = \frac{1 + \alpha_T^2}{2\mu B} P_1, \tag{1.3.39}$$

with the relation between the potentials as,

$$\frac{\partial \phi}{\partial x}\Big|_{z=0} = \frac{2}{1+\alpha_T^2} \frac{\partial \psi}{\partial z} \quad \text{or} \quad \phi\Big|_{z=0} = -\frac{2\alpha_T}{1+\alpha_T^2} \psi_c\Big|_{z=0}, \tag{1.3.40}$$

where  $\psi_c$  is the Hilbert transform of the function  $\psi$ .

Moreover, the elliptic equations governing the propagation of Rayleigh wave in the interior are same as that of Eq. (1.3.37).

Analogous to Eq. (1.3.38), the hyperbolic equations presented in Eq. (1.3.39) can be reformulated in terms of the vertical displacement,  $u_3$ , as follows:

$$\left(\frac{\partial^2}{\partial x^2} - \frac{1}{c_R^2} \frac{\partial^2}{\partial t^2}\right) u_3(x, 0, t) = \frac{1 - \alpha_T^4}{4\mu B} \frac{\partial P_1}{\partial x}.$$
 (1.3.41)

Case 3: In case of non-zero stress components,  $P_1 \neq 0$ ,  $P_3 \neq 0$ , we get the hyperbolic equation at the surface as,

$$\left[ \frac{\partial^2}{\partial x^2} - \frac{1}{v^2} \frac{\partial^2}{\partial t^2} \right] \phi(x, 0, t) = \frac{1 + \beta^2}{2\mu B} \left[ P_2 + \nu^{-1} (P_1)_c \right], \tag{1.3.42}$$

where  $(P_1)_c$  is the Hilbert transform of the function  $P_1$  and  $\nu$  assuming the value,

$$\nu = \frac{2\alpha_L}{1 + \alpha_T^2}.$$

The relation between the potentials is same as that given in Eq. (1.3.36).

Thus, an explicit asymptotic hyperbolic-elliptic model is derived for the propagation of Rayleigh waves. This model demonstrates the dual nature of these waves, characterized by hyperbolic equations in Eq. (1.3.35) or (1.3.39) at the surface and elliptic equations provided in Eq. (1.3.37) within the interior of the medium.

# 1.3.2.1 Viscoelasticity

Viscoelasticity is a material property characterized by a combination of viscous and elastic behavior during deformation. In viscoelastic materials, the relationship between stress and strain is time-dependent, exhibiting three prominent characteristics:

- Stress relaxation: The gradual decay of stress over time under a constant strain.
- Creep: The gradual increase of strain over time under a constant stress.
- **Hysteresis**: A phase lag observed between stress and strain during cyclic loading.

A typical dynamic test is carried out to study the behavior of viscoelastic materials by measuring the stress resulted from the small strain. Consider a sample subjected to a complex strain,

$$\epsilon(t) = \overline{\epsilon} e^{i\omega t},$$

where  $\omega$  is the angular frequency and  $\bar{\epsilon}$  is the small amplitude.

For a **purely elastic material**, the stress is directly proportional to strain, i.e.,  $\sigma(t) = C\epsilon(t)$ . In other words, stress components are in-phase with the strain components.

For a **purely viscous material**, the stress is proportional to the strain rate, i.e.,  $\sigma(t) = \eta \frac{d\epsilon}{dt}$ . It can be deduced that the stress and strain are 90 degrees out of phase.

In a one-dimensional linear viscoelastic material, a steady state will be eventually reached in which stress behavior is similar to strain with the same angular frequency  $\omega$ , but with a phase shift of  $\theta$ . In other words,

$$\sigma(t) = \overline{\sigma} \, e^{i(\omega t + \theta)}.$$

This equation can be further re-written as,

$$\sigma(t) = G \epsilon(t),$$

where G = G' + iG'' is the complex dynamic modulus with the coefficients,

$$G' = \frac{\overline{\sigma}}{\overline{\epsilon}} \cos \theta$$
 and  $G'' = \frac{\overline{\sigma}}{\overline{\epsilon}} \sin \theta$ .

The coefficient G' is the storage modulus, representing the energy stored and recovered per cycle, and corresponds to the in-phase response. G'' is the loss modulus, characterizing energy dissipation within the material, and corresponds to the out-of-phase response.

The development of constitutive equations for linear viscoelastic materials has traditionally relied on two fundamental approaches (a) the utilization of mechanical analogs, which employ idealized mechanical elements to represent material behavior (b) the application of the Boltzmann superposition principle, which accounts for the material's response to past loading history. The more generalized approach widely used to model the linear viscoelastic materials is Boltzmann superposition model. According to this, the constitutive relation relating stress with strain is given by,

$$\sigma(t) = \int_0^t G(t - t') \frac{\mathrm{d}\epsilon}{\mathrm{d}t'} \, \mathrm{d}t',$$

where G(t) denotes the relaxation modulus function. However, choosing an appropriate relaxation function in Boltzmann model, one can easily obtain the mechanical analog models, like Maxwell model, Kelvin-Voigt model, and standard linear model. For more details on this theory of viscoelasticity, interested readers can refer [257,258]. An advance discussion on the fault propagation in such a medium can be found in [260, 261]

#### 1.3.3 Nonlocal elasticity theory

Nonlocal elasticity theory incorporates the influence of long-range interatomic forces, leading to a dependence of stress at a given point on the strain field throughout the entire body, rather than solely on the strain at that specific point. Building upon the pioneering

works of Rogula [259, 262], Kröner [145], Krumhansl [263], and Kunin [133], Eringen formulated an integral model [60] for nonlocal elasticity, demonstrating its effectiveness in solving problems such as Rayleigh wave propagation and screw dislocation.

According to this integral nonlocal model [151], the governing equations in the absence of body forces for a homogeneous elastic solid is given as,

$$\tau_{mn,m} = \rho \, u_{n,tt}, \ m, n = 1, 2, 3,$$
(1.3.43)

where  $u_n$ , n = 1, 2, 3 denotes the displacement components,  $\rho$  is the density and

$$\tau_{mn}(\mathbf{x}) = \int_{\Omega} \beta(|\mathbf{x} - \overline{\mathbf{x}}|, \zeta) \,\sigma_{mn}(\overline{\mathbf{x}}) \,d\Omega(\overline{\mathbf{x}}), \,\, \zeta = e_0 \frac{\aleph}{l}.$$
(1.3.44)

Here  $\beta$  represents a nonlocality kernel that depends on the material properties of the medium and characteristic length ratio  $\zeta$ ;  $\aleph$  denotes the internal characteristic length (eg. granular distance, lattice parameter); l denotes the external characteristic length (eg. wavelength, crack-length) and  $e_0$  is the material constant.

Further,  $\Omega$  denotes the volume of the region over which the deformation has occurred;  $\tau_{mn}$ ,  $\sigma_{mn}$  are the nonlocal and local stress tensors, respectively, at a time t and  $\mathbf{x}$  is the reference position.

The nonlocal elastic moduli  $\beta(|\mathbf{x} - \overline{\mathbf{x}}|, \zeta)$  which constitute the kernal of the integral relation in Eq. (1.3.44) contains the parameters that corresponds to nonlocal characteristics. These kernels must possess certain physically applicable properties, detailed as below [264]:

(i)  $\beta(|\mathbf{x} - \overline{\mathbf{x}}|, \zeta)$  is a delta-sequence, tending to Dirac-delta function as  $\aleph \to 0$ . In other words,

$$\lim_{\aleph \to 0} \beta(|\mathbf{x} - \overline{\mathbf{x}}|, \zeta) = \delta(|\mathbf{x} - \overline{\mathbf{x}}|), \qquad (1.3.45)$$

i.e., the nonlocal theory transforms to the local theory in this limit.

- (ii)  $\beta(|\mathbf{x} \overline{\mathbf{x}}|, \zeta)$  is a continuous and bounded function of  $|\mathbf{x} \overline{\mathbf{x}}|$ , at least for the case when  $\zeta \neq 0$ .
- (iii) In the limit of vanishing internal characteristic lengths  $\zeta \to 1$ , the nonlocal theory should approach atomic lattice dynamics.
- (iv)  $\beta(|\mathbf{x} \overline{\mathbf{x}}|, \zeta)$  attains a maximum at  $\overline{\mathbf{x}} = \mathbf{x}$  and decreases rapidly to zero as  $|\mathbf{x} \overline{\mathbf{x}}|$  increases.
- (v) The integral value  $\int_{\Omega} \beta\left(\left|\mathbf{x}-\overline{\mathbf{x}}\right|,\zeta\right) \, d\Omega(\overline{\mathbf{x}}) = 1$ .

(vi) The kernel  $\beta(|\mathbf{x} - \overline{\mathbf{x}}|, \zeta)$  is Green's function for a linear differential operator  $\mathcal{L}$ , i.e.,

$$\mathcal{L}\left[\beta\left(\left|\mathbf{x}-\overline{\mathbf{x}}\right|,\zeta\right)\right] = \delta\left(\left|\mathbf{x}-\overline{\mathbf{x}}\right|\right).$$

In case such an operator exists, then on applying  $\mathcal{L}$  to Eq. (1.3.44), we have

$$\mathcal{L}\left[\tau_{mn}\right] = \sigma_{mn}.\tag{1.3.46}$$

Below are the several kernel functions, proposed by Eringen [60] that satisfy properties (i) - (vi) and have practical physical applications:

### I. One-dimensional kernel

$$\beta(|\mathbf{x}|,\zeta) = \begin{cases} \frac{1}{\zeta l} \left(1 - \frac{|x|}{\zeta l}\right), & \text{if } |x| \le \zeta l \\ 0, & \text{otherwise} \end{cases}$$
 (1.3.47)

$$\beta(|\mathbf{x}|,\zeta) = \frac{1}{l\sqrt{\pi\zeta}} \exp\left(-\frac{x^2}{\zeta l^2}\right)$$
 (1.3.48)

$$\beta(|\mathbf{x}|,\zeta) = \frac{1}{2\zeta l} \exp\left(-\frac{|x|}{\zeta l}\right) \tag{1.3.49}$$

#### II. Two-dimensional kernel

$$\beta(|\mathbf{x}|,\zeta) = \frac{1}{\pi\zeta l^2} \exp\left(-\frac{\mathbf{x}\cdot\mathbf{x}}{\zeta l^2}\right)$$
 (1.3.50)

$$\beta(|\mathbf{x}|,\zeta) = \frac{1}{2\pi\zeta^2 l^2} K_0\left(\frac{\sqrt{\mathbf{x}\cdot\mathbf{x}}}{\zeta l}\right)$$
 (1.3.51)

where  $K_0(\cdot)$  is the modified Bessel function of zero order.

### III. Three-dimensional kernel

$$\beta(|\mathbf{x}|,\zeta) = \frac{1}{4\pi\zeta^2 l^2 \sqrt{\mathbf{x} \cdot \mathbf{x}}} \exp\left(\frac{\sqrt{\mathbf{x} \cdot \mathbf{x}}}{\zeta l}\right)$$
(1.3.52)

$$\beta(|\mathbf{x}|,\zeta) = \frac{1}{(\pi\zeta l^2)^{\frac{3}{2}}} \exp\left(-\frac{\mathbf{x}\cdot\mathbf{x}}{\zeta l^2}\right)$$
 (1.3.53)

In his works [60, 151], Eringen demonstrated that by employing a two-dimensional kernel of the form given in Eq. (1.3.51), the integral operator  $\mathcal{L}$ , can be approximated as

$$\mathcal{L} = \left(1 - \zeta^2 l^2 \,\nabla^2\right),\tag{1.3.54}$$

where  $\nabla^2$  is the two-dimensional Laplacian operator.

#### 1.3.3.1 Eringen's theory for nonlocal surface Rayleigh waves

Consider Rayleigh wave propagation in a homogeneous, isotropic, nonlocal elastic semi-infinite medium with displacement vector  $\mathbf{u} = (u_1, 0, u_3)$ . Employing a two-dimensional Bessel function kernel as defined in Eq. (1.3.52) within the integral formulation (1.3.44), and applying the operator  $\mathcal{L}$  to the governing equations in Eq. (1.3.4) (with  $F_n = 0$ ) under plane strain conditions, while utilizing the relationships in Eqs. (1.3.2), (1.3.3), and (1.3.46), yields,

$$\mu u_{mm} + (\Lambda + \mu) u_{m,mn} - \rho \left( 1 - \aleph^2 \nabla^2 \right) u_{n,tt} = 0, \ m, n = 1, 3.$$
 (1.3.55)

As discussed in previous sections, for plain strain.

$$u_1 = \frac{\partial \phi}{\partial x} - \frac{\partial \psi}{\partial z}, \qquad u_3 = \frac{\partial u_3}{\partial z} + \frac{\partial \psi}{\partial x},$$
 (1.3.56)

decouples the equations of motion into,

$$c_L^2 \nabla^2 \phi = (1 - \aleph^2 \nabla^2) \phi_{,tt}, \qquad c_T^2 \nabla^2 \psi = (1 - \aleph^2 \nabla^2) \psi_{,tt}, \qquad (1.3.57)$$

with the body wave velocities  $c_L = \sqrt{\frac{\Lambda + 2\mu}{\rho}}$  and  $c_T = \sqrt{\frac{\mu}{\rho}}$ .

We seek the solutions of Eq. (1.3.57) to be in the form of surface waves given by,

$$\phi = P e^{-m_1 z} e^{i(kx - \omega t)}, \qquad \psi = Q e^{-m_2 z} e^{i(kx - \omega t)}.$$
 (1.3.58)

The above equations satisfies Eq. (1.3.57) only when  $m_1, m_2$  takes the values,

$$m_1 = \sqrt{1 - \frac{c^2}{c_L^2 - \aleph^2 \omega^2}}, \qquad m_2 = \sqrt{1 - \frac{c^2}{c_T^2 - \aleph^2 \omega^2}}.$$
 (1.3.59)

By substituting Eq. (1.3.58) into Eq. (1.3.56), we arrive at the expressions for the displacement field. Subsequently, we can obtain at the corresponding stress field as,

$$\tau_{11} = \left[\frac{c_L^2}{c_T^2} \left(m_1^2 - 1\right) - 2m_1^2\right] I_1 P - 2i \, m_2 I_2 Q, 
\tau_{31} = -2i \, m_1 I_1 P + \left(1 + m_2^2\right) I_2 Q, 
\tau_{33} = \left[2 + \frac{c_L^2}{c_T^2} \left(m_1^2 - 1\right)\right] I_1 P + 2i \, m_2 I_2 Q,$$
(1.3.60)

where

$$I_{j} = \int_{0}^{\infty} \int_{-\infty}^{\infty} K_{0} \left[ \frac{\sqrt{(x - \overline{x})^{2} + \overline{z}^{2}}}{\aleph} \right] e^{-km_{j}\overline{z}} \exp\left[i(k\overline{x} - \omega t)\right] d\overline{x} d\overline{z}, \ j = 1, 2 \quad (1.3.61)$$

The nonlocal stress-free boundary conditions at z=0 suggests  $\tau_{31}=\tau_{33}=0$ . Since  $I_1,I_2\neq 0$ , a non-trivial solution exists if

$$[2 + \Gamma^{-2}(m_1^2 - 1)] (1 + m_2^2) - 4m_1 m_2 = 0, \qquad (1.3.62)$$

where  $\Gamma = \frac{c_T}{c_L}$ . The Eq. (1.3.62) is referred as the Rayleigh wave dispersion relation in a nonlocal elastic semi-infinite medium (as per Eringen's theory [60]). On rearranging the terms of Eq. (1.3.62) while using Eq. (1.3.59) simplifies the dispersion relation as,

$$\Theta\left(\alpha_1\Theta^3 + \alpha_2\Theta^2 + \alpha_3\Theta + \alpha_4\right) = 0, (1.3.63)$$

in which

$$\alpha_1 = \frac{1}{16} + \epsilon^2 \left( \frac{1+\beta}{4} \right) + \epsilon^4 \left( \frac{1+4\beta - 3\beta^2}{4} \right) + \epsilon^6 \beta \left( 1 - \beta \right),$$

$$\alpha_2 = -\frac{1}{2} + \epsilon^2 \left( \frac{2\beta^2 - \beta - 3}{2} \right) - \epsilon^4 \left( 1 + \beta - 2\beta^2 \right),$$

$$\alpha_3 = \frac{3}{2} - \beta + \epsilon^2 \left( 2 - \beta - \beta^2 \right),$$

$$\alpha_4 = 1 - \beta,$$

$$\Theta = \frac{c^2}{c_T^2}, \ \epsilon = \aleph k, \ \beta = \frac{1-p}{2\left( 1 - p \right)},$$

where p is the Poisson's ratio.

By simplifying Eq. (1.3.62) and performing a Taylor series expansion about  $\epsilon = 0$ , we can also arrive at a corrected dispersion relation characterized by an expansion that includes only even powers of the nonlocal parameter  $\epsilon$ .

$$\left[ \left( 2 - \Theta^2 \right)^2 - 4\sqrt{1 - \Theta^2} \sqrt{1 - \frac{\Theta^2}{\gamma}} \right]$$

$$+ \epsilon^2 \left[ \frac{2\Theta^4 \left( -\gamma^2 + \gamma\Theta^2 + \Theta^2 - 1 \right) \sqrt{1 - \frac{\Theta^2}{\gamma}}}{\gamma \sqrt{1 - \Theta^2} \left( \Theta^2 - \gamma \right)} + \frac{\gamma\Theta^6 - 2\gamma\Theta^4 + \Theta^6 - 2\Theta^4}{\gamma} \right] + O\left( \epsilon^4 \right).$$

$$(1.3.64)$$

Further we note that, the leading order term in the dispersion relation given in Eq. (1.3.64) coincides with the well known secular equation of Rayleigh waves derived in Eq. (1.3.14). However, the absence of first-order correction terms in this expansion may limit the accuracy of the corrected dispersion relation.

As pointed out by Eringen [151], the nonlocal moduli,  $\beta(|\mathbf{x} - \overline{\mathbf{x}}|, \zeta)$  are strictly applicable

to homogeneous and isotropic solids. Near the surface, material inhomogeneities emerge within a boundary layer of a few atomic distances. This necessitates the development of refined theory that accounts for boundary layer effects within the framework of nonlocal elasticity to address this limitation and thereby improve upon Eringen's original theory.

#### 1.3.3.2 Refined theory for nonlocal surface Rayleigh waves

The use of differential operator  $\mathcal{L}$  often neglects the boundary layer near the surface, leading to discrepancies between solutions obtained from integral and differential formulations. This section briefly demonstrates that the solution of the conventional differential model presented in [60] fails to satisfy the equation of motion for nonlocal stresses derived from the integral theory, necessitating the derivation of refined boundary conditions. The readers are advised to refer Kaplunov et al. [204] for detailed calculations.

Now, define the dimensionless quantities

$$\xi = \frac{x}{\lambda}, \ \eta = \frac{z}{\lambda}, \ \epsilon = \frac{\aleph}{\lambda}.$$

where  $\lambda$  is the wavelength of the propagating wave. Assuming slow variations of local stresses  $\sigma_{mn}$  along x-direction, a two-term Taylor series expansion of  $\sigma_{mn}$  in terms of  $\xi$  about the point  $\overline{\xi} = \xi$  can be constructed, resulting in,

$$\tau_{mn}(\xi,\eta) = \frac{1}{2\pi\epsilon^2} \int_0^{\infty} \int_{-\infty}^{\infty} K_0 \left[ \frac{\sqrt{(\xi - \overline{\xi})^2 + \overline{\eta}^2}}{\aleph} \right] \left[ 1 + \frac{(\overline{\xi} - \xi)^2}{2} \frac{\partial^2}{\partial \xi^2} + \cdots \right] \sigma_{mn}(\xi,\overline{\eta}) d\overline{\xi} d\overline{\eta}.$$
(1.3.65)

Utilizing the integral identity, see Gradshteyn and Ryzhik [265],

$$\int_0^\infty z^{2m} K_0 \left( a\sqrt{x^2 + z^2} \right) dz = \frac{\pi}{2a^{2m+1}} \left( 1 + amx \right) \exp\left( -ax \right), \text{ for } m = 1, 2, (1.3.66)$$

Eq. (1.3.65) can be reduced and further by neglecting higher-order terms  $O(\epsilon^4)$ , we get

$$\tau_{mn}\left(\xi,\eta\right) = \frac{1}{2\epsilon} \int_{0}^{\infty} \left[ 1 + \frac{\epsilon^{2}}{2} \left( 1 + \frac{|\overline{\eta} - \eta|}{\epsilon} \right) \frac{\partial^{2}}{\partial \xi^{2}} + \cdots \right] \sigma_{mn}\left(\xi,\overline{\eta}\right) \exp\left( -\frac{|\overline{\eta} - \eta|}{\epsilon} \right) d\overline{\eta}.$$

$$(1.3.67)$$

As a result, the double integral  $I_j$ , j = 1, 2 defined in Eq. (1.3.61) can be approximated using Eq. (1.3.67). This gives,

$$I_{j} = e^{i(kx - \omega t)} \left\{ \left[ 1 - \epsilon^{2} \left( 1 - m_{j0}^{2} \right) \right] \exp\left( -km_{j}z \right) - \frac{1}{2} \left[ 1 + \epsilon m_{j0} - \epsilon^{2} \left( 1 - m_{k0}^{2} + \frac{z}{2\aleph} \right) \right] \exp\left( -\frac{z}{\aleph} \right) \right\}.$$

$$(1.3.68)$$

Here  $m_{j0}$  are the leading order terms in the expansion of  $m_j$  in Eq. (1.3.59), i.e.,

$$m_1 = \sqrt{1 - \frac{c^2}{c_L^2}}, \qquad m_2 = \sqrt{1 - \frac{c^2}{c_T^2}}.$$
 (1.3.69)

The coefficients of  $\exp\left(-\frac{z}{\aleph}\right)$  in Eq. (1.3.68) are associated with the nonlocal boundary layer.

Applying the stress-free boundary condition  $\tau_{31} = 0$ , yields a relationship between the constants P and Q. Substituting this relation into the expressions for nonlocal stresses and considering the leading-order terms, we obtain

$$Q\left(1 - 2m_{20}^2 + m_{20}^4\right) \left(1 + m_{20}^2\right) \exp\left(-\frac{z}{\epsilon}\right) \neq 0. \tag{1.3.70}$$

Thus, we can conclude that the solutions obtained in Eq. (1.3.58) for Eringen's theory do not satisfy the equations of motion in Eq. (1.3.55), indicating an inconsistency within the integral model.

In order to have an equivalence between the differential and the integral formulations of nonlocal elasticity, substitute the differential formulation,

$$\widetilde{\sigma}_{mn} = \left(1 - \epsilon^2 \nabla^2\right) \widetilde{\tau}_{mn},$$

in the integral formulation given in Eq. (1.3.67).

This will yield on rigorous calculations, the additional conditions for which the equivalence holds good. These are given by,

$$\left[1 - \aleph \frac{\partial}{\partial z} - \frac{\aleph^3}{2} \frac{\partial^3}{\partial x^2 \partial z}\right] \tau_{mn} \bigg|_{z=0} = 0, \ m, n = 1, 3.$$
 (1.3.71)

Due to pre-imposed restrictions on  $\tau_{31}$  and  $\tau_{33}$  in case of a stress-free surface (i.e.,  $\tau_{31} = \tau_{33} = 0$ ), it may not be possible to satisfy all conditions simultaneously. This could potentially lead to an ill-posed problem. As a result, the additional condition is applied only to the specific stress component,  $\tau_{11}$ . This implies that

$$\left[1 - \aleph \frac{\partial}{\partial z} - \frac{\aleph^3}{2} \frac{\partial^3}{\partial x^2 \partial z}\right] \tau_{11} \bigg|_{z=0} = 0. \tag{1.3.72}$$

Asymptotic analysis is then carried out to capture the effects of the boundary layer arising from the application of nonlocal elasticity.

Boundary layer theory and asymptotic analysis [269] are considered the most valuable tools in geomechanics for investigating the impact of boundary layers on the overall complex non-local behavior of geological materials.

To elucidate the behavior along the z-coordinate within the semi-infinite medium and in the vicinity of the boundary layer, respectively, we define fast  $(\eta_f)$  and slow  $(\eta_s)$  variables,

$$\eta_f = \frac{z}{\aleph}, \qquad \eta_s = \frac{z}{\lambda}.$$

The following dimensionless quantities are adopted through out this section,

$$\begin{split} \xi &= \frac{x}{\lambda}, \quad \epsilon &= \frac{\aleph}{\lambda}, \quad \widetilde{t} = \frac{c_T}{\lambda} \, t, \\ \widetilde{u}_j &= \frac{u_j}{\lambda}, \quad \widetilde{\sigma}_{mn} = \frac{\sigma_{mn}}{\mu}, \quad \widetilde{\tau}_{mn} = \frac{\tau_{mn}}{\mu}. \end{split}$$

The nonlocal stresses are decomposed into fast components,  $q_{mn}$  and slow components  $p_{mn}$  as,

$$\widetilde{\tau}_{11} = p_{11} + q_{11}, 
\widetilde{\tau}_{31} = p_{31} + \epsilon q_{31}, 
\widetilde{\tau}_{33} = p_{33} + \epsilon^2 q_{33}.$$
(1.3.73)

As a result, the governing equations are reformulated into equations involving the slow-varying and fast-varying components. This gives,

$$\frac{\partial p_{1n}}{\partial \xi} + \frac{\partial p_{3n}}{\partial \eta_s} = \frac{\partial^2 \widetilde{u}_n}{\partial \widetilde{t}^2}, \qquad \frac{\partial q_{1m}}{\partial \xi} + \frac{\partial q_{3m}}{\partial \eta_f} = 0, \qquad (1.3.74)$$
and
$$\epsilon^2 \left( \frac{\partial p_{mn}}{\partial \xi^2} + \frac{\partial^2 p_{mn}}{\partial \eta_s^2} \right) - p_{mn} = -\widetilde{\sigma}_{mn}, \qquad \epsilon^2 \frac{\partial^2 q_{mn}}{\partial \xi^2} + \frac{\partial^2 q_{mn}}{\partial \eta_f^2} - q_{mn} = 0, \quad (1.3.75)$$

with

$$\widetilde{\sigma}_{11} = \Gamma^{-2} \frac{\partial \widetilde{u}_{1}}{\partial \xi} + (\Gamma^{-2} - 2) \frac{\partial \widetilde{u}_{3}}{\partial \eta_{s}}, 
\widetilde{\sigma}_{31} = \frac{\partial \widetilde{u}_{1}}{\partial \eta_{s}} + \frac{\partial \widetilde{u}_{3}}{\partial \xi}, 
\widetilde{\sigma}_{33} = \Gamma^{-2} \frac{\partial \widetilde{u}_{3}}{\partial \eta_{s}} + (\Gamma^{-2} - 2) \frac{\partial \widetilde{u}_{1}}{\partial \xi},$$
(1.3.76)

where  $\Gamma = \sqrt{\frac{\mu}{\Lambda + 2\mu}}$  and subjected to the boundary conditions,

$$p_{31}\Big|_{\eta_{s}=0} + \epsilon \, q_{31}\Big|_{\eta_{f}=0} = 0,$$

$$p_{33}\Big|_{\eta_{s}=0} + \epsilon^{2} \, q_{33}\Big|_{\eta_{f}=0} = 0,$$

$$r_{32}\Big|_{\eta_{s}=0} + \epsilon \, s_{32}\Big|_{\eta_{f}=0} = 0,$$

$$p_{11}\Big|_{\eta_{s}=0} + q_{11}\Big|_{\eta_{f}=0} - \epsilon \, \frac{\partial p_{11}}{\partial \eta_{s}}\Big|_{\eta_{s}=0} - \frac{\partial q_{11}}{\partial \eta_{f}}\Big|_{\eta_{f}=0} - \frac{\epsilon^{2}}{2} \, \frac{\partial^{3} q_{11}}{\partial \xi^{2} \, \partial \eta_{f}}\Big|_{\eta_{f}=0} = 0.$$

$$(1.3.77)$$

Also, on expanding certain quantities in asymptotic series as

$$\mathfrak{F}_{mn} = \mathfrak{F}_{mn}^{(0)} + \epsilon \,\mathfrak{F}_{mn}^{(1)} + \epsilon^2 \mathfrak{F}_{mn}^{(2)} + \cdots \tag{1.3.78}$$

where  $\mathfrak{F}_{mn} = \{u_n, \sigma_{mn}, p_{mn}, q_{mn}\}.$ 

As a result, we can rewrite the Eqs. (1.3.74)-(1.3.77) for various asymptotic orders  $i = 0, 1, 2, \dots$  as,

$$\frac{\partial p_{1n}^{(i)}}{\partial \xi} + \frac{\partial p_{3n}^{(i)}}{\partial \eta_s} = \frac{\partial^2 \widetilde{u}_n^{(i)}}{\partial \widetilde{t}^2}, \qquad \frac{\partial q_{1m}^{(i)}}{\partial \xi} + \frac{\partial q_{3m}^{(i)}}{\partial \eta_f} = 0, \tag{1.3.79}$$

and

$$\frac{\partial^2 p_{mn}^{(i-2)}}{\partial \xi^2} + \frac{\partial^2 p_{mn}^{(i-2)}}{\partial \eta_s^2} - p_{mn}^{(i)} = -\widetilde{\sigma}_{mn}^{(i)}, \qquad \frac{\partial^2 q_{mn}^{(i-2)}}{\partial \xi^2} + \frac{\partial^2 q_{mn}^{(i)}}{\partial \eta_f^2} - q_{mn}^{(i)} = 0, \qquad (1.3.80)$$

with

$$\widetilde{\sigma}_{11}^{(i)} = \Gamma^{-2} \frac{\partial \widetilde{u}_{1}^{(i)}}{\partial \xi} + (\Gamma^{-2} - 2) \frac{\partial \widetilde{u}_{3}^{(i)}}{\partial \eta_{s}}, 
\widetilde{\sigma}_{31}^{(i)} = \frac{\partial \widetilde{u}_{1}^{(i)}}{\partial \eta_{s}} + \frac{\partial \widetilde{u}_{3}^{(i)}}{\partial \xi}, 
\widetilde{\sigma}_{33}^{(i)} = \Gamma^{-2} \frac{\partial \widetilde{u}_{3}^{(i)}}{\partial \eta_{s}} + (\Gamma^{-2} - 2) \frac{\partial \widetilde{u}_{1}^{(i)}}{\partial \xi},$$

$$(1.3.81)$$

and the boundary conditions at the surface  $\eta_s = \eta_f = 0$  as,

$$p_{31}^{(i)}\Big|_{\eta_{s}=0} + q_{31}^{(i-1)}\Big|_{\eta_{f}=0} = 0,$$

$$p_{33}^{(i)}\Big|_{\eta_{s}=0} + q_{33}^{(i-2)}\Big|_{\eta_{f}=0} = 0,$$

$$p_{11}^{(i)}\Big|_{\eta_{s}=0} + q_{11}^{(i)}\Big|_{\eta_{f}=0} - \frac{\partial p_{11}^{(i-1)}}{\partial \eta_{s}}\Big|_{\eta_{s}=0} - \frac{\partial q_{11}^{(i)}}{\partial \eta_{f}}\Big|_{\eta_{f}=0} - \frac{1}{2} \frac{\partial^{3} q_{11}^{(i-2)}}{\partial \xi^{2} \partial \eta_{f}}\Big|_{\eta_{f}=0} = 0.$$

$$(1.3.82)$$

By comparing the leading-order terms in Eqs. (1.3.80), we obtain the differential equation for the zeroth order. Solving this equation yields a decaying solution of the form,

$$q_{mn}^{(0)} = Q_{mn}^{(0)}(\xi, \tilde{t}) e^{-\eta_f}. \tag{1.3.83}$$

The values for the coefficients  $Q_{mn}^{(0)}$  can be easily obtained using Eqs. (1.3.77)(iv) and (1.3.79) as,

$$Q_{11}^{(0)} = -\frac{1}{2} \widetilde{\sigma}_{11}^{(0)} \Big|_{\eta_s = 0}, \qquad Q_{31}^{(0)} = -\frac{1}{2} \frac{\partial \widetilde{\sigma}_{11}^{(0)}}{\partial \xi} \Big|_{\eta_s = 0}, \qquad Q_{33}^{(0)} = -\frac{1}{2} \frac{\partial^2 \widetilde{\sigma}_{11}^{(0)}}{\partial \xi^2} \Big|_{\eta_s = 0}$$
(1.3.84)

As a result, the boundary conditions at the leading order becomes,

$$\tilde{\sigma}_{31}^{(0)} = 0, \qquad \tilde{\sigma}_{33}^{(0)} = 0, \tag{1.3.85}$$

which coincides the traditional boundary conditions in a local elastic semi-infinite medium. At the first order, the solution to the differential equation in  $q_{mn}^{(1)}$  takes the form,

$$q_{mn}^{(1)} = Q_{mn}^{(1)} \left(\xi, \tilde{t}\right) e^{-\eta_f}, \tag{1.3.86}$$

where

$$Q_{11}^{(1)} = -\frac{1}{2} \left( \widetilde{\sigma}_{11}^{(1)} \Big|_{\eta_{s}=0} - \frac{\partial \widetilde{\sigma}_{11}^{(0)}}{\partial \eta_{s}} \Big|_{\eta_{s}=0} \right),$$

$$Q_{31}^{(1)} = -\frac{1}{2} \left( \frac{\partial \widetilde{\sigma}_{11}^{(1)}}{\partial \xi} \Big|_{\eta_{s}=0} - \frac{\partial^{2} \widetilde{\sigma}_{11}^{(0)}}{\partial \eta_{s} \partial \xi} \Big|_{\eta_{s}=0} \right),$$

$$Q_{33}^{(1)} = -\frac{1}{2} \left( \frac{\partial^{2} \widetilde{\sigma}_{11}^{(1)}}{\partial \xi^{2}} \Big|_{\eta_{s}=0} - \frac{\partial^{3} \widetilde{\sigma}_{11}^{(0)}}{\partial \eta_{s} \partial \xi^{2}} \Big|_{\eta_{s}=0} \right).$$

$$(1.3.87)$$

Subsequently, the boundary conditions at the first order results in,

$$\widetilde{\sigma}_{31}^{(1)} - \frac{1}{2} \frac{\partial \widetilde{\sigma}_{11}^{(0)}}{\partial \xi} = 0, \qquad \widetilde{\sigma}_{33}^{(1)} = 0.$$
(1.3.88)

Notably, the first-order boundary conditions for a nonlocal semi-infinite medium include an additional term that depends on  $\tilde{\sigma}_{11}$ .

Subsequently, at second order, the equation of motion presented in Eq. (1.3.79) can be rewritten as,

$$\frac{\partial \widetilde{\sigma}_{1n}^{(2)}}{\partial \xi} + \frac{\partial \widetilde{\sigma}_{3n}^{(2)}}{\partial \eta_s} = \frac{\partial^2 \widetilde{u}_n^{(2)}}{\partial \widetilde{t}^2} - \frac{\partial^2}{\partial \widetilde{t}^2} \left( \frac{\partial^2 \widetilde{u}_n^{(0)}}{\partial \xi^2} + \frac{\partial^2 \widetilde{u}_n^{(0)}}{\partial \eta_s^2} \right). \tag{1.3.89}$$

As a result, the boundary conditions at the second order becomes,

$$\widetilde{\sigma}_{31}^{(2)} + \frac{\partial^{2} \widetilde{\sigma}_{31}^{(0)}}{\partial \xi^{2}} + \frac{\partial^{2} \widetilde{\sigma}_{31}^{(0)}}{\partial \eta_{s}^{2}} - \frac{1}{2} \left( \frac{\partial \widetilde{\sigma}_{11}^{(1)}}{\partial \xi} - \frac{\partial^{2} \widetilde{\sigma}_{11}^{(0)}}{\partial \eta_{s} \partial \xi} \right) = 0, 
\widetilde{\sigma}_{33}^{(2)} + \frac{\partial^{2} \widetilde{\sigma}_{33}^{(0)}}{\partial \xi^{2}} + \frac{\partial^{2} \widetilde{\sigma}_{33}^{(0)}}{\partial \eta_{s}^{2}} - \frac{1}{2} \frac{\partial^{2} \widetilde{\sigma}_{11}^{(0)}}{\partial \xi^{2}} = 0.$$
(1.3.90)

Using the fact that,  $\widetilde{\sigma}_{mn}^{(1)} \approx \frac{1}{\epsilon} \widetilde{\sigma}_{mn}$ ,  $\widetilde{\sigma}_{mn}^{(2)} \approx \frac{1}{\epsilon^2} \widetilde{\sigma}_{mn}$ , the boundary value problem can now be given as,

$$\frac{\partial \widetilde{\sigma}_{1n}}{\partial \xi} + \frac{\partial \widetilde{\sigma}_{3n}}{\partial \eta_s} = \frac{\partial^2 \widetilde{u}_n}{\partial \widetilde{t}^2} - \epsilon^2 \frac{\partial^2}{\partial \widetilde{t}^2} \left( \frac{\partial^2 \widetilde{u}_n}{\partial \xi^2} + \frac{\partial^2 \widetilde{u}_n}{\partial \eta_s^2} \right), \tag{1.3.91}$$

subjected to,

$$\widetilde{\sigma}_{31} - \frac{\epsilon}{2} \frac{\partial \widetilde{\sigma}_{11}}{\partial \xi} + \epsilon^2 \left( \frac{\partial^2 \widetilde{\sigma}_{31}}{\partial \xi^2} + \frac{\partial^2 \widetilde{\sigma}_{31}}{\partial \eta_s^2} + \frac{1}{2} \frac{\partial^2 \widetilde{\sigma}_{11}}{\partial \eta_s \partial \xi} \right) = 0, 
\widetilde{\sigma}_{33} + \epsilon^2 \left( \frac{\partial^2 \widetilde{\sigma}_{33}}{\partial \xi^2} + \frac{\partial^2 \widetilde{\sigma}_{33}}{\partial \eta_s^2} - \frac{1}{2} \frac{\partial^2 \widetilde{\sigma}_{11}}{\partial \xi^2} \right) = 0.$$
(1.3.92)

Upon recasting the refined boundary conditions in terms of the original variables employed in the analysis, the governing equations that describe the propagation of Rayleigh waves on the surface of a nonlocal elastic semi-infinite medium can be expressed as

$$\frac{\partial \sigma_{11}}{\partial x} + \frac{\partial \sigma_{31}}{\partial z} = \rho \left( 1 - \aleph^2 \nabla^2 \right) \frac{\partial^2 u_1}{\partial t^2}, 
\frac{\partial \sigma_{13}}{\partial x} + \frac{\partial \sigma_{33}}{\partial z} = \rho \left( 1 - \aleph^2 \nabla^2 \right) \frac{\partial^2 u_3}{\partial t^2},$$
(1.3.93)

with the refined boundary conditions prescribed at the surface z=0 as,

$$\sigma_{31} - \frac{\aleph}{2} \frac{\partial \sigma_{11}}{\partial x} + \aleph^2 \left( \frac{\partial^2 \sigma_{31}}{\partial x^2} + \frac{\partial^2 \sigma_{31}}{\partial z^2} + \frac{1}{2} \frac{\partial^2 \sigma_{11}}{\partial x \partial z} \right) = 0,$$

$$\sigma_{33} + \aleph^2 \left( \frac{\partial^2 \sigma_{33}}{\partial x^2} + \frac{\partial^2 \sigma_{33}}{\partial z^2} - \frac{1}{2} \frac{\partial^2 \sigma_{11}}{\partial x^2} \right) = 0.$$

$$(1.3.94)$$

Employing these boundary conditions, the dispersion relation can be derived within an error of  $O(\epsilon^2)$  for Rayleigh waves propagating in a nonlocal elastic semi-infinite medium as,

$$(1 + m_{20}^2)^2 - 4m_{10} m_{20} - 2\epsilon m_{20} (1 - \Gamma^{-2}) (1 - m_{10}^2) = 0.$$
 (1.3.95)

The leading-order analysis recovers the classical dispersion relation. This analysis gives a first-order corrected dispersion relation, offering a more refined correction to the effects of nonlocality compared to the correction established by Eringen's theory [60].

### 1.3.4 Micropolar elasticity theory

Classical elasticity theory faces limitations in accurately modeling materials with complex microstructures or scenarios involving significant stress gradients. For instance, it struggles to predict the behavior of materials like composites, polymers, soil, and bone, where internal structures play a crucial role [266]. Additionally, it cannot adequately address situations where the stress-strain relationship is asymmetric, such as those encountered in an elastic continuum subjected to a volume moment distribution. To overcome these limitations, Eringen [51] followed by Nowacki [52] extended the theory by incorporating body microinertia effects, leading to the development of micropolar elasticity theory. In essence, micropolar elasticity models a material as a continuum embedded with uniformly distributed rigid particles of infinitesimal size, allowing for a more intricate description of material behavior.

In this section, we will present the fundamental relations, including the constitutive stressstrain relations and governing equations, within the context of a general linear micropolar elasticity theory for a homogeneous, isotropic solid.

In a linear micropolar elastic solid, the displacement field vector  $\mathbf{u}$  is complemented by a microrotation field vector  $\Phi$ , which is independent of the displacement field. A micropolar deformation is fully characterized by the asymmetric strain tensor  $\varepsilon_{ij}$  and the curvature tensor  $\Gamma_{ij}$ , defined as,

$$\begin{cases}
\varepsilon_{mn} = u_{n,m} - \epsilon_{mnp} \Phi_p, \\
\Gamma_{mn} = \Phi_{m,n},
\end{cases}$$

$$mn = 1, 2, 3. \tag{1.3.96}$$

where  $\epsilon_{mnp}$  stands for the permutation symbol.

Using these definitions in Eq. (1.3.96), the relation for the microrotation vector can be given as,

$$\Phi_m = \frac{1}{2} \epsilon_{mnp} (u_{p,n} - \varepsilon_{np}), \ m, n, p = 1, 2, 3.$$

The strain tensor written in Eq. (1.3.96) is clearly an asymmetric vector, as a result it can be decomposed into symmetric  $\varepsilon_{mn}^{\dagger}$  and asymmetric components  $\varepsilon_{mn}^{\ddagger}$  as,

$$\varepsilon_{mn} = \varepsilon_{mn}^{\dagger} + \varepsilon_{mn}^{\ddagger}.$$

where

$$\varepsilon_{mn}^{\dagger} = \frac{1}{2} \left( u_{n,m} + u_{m,n} \right), \qquad \varepsilon_{mn}^{\ddagger} = \frac{1}{2} \left( u_{n,m} - u_{m,n} \right) - \epsilon_{mnp} \Phi_p.$$

Now, for a linear isotropic micropolar medium, the theory proposes two sets of constitutive relations as,

$$\sigma_{mn} = \Lambda \,\varepsilon_{pp} \,\delta_{mn} + (\mu + \kappa) \,\varepsilon_{mn} + \mu \,\varepsilon_{nm}, 
\Pi_{mn} = \alpha \,\Gamma_{pp} \,\delta_{mn} + \beta \,\Gamma_{mn} + \gamma \,\Gamma_{nm},$$

$$mathred{m, n = 1, 2, 3.}$$
(1.3.97)

where  $\Lambda$  and  $\mu$  are the well-know Lamé's constants;  $\kappa$ ,  $\alpha$ ,  $\beta$ ,  $\gamma$  are the micropolar constants;  $\delta_{mn}$  denotes the Kronecker's delta tensor.

In a micropolar continuum subjected to a body force,  $F_n$ , and a body moment,  $M_n$ , the internal loads between adjacent elements are characterized by a classical force stress tensor,  $\sigma_{mn}$ , and a micropolar couple stress tensor,  $\Pi_{mn}$ . These stress tensors must satisfy the balance of linear and angular momenta, resulting in governing equations expressed as,

$$\sigma_{mn,m} + \rho F_n = \rho u_{n,tt},$$

$$\Pi_{mn,m} + \epsilon_{nmp} \sigma_{mp} + \rho M_n = j \rho \Phi_{n,tt},$$
(1.3.98)

in which  $\rho$  is the material mass density and j is the microinertia.

Substituting the constitutive relations in Eq. (1.3.97) into the governing equation in Eq. (1.3.98), we can obtain the system of governing equations for a micropolar elastic solids as,

$$(\Lambda + 2\mu) u_{m,mn} + (\mu + \kappa) u_{n,mm} + \kappa \epsilon_{npm} \Phi_{m,p} + \rho F_n = \rho u_{n,tt},$$

$$(\alpha + \beta) \Phi_{m,mn} + \gamma u_{n,mm} - 2\kappa \Phi_n + \rho M_n = j \rho \Phi_{n,tt}.$$

$$(1.3.99)$$

The strain energy density  $\mathcal{E}$  for a linear isotropic micropolar continuum is given as [52],

$$\mathcal{E} = \frac{1}{2} \left( \sigma_{mn} \varepsilon_{mn} + \Pi_{mn} \Gamma_{mn} \right).$$

A positive definite quadratic form for the strain energy density  $\mathcal{E}$  imposes the following restrictions on the material constants,

$$\mu > 0, \quad \kappa > 0, \quad 3\Lambda + 2\mu + \kappa > 0,$$
  
 $\gamma > 0, \quad \beta > 0, \quad 3\alpha + \beta + \gamma > 0.$ 

#### 1.3.5 Nonlocal micropolar elasticity theory

Classical continuum mechanics treats material as a collection of point particles, each capable of only translational motion and interacting solely with its immediate neighbors. This limits its applicability, failing to capture the discrete nature of materials and microscopic phenomena such as micro-deformations and micro-dislocations. Recognizing this limitation, a more generalized perspective emerged, acknowledging the material particle as a finite volume element capable of both deformation and rotation. Furthermore, the behavior of any given particle cannot be fully understood in isolation, as it is influenced by interactions with other particles throughout the material. These considerations have led to the development of nonlocal microcontinuum theories, which provide a more comprehensive framework for understanding material behavior beyond the limitations of classical continuum mechanics.

Here, we will write the constitutive stress-strain relations and equations of motion in a non-local micropolar elastic medium.

A nonlocal micropolar elastic solid exhibits both translational and rotational motions, which give rise to nonlocal force stresses and nonlocal couple stresses within the medium. The integral formulation that relates nonlocal force and couple stresses with local force and couple stresses, respectively are given similar to Eq. (1.3.44) as,

$$\tau_{mn}(\mathbf{x}) = \int_{\Omega} \beta(|\mathbf{x} - \overline{\mathbf{x}}|, \aleph) \, \sigma_{mn}(\overline{\mathbf{x}}) \, d\Omega(\overline{\mathbf{x}})$$

$$\pi_{mn}(\mathbf{x}) = \int_{\Omega} \beta(|\mathbf{x} - \overline{\mathbf{x}}|, \aleph) \, \Pi_{mn}(\overline{\mathbf{x}}) \, d\Omega(\overline{\mathbf{x}}),$$

$$mn(\mathbf{x}) = \int_{\Omega} \beta(|\mathbf{x} - \overline{\mathbf{x}}|, \aleph) \, \Pi_{mn}(\overline{\mathbf{x}}) \, d\Omega(\overline{\mathbf{x}}),$$

$$(1.3.100)$$

where  $\beta(|\mathbf{x} - \overline{\mathbf{x}}|)$  represents the nonlocal kernel, which can assume any of the forms defined in Eqs. (1.3.47) - (1.3.53).

The constitutive relations that relate these local stresses with the strain tensor  $(\epsilon)$  and

curvature tensor  $(\Gamma)$  are given as [61],

$$\sigma_{mn} = \Lambda \,\varepsilon_{pp} \,\delta_{mn} + (\mu + \kappa) \,\varepsilon_{mn} + \mu \,\varepsilon_{nm}, 
\Pi_{mn} = \alpha \,\Gamma_{pp} \,\delta_{mn} + \beta \,\Gamma_{mn} + \gamma \,\Gamma_{nm},$$

$$mathred{mn} m = 1, 2, 3.$$
(1.3.101)

Here  $\kappa$ ,  $\alpha$ ,  $\beta$  and  $\gamma$  are the micropolar constants;  $\Lambda$ ,  $\mu$  are the elastic constants;  $\delta_{mn}$  denotes the well-known Kronecker delta symbol. Moreover, the relation between the curvature tensor and strain tensor with the displacement components and rotational components are given as,

$$\begin{cases}
\varepsilon_{mn} = u_{n,m} - \epsilon_{mnp} \Phi_p, \\
\Gamma_{mn} = \Phi_{m,n},
\end{cases}$$

$$mn = 1, 2, 3, \qquad (1.3.102)$$

where  $u_n$  and  $\Phi_n$  are the displacement components and microrotation vector components of the surface wave, respectively.

Further, the governing equations in a non-local micropolar elastic solid (without any body forces or moments) are given by,

$$\tau_{mn,m} - \rho u_{n,tt} = 0,$$

$$\pi_{12,x} + \pi_{32,z} + \epsilon_{nmp} \sigma_{mp} - \rho j \Phi_{2,tt} = 0,$$

$$m, n = 1, 3.$$
(1.3.103)

Having established these fundamental concepts and mathematical tools in this section, we now proceed to delve into the core research problems addressed in this thesis.

# CHAPTER 2

Rayleigh Wave Propagation in Nonlocal Micropolar Semi-infinite Medium

This chapter investigates wave propagation in a semi-infinite medium characterized by nonlocal and micropolar elastic properties. We begin the study by considering the constitutive equations and governing equation of motion under nonlocal micropolar elasticity, as outlined in Eqs. (1.3.100)-(1.3.103). Utilizing asymptotic analysis, we derive refined boundary conditions for the propagation of Rayleigh waves. As a practical application, we then examine and analyze the boundary value problem of the propagation of Rayleigh waves within a viscoelastic semi-infinite medium.

# 2.1 Derivation of refined boundary conditions on the surface of a nonlocal micropolar semi-infinite medium\*

#### 2.1.1 Mathematical formulation

Consider the two-dimensional singular non-local kernel as provided in Eringen's theory [60],

$$\beta(|\mathbf{x}' - \mathbf{x}|, \aleph) = \frac{1}{2\pi\aleph^2} K_0 \left( \frac{\sqrt{(\mathbf{x}' - \mathbf{x}) \cdot (\mathbf{x}' - \mathbf{x})}}{\aleph} \right)$$
(2.1.1)

where  $\aleph$  is the non-locality parameter associated with the micropolar medium.

Consequently, the relationship between conventional local stresses and non-local stresses can be established through the integral formulation (1.3.100) as follows:

$$\tau_{mn} = \frac{1}{2\pi\aleph^{2}} \int_{0}^{\infty} \int_{-\infty}^{\infty} K_{0} \left( \frac{\sqrt{(x-x')^{2} + (z-z')^{2}}}{\aleph} \right) \sigma_{mn} (x', z') dx' dz' 
\pi_{mn} = \frac{1}{2\pi\aleph^{2}} \int_{0}^{\infty} \int_{-\infty}^{\infty} K_{0} \left( \frac{\sqrt{(x-x')^{2} + (z-z')^{2}}}{\aleph} \right) \Pi_{mn} (x', z') dx' dz' \right)$$
(2.1.2)

Additionally, utilizing the same two-dimensional kernel as specified in Eq. (2.1.1), the differential model proposed by Eringen [60] relates the local and non-local stresses as,

$$\begin{aligned}
(1 - \aleph^2 \nabla^2) \, \tau_{mn} &= \sigma_{mn} \\
(1 - \aleph^2 \nabla^2) \, \pi_{mn} &= \Pi_{mn}
\end{aligned}$$
(2.1.3)

Introduce the dimensionless variables,

$$\chi = \frac{x}{\lambda}, \ \eta = \frac{z}{\lambda}, \ \text{and} \ \epsilon = \frac{\aleph}{\lambda} << 1$$

<sup>\*</sup> Published in **Zeitschrift für angewandte Mathematik und Physik** (Springer), (2024), DOI: 10.1007/s00033-024-02407-4

is the small dimensionless parameter associated with non-locality in the micropolar medium. Utilizing the approximation provided in Eqs. (1.3.67), that takes into account the assumption of slow variation of local stresses  $\sigma_{mn}$  along x-direction, we approximate Eqs. (2.1.2) as,

$$\tau_{mn} \approx \frac{1}{2\epsilon} \int_0^\infty \left[ 1 + \frac{\epsilon^2}{2} \left( 1 + \frac{|\eta' - \eta|}{\epsilon} \right) \frac{\partial^2}{\partial \chi^2} \right] \sigma_{mn}(\chi, \eta') \exp\left( -\frac{|\eta' - \eta|}{\epsilon} \right) d\eta' \qquad (2.1.4)$$

$$\pi_{mn} \approx \frac{1}{2\epsilon} \int_0^\infty \left[ 1 + \frac{\epsilon^2}{2} \left( 1 + \frac{|\eta' - \eta|}{\epsilon} \right) \frac{\partial^2}{\partial \chi^2} \right] \Pi_{mn}(\chi, \eta') \exp\left( -\frac{|\eta' - \eta|}{\epsilon} \right) d\eta' \qquad (2.1.5)$$

Using the differential formulation of non-local stresses as in Eq. (2.1.3), the equation of motion for the propagation of Rayleigh waves with the displacement components in the form of local stresses can be written with the help of Eq. (1.3.103) as,

$$\left. \begin{array}{l}
\sigma_{1n,x} + \sigma_{3n,z} - \rho \left( 1 - \aleph^2 \nabla^2 \right) u_{n,tt} = 0, \\
\Pi_{12,x} + \Pi_{32,z} + \sigma_{31} - \sigma_{13} - \rho j \left( 1 - \aleph^2 \nabla^2 \right) \Phi_{2,tt} = 0
\end{array} \right\} n = 1, 3$$
(2.1.6)

To decouple the system in Eq. (2.1.6), we shall apply the method of potentials in which the displacement components are decomposed into the sum of a scalar function  $\phi$  and a vector potential  $\Psi = (\psi_1, \psi, \psi_3)$  as,

$$u_1(x, z, t) = \phi_{,x} - \psi_{,z}, \ u_3(x, z, t) = \phi_{,z} + \psi_{,x}$$
 (2.1.7)

This reduces the governing coupled equations of motion given in Eq. (2.1.6) as,

$$(\Lambda + 2\mu + \kappa) \nabla^2 \phi - \rho (1 - \aleph^2 \nabla^2) \phi_{,tt} = 0,$$

$$(\mu + \kappa) \nabla^2 \psi + \kappa \Phi_2 - \rho (1 - \aleph^2 \nabla^2) \psi_{,tt} = 0,$$

$$\gamma \nabla^2 \Phi_2 - \kappa \nabla^2 \psi - 2 \kappa \Phi_2 - \rho j (1 - \aleph^2 \nabla^2) \Phi_{2,tt} = 0.$$

$$(2.1.8)$$

Let us define certain velocity parameters for the micropolar elastic media as

$$c_1 = \sqrt{\frac{\Lambda + 2\mu + \kappa}{\rho}}, \ c_2 = \sqrt{\frac{\mu + \kappa}{\rho}}, \ c_3 = \sqrt{\frac{\kappa}{\rho}}, \ c_4 = \sqrt{\frac{\gamma}{\rho j}}.$$

and assume that the solutions to the system of equations to be propagating in a timeharmonic form as,

$$\{\phi, \psi, \Phi_2\} = \{P, Y, Z\} e^{-krz} e^{i(kx - \omega t)},$$
 (2.1.9)

Substituting Eq. (2.1.9) in decoupled system of equations of Eq. (2.1.8), we get,

$$\phi(x, z, t) = P e^{-kr_1 z} e^{i(kx - \omega t)}, 
\psi(x, z, t) = \left[ Q e^{-kr_2 z} + R e^{-kr_3 z} \right] e^{i(kx - \omega t)}, 
\Phi_2(x, z, t) = s k^2 R e^{-kr_3 z} e^{i(kx - \omega t)},$$
(2.1.10)

where

$$\begin{split} r_1^2 &= 1 - \frac{v^2}{c_1^2 - \epsilon^2 v^2}, \ r_2^2 = 1 - \frac{v^2}{c_2^2 - \epsilon^2 v^2}, \\ r_3^2 &= 1 - \frac{v^2}{c_4^2 - \epsilon^2 v^2} \left( 1 - \frac{2c_3^2}{j\omega^2} \right), \ s = \frac{v^2}{c_3^2} \left[ 1 - \frac{c_2^2 - \epsilon^2 v^2}{c_4^2 - \epsilon^2 v^2} \left( 1 - \frac{2c_3^2}{j\omega^2} \right) \right], \end{split}$$

are such that  $Re(r_i) > 0$  for i = 1, 2, 3 to ensure the exponential decay of the waves from the surface.

The traction-free boundary conditions at the surface z=0 indicate the vanishing of force-stresses and couple-stresses at the surface, i.e., at z=0,

$$\tau_{31} = 0, \ \tau_{33} = 0, \ \pi_{32} = 0.$$
(2.1.11)

## 2.1.2 Failure of equivalence

This section aims to verify the equivalence between the integral and differential formulations of Eringen's non-local elasticity theory. We will utilize the differential form of the non-local model in the equation of motion, while employing the integral formulation for the boundary conditions, and subsequently assess their equivalence. For our convenience, we will omit the time-harmonic terms for further studies.

Now, the non-local stresses can be explicitly written from Eqs. (2.1.4) and (2.1.5) using Eq. (1.3.97) as,

$$\begin{split} \tau_{11} &= k^2 \left[ -\left(\Lambda + 2\mu + \kappa - \Lambda \, r_1^2\right) \, P \, I_1 + i \, r_2 \, (2\mu + \kappa) \, Q \, I_2 + i \, r_3 \, (2\mu + \kappa) \, R \, I_3 \right] \\ \tau_{13} &= k^2 \, \left[ -i \, r_1 \, (2\mu + \kappa) \, P \, I_1 - \left(\mu + \kappa + \mu \, r_2^2\right) \, Q \, I_2 + \left(s \, \kappa - (\mu + \kappa) - \mu \, r_3^2\right) \, R \, I_3 \right] \\ \tau_{31} &= k^2 \, \left[ -i \, r_1 \, (2\mu + \kappa) \, P \, I_1 - \left(\mu + (\mu + \kappa) \, r_2^2\right) \, Q \, I_2 - \left(s \, \kappa + \mu + (\mu + \kappa) \, r_3^2\right) \, R \, I_3 \right] \\ \tau_{33} &= k^2 \, \left[ \left( (\Lambda + 2\mu + \kappa) \, r_1^2 - \Lambda \right) \, P \, I_1 - i \, r_2 \, (2\mu + \kappa) \, Q \, I_2 - i \, r_3 \, (2\mu + \kappa) \, R \, I_3 \right] \\ \tau_{12} &= i \, s \, k^3 \, \gamma \, R \, I_3 \\ \tau_{32} &= -s \, k^3 \, \gamma \, r_3 \, R \, I_3 \end{split}$$

where

$$I_{i} = \frac{1}{2\aleph} \int_{0}^{\infty} \left[ 1 + \frac{\aleph^{2}}{2} \left( 1 + \frac{|x' - x|}{\aleph} \right) \frac{\partial^{2}}{\partial x^{2}} \right] \exp\left(ikx - kr_{i}z\right) \exp\left(-\frac{|z' - z|}{\aleph}\right) dz', \quad i = 1, 2, 3$$
 (2.1.12)

On splitting  $I_i$  in Eq. (2.1.12) over the interval from 0 to z and from z to z' following the approach of Kaplunov et al. [204], and subsequently simplifying, we obtain,

$$I_{i} = \left[1 + \epsilon^{2} \left(r_{i0}^{2} - 1\right)\right] \exp\left(-kr_{i}z\right) - \frac{1}{2} \left[1 + \epsilon r_{i0} + \epsilon^{2} \left(r_{i0}^{2} - 1 - \frac{kz}{2\epsilon}\right)\right] \exp\left(-\frac{kz}{\epsilon}\right)$$
(2.1.13)

The coefficients of  $\exp\left(\frac{-kz}{\epsilon}\right)$  in Eq. (2.1.13) are linked with the boundary layer formed as a result of the non-local elasticity effects in the medium.

Substituting in Eq. (2.1.11), a system of equations in P, Q, R is obtained. This system is then solved for the non-trivial solution to obtain the dispersion relations for Rayleigh waves within an error of  $O(\epsilon^2)$  as,

$$(1+d)^2 r_{10} r_{20} - (r_{20}^2 + d)^2 = 0 (2.1.14)$$

$$r_{30} = 0 (2.1.15)$$

with  $d = \frac{\mu}{\mu + \kappa}$ . Also,  $r_{10}$ ,  $r_{20}$  and  $r_{30}$  are the leading order Taylor series approximations of  $r_1$ ,  $r_2$  and  $r_3$ , respectively within an error of  $O(\epsilon^2)$  and are given by,

$$r_{10}^2 = 1 - \frac{v^2}{c_1^2}, \ r_{20}^2 = 1 - \frac{v^2}{c_2^2}, \ r_{30}^2 = 1 - \frac{v^2}{c_4^2} \left( 1 - \frac{2c_3^2}{j\omega^2} \right)$$

Eqs. (2.1.14) and (2.1.15) represent the dispersion relations consisting of two modes of Rayleigh waves, one of which is entirely due to the micropolarity in the medium. Also, these two modes do not coexist at the same period. In other words, the relations in Eqs. (2.1.14) and (2.1.15) cannot be zero simultaneously.

For the mode corresponding to Eq. (2.1.14) and from the boundary conditions at z = 0, the arbitrary constants P, Q and R are related by,

$$P = \frac{i \left(r_{20}^2 + d\right) \left(1 + \left(r_{10} - r_{20}\right) \left(\epsilon - \epsilon^2 r_{20}\right)\right)}{\left(1 + d\right) r_{10}} Q, \ R = 0$$

Substituting these values of P, Q, R into the equation of motion given in Eq. (2.1.6) for n = 1 and analyzing the leading order term that is associated with the boundary layer near the vicinity of the surface, we observe that,

$$\frac{k^3}{2(1+d)^2 r_{10}} \left[ (1+d)^2 r_{10}^2 - 2 r_{20}^2 \left( d + r_{20}^2 - 1 \right) - (1+d^2) \right] \exp\left( -\frac{kz}{\epsilon} \right) \neq 0 \quad (2.1.16)$$

Similarly, for the micropolar mode corresponding to Eq. (2.1.15), the relation between the arbitrary constants is given as,

$$P = \frac{i(1+d)r_{20}}{r_{20}^2 + d} \left[ 1 + (r_{10} - r_{20}) \left( \epsilon - \epsilon^2 r_{20} \right) \right] Q$$

$$R = \frac{(r_{20}^2 + d)^2 - (1+d)^2 r_{10} r_{20}}{r_{20}^2 + d} \left[ 1 + (r_{30} - r_{20}) \left( \epsilon - \epsilon^2 r_{20} \right) \right] Q,$$

Substituting the same into the equation of motion in Eq. (2.1.6) at n = 1, we have at the leading order,

$$\frac{k^3}{r_{20}^2 + d} \left[ (1+d)^2 r_{10} r_{20} - \left(r_{20}^2 + d\right)^2 \right] \exp\left(\frac{-kz}{\epsilon}\right) \neq 0$$
 (2.1.17)

which is true as this mode does not coexist with the mode corresponding to Eq. (2.1.14). Eqs. (2.1.16) and (2.1.17) indicate that the solution for the Rayleigh wave obtained from a differential non-local model does not comply with the original governing equations derived under the framework of the integral non-local elastic model. This suggests the failure of the equivalence between the differential and integral formulations of the non-local model in case of a non-local micropolar semi-infinite medium.

## 2.1.3 Equivalence conditions

Upon substituting the differential form of the local stresses provided in Eq. (2.1.2) into Eqs. (2.1.3) and (2.1.4), which represents the integral formulation of the non-local stresses at the boundary, we get,

$$\tau_{mn}\Big|_{\eta=0} = \frac{1}{2\epsilon} \int_0^\infty \left[ 1 + \frac{\epsilon^2}{2} \left( 1 + \frac{\eta'}{\epsilon} \right) \frac{\partial^2}{\partial \chi^2} \right] \left[ 1 - \epsilon^2 \left( \frac{\partial^2}{\partial \chi^2} + \frac{\partial^2}{\partial \eta'^2} \right) \right] \tau_{mn} \left( \chi, \eta' \right) e^{-\frac{\eta'}{\epsilon}} d\eta' \quad (2.1.18)$$

$$\pi_{mn}\Big|_{\eta=0} = \frac{1}{2\epsilon} \int_0^\infty \left[ 1 + \frac{\epsilon^2}{2} \left( 1 + \frac{\eta'}{\epsilon} \right) \frac{\partial^2}{\partial \chi^2} \right] \left[ 1 - \epsilon^2 \left( \frac{\partial^2}{\partial \chi^2} + \frac{\partial^2}{\partial \eta'^2} \right) \right] \pi_{mn} \left( \chi, \eta' \right) e^{-\frac{\eta'}{\epsilon}} d\eta' \quad (2.1.19)$$

This is further simplified by ignoring the higher order terms of  $O(\epsilon^4)$  to get,

$$\tau_{mn}\Big|_{\eta=0} = \frac{1}{2} \left[ \tau_{mn}\Big|_{\eta=0} + \epsilon \frac{\partial \tau_{mn}}{\partial \eta} \Big|_{\eta=0} + \frac{\epsilon^3}{2} \frac{\partial^3 \tau_{mn}}{\partial \chi^2 \partial \eta} \Big|_{\eta=0} \right]$$
(2.1.20)

$$\left. \pi_{mn} \right|_{\eta=0} = \frac{1}{2} \left[ \pi_{mn} \right|_{\eta=0} + \epsilon \left. \frac{\partial \pi_{mn}}{\partial \eta} \right|_{\eta=0} + \frac{\epsilon^3}{2} \left. \frac{\partial^3 \pi_{mn}}{\partial \chi^2 \partial \eta} \right|_{\eta=0} \right]$$
(2.1.21)

Further rearrangement gives a set of conditions,

$$\left[1 - \epsilon \frac{\partial}{\partial \eta} - \frac{\epsilon^3}{2} \frac{\partial^3}{\partial \chi^2 \partial \eta}\right] \tau_{mn} \bigg|_{n=0} = 0$$
 (2.1.22)

$$\left[1 - \epsilon \frac{\partial}{\partial \eta} - \frac{\epsilon^3}{2} \frac{\partial^3}{\partial \chi^2 \partial \eta}\right] \pi_{mn} \bigg|_{\eta=0} = 0$$
 (2.1.23)

for which the equivalence between the differential and integral non-local model is possible. However, for the equations of motion described in Eq. (2.1.5), the boundary conditions derived from Eqs. (2.1.22) and (2.1.23), along with the already prescribed boundary conditions in Eq. (2.1.11), result in an ill-posed problem. Thus, we conclude that not all the conditions in Eqs. (2.1.22) and (2.1.23) can be satisfied at the boundary.

# 2.1.4 Singularly perturbed differential model

Here, we redefine the proposed problem by considering the singularly perturbed differential equations as

$$\tau_{1n,x} + \tau_{3n,z} - \rho u_{n,tt} = 0, \quad n = 1, 3 
\pi_{12,x} + \pi_{32,z} + \tau_{31} - \tau_{13} - \rho j \Phi_{2,tt} = 0$$
(2.1.24)

and 
$$\begin{cases} \aleph^{2} \left( \tau_{mn,xx} + \tau_{mn,zz} \right) - \tau_{mn} = -\sigma_{mn}, \\ \aleph^{2} \left( \pi_{m2,xx} + \pi_{m2,zz} \right) - \pi_{m2} = -\Pi_{m2}, \end{cases}$$
  $m = 1, 3$  (2.1.25)

with the boundary conditions prescribed on the surface z = 0 as,

$$\tau_{31}\big|_{z=0} = 0, \ \tau_{33}\big|_{z=0} = 0, \ \pi_{32}\big|_{z=0} = 0$$
 (2.1.26)

$$\left[1 - \aleph \frac{\partial}{\partial z} - \frac{\aleph^3}{2} \frac{\partial^3}{\partial x^2 \partial z}\right] \tau_{11} \bigg|_{z=0} = 0, \quad \left[1 - \aleph \frac{\partial}{\partial z} - \frac{\aleph^3}{2} \frac{\partial^3}{\partial x^2 \partial z}\right] \pi_{12} \bigg|_{z=0} = 0 \quad (2.1.27)$$

This suggests that by employing the singularly perturbed differential model as defined above, an equivalence between the differential and integral formulation can be obtained for the non-local force stress  $\tau_{11}$  and couple stress  $\pi_{12}$ .

# Asymptotic analysis

We shall employ asymptotic analysis to study the behavior of the solutions of the singularly perturbed differential problem presented in Eqs. (2.1.24)-(2.1.27).

To do this, we shall introduce the dimensionless parameter,

$$\epsilon = \frac{\aleph}{\lambda},$$

The presence of this small parameter  $\epsilon$  leads to two distinct scales of behavior in the differential equation. To interprete this behavior, we introduce the following slow and fast dimensionless variables along the length scale as,

$$u_s = \frac{z}{\lambda}, \ \varkappa_f = \frac{z}{\aleph}.$$

Here,  $\varkappa_s$  represents the slow behavior of the system, governed by simpler dynamics, while  $\varkappa_f$  captures the rapid changes occurring in the boundary layer of the system due to the presence of  $\epsilon$ .

Further, define the following dimensionless parameters,

$$\chi = \frac{x}{\lambda}, \ \widetilde{t} = \frac{c_2}{\lambda} t,$$

$$\widetilde{\tau}_{mn} = \frac{\tau_{mn}}{\mu + \kappa}, \ \widetilde{\sigma}_{mn} = \frac{\sigma_{mn}}{\mu + \kappa}, \ \widetilde{\pi}_{mn} = \frac{\pi_{mn}}{(\mu + \kappa) \lambda}, \ \widetilde{\Pi}_{mn} = \frac{\Pi_{mn}}{(\mu + \kappa) \lambda}$$

$$J = \frac{j}{\lambda^2}, \ \widetilde{\Phi}_2 = \Phi_2, \ \widetilde{u}_m = \frac{u_m}{\lambda}, \ m, n = 1, 2, 3$$

Following the approach of Chebakov et al. [203] and Kaplunov et al. [204], we decompose the non-local force stresses, and couple stresses into slow and fast components as,

$$\widetilde{\tau}_{11} = p_{11} + q_{11} 
\widetilde{\tau}_{31} = p_{31} + \epsilon q_{31} 
\widetilde{\tau}_{13} = p_{13} + \epsilon q_{31} 
\widetilde{\tau}_{13} = p_{13} + \epsilon q_{31} 
\widetilde{\tau}_{33} = p_{33} + \epsilon^2 q_{33}$$
(2.1.28)

for non-local couple stresses: 
$$\widetilde{\pi}_{12} = r_{12} + s_{12}$$

$$\widetilde{\pi}_{32} = r_{32} + \epsilon s_{32}$$

$$(2.1.29)$$

where  $p_{mn}, r_{mn}$  for m, n = 1, 2, 3 represents the slow-varying components of the force stresses and couple stresses, respectively, while  $q_{mn}, s_{mn}$  for m, n = 1, 2, 3 represents the fast-varying components of force stresses and couple stresses, respectively. In the context of a micropolar solid, it is significant to acknowledge that the force stresses lose their symmetry. Specifically, for slow-varying quantities, we assume that the quantitites  $p_{mn} \neq p_{nm}$ . However, in contrast, the fast-varying stress components within the boundary layer retain symmetry, i.e  $q_{mn} = q_{nm}$ . This symmetry vanishes as we move away from the boundary layer.

As a result, the governing equations are reformulated into slow and fast-varying components, yielding the following expressions,

$$\frac{\partial p_{1n}}{\partial \chi} + \frac{\partial p_{3n}}{\partial \varkappa_s} = \frac{\partial^2 \widetilde{u}_n}{\partial \widetilde{t}^2}, \quad \frac{\partial q_{1m}}{\partial \chi} + \frac{\partial q_{3m}}{\partial \varkappa_f} = 0$$

$$\frac{\partial r_{12}}{\partial \chi} + \frac{\partial r_{32}}{\partial \varkappa_s} + p_{31} - p_{13} = J \frac{\partial^2 \widetilde{\Phi}_2}{\partial \widetilde{t}^2}, \quad \frac{\partial s_{12}}{\partial \chi} + \frac{\partial s_{32}}{\partial \varkappa_f} = 0$$
and
$$\epsilon^2 \left( \frac{\partial p_{mn}}{\partial \chi^2} + \frac{\partial^2 p_{mn}}{\partial \varkappa_s^2} \right) - p_{mn} = -\widetilde{\sigma}_{mn}, \quad \epsilon^2 \frac{\partial^2 q_{mn}}{\partial \chi^2} + \frac{\partial^2 q_{mn}}{\partial \varkappa_f^2} - q_{mn} = 0$$

$$\epsilon^2 \left( \frac{\partial r_{m2}}{\partial \chi^2} + \frac{\partial^2 r_{mn}}{\partial \varkappa_s^2} \right) - r_{mn} = -\widetilde{\Pi}_{mn}, \quad \epsilon^2 \frac{\partial^2 s_{mn}}{\partial \chi^2} + \frac{\partial^2 s_{mn}}{\partial \varkappa_f^2} - s_{mn} = 0 \right\} (2.1.31)$$

$$\widetilde{\sigma}_{11} = \alpha_1^2 \frac{\partial \widetilde{u}_1}{\partial \chi} + (\alpha_1^2 - 2 + \alpha_2^2) \frac{\partial \widetilde{u}_3}{\partial \varkappa_s}$$

$$\widetilde{\sigma}_{13} = \frac{\partial \widetilde{u}_3}{\partial \chi} + (1 - \alpha_2^2) \frac{\partial \widetilde{u}_1}{\partial \varkappa_s} + \alpha_2^2 \widetilde{\Phi}_2$$
with
$$\widetilde{\sigma}_{31} = \frac{\partial \widetilde{u}_1}{\partial \varkappa_s} + (\alpha_1^2 - 2 + \alpha_2^2) \frac{\partial \widetilde{u}_1}{\partial \chi}$$

$$\widetilde{\sigma}_{33} = \alpha_1^2 \frac{\partial \widetilde{u}_3}{\partial \varkappa_s} + (\alpha_1^2 - 2 + \alpha_2^2) \frac{\partial \widetilde{u}_1}{\partial \chi}$$

$$\widetilde{\Pi}_{12} = \alpha_3^2 J \frac{\partial \widetilde{\Phi}_2}{\partial \chi}$$

$$\widetilde{\Pi}_{32} = \alpha_3^2 J \frac{\partial \widetilde{\Phi}_2}{\partial \chi}$$

subjected to the boundary conditions,

$$p_{31}\Big|_{\varkappa_{s}=0} + \epsilon q_{31}\Big|_{\varkappa_{f}=0} = 0,$$

$$p_{33}\Big|_{\varkappa_{s}=0} + \epsilon^{2} q_{33}\Big|_{\varkappa_{f}=0} = 0,$$

$$r_{32}\Big|_{\varkappa_{s}=0} + \epsilon s_{32}\Big|_{\varkappa_{f}=0} = 0$$

$$p_{11}\Big|_{\varkappa_{s}=0} + q_{11}\Big|_{\varkappa_{f}=0} - \epsilon \frac{\partial p_{11}}{\partial \varkappa_{s}}\Big|_{\varkappa_{s}=0} - \frac{\partial q_{11}}{\partial \varkappa_{f}}\Big|_{\varkappa_{f}=0} - \frac{\epsilon^{2}}{2} \frac{\partial^{3} q_{11}}{\partial \chi^{2} \partial \varkappa_{f}}\Big|_{\varkappa_{f}=0} = 0$$

$$r_{12}\Big|_{\varkappa_{s}=0} + s_{12}\Big|_{\varkappa_{f}=0} - \epsilon \frac{\partial r_{12}}{\partial \varkappa_{s}}\Big|_{\varkappa_{s}=0} - \frac{\partial s_{12}}{\partial \varkappa_{f}}\Big|_{\varkappa_{f}=0} - \frac{\epsilon^{2}}{2} \frac{\partial^{3} s_{12}}{\partial \chi^{2} \partial \varkappa_{f}}\Big|_{\varkappa_{f}=0} = 0$$

where  $\alpha_1 = \frac{c_1}{c_2}$ ,  $\alpha_2 = \frac{c_3}{c_2}$ ,  $\alpha_3 = \frac{c_4}{c_2}$  are the dimensionless quantities.

The quantities  $p_{mn}, q_{mn}, \widetilde{\sigma}_{mn}, r_{mn}, s_{mn}, \widetilde{\Pi}_{mn}, \widetilde{u}_n, \widetilde{\Phi}_2$  are now expanded in an asymptotic series of the form,

$$g = g^{(0)} + \epsilon g^{(1)} + \epsilon^2 g^{(2)} + \dots$$
 (2.1.34)

where  $g \in \{p_{mn}, q_{mn}, \widetilde{\sigma}_{mn}, r_{mn}, s_{mn}, \widetilde{\Pi}_{mn}, \widetilde{u}_n, \widetilde{\Phi}_2\}.$ 

As a result of the asymptotic expansion sought in Eq. (2.1.34), we can rewrite the Eqs. (2.1.30)-(2.1.33) for different asymptotic orders i = 0, 1, 2, ..., as,

$$\frac{\partial p_{1n}^{(i)}}{\partial \chi} + \frac{\partial p_{3n}^{(i)}}{\partial \varkappa} = \frac{\partial^2 \tilde{u}_n^{(i)}}{\partial t^2}, \quad \frac{\partial q_{1m}^{(i)}}{\partial \chi} + \frac{\partial q_{3m}^{(i)}}{\partial \varkappa} = 0$$

$$\frac{\partial r_{12}^{(i)}}{\partial \chi} + \frac{\partial r_{32}^{(i)}}{\partial \varkappa} + p_{31}^{(i)} - p_{13}^{(i)} = J \frac{\partial^2 \tilde{\Phi}_2^{(i)}}{\partial t^2}, \quad \frac{\partial s_{12}^{(i)}}{\partial \chi} + \frac{\partial s_{32}^{(i)}}{\partial \varkappa} = 0$$
and
$$\frac{\partial^2 p_{mn}^{(i)-2}}{\partial \chi^2} + \frac{\partial^2 p_{mn}^{(i)-2}}{\partial \varkappa^2} - p_{mn}^{(i)} = -\tilde{\sigma}_{mn}^{(i)}, \quad \frac{\partial^2 q_{mn}^{(i)-2}}{\partial \chi^2} + \frac{\partial^2 q_{mn}^{(i)}}{\partial \varkappa^2} - q_{mn}^{(i)} = 0$$

$$\frac{\partial^2 r_{m2}^{(i)-2}}{\partial \chi^2} + \frac{\partial^2 r_{mn}^{(i)-2}}{\partial \varkappa^2} - r_{mn}^{(i)} = -\tilde{\Pi}_{mn}^{(i)}, \quad \frac{\partial^2 s_{mn}^{(i)-2}}{\partial \chi^2} + \frac{\partial^2 s_{mn}^{(i)}}{\partial \varkappa^2} - s_{mn}^{(i)} = 0$$

$$\tilde{\sigma}_{11}^{(i)} = \alpha_1^2 \frac{\partial \tilde{u}_1^{(i)}}{\partial \chi} + (\alpha_1^2 - 2 + \alpha_2^2) \frac{\partial \tilde{u}_3^{(i)}}{\partial \varkappa}$$

$$\tilde{\sigma}_{13}^{(i)} = \frac{\partial \tilde{u}_3^{(i)}}{\partial \chi} + (1 - \alpha_2^2) \frac{\partial \tilde{u}_3^{(i)}}{\partial \varkappa} + \alpha_2^2 \tilde{\Phi}_2^{(i)}$$
with
$$\tilde{\sigma}_{33}^{(i)} = \frac{\partial \tilde{u}_1^{(i)}}{\partial \varkappa} + (\alpha_1^2 - 2 + \alpha_2^2) \frac{\partial \tilde{u}_1^{(i)}}{\partial \chi}$$

$$\tilde{\Pi}_{12}^{(i)} = \alpha_3^2 J \frac{\partial \tilde{\Phi}_2^{(i)}}{\partial \chi}$$

$$\tilde{\Pi}_{32}^{(i)} = \alpha_3^2 J \frac{\partial \tilde{\Phi}_2^{(i)}}{\partial \chi}$$

$$\tilde{\Pi}_{32}^{(i)} = \alpha_3^2 J \frac{\partial \tilde{\Phi}_2^{(i)}}{\partial \chi}$$

and the boundary conditions at the surface  $\varkappa_s = \varkappa_f = 0$  as,

$$\begin{aligned} p_{31}^{(i)}\Big|_{\varkappa_{s}=0} + q_{31}^{(i-1)}\Big|_{\varkappa_{f}=0} &= 0, \\ p_{33}^{(i)}\Big|_{\varkappa_{s}=0} + q_{33}^{(i-2)}\Big|_{\varkappa_{f}=0} &= 0, \\ r_{32}^{(i)}\Big|_{\varkappa_{s}=0} + s_{32}^{(i-1)}\Big|_{\varkappa_{f}=0} &= 0 \\ p_{11}^{(i)}\Big|_{\varkappa_{s}=0} + q_{11}^{(i)}\Big|_{\varkappa_{f}=0} - \frac{\partial p_{11}^{(i-1)}}{\partial \varkappa_{s}}\Big|_{\varkappa_{s}=0} - \frac{\partial q_{11}^{(i)}}{\partial \varkappa_{f}}\Big|_{\varkappa_{f}=0} - \frac{1}{2} \frac{\partial^{3} q_{11}^{(i-2)}}{\partial \chi^{2} \partial \varkappa_{f}}\Big|_{\varkappa_{f}=0} &= 0 \\ r_{12}^{(i)}\Big|_{\varkappa_{s}=0} + s_{12}^{(i)}\Big|_{\varkappa_{f}=0} - \frac{\partial r_{12}^{(i-1)}}{\partial \varkappa_{s}}\Big|_{\varkappa_{s}=0} - \frac{\partial s_{12}^{(i)}}{\partial \varkappa_{f}}\Big|_{\varkappa_{f}=0} - \frac{1}{2} \frac{\partial^{3} s_{12}^{(i-2)}}{\partial \chi^{2} \partial \varkappa_{f}}\Big|_{\varkappa_{f}=0} &= 0 \end{aligned}$$

Comparing the leading order terms in Eqs. (2.1.36), we have

$$p_{mn}^{(0)} = \widetilde{\sigma}_{mn}^{(0)}, \ r_{mn}^{(0)} = \widetilde{\Pi}_{mn}^{(0)}$$
 (2.1.39)

$$\frac{\partial^2 q_{mn}^{(0)}}{\partial \varkappa_f^2} - q_{mn}^{(0)} = 0, \quad \frac{\partial^2 s_{mn}^{(0)}}{\partial \varkappa_f^2} - s_{mn}^{(0)} = 0$$
 (2.1.40)

The differential equations in Eqs. (2.1.40) are solved for the decaying solution to obtain,

$$q_{mn}^{(0)} = Q_{mn}^{(0)} \left(\chi, \tilde{t}\right) e^{-\varkappa_f}, \ s_{mn}^{(0)} = S_{mn}^{(0)} \left(\chi, \tilde{t}\right) e^{-\varkappa_f}$$
(2.1.41)

where the values for some of the coefficients  $Q_{mn}^{(0)}$  can be easily obtained using Eqs. (2.1.38)(iv) and (2.1.35) as,

$$Q_{11}^{(0)} = -\frac{1}{2} \widetilde{\sigma}_{11}^{(0)} \Big|_{\varkappa_s = 0}, \ Q_{31}^{(0)} = -\frac{1}{2} \frac{\partial \widetilde{\sigma}_{11}^{(0)}}{\partial \chi} \Big|_{\varkappa_s = 0}, \ Q_{33}^{(0)} = -\frac{1}{2} \frac{\partial^2 \widetilde{\sigma}_{11}^{(0)}}{\partial \chi^2} \Big|_{\varkappa_s = 0}$$
(2.1.42)

The values of  $S_{mn}^{(0)}$  evaluated from the leading order term analysis are,

$$S_{12}^{(0)} = -\frac{1}{2} \left. \widetilde{\Pi}_{12}^{(0)} \right|_{\varkappa_s = 0}, \ S_{32}^{(0)} = -\frac{1}{2} \left. \frac{\partial \widetilde{\Pi}_{12}^{(0)}}{\partial \chi} \right|_{\varkappa_s = 0}$$
 (2.1.43)

As a result, the boundary conditions at the leading order becomes,

$$\widetilde{\sigma}_{31}^{(0)} = 0, \ \widetilde{\sigma}_{33}^{(0)} = 0, \ \widetilde{\Pi}_{32}^{(0)} = 0$$
 (2.1.44)

which is the classical boundary conditions in a local micropolar elastic semi-infinite medium.

Further analysing the first order terms at i = 1 for Eq. (2.1.36), we get

$$p_{mn}^{(1)} = \widetilde{\sigma}_{mn}^{(1)}, \ r_{mn}^{(1)} = \widetilde{\Pi}_{mn}^{(1)},$$
 (2.1.45)

$$\frac{\partial^2 q_{mn}^{(1)}}{\partial \varkappa_f^2} - q_{mn}^{(1)} = 0. \tag{2.1.46}$$

The solution to the differential equation in Eq. (2.1.46) takes the form,

$$q_{mn}^{(1)} = Q_{mn}^{(1)} \left(\chi, \tilde{t}\right) e^{-\varkappa_f}, \tag{2.1.47}$$

where

$$Q_{11}^{(1)} = -\frac{1}{2} \left( \widetilde{\sigma}_{11}^{(1)} \Big|_{\varkappa_{s}=0} - \frac{\partial \widetilde{\sigma}_{11}^{(0)}}{\partial \varkappa_{s}} \Big|_{\varkappa_{s}=0} \right)$$

$$Q_{31}^{(1)} = -\frac{1}{2} \left( \frac{\partial \widetilde{\sigma}_{11}^{(1)}}{\partial \chi} \Big|_{\varkappa_{s}=0} - \frac{\partial^{2} \widetilde{\sigma}_{11}^{(0)}}{\partial \varkappa_{s} \partial \chi} \Big|_{\varkappa_{s}=0} \right)$$

$$Q_{33}^{(1)} = -\frac{1}{2} \left( \frac{\partial^{2} \widetilde{\sigma}_{11}^{(1)}}{\partial \chi^{2}} \Big|_{\varkappa_{s}=0} - \frac{\partial^{3} \widetilde{\sigma}_{11}^{(0)}}{\partial \varkappa_{s} \partial \chi^{2}} \Big|_{\varkappa_{s}=0} \right)$$

$$(2.1.48)$$

Moreover, using the boundary conditions in Eq. (2.1.38), the values of  $S_{mn}^{(1)}$  is obtained as,

$$S_{12}^{(1)} = -\frac{1}{2} \left( \widetilde{\Pi}_{12}^{(1)} \Big|_{\varkappa_{s}=0} - \frac{\partial \widetilde{\sigma}_{11}^{(0)}}{\partial \varkappa_{s}} \Big|_{\varkappa_{s}=0} \right)$$

$$S_{32}^{(1)} = -\frac{1}{2} \left( \frac{\partial \widetilde{\Pi}_{12}^{(1)}}{\partial \chi} \Big|_{\varkappa_{s}=0} - \frac{\partial^{2} \widetilde{\Pi}_{12}^{(0)}}{\partial \varkappa_{s} \partial \chi} \Big|_{\varkappa_{s}=0} \right)$$

$$(2.1.49)$$

Subsequently, the boundary conditions at the first order results in,

$$\widetilde{\sigma}_{31}^{(1)} - \frac{1}{2} \frac{\partial \widetilde{\sigma}_{11}^{(0)}}{\partial \chi} = 0, \ \widetilde{\sigma}_{33}^{(1)} = 0, \ \widetilde{\Pi}_{32}^{(1)} - \frac{1}{2} \frac{\partial \widetilde{\Pi}_{12}^{(0)}}{\partial \chi} = 0$$
 (2.1.50)

It is noteworthy that in the first-order boundary conditions of a non-local semi-infinite medium, an additional term dependent on  $\tilde{\sigma}_{11}$  appears.

Now, at the second order, the Eqs. (2.1.36) can be expressed using Eq. (2.1.40) as

$$\widetilde{\sigma}_{mn}^{(2)} + \frac{\partial^{2} \widetilde{\sigma}_{mn}^{(0)}}{\partial \chi^{2}} + \frac{\partial^{2} \widetilde{\sigma}_{mn}^{(0)}}{\partial \varkappa_{s}^{2}} = p_{mn}^{(2)} 
\widetilde{\Pi}_{32}^{(2)} + \frac{\partial^{2} \widetilde{\Pi}_{32}^{(0)}}{\partial \chi^{2}} + \frac{\partial^{2} \widetilde{\Pi}_{32}^{(0)}}{\partial \varkappa_{s}^{2}} = r_{32}^{(2)}$$
(2.1.51)

This rewrites the equation of motion presented in Eq. (2.1.35) as,

$$\frac{\partial \widetilde{\sigma}_{1n}^{(2)}}{\partial \chi} + \frac{\partial \widetilde{\sigma}_{3n}^{(2)}}{\partial \varkappa_{s}} = \frac{\partial^{2} \widetilde{u}_{n}^{(2)}}{\partial \widetilde{t}^{2}} - \frac{\partial^{2}}{\partial \widetilde{t}^{2}} \left( \frac{\partial^{2} \widetilde{u}_{n}^{(0)}}{\partial \chi^{2}} + \frac{\partial^{2} \widetilde{u}_{n}^{(0)}}{\partial \varkappa_{s}^{2}} \right), 
\frac{\partial \widetilde{\Pi}_{12}^{(2)}}{\partial \chi} + \frac{\partial \widetilde{\Pi}_{32}^{(2)}}{\partial \varkappa_{s}} + \widetilde{\sigma}_{31}^{(2)} - \widetilde{\sigma}_{13}^{(2)} = J \frac{\partial^{2} \widetilde{\Phi}_{2}^{(2)}}{\partial \widetilde{t}^{2}} - J \frac{\partial^{2}}{\partial \widetilde{t}^{2}} \left( \frac{\partial^{2} \widetilde{\Phi}_{2}^{(0)}}{\partial \chi^{2}} + \frac{\partial^{2} \widetilde{\Phi}_{2}^{(0)}}{\partial \varkappa_{s}^{2}} \right).$$
(2.1.52)

As a result, the boundary conditions at the second order can be written using Eq. (2.1.38) as,

$$\widetilde{\sigma}_{31}^{(2)} + \frac{\partial^{2} \widetilde{\sigma}_{31}^{(0)}}{\partial \chi^{2}} + \frac{\partial^{2} \widetilde{\sigma}_{31}^{(0)}}{\partial \varkappa_{s}^{2}} - \frac{1}{2} \left( \frac{\partial \widetilde{\sigma}_{11}^{(1)}}{\partial \chi} - \frac{\partial^{2} \widetilde{\sigma}_{11}^{(0)}}{\partial \varkappa_{s} \partial \chi} \right) = 0, 
\widetilde{\sigma}_{33}^{(2)} + \frac{\partial^{2} \widetilde{\sigma}_{33}^{(0)}}{\partial \chi^{2}} + \frac{\partial^{2} \widetilde{\sigma}_{33}^{(0)}}{\partial \varkappa_{s}^{2}} - \frac{1}{2} \frac{\partial^{2} \widetilde{\sigma}_{11}^{(0)}}{\partial \chi^{2}} = 0, 
\widetilde{\Pi}_{32}^{(2)} + \frac{\partial^{2} \widetilde{\Pi}_{32}^{(0)}}{\partial \chi^{2}} + \frac{\partial^{2} \widetilde{\Pi}_{32}^{(0)}}{\partial \varkappa_{s}^{2}} - \frac{1}{2} \left( \frac{\partial \widetilde{\Pi}_{12}^{(1)}}{\partial \chi} - \frac{\partial^{2} \widetilde{\Pi}_{12}^{(0)}}{\partial \varkappa_{s} \partial \chi} \right) = 0.$$
(2.1.53)

Using the fact that,  $f^{(1)} \approx \frac{1}{\epsilon} f$ ,  $f^{(2)} \approx \frac{1}{\epsilon^2} f$  for  $f \in \{\widetilde{\sigma}_{mn}, \widetilde{\Pi}_{mn}\}$ , the boundary value problem can now be given as,

$$\frac{\partial \tilde{\sigma}_{1n}}{\partial \chi} + \frac{\partial \tilde{\sigma}_{3n}}{\partial \varkappa_{s}} = \frac{\partial^{2} \tilde{u}_{n}}{\partial \tilde{t}^{2}} - \epsilon^{2} \frac{\partial^{2}}{\partial \tilde{t}^{2}} \left( \frac{\partial^{2} \tilde{u}_{n}}{\partial \chi^{2}} + \frac{\partial^{2} \tilde{u}_{n}}{\partial \varkappa_{s}^{2}} \right), 
\frac{\partial \tilde{\Pi}_{12}}{\partial \chi} + \frac{\partial \tilde{\Pi}_{32}}{\partial \varkappa_{s}} + \tilde{\sigma}_{31} - \tilde{\sigma}_{13} = J \frac{\partial^{2} \tilde{\Phi}_{2}}{\partial \tilde{t}^{2}} - J \epsilon^{2} \frac{\partial^{2}}{\partial \tilde{t}^{2}} \left( \frac{\partial^{2} \tilde{\Phi}_{2}}{\partial \chi^{2}} + \frac{\partial^{2} \tilde{\Phi}_{2}}{\partial \varkappa_{s}^{2}} \right),$$
(2.1.54)

subjected to,

$$\widetilde{\sigma}_{31} - \frac{\epsilon}{2} \frac{\partial \widetilde{\sigma}_{11}}{\partial \chi} + \epsilon^{2} \left( \frac{\partial^{2} \widetilde{\sigma}_{31}}{\partial \chi^{2}} + \frac{\partial^{2} \widetilde{\sigma}_{31}}{\partial \varkappa_{s}^{2}} + \frac{1}{2} \frac{\partial^{2} \widetilde{\sigma}_{11}}{\partial \varkappa_{s} \partial \chi} \right) = 0$$

$$\widetilde{\sigma}_{33} + \epsilon^{2} \left( \frac{\partial^{2} \widetilde{\sigma}_{33}}{\partial \chi^{2}} + \frac{\partial^{2} \widetilde{\sigma}_{33}}{\partial \varkappa_{s}^{2}} - \frac{1}{2} \frac{\partial^{2} \widetilde{\sigma}_{11}}{\partial \chi^{2}} \right) = 0$$

$$\widetilde{\Pi}_{32} - \frac{\epsilon}{2} \frac{\partial \widetilde{\Pi}_{12}}{\partial \chi} + \epsilon^{2} \left( \frac{\partial^{2} \widetilde{\Pi}_{32}}{\partial \chi^{2}} + \frac{\partial^{2} \widetilde{\Pi}_{32}}{\partial \varkappa_{s}^{2}} + \frac{1}{2} \frac{\partial^{2} \widetilde{\Pi}_{12}}{\partial \varkappa_{s} \partial \chi} \right) = 0$$

$$(2.1.55)$$

# Refined boundary value problem

After recasting the refined boundary conditions in terms of the original variables employed throughout the analysis, the governing equations describing Rayleigh wave propagation on the surface of a non-local micropolar semi-infinite medium can be expressed as:

$$\frac{\partial \sigma_{11}}{\partial x} + \frac{\partial \sigma_{31}}{\partial z} = \rho \left( 1 - \aleph^2 \nabla^2 \right) \frac{\partial^2 u_1}{\partial t^2},$$

$$\frac{\partial \sigma_{13}}{\partial x} + \frac{\partial \sigma_{33}}{\partial z} = \rho \left( 1 - \aleph^2 \nabla^2 \right) \frac{\partial^2 u_3}{\partial t^2},$$

$$\frac{\partial \Pi_{12}}{\partial x} + \frac{\partial \Pi_{32}}{\partial z} + \sigma_{31} - \sigma_{13} = \rho j \left( 1 - \aleph^2 \nabla^2 \right) \frac{\partial^2 \tilde{\Phi}_2}{\partial t^2},$$
(2.1.56)

with the refined boundary conditions prescribed at the surface z=0 as,

$$\sigma_{31} - \frac{\aleph}{2} \frac{\partial \sigma_{11}}{\partial x} + \aleph^2 \left( \frac{\partial^2 \sigma_{31}}{\partial x^2} + \frac{\partial^2 \sigma_{31}}{\partial z^2} + \frac{1}{2} \frac{\partial^2 \sigma_{11}}{\partial x \partial z} \right) = 0$$

$$\sigma_{33} + \aleph^2 \left( \frac{\partial^2 \sigma_{33}}{\partial x^2} + \frac{\partial^2 \sigma_{33}}{\partial z^2} - \frac{1}{2} \frac{\partial^2 \sigma_{11}}{\partial x^2} \right) = 0$$

$$\Pi_{32} - \frac{\aleph}{2} \frac{\partial \Pi_{12}}{\partial x} + \aleph^2 \left( \frac{\partial^2 \Pi_{32}}{\partial x^2} + \frac{\partial^2 \Pi_{32}}{\partial z^2} + \frac{1}{2} \frac{\partial^2 \Pi_{12}}{\partial x \partial z} \right) = 0$$

$$(2.1.57)$$

# Dispersion relations

Substitutition of the solutions obtained for the displacement potentials and microrotation components in Eq. (2.1.10) into the refined boundary conditions in Eq. (2.1.57) gives the system of linear equations in P, Q and R.

This system is solved for non-trivial solution by ignoring the terms of order greater than or equal to  $O(\epsilon^2)$  to obtain the dispersion relations as follows,

$$(2 - \alpha_2^2)^2 r_{10} r_{20} - (1 + r_{20}^2 - \alpha_2^2)^2 + \epsilon \left[ \frac{1}{2} r_{20} (1 - r_{10}^2) (2 - \alpha_2^2) (2 - 2\alpha_1^2 - \alpha_2^2) \right] = 0,$$
(2.1.58)

$$r_{30} - \frac{1}{2}\epsilon = 0. {(2.1.59)}$$

This suggests the existence of two modes of Rayleigh waves that can propagate in a non-local micropolar elastic semi-infinite medium, with one mode arising solely from the micropolarity of the medium and disappearing in its absence.

If v is the velocity of Rayleigh waves propagating in a non-local micropolar elastic semiinfinite medium, then the dispersion relations given in Eqs. (2.1.58) and (2.1.59) can be rewritten as,

$$(2 - \alpha_2^2)^2 \sqrt{1 - \frac{v^2}{c_1^2}} \sqrt{1 - \frac{v^2}{c_2^2}} - \left(2 - \alpha_2^2 - \frac{v^2}{c_2^2}\right)^2 + \epsilon \left[\frac{1}{2} \left(2 - \alpha_2^2\right) \left(2 - 2\alpha_1^2 - \alpha_2^2\right) \frac{v^2}{c_1^2} \sqrt{1 - \frac{v^2}{c_2^2}}\right] = 0,$$

$$(2.1.60)$$

$$\sqrt{1 - \frac{v^2}{c_4^2} \left( 1 - \frac{2c_3^2}{j\omega^2} \right)} - \frac{1}{2} \epsilon = 0.$$
 (2.1.61)

As expected, the dispersion relations obtained at the leading order align exactly with the previously established results for a local micropolar elastic semi-infinite medium (see, Eringen et al. [60], Rayleigh [14]).

Now, let  $c = \frac{v}{c_2}$  be the dimensionless phase velocity of Rayleigh waves propagating in

a nonlocal micropolar elastic solid. Also, let  $d = \frac{\kappa}{\mu}$  denote the dimensionless parameter characterizing the micropolar constant within the semi-infinite medium domain. It follows that  $\alpha_2^2$  can be approximated by d with an error of  $O(d^2)$ .

As a result, the dispersion equation in Eq. (2.1.60) can be rewritten as,

$$(2-d)^{2} \sqrt{1-\frac{c^{2}}{\alpha_{1}^{2}}} \sqrt{1-c^{2}} - (2-d-c^{2})^{2} + \epsilon \left[\frac{1}{2} (2-d) (2-2\alpha_{1}^{2}-d) \frac{c^{2}}{\alpha_{1}^{2}} \sqrt{1-c^{2}}\right] = 0$$
(2.1.62)

, in which  $\alpha_1^2 = \frac{2(1-\nu)}{1-2\nu}$  relating with Poisson's ratio,  $\nu$ .

To understand explicitly the nonlocal and micropolar effects on the phase velocity of the Rayleigh waves, we shall expand c in an asymptotic series of the form upto an error of  $O(\epsilon^2)$  and  $O(d^2)$ ,

$$c = c_r^{(0)} + d c_m^{(0)} + \epsilon \left( c_r^{(1)} + d c_m^{(1)} \right) + \dots, \tag{2.1.63}$$

where  $c_r^{(0)} = c_r$  is the dimensionless phase velocity of Rayleigh waves propagating in an elastic semi-infinite medium in absence of both nonlocal and micropolar effects.

Expanding Eq. (2.1.62) in a Taylor series about the point  $c = c_r$  and using the asymptotic series, we get the values of the corrections as,

$$c_m^{(0)} = -\frac{c_r (2 - c_r^2)^3}{4 \left[ (2 - c_r^2)^3 - 4 \left( 1 + \frac{1}{\alpha_1^2} (1 - 2c_r^2) \right) \right]}$$
(2.1.64)

$$c_r^{(1)} = -\frac{c_r \sqrt{1 - c_r^2} (2 - c_r^2)^2 \left(\frac{1}{\alpha_1^2} - 1\right)}{2 \left[ (2 - c_r^2)^3 - 4 \left(1 + \frac{1}{\alpha_1^2} (1 - 2c_r^2)\right) \right]},$$
(2.1.65)

$$c_r \left(c_r^2 - 1\right) \frac{1}{\alpha_1^2} \sqrt{1 - \frac{c_r^2}{\alpha_1^2}} - 2 c_m^{(0)} \left(3c_r^2 - 2\right) \left(\frac{1}{\alpha_1^2} - 1\right) \sqrt{1 - \frac{c_r^2}{\alpha_1^2}},$$

$$c_m^{(1)} = -\frac{-c_r^{(1)} \left[ \left(2 - c_r^2\right)^2 - 4 \left(1 + \frac{1}{\alpha_1^2} \left(1 - 2c_r^2\right)\right) \right]}{\left(2 - c_r^2\right)^3 - 4 \left(1 + \frac{1}{\alpha_1^2} \left(1 - 2c_r^2\right)\right)}. (2.1.66)$$

It can be easily verified that the micropolar mode of Rayleigh waves corresponding to Eq. (2.1.61) propagates in a non-local micropolar semi-infinite medium with a velocity,

$$v = \sqrt{c_4^2 \left(1 - \frac{\epsilon^2}{4}\right) + \frac{2c_3^2}{jk^2}}. (2.1.67)$$

This equation clearly highlights the dispersive nature of the wave mode even in the absence of nonlocal elasticity.

# 2.1.5 Graphical discussions

# Dispersion analysis

Dispersion plots are generated to analyze the wave behavior. Figure 2.1.1 represents the phase velocity curves for the mode corresponding to Eq. (2.1.58) in a nonlocal micropolar semi-infinite medium. In a purely local model (without nonlocal elasticity), the wave is non-dispersive (constant velocity). However, the presence of nonlocality introduces dispersion, as shown by the first-order approximation in the dispersion relation, and the corresponding variation in phase velocity with wave number is depicted in Figure 2.1.1.

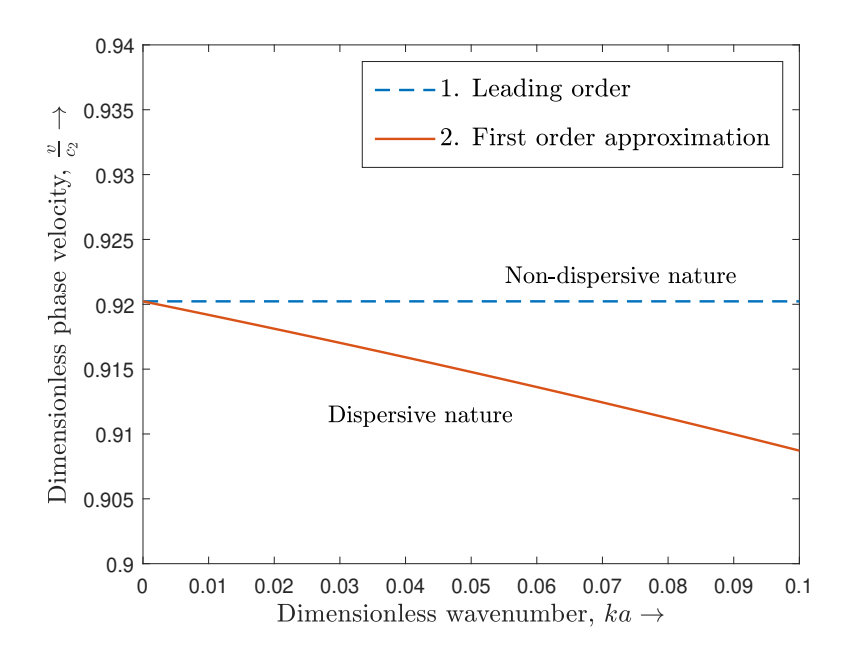


Figure 2.1.1: Corrected phase velocity curves for one of the modes corresponding to elastic counterpart

Furthermore, the micropolar mode of Rayleigh waves exhibits dispersion in both local and nonlocal elasticity scenarios. Figure 2.1.2 illustrates this by plotting the phase velocity variation versus wavenumber. Curve 1 represents the local elastic case, while curves 2, 3, and 4 correspond to the nonlocal elastic case based on the first-order approximation in the dispersion relation provided in Eq. (2.1.59).

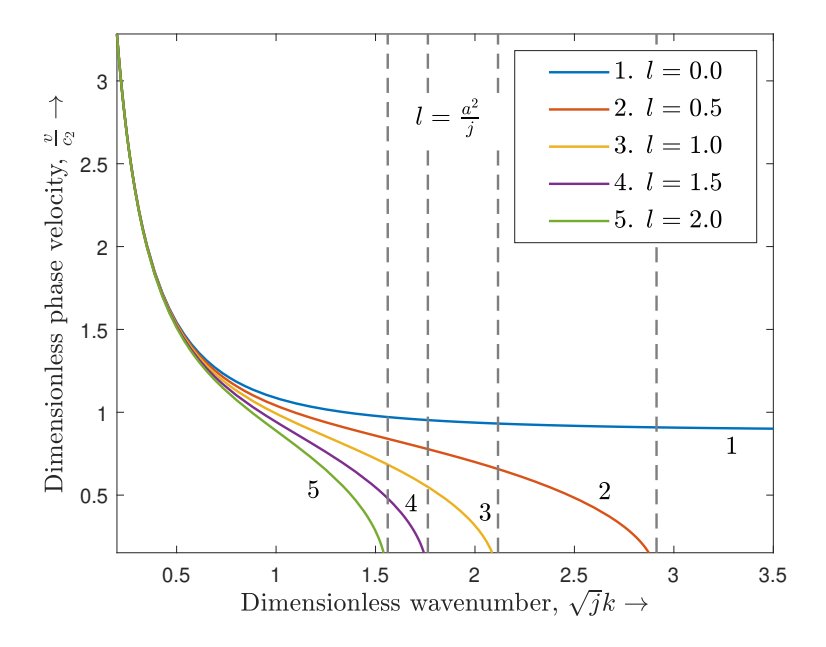


Figure 2.1.2: Corrected phase velocity curves for micropolar dispersive mode for different values of  $l = \frac{a^2}{j}$ 

# Sensitivity analysis

A sensitivity analysis is then performed to understand how small perturbations in micropolar or nonlocal effects affect the wave propagation. This helps us to assess the robustness of our model.

The linear relationship observed in the Figure 2.1.3(a) indicates a direct and predictable interaction between the micropolar parameter d and the sensitivity of the phase velocity to changes in the non-local parameter  $\epsilon$ . The negative values of  $\frac{dc}{d\epsilon}$  throughout suggests that an increase in the nonlocal parameter  $\epsilon$  consistently leads to a decrease in the phase velocity c. This finding is significant as it highlights the dampening effect of the nonlocal properties on wave propagation velocity.

The sensitivity analysis graph of  $\frac{dc}{d\epsilon}$  versus Poisson's ratio  $\nu$  as described in Figure 2.1.3(b) for varying micropolar parameter values reveals important interactions in the non-local micropolar model. The consistently negative  $\frac{dc}{d\epsilon}$  demonstrates a general reduction in phase velocity with increasing  $\epsilon$ . The moderation effect observed with increasing  $\nu$  highlights that the materials with higher Poisson's ratios reduce the sensitivity to non-local effects. Furthermore, the convergence of curves at higher  $\nu$  values signifies that the influence of micropolarity diminishes in materials with high Poisson's ratios.

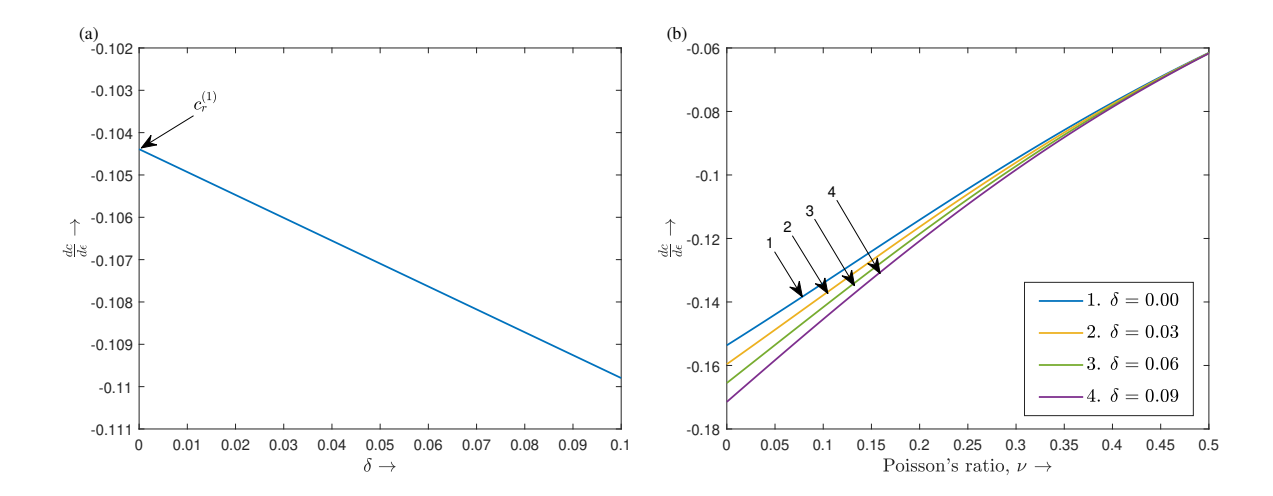


Figure 2.1.3: Variation of the sensitivity of phase velocity c with respect to nonlocal elastic parameter  $\epsilon$  as a function of (a) micropolarity parameter d (or  $\delta$ ) (b) Poisson's ratio  $\nu$ 

The positive values of  $\frac{dc}{dd}$  in Figure 2.1.4(a) indicates that micropolar effects in the medium always contribute to an increase in the phase velocity of Rayleigh waves. However, the negative slope of the graph shows that the rate of this increase diminishes as the nonlocal parameter  $\epsilon$  grows. In practical terms, this means that while micropolar elasticity inherently increases wave speed, the presence of nonlocal effects can moderate this increase. The negative slope further illustrates that the impact of nonlocal effects on reducing phase velocity becomes more significant as the micropolar parameter d increases in the medium.

The sensitivity analysis of  $\frac{dc}{dd}$  with respect to Poisson's ratio  $\nu$  as depicted in Figure 2.1.4(b) for varying non-local parameter values reveals significant insights into the interplay between material properties, non-local effects, and micropolar characteristics. The consistently positive  $\frac{dc}{dd}$  indicates that the phase velocity increases with the micropolar parameter across all examined Poisson's ratios. However, the decreasing  $\frac{dc}{dd}$  with higher  $\nu$  suggests that the impact of micropolarity on phase velocity weakens as Poisson's ratio increases. Moreover, the convergence of curves at higher  $\nu$  values signifies that, in materials with high Poisson's ratios, the effect of the non-local parameter on phase velocity becomes minimal.

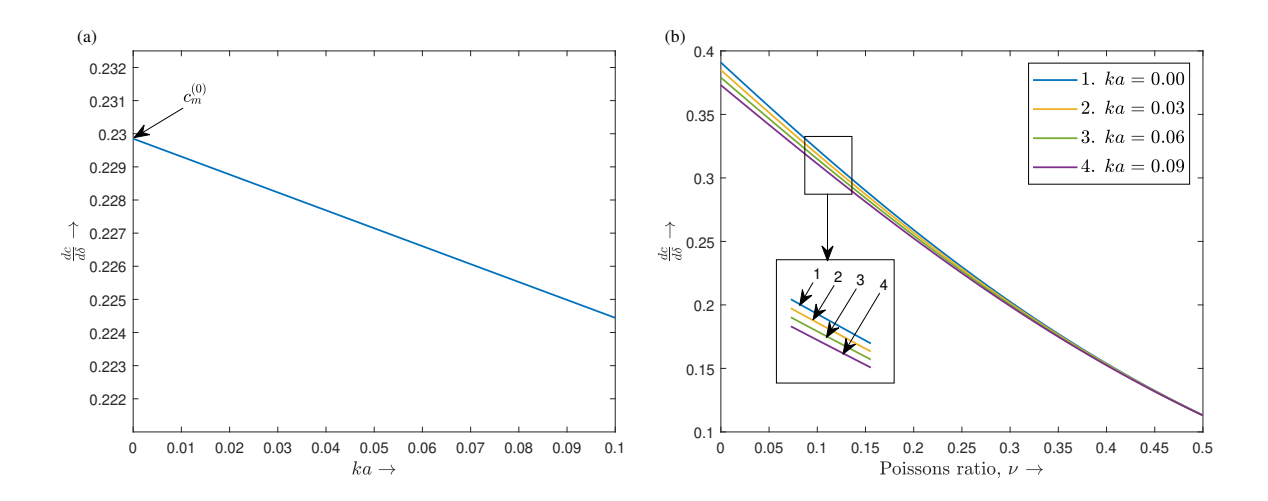


Figure 2.1.4: Variation of the sensitivity of phase velocity c with respect to micropolar parameter  $d(\text{or }\delta)$  as a function of (a) nonlocal elastic parameter  $\epsilon$  (b) Poisson's ratio  $\nu$ 

#### 2.1.6 Conclusions

This study demonstrates that the equivalence between nonlocal integral and differential formulations breaks down for Rayleigh waves in a nonlocal micropolar semi-infinite medium. The analysis reveals that this equivalence can only be restored with specific additional boundary conditions, particularly for certain force and couple stress distributions. The presence of a heterogeneous boundary layer near the surface necessitates refined boundary conditions, leading to second-order corrections to the traditional traction-free and couple stress-free conditions. These corrections account for nonlocal effects and accurately capture boundary layer influences. The refined conditions yield nonlocal-corrected dispersion relations, revealing two distinct Rayleigh wave modes, one uniquely due to the micropolar nature of the medium. The findings highlight the significant role of micropolar effects, especially in materials with high Poisson's ratios, while nonlocal effects are less influential in such cases.

# 2.2 Application in a nonlocal micropolar viscoelastic medium\*

Building upon the refined nonlocal traction-free boundary conditions established in the previous sub-chapter, this section investigates Rayleigh wave propagation in a viscoelastic medium within the framework of nonlocal and micropolar elasticity. We derive leading-order nonlocal corrected dispersion relations, revealing distinct modes, including micropolar-specific modes and nonlocal quasi-elastic modes. We analyze two specific viscoelastic models and examine the influence of material and nonlocal parameters on Rayleigh wave propagation, including particle trajectories. MATLAB simulations are carried out to visualize phase velocity behavior and understand the interplay of various parameters across all identified modes.

#### 2.2.1 Formulation of the problem

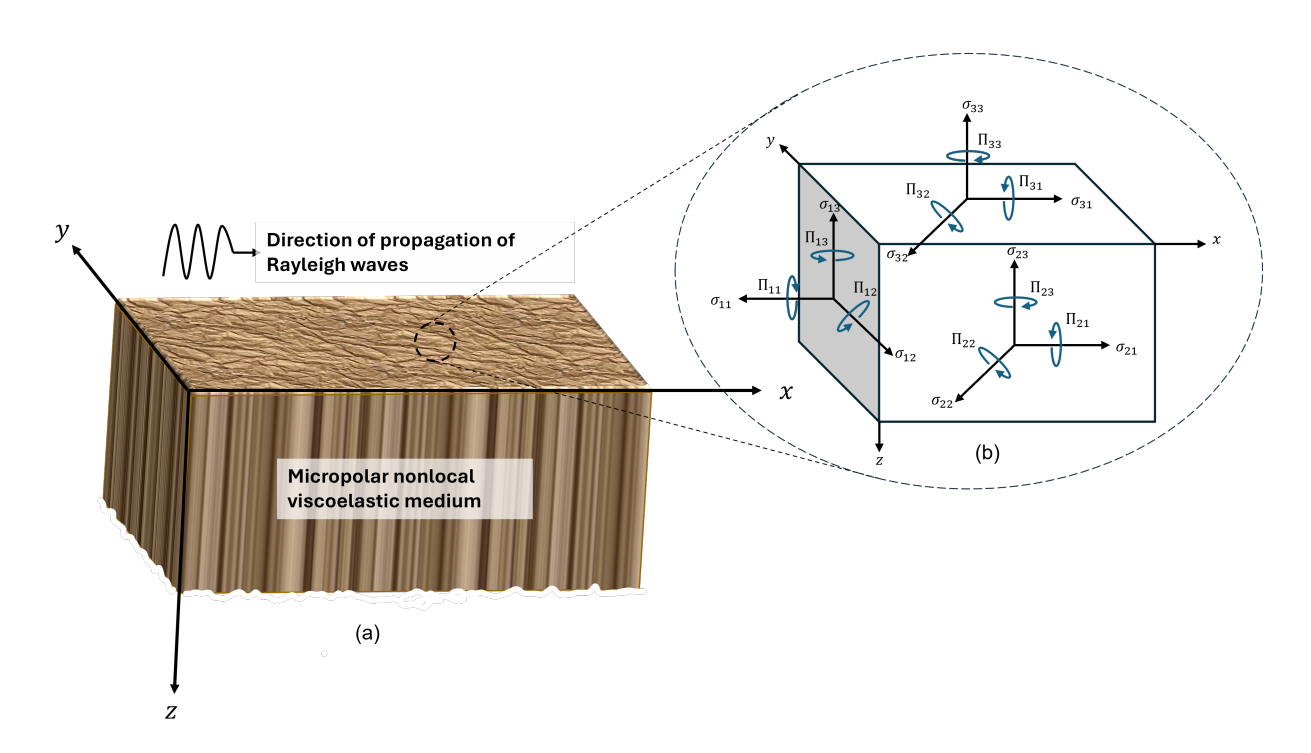


Figure 2.2.1: (a) Geometry of the model (b) A unit micropolar cell displaying force stresses and couple stresses

Consider the propagation of Rayleigh wave fields along x-direction having the displacement vector  $\mathbf{u} = (u_1, 0, u_3)$  and the microrotation vector  $\mathbf{\Phi} = (0, \Phi_2, 0)$ . Since the

<sup>\*</sup> Published in ZAMM Journal of Applied Mathematics and Mechanics/Zeitschrift für Angewandte Mathematik und Mechanik (Wiley), (2024), DOI: 10.1002/zamm.202400604

motion of Rayleigh wave fields is confined to the xz-plane, we have  $\frac{\partial}{\partial y} \equiv 0$  in this problem. The waves are propagating over the free surface z=0 of the nonlocal micropolar viscoelastic medium occupying the semi-infinite medium  $z\leq 0$  as described in Figure 2.2.1.

Introducing the conventional scalar potential  $\phi$  and a vector potential  $\psi = (\psi_1, \psi_2, \psi_3)$  for the displacement vector through,

$$u_1 = \frac{\partial \phi}{\partial x} - \frac{\partial \psi_2}{\partial z}, \ u_3 = \frac{\partial \phi}{\partial z} + \frac{\partial \psi_2}{\partial x},$$

the field equations given in Eq. (1.3.103) may be reduced as,

$$(\Lambda + 2\mu + \kappa) \nabla^{2}\phi - \rho (1 - \aleph^{2}\nabla^{2}) \ddot{\phi} = 0,$$

$$(\mu + \kappa) \nabla^{2}\psi_{2} + \kappa \Phi_{2} - \rho (1 - \aleph^{2}\nabla^{2}) \ddot{\psi}_{2} = 0,$$

$$\gamma \nabla^{2}\Phi_{2} - \kappa \nabla^{2}\psi_{2} - 2\kappa\Phi_{2} - \rho j (1 - \aleph^{2}\nabla^{2}) \ddot{\Phi}_{2} = 0.$$

$$(2.2.1)$$

Assume a suitable complex notation for scalar, vector potentials, and microrotation vector components with the real angular frequency  $\omega = \frac{k}{s}$  as

$$\{\phi, \psi_2, \Phi_2\} = \{\mathcal{X}, \mathcal{Y}, \zeta \mathcal{Y}\} e^{i\omega(sx+qz-t)}, \tag{2.2.2}$$

where  $\mathcal{X}, \mathcal{Y}$  are the complex amplitudes and s is the complex slowness vector component along x-direction with  $\mathfrak{Re}(s) > 0$  and  $\mathfrak{Im}(s) \geq 0$  ensuring the decay of the amplitude along positive x-direction; k is the wavenumber;  $q, \zeta$  are the complex variables to be determined.

Substituting the field form given in Eq. (2.2.2) into the reduced field equations given in Eq. (2.2.1), we get

$$\phi(x, z, t) = \mathcal{X}e^{i\omega(sx+q_1z-t)}, 
\psi_2(x, z, t) = \mathcal{Y}_1 e^{i\omega(sx+q_2z-t)} + \mathcal{Y}_2 e^{i\omega(sx+q_3z-t)}, 
\Phi_2(x, z, t) = \zeta \mathcal{Y}_2 e^{i\omega(sx+q_3z-t)},$$
(2.2.3)

where

$$q_1 = \sqrt{\frac{\rho}{\Lambda + 2\mu + \kappa - \rho \aleph^2 \omega^2} - s^2}, \quad q_2 = \sqrt{\frac{\rho}{\mu + \kappa - \rho \aleph^2 \omega^2} - s^2}$$
$$q_3 = \sqrt{\frac{\rho j \omega^2 - 2\kappa}{\omega^2 \left(\gamma - \rho j \aleph^2 \omega^2\right)} - s^2}, \quad \zeta = \frac{\omega^2 \left(\rho - (\mu + \kappa - \rho \aleph^2 \omega^2)(q_3^2 + s^2)\right)}{\kappa}.$$

As a result, the final expressions for the displacement and microrotation vector fields for Rayleigh wave fields propagating in a nonlocal micropolar viscoelastic medium are as follows:

$$u_{1}(x, z, t) = i\omega \left(s\mathcal{X} e^{i\omega q_{1}z} - q_{2}\mathcal{Y}_{1} e^{i\omega q_{2}z} - q_{3}\mathcal{Y}_{2} e^{i\omega q_{3}z}\right) e^{i\omega(sx-t)},$$

$$u_{3}(x, z, t) = i\omega \left(q_{1}\mathcal{X} e^{i\omega q_{1}z} + s\mathcal{Y}_{1} e^{i\omega q_{2}z} + s\mathcal{Y}_{2} e^{i\omega q_{3}z}\right) e^{i\omega(sx-t)},$$

$$\Phi_{2}(x, z, t) = \zeta \mathcal{Y}_{2} e^{i\omega q_{3}z} e^{i\omega(sx-t)}.$$
(2.2.4)

#### 2.2.2 Dispersion relations

In a mechanical stress-free surface, the nonlocal force stress components and couple stress components at the boundary of the viscoelastic semi-infinite medium z=0 vanishes. This means,

$$\tau_{31} = 0, \ \tau_{33} = 0, \ \pi_{32} = 0, \ \text{at } z = 0.$$
 (2.2.5)

#### Refined boundary conditions

To account for the nonlocal boundary layer localized near the surface, a modified differential model was developed by Kaplunov et al. [204, 205] for an isotropic elastic semi-infinite medium. This theory could further be extended for a nonlocal micropolar semi-infinite medium, and as a result, the refined boundary conditions for such a medium can be determined as follows:

$$\sigma_{31} - \frac{\aleph}{2} \frac{\partial \sigma_{11}}{\partial x} + \aleph^2 \left( \frac{\partial^2 \sigma_{31}}{\partial x^2} + \frac{\partial^2 \sigma_{31}}{\partial z^2} + \frac{1}{2} \frac{\partial^2 \sigma_{11}}{\partial x \partial z} \right) = 0, \text{ at } z = 0, \qquad (2.2.6)$$

$$\sigma_{33} - \aleph^2 \left( \frac{1}{2} \frac{\partial^2 \sigma_{11}}{\partial x^2} - \frac{\partial^2 \sigma_{33}}{\partial x^2} - \frac{\partial^2 \sigma_{33}}{\partial z^2} \right) = 0 \text{ at } z = 0, \qquad (2.2.7)$$

$$\Pi_{32} - \frac{\aleph}{2} \frac{\partial \Pi_{12}}{\partial x} + \aleph^2 \left( \frac{\partial^2 \Pi_{32}}{\partial x^2} + \frac{\partial^2 \Pi_{32}}{\partial z^2} + \frac{1}{2} \frac{\partial^2 \Pi_{12}}{\partial x \partial z} \right) = 0 \text{ at } z = 0.$$
 (2.2.8)

On inserting the expressions of stresses using Eqs. (2.2.4) into Eqs. (2.2.6)-(2.2.8), a homogeneous linear system of equations with the coefficient matrix denoted by A is obtained for  $\mathcal{X}$ ,  $\mathcal{Y}_1$  and  $\mathcal{Y}_2$  (see Appendix A). Assuming a long-wave regime in which the small parameter becomes  $\epsilon = \aleph k$ , this system of linear homogeneous equations can be solved for a non-trivial solution, and a dispersion relation can be obtained within an error

of  $O(\epsilon^2)$ .

$$s^{2} q_{10} q_{20} (\beta - 2)^{2} + (q_{20}^{2} + s^{2} (\beta - 1)) (\alpha q_{10}^{2} + s^{2} (\alpha + \beta - 2))$$

$$-\epsilon \left(\frac{i s}{2} (2 - \beta) (2\alpha + \beta - 2) (q_{10}^{2} + s^{2}) q_{20}\right) = 0, \quad (2.2.9)$$

$$s \epsilon + 2 i q_{30} = 0, \quad (2.2.10)$$

where,

$$q_{10} = \sqrt{\frac{\rho}{\Lambda + 2\mu + \kappa} - s^2}, \ q_{20} = \sqrt{\frac{\rho}{\mu + \kappa} - s^2}, \ q_{30} = \sqrt{\frac{\rho j \omega^2 - 2\kappa}{\omega^2 \gamma} - s^2}, \ \alpha = \frac{\Lambda + 2\mu + \kappa}{\mu + \kappa}, \ \beta = \frac{\kappa}{\mu + \kappa}.$$

Eqs. (2.2.9) and (2.2.10) are the **dispersion relations** obtained for the Rayleigh wave fields propagating in a nonlocal micropolar viscoelastic medium. It is essential to emphasize that Rayleigh waves propagating in a nonlocal micropolar medium yield two modes: one, as described in Eq. (2.2.9), mimics the elastic mode of the classical elastic medium, while the mode corresponding to Eq. (2.2.10) solely arise due to micropolarity in the medium. This mode ceases to exist when micropolarity is absent.

# Analysis of dispersion modes

On introducing some dimensionless quantities,

$$c = \frac{\rho}{s^2 (2\mu + \kappa)}, \ \alpha_1 = \frac{2\mu + \kappa}{\Lambda + 2\mu + \kappa}, \ \alpha_2 = \frac{2\mu + \kappa}{\mu + \kappa},$$

the dispersion relation for the first mode described in Eq. (2.2.9) becomes,

$$q_{10} q_{20} + s^2 (c-1)^2 - \epsilon \left(\frac{i}{2} s \, c \, q_{20} (2 - \alpha_1)\right) = 0,$$
 (2.2.11)

As expected, the leading order (for  $\epsilon = 0$ ) yields the dispersion equation for Rayleigh waves in a micropolar viscoelastic solid.

By selecting the positive real x-axis as the branch cut, we guarantee that the complex slowness vector s has the desired positive real and imaginary components. Subsequently, employing a Taylor series expansion of  $q_{20}$  around c = 0, truncated to the first-order term, and squaring the resulting expression to eliminate the square roots, we arrive at a cubic equation in c as

$$c^{3} \left[ -2 + \epsilon \left( \alpha_{1} \alpha_{2} - 2\alpha_{2} \right) \right] + c^{2} \left[ 8 + \epsilon \left( -2\alpha_{2} \alpha_{1} - 2\alpha_{1} + 4\alpha_{2} + 4 \right) \right]$$
$$+ c \left[ 2\alpha_{1} \alpha_{2} - 12 + \epsilon \left( \alpha_{2} \alpha_{1} + 4\alpha_{1} - 2\alpha_{2} - 8 \right) \right] + 8 - 2\alpha_{1} - 2\alpha_{2} + \epsilon \left( 4 - 2\alpha_{1} \right) = 0. \quad (2.2.12)$$

It is very important to note that not all the roots of Eq. (2.2.12) satisfy the dispersion equation given in Eq. (2.2.11). Some non-admissible (spurious) roots are introduced due to the squaring of the dispersion equation given in Eq. (2.2.11). Thus, we can conclude that a root c of Eq. (2.2.12) is admissible if for such a c,

- the dispersion equation (2.2.11) is satisfied,
- $\mathfrak{Re}(s) > 0$  and  $\mathfrak{Im}(s) \ge 0$  (as amplitude does not increase with the wave propagation along x-direction),
- $\mathfrak{Im}(q_{10}) < 0$ ,  $\mathfrak{Im}(q_{20}) < 0$  (as Rayleigh surface wave decay along the depth from the surface).

Additionally, we will simplify the expression in Eq. (2.2.10) to examine the micropolar mode. This yields the complex slowness component s as:

$$s = 2\sqrt{\frac{\rho j\omega^2 - 2\kappa}{(4 - \epsilon^2)\,\omega^2\,\gamma}}. (2.2.13)$$

The reciprocal of the expression in Eq. (2.2.13) represents the velocity of the micropolar mode of the Rayleigh waves propagating in a nonlocal micropolar viscoelastic medium. Now, for a purely micropolar elastic medium in the absence of nonlocal elasticity ( $\epsilon = 0$ ), the velocity v, which is the reciprocal of the slowness component s in any medium, can be given as,

$$\frac{v}{v_2} = \sqrt{\frac{2\kappa}{\mu j k^2} + \frac{\gamma}{\mu j}} \approx \sqrt{\frac{2\kappa}{\mu j k^2}} \tag{2.2.14}$$

as the second term inside the square root is indeed a very smaller quantity. Here  $v_2 = \sqrt{\frac{\mu}{\rho}}$ . This velocity clearly matches exactly with the results of Suhubi and Eringen [106]. Further, it is intriguing to observe that these two distinct modes of Rayleigh wave fields, one of which is solely due to micropolarity in the viscoelastic medium, do not coexist in the same space for an extended period within a longer wavelength regime. This fact could be simply proven by the method of contradiction.

If the determinant of the coefficient matrix, |A| = 0, implying  $a_{11}a_{22} - a_{12}a_{21} = 0$  and  $a_{33} = 0$ , then  $\mathcal{Y}_2$  that explicitly determines the amplitude of the micro-rotation vector component  $\Phi_2$  can never be zero (for if  $\mathcal{Y}_2 = 0$ , then  $\Phi_2 = 0$  suggesting that the micro-rotation vanishes which is absurd). For  $\mathcal{Y}_2 = t_3(\neq 0)$ , the system has infinitely many solutions due to the vanishing determinant of the coefficient matrix. Now, by setting  $\mathcal{Y}_1 = t_2(\neq 0)$  and determining  $\mathcal{X}$  from the system, we arrive at  $t_3 = 0$ , a contradiction.

Thus, we conclude that both Rayleigh modes do not coexist in the same space. Physically, this means that one of the modes might propagate faster or slower than the other, leading to a spatial separation between them. This dispersion mismatch prevents the coexistence of both modes. In the following sections, we will analyze the velocities of these modes in detail.

# 2.2.3 Particle motion and dynamics

In this section, we will explore both the trajectory and the behavior exhibited by oscillating particles of a nonlocal micropolar viscoelastic solid during the propagation of Rayleigh wave fields.

# Particle trajectories

For the present problem considered in xz-plane, the displacement components are obtained as the resultant of the superposition of plane-polarized scalar and vector potentials. Every point in the viscoelastic semi-infinite medium will trace a curve, and the locus of this curve is determined by computing the real parts of the displacement components,  $u_1$  and  $u_3$ . Now, from Eq. (2.2.4)

$$\{\Re(u_1), \Re(u_3)\} = -\omega \{|A_1(z)| \sin(\theta_1), |A_3(z)| \sin(\theta_3)\} e^{-\Im(s)\omega x}, \qquad (2.2.15)$$

where

$$A_1(z) = s e^{i\omega q_1 z} \mathcal{X} - q_2 e^{i\omega q_2 z} \mathcal{Y}_1, \quad A_3(z) = q_1 e^{i\omega q_1 z} \mathcal{X} + s e^{i\omega q_2 z} \mathcal{Y}_1,$$

$$\text{and } \theta_i = \arg(A_i(z)) + \omega \left(\Re \mathfrak{e}(s) - t\right) \text{ for } i = 1, 3.$$

$$(2.2.16)$$

At a given coordinate x and z, the conic traced by the particles of Rayleigh wave fields is obtained by eliminating t from Eq. (2.2.15)). This yields,

$$[P_0 \Re \mathfrak{e}(u_1)]^2 + [Q_0 \Re \mathfrak{e}(u_3)]^2 - 2 \cos \eta \, P_0 \, Q_0 \Re \mathfrak{e}(u_1) \Re \mathfrak{e}(u_3) = \sin^2 \eta, \qquad (2.2.17)$$

where 
$$P_0 = -\frac{1}{\omega |A_1(z)|e^{-\Im \mathfrak{m}(s)\,\omega x}}$$
,  $Q_0 = -\frac{1}{\omega |A_3(z)|e^{-\Im \mathfrak{m}(s)\,\omega x}}$  and  $\eta = \arg\left[A_1(z)\right] - \arg\left[A_3(z)\right]$ .

Also, it is easy to verify that the discriminant of Eq. (2.2.17) is negative for all  $\eta \neq 0$ . This implies that the particles of the Rayleigh wave field in any mode trace an *elliptical* orbit for all  $\eta \neq 0$ .

When  $\eta = 0$ , the ellipse degenerates into a *straight line*, as can be seen from Eq. (2.2.16). We further attempt to rewrite the equation of the ellipse given in Eq. (2.2.17) to a standard form by deriving the tilted angle of the ellipse with respect to z-axis. By

choosing an appropriate rotation of the coordinates, it is possible to determine the angle of rotation, denoted by  $\beta$  as

$$\beta = \begin{cases} \frac{1}{2} \cot^{-1} \left( \frac{Q_0^2 - P_0^2}{2 \cos \eta P_0 Q_0} \right) & Q_0 \neq P_0, \\ \frac{\pi}{4} & Q_0 = P_0. \end{cases}$$

This angle of rotation,  $\beta \neq \frac{\pi}{4}$  determines the tilt of the elliptical path of Rayleigh wave field particles and depends on complex angular frequency  $\omega$ , nonlocal elastic parameter  $\aleph$  and complex moduli of the viscoelastic medium. When  $\beta = \frac{\pi}{4}$ , a circular path is traced by the oscillating particles during Rayleigh wave field propagation. Using this angle of rotation  $\beta$ , the standard form of the ellipse traced by the particles can be given as,

$$\left(\frac{\Re\mathfrak{e}(u_1)}{P}\right)^2 + \left(\frac{\Re\mathfrak{e}(u_3)}{Q}\right)^2 = 1,\tag{2.2.18}$$

where

$$P = \sin \eta \, \left( P_0^2 \, \cos^2 \beta + Q_0^2 \, \sin^2 \beta - 2 \, P_0 \, Q_0 \, \cos \eta \, \sin \beta \, \cos \beta \right)^{\frac{-1}{2}},$$

$$Q = \sin \eta \, \left( P_0^2 \, \sin^2 \beta + Q_0^2 \, \cos^2 \beta + 2 \, P_0 \, Q_0 \, \cos \eta \, \sin \beta \, \cos \beta \right)^{\frac{-1}{2}}.$$

# Prograde and retrograde dynamics

To determine the type of elliptical motion (prograde or retrograde) of the Rayleigh wave field particles, we need to realize the nature of the time derivative of the polar angle. Let us define this polar angle  $\chi$  as,

$$\chi = \arg \left[ \frac{\mathfrak{Re}(u_1)}{\mathfrak{Re}(u_3)} \right] \text{ or } \chi = \tan^{-1} \left[ \frac{\mathfrak{Re}(u_1)}{\mathfrak{Re}(u_3)} \right].$$

A time derivative of this polar angle  $\chi$  is evaluated by using Eq. (2.2.15) as,

$$\frac{d\chi}{dt} = \frac{\omega}{\sin^2 \theta_3 + \sin^2 \theta_1} \cdot \frac{|A_1(z)|}{|A_3(z)|} \cdot \sin \eta.$$

Note that when  $\sin \eta < 0$  (> 0), the polar angle  $\chi$  decreases (increases) with time, suggesting that the Rayleigh wave field particles in an elliptical orbit will exhibit a prograde (retrograde) motion.

Moreover, on simplifying the term  $\sin \eta$ , it can be further inferred that the elliptical orbit describes a prograde (retrograde) motion if

$$\mathfrak{Im}\left[\overline{A_{1}(z)}\,A_{3}(z)\right] = \mathfrak{Re}[A_{1}(z)]\,\mathfrak{Im}[A_{3}(z)] - \mathfrak{Re}[A_{3}(z)]\,\mathfrak{Im}[A_{1}(z)] < 0\,(>0). \tag{2.2.19}$$

Further, the dispersive properties of Rayleigh waves that arise due to the elastic counterpart of the medium for two specific viscoelastic solids in detail: (i) an incompressible solid and (ii) a Poisson solid. Both of these solids are assumed to be meeting criteria akin to that of a Hardtwig solid [267] as  $\Re \mathfrak{e}(\mu)/\Re \mathfrak{e}(K) = \Im \mathfrak{m}(\mu)/\Im \mathfrak{m}(K)$ .

#### 2.2.4 Incompressible solid semi-infinite medium

An incompressible solid preserves its volume when a body deforms; in other words, there is no volumetric strain in such a medium. This suggests that the bulk modulus is infinitely very large, or equivalently,  $\Lambda \to \infty$ .

#### Mode analysis

Define a new parameter d as,  $d = \frac{\mu}{\mu + \kappa}$ . On decomposing the components of d into its corresponding real and imaginary parts, we have

$$\begin{split} \mathfrak{Re}(d) &= \frac{\mathfrak{Re}(\mu) \left(\mathfrak{Re}(\mu) + \mathfrak{Re}(\kappa)\right) + \mathfrak{Im}(\mu) \left(\mathfrak{Im}(\mu) + \mathfrak{Im}(\kappa)\right)}{\left(\mathfrak{Re}(\mu) + \mathfrak{Re}(\kappa)\right)^2 + \left(\mathfrak{Im}(\mu) + \mathfrak{Im}(\kappa)\right)^2} \\ \mathfrak{Im}(d) &= \frac{\mathfrak{Im}(\mu) \left(\mathfrak{Re}(\mu) + \mathfrak{Re}(\kappa)\right) - \mathfrak{Re}(\mu) \left(\mathfrak{Im}(\mu) + \mathfrak{Im}(\kappa)\right)}{\left(\mathfrak{Re}(\mu) + \mathfrak{Re}(\kappa)\right)^2 + \left(\mathfrak{Im}(\mu) + \mathfrak{Im}(\kappa)\right)^2} \end{split}$$

Using the fact that  $\Re(\mu)/\Re(K) = \Im(\mu)/\Im(K)$ , we get  $\Im(\mu) = 0$  and as a result,

$$d = \mathfrak{Re}(d) = \frac{\left(\mathfrak{Re}(\mu)\right)^2 + \left(\mathfrak{Im}(\mu)\right)^2 + \mathfrak{Re}(\mu)\mathfrak{Re}(\kappa) + \mathfrak{Im}(\mu)\mathfrak{Im}(\kappa)}{\left(\mathfrak{Re}(\mu) + \mathfrak{Re}(\kappa)\right)^2 + \left(\mathfrak{Im}(\mu) + \mathfrak{Im}(\kappa)\right)^2}$$

which is clearly less than 1.

Thus, we conclude that d is a real number (i.e.,  $d \in \mathbb{R}$ ) and falls within the range  $0 < d \le 1$ . Hence, by allowing  $\Lambda \to \infty$  in Eq. (2.2.12), the dispersion relation for the Rayleigh waves in an incompressible solid can be derived, resulting in:

$$2c^{3}\left[-1 - \epsilon\left(1 + d\right)\right] + 4c^{2}\left[2 + \epsilon\left(2 + d\right)\right] - 2c\left[6 + (d + 5)\epsilon\right] + 6 - 2d + 4\epsilon = 0, \quad (2.2.20)$$

with small  $\epsilon \geq 0$  and  $0 < d \leq 1$ . A detailed analysis of this equation is conducted to determine the exact roots of the dispersion relation.

Consider a complex polynomial with real coefficients in z given by,

$$h(z) = 2z^{3} \left[ -1 - \epsilon (1+d) \right] + 4z^{2} \left[ 2 + \epsilon (2+d) \right] - 2z \left[ 6 + (d+5)\epsilon \right) \right] + 6 - 2d + 4\epsilon = 0,$$
(2.2.21)

satisfying the dispersion relation given in Eq. (2.2.20) at z=c.

Quasi-elastic mode: Now, according to Descartes' rule of signs, it is evident that Eq. (2.2.21) possesses at least one positive real root and no negative real roots. Furthermore, it is worth recalling that a cubic equation possesses three distinct real roots only if the polynomial discriminant is strictly positive [268]. Applying this principle, it is easy to check that the polynomial discriminant for the cubic equation h(z) in Eq. (2.2.21) remains less than or equal to zero for all possible values of  $\epsilon$  and d. Consequently, Eq. (2.2.21) has to have only one positive real root, say  $c_r$  and this real root is less than unity for every possible value of  $\epsilon$  and d.

Now, it remains to check if this positive real root satisfies the exact dispersion relation given in Eq. (2.2.11).

As  $\Lambda$  approaches infinity, we observe  $q_1 = \pm is$ . Given that  $\mathfrak{Im}(q_{10}) < 0$ , we can only assume  $q_{10} = -is$ , considering the fact that  $\mathfrak{Re}(s) > 0$ . Using this value of  $q_{10}$ , we could write the expression for  $q_{20}$  from Eq. (2.2.11) as,

$$q_{20} = -is \left[ \frac{2(c-1)^2}{2 + \epsilon c (1-d)} \right]. \tag{2.2.22}$$

Observe that for  $c = c_r < 1 \in \mathbb{R}$  and for all the possible values of  $\epsilon$  and d,  $\mathfrak{Im}(q_{20}) < 0$  as  $\mathfrak{Re}(s) > 0$ . In other words, the positive real root of the cubic equation (2.2.20) satisfies the exact dispersion relation giving rise to a *quasi-elastic mode* of Rayleigh wave field propagating in a nonlocal micropolar incompressible solid semi-infinite medium.

Viscoelastic mode: This mode arises due to the complex roots in the dispersion relation in Eq. (2.2.20). It is essential to determine which of the two complex roots of the cubic equation h(z) in Eq. (2.2.21) satisfies the dispersion relation (2.2.11). It is essential to verify conditions under which these complex roots will satisfy  $\mathfrak{Im}(q_2) < 0, \mathfrak{Im}(q_1) < 0$ .

Checking these conditions is algebraically complicated, thus we consider a numerical example of an incompressible solid semi-infinite medium with small viscous terms and thereby determine the conditions for which the viscoelastic mode arises.

# Numerical example

We shall now describe a particular viscoelastic incompressible solid semi-infinite medium with small viscous terms in detail. We take

$$\mu = \mu_0 (1 - i \, \delta a), \ \kappa = \kappa_0 (1 - i \, \delta b),$$
 (2.2.23)

where  $\delta > 0$  is small and  $0 < \delta a < 1$ . Also, since  $\Re \mathfrak{e}(\mu)/\Re \mathfrak{e}(K) = \Im \mathfrak{m}(\mu)/\Im \mathfrak{m}(K)$ , we get a = b. Let us consider a case where  $\mu_0 = \kappa_0 = 0.4 \times 10^{11} \text{ N m}^{-2}$ ,  $\rho = 1740 \text{ kg m}^{-3}$  and dimensionless nonlocal elastic parameter  $\epsilon = 0.04$ . Then the roots of the dispersion relation are,

$$c_r = 0.659793,$$
  
 $c_1 = 1.65124 + 0.981019 i,$   
 $c_2 = 1.65124 - 0.981019 i.$ 

Quasi-elastic mode: For the root  $c_r$ , the value of s for which  $\Re \mathfrak{e}(s) > 0$  can be calculated as,

$$s = 0.0001482 + 0.00007412 \delta a i$$

with the condition that  $\delta a > 0$ . Further, we have

$$q_{10} = 0.00007412 \,\delta a - 0.0001482 \,i,$$
  
 $q_{20} = 0.000008522 \,\delta a - 0.0000170455 \,i.$ 

As seen in the previous section, the only positive real root of the cubic equation (2.2.21) satisfies the exact dispersion relation given in Eq. (2.2.11) for every value of d and  $\epsilon << 1$ . The variation of real phase velocity  $v = \frac{\rho}{s^2(\mu + \kappa)}$  of quasi-elastic mode with the material parameter  $\frac{\kappa}{\mu}$  for different values of small  $\epsilon$  is presented in the Figure 2.2.2. The data in Figure 2.2.2 demonstrates that the phase velocity of Rayleigh waves in the quasi-elastic mode rises as the material parameter of the micropolar media increases up to a certain threshold, beyond which it reaches a steady value. Moreover, when micropolarity is absent in the medium, the y-intercepts offer insights into the phase velocity at which the wave propagates. It can be further noted that as the nonlocal parameter of the media increases, there is a corresponding rise in the phase velocity of the propagating waves.

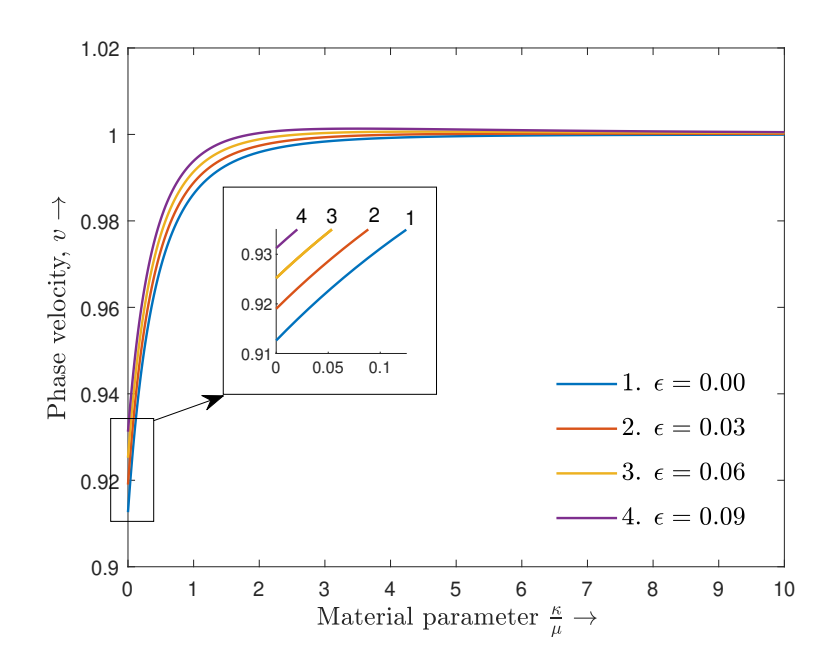
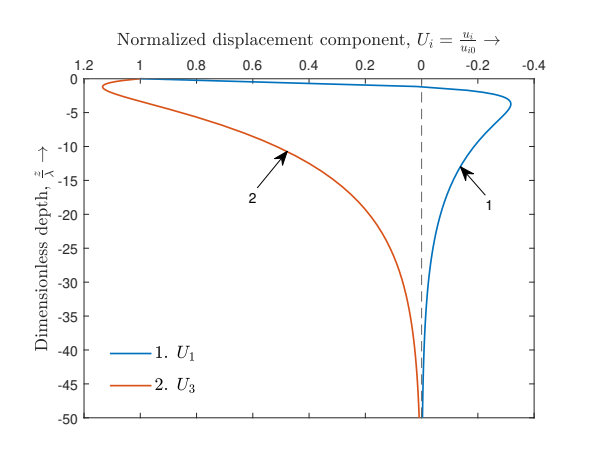
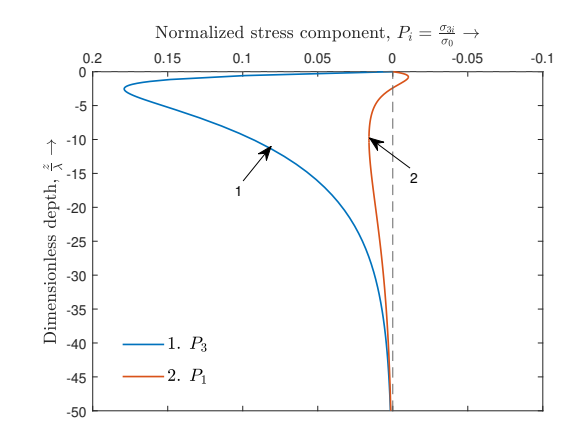


Figure 2.2.2: Variation of phase velocity (v) with the material parameter  $\left(\frac{\kappa}{\mu}\right)$  for different values of  $\epsilon$  in an incompressible solid semi-infinite medium





- (a) Normalized displacement variation
- (b) Normalized stress variation

Figure 2.2.3: Normalized (a) displacement components  $(U_i)$  (b) stress components  $(P_i)$  versus dimensionless depth  $\left(\frac{z}{\Lambda}\right)$  for a quasi-elastic mode of Rayleigh waves in an incompressible solid

Figure 2.2.3 illustrates the depth-dependent variation of normalized displacement  $U_i = \frac{u_i}{u_{i0}}$ , i = 1, 3 and stress components  $P_i = \frac{\sigma_{3i}}{\sigma_0}$ , i = 1, 3 for Rayleigh wave fields

propagating in a quasi-elastic mode of an incompressible semi-infinite medium. The normalization of the displacement and stress is based on the respective displacement components at z = 0 (i.e.,  $u_{10}, u_{30}$ ) and the stress component  $\sigma_{11}$  at z = 0 ( $\sigma_{0}$ ), respectively. As depicted in Figures 2.2.3a and 2.2.3b, the displacement and stress profiles exhibit a characteristic exponential decay with depth, confirming the localized nature of the wave energy near the surface.

**Viscoelastic mode:** For the root  $c_1$ , the possible value of s that satisfies  $\mathfrak{Re}(s) > 0$  is

$$s = 0.00008379 + 0.00001151 \delta a + (0.00004189 \delta a - 0.00002301) i.$$

This further gives,

$$q_{10} = 0.00004189 \,\delta a - 0.00002301 + (-0.00001151 \,\delta a - 0.00008379) i,$$
  
 $q_{20} = 0.0001176 - 0.000007153 \,\delta a + (0.00005882 \,\delta a + 0.00001431) i.$ 

It is easy to check that there exists no  $\delta a$  for which the root  $c_1$  satisfies the exact dispersion relation given in Eq. (2.2.11). Thus, root  $c_1$  does not account for any viscoelastic mode of Rayleigh waves in the medium.

For the root  $c_2$ , The value of s satisfying  $\Re \mathfrak{e}(s) > 0$  can be computed as:

$$s = 0.00008379 - 0.00001151 \delta a + (0.00004189 \delta a + 0.00002301) i.$$

As a result, we have

$$q_{10} = 0.00002301 + 0.00004189 \,\delta a + (0.00001151 \,\delta a - 0.00008379) i,$$
  
 $q_{20} = -0.000007153 \,\delta a - 0.0001176 + (0.0000143075 - 0.0000588204 \,\delta a) i.$ 

For  $c_2$  to satisfy the dispersion relation in Eq. (2.2.11), we derive the condition on  $\delta a$  such that  $\Re \mathfrak{e}(s) > 0$ ,  $\Im \mathfrak{m}(q_{10}) < 0$ , and  $\Im \mathfrak{m}(q_{20}) < 0$ . This on reduction gives, 0.243241  $< \delta a < 7.28203$ .

Therefore, we conclude that the viscoelastic mode of Rayleigh waves propagates only under the condition that the material parameters specified in Eq. (2.2.23) satisfy

$$0.243241 < \delta a < 1.$$

In general, a specific critical value of  $\delta a_c(<1)$  exists for every d, beyond which the viscoelastic mode of the Rayleigh wave can propagate.

Figure 2.2.4 is plotted to understand the variation of these critical values with the material parameter d. The analysis indicates that the minimum critical value of  $\delta a$  occurs for a local non-micropolar solid. Moreover, there is a significant decrease in  $\delta a_c$  with the increase in the nonlocal parameter of the medium up to a certain value of d, after which a reverse behavior is observed. This further validates the existence of specific d and  $\delta a_c$  values for which every curve, corresponding to a different nonlocal parameter, intersects. The phase velocity of Rayleigh wave fields propagating in a viscoelastic mode decreases

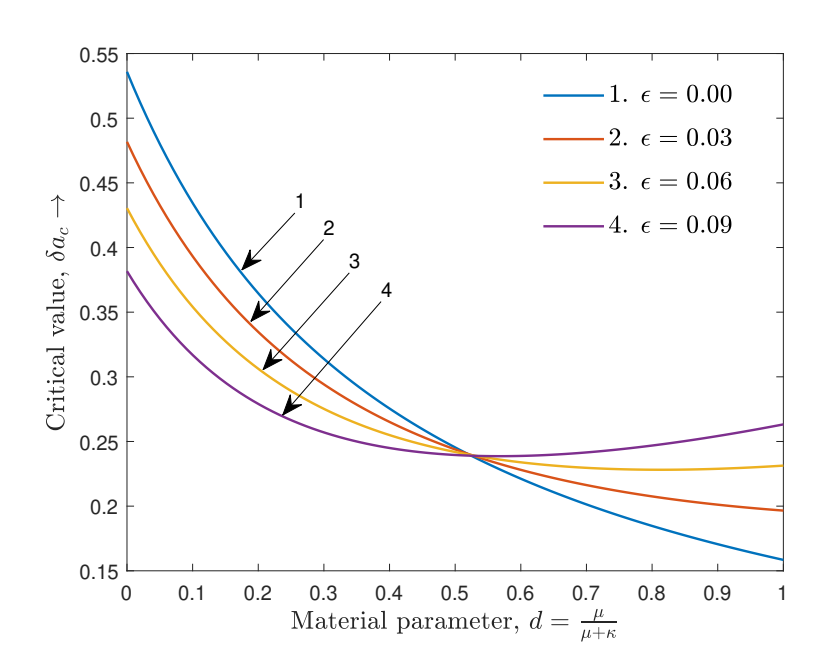


Figure 2.2.4: Variation of critical  $\delta a_c$  with material parameter d for different  $\epsilon$ 

with the increase in the material parameter. This behavior is clearly depicted in Figure 2.2.5, which is in contrast to the behavior observed in the case of Rayleigh waves propagating in a quasi-elastic mode. Furthermore, as the nonlocal parameter of the medium increases, the phase velocity decreases up to a specific value of d, after which the trend reverses. In contrast to the quasi-elastic case, Rayleigh waves propagating through a viscoelastic semi-infinite medium exhibit a more complex depth-dependent behavior as presented in Figure 2.2.6. While the displacement and stress components still demonstrate an oscillatory pattern as illustrated in Figure 2.2.6a and 2.2.6b, the amplitude of

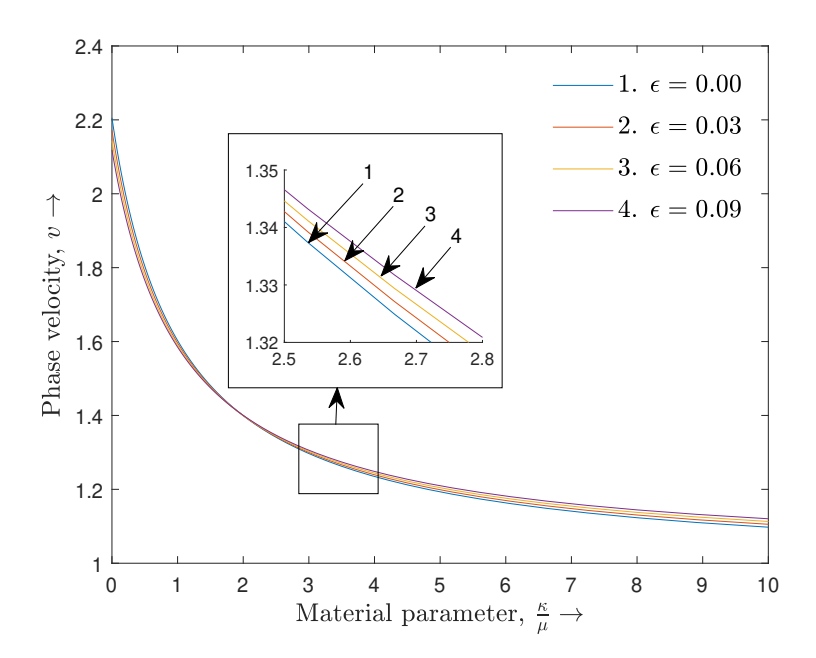
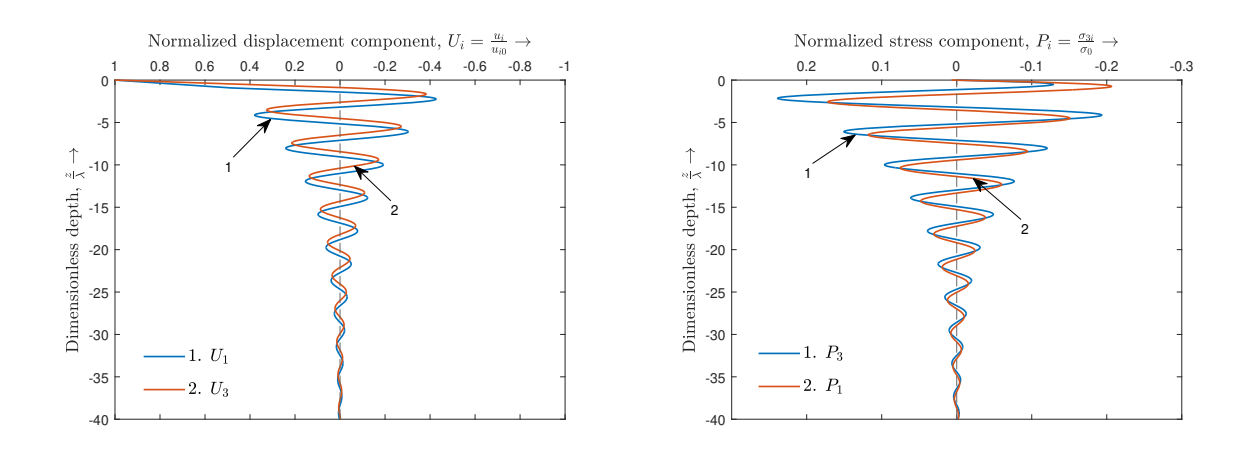


Figure 2.2.5: Variation of phase velocity v with material parameter  $\frac{\kappa}{\mu}$  for different  $\epsilon$ 



- (a) Normalized displacement variation
- (b) Normalized stress variation

Figure 2.2.6: Normalized (a) displacement components  $(U_i)$  (b) stress components  $(P_i)$  versus dimensionless depth  $(\frac{z}{\Lambda})$  for a viscoelastic mode of Rayleigh waves in an incompressible solid

these oscillations gradually diminishes with increasing depth. This attenuation of the wave energy is a direct consequence of the viscoelastic properties of the medium, which

introduce energy dissipation mechanisms not present in a purely elastic medium. Ultimately, the oscillations decay to zero, confirming the localized nature of the wave field near the surface.

## Particle motion

We will further analyze the type of particle motion (prograde or retrograde) exhibited by Rayleigh wave field particles propagating in the quasi-elastic and viscoelastic modes at the surface.

At the surface of an incompressible solid semi-infinite medium, the quantities  $A_1(z)$  and  $A_3(z)$  as defined in Eq. (2.2.16) becomes,

$$A_1(0) = A_1 = s \mathcal{X} - q_2 \mathcal{Y}_1$$
, and  $A_3(0) = A_3 = q_1 \mathcal{X} + s \mathcal{Y}_1$ . (2.2.24)

By approximating Eq. (2.2.24) within an error of  $O(\epsilon^2)$  and incorporating the boundary conditions in Eqs. (2.2.6)-(2.2.9), a relationship between  $\mathcal{X}$  and  $\mathcal{Y}_1$  is derived. Subsequently, upon substituting this relation along with the corresponding values of  $q_1$  and  $q_2$  from Eq. (2.2.22) for an incompressible solid semi-infinite medium, we obtain,

$$A_1 = cs$$
, and  $A_3 = i s c \left(\frac{1+\epsilon}{1-c}\right)$ . (2.2.25)

Quasi-elastic mode: For real c, the quantity

$$\mathfrak{Im}(\overline{A_1}A_3) < 0 \ (>0), \text{ only when } 1-c < 0 \ (>0).$$

We have the value c < 1 from previous results in a quasi-elastic mode. As a result, the particles of the Rayleigh wave fields in a quasi-elastic mode maintain their elliptical motion and remain retrograde for all values of  $\epsilon$  and d.

**Viscoelastic mode:** For a complex root  $c = \Re \mathfrak{e}(c) + i \Im \mathfrak{m}(c)$ , the quantity

$$\mathfrak{Im}(\overline{A_1} A_3) < 0 \ (> 0), \text{ only when } 1 - \mathfrak{Re}(c) < 0 \ (> 0).$$

Thus, we conclude that the particles exhibit a prograde (retrograde) motion correspondingly when  $\Re \mathfrak{e}(c) > 1$  (< 1). For the numerical example described in section 2.2.4, the Rayleigh wave field particles propagating in a viscoelastic mode exhibit a *prograde* elliptical motion for all possible  $\epsilon$  and d.

## 2.2.5 Poisson solid semi-infinite medium

In the context of classical elasticity theory, a Poisson solid refers to an isotropic solid whose elastic constants ( $\Lambda$  and  $\mu$ ) are equal. In other words, such as solid has a Poisson ratio,  $\nu = 0.25$ . Further, extending this concept to micropolar elasticity theory (cf. Eringen [51]), we have for a Poisson solid,  $\Lambda = \mu + K/2$ .

# Mode analysis

Similar to the section 2.2.4, we reintroduce the parameter  $d = \frac{\mu}{\mu + \kappa}$  lying between 0 and 1 for further analysis. Taking  $\Lambda = \mu + \frac{\kappa}{2}$ , the dispersion relation in Eq. (2.2.12) now becomes,

$$2c^{3}\left[-3-2\epsilon(1+d)\right]+8c^{2}\left[3+\epsilon(2+d)\right]-4c\left[8-d+\epsilon(5+d)\right]+14-6d+8\epsilon=0,\ (2.2.26)$$

for  $0 < \epsilon << 1$  and 0 < d < 1.

Let g(z) denotes a complex polynomial with the real coefficients given by,

$$g(z) = 2z^{3} \left[ -3 - 2\epsilon(1+d) \right] + 8z^{2} \left[ 3 + \epsilon(2+d) \right] - 4z \left[ 8 - d + \epsilon(5+d) \right] + 14 - 6d + 8\epsilon,$$
(2.2.27)

and has roots at z = c. Now, we will examine the values of c that give rise to quasi-elastic and viscoelastic modes of Rayleigh wave fields during their propagation in a nonlocal micropolar viscoelastic medium.

It can be easily verified from Descartes' rule of signs that Eq. (2.2.27) has at least one positive real root and no negative real roots for all the possible values of small  $\epsilon$  and d. Moreover, evaluation of the polynomial discriminant yields the range of values for  $\epsilon$  and d where Eq. (2.2.27) possesses either one or all positive real roots. The graph of the polynomial discriminant for different values of  $\epsilon$  and d is plotted in Figure 2.2.7.

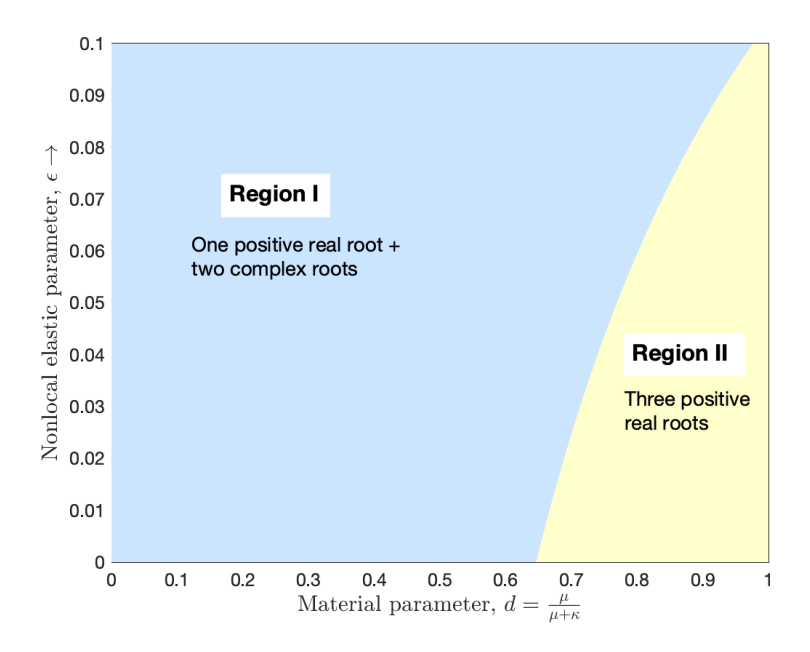


Figure 2.2.7: Nature of roots c for different values of  $\epsilon$  and d

Figure 2.2.7 indicates a critical value of the material parameter d for each fixed  $\epsilon$ , beyond which the polynomial discriminant is consistently positive. This implies that there exists a d corresponding to every  $\epsilon$  where the cubic equation in Eq. (2.2.27) possesses exactly three positive real roots. To distinguish between the root nature, the graph is divided into two regions: Region I and Region II. In Region I, the cubic equation has one positive real root and two complex roots, while in Region II, it has all three positive real roots.

Now, we shall investigate the conditions under which the real roots of Eq. (2.2.27) satisfy the exact dispersion relation in Eq. (2.2.11).

Quasi-elastic mode: For real root c < 3/2, the values of  $q_{10}$  and  $q_{20}$  are determined using the fact that  $\Re \mathfrak{e}(s) > 0$ ,  $\Im \mathfrak{m}(s) > 0$ . This gives,

$$q_{10} = -i s \sqrt{1 - \frac{2c}{3}}, \ q_{20} = -i s \left( \frac{3(c-1)^2}{2c\epsilon + 3\sqrt{1 - \frac{2c}{3}}} \right).$$
 (2.2.28)

From Eq. (2.2.28), it is evident that  $\mathfrak{Im}(q_{10}) < 0$  and  $\mathfrak{Im}(q_{20}) < 0$  for all  $\epsilon, d$ , indicating that a real root  $c < \frac{3}{2}$  of Eq. (2.2.27) satisfies the exact dispersion relation given in Eq. (2.2.11), thus leading to the propagation of quasi-elastic mode of Rayleigh wave fields.

Similarly, for  $c > \frac{3}{2}$ , the values of  $q_1$  and  $q_2$  can be determined as,

$$q_{10} = -s\sqrt{\frac{2c}{3} - 1}, \ q_{20} = -is\left(\frac{3(c-1)^2}{2c\epsilon - 3i\sqrt{\frac{2c}{3} - 1}}\right).$$
 (2.2.29)

Clearly,  $\mathfrak{Im}(q_{10}) < 0$  given that  $\mathfrak{Im}(s) < 0$ . And  $\mathfrak{Im}(q_{20}) < 0$ , provided that

$$\frac{\mathfrak{Im}(s)}{\mathfrak{Re}(s)} < \left(\frac{2c\epsilon}{3\sqrt{\frac{2c}{3}-1}}\right). \tag{2.2.30}$$

Thus, we infer that for  $c > \frac{3}{2}$ , the quasi-elastic mode of Rayleigh wave fields propagate in a medium when Eq. (2.2.30) is satisfied. Moreover, we shall discuss this briefly by taking a numerical example in the next section.

Viscoelastic mode: The viscoelastic mode of Rayleigh wave fields propagate in a non-local micropolar medium when the material parameter d and the nonlocal parameter  $\epsilon$  lies in the Region I. These modes emerge when the complex roots of Eq. (2.2.27) satisfy Eq. (2.2.11).

For a comprehensive analysis of the occurrence of these modes, we explore a numerical example involving a Poisson solid semi-infinite medium with minor viscous terms to identify the conditions under which both quasi-elastic and viscoelastic modes propagate.

#### Numerical example

Consider a viscoelastic Poisson solid semi-infinite medium with small viscous terms as,

$$\mu = \mu_0(1 - i \delta a), \ \kappa = \kappa_0(1 - i \delta b), \ \Lambda = \mu_0(1 - i \delta a) + \frac{\kappa_0}{2}(1 - i \delta b),$$

with  $\delta > 0$  and  $\delta a < 1$ . We also have a = b similar to section 2.2.4.

Suppose we consider a viscoelastic solid where  $\mu_0 = 0.4 \times 10^{11}$  and  $\kappa_0 = 0.1 \times 10^{11}$  N m<sup>-2</sup>,  $\rho = 1740$  kg m<sup>-3</sup>. We shall study the modes for four cases of  $\epsilon$  and d.

A table is constructed to examine the real roots across various intervals of  $\epsilon$  and d, thereby checking the conditions on  $\delta a$  for which these roots satisfy exact dispersion relation given in Eq. (2.2.11).

Case 1 is studied for a viscoelastic solid in which  $\epsilon$  and d lie in Region I. Here the cubic equation Eq. (2.2.21) has only one positive real root. Clearly, this root satisfies Eq. (2.2.11) for every possible value of  $\delta a > 0$ . Similarly, Case 2 is studied for a solid in which

Table 2.2.1: Conditions for which the real roots satisfy the exact dispersion relation

Cases	Real roots	$\mathfrak{Im}(q_{i0})$	Quasi-elastic mode propagates for	
Case 1: $(\epsilon, d) = (0.06, 0.8)$	0.512235	$\mathfrak{Im}(q_{10}) = -0.000157652$ $\mathfrak{Im}(q_{20}) = -0.0000555558$	all values of $\delta a < 1$	
	0.510007	$\mathfrak{Im}(q_{10}) = -0.000158174$ $\mathfrak{Im}(q_{20}) = -0.0000565933$	all values of $\delta a < 1$	
Case 2:	1.64845	$\Im \mathfrak{m}(q_{10}) = -0.0000170344 \delta a$ $\Im \mathfrak{m}(q_{20}) = -0.0000198394 \delta a$ $+0.0000709899$	$\delta a < 0.279468$	
$(\epsilon, d) = (0.04, 0.8)$	1.80083	$\Im \mathfrak{m}(q_{10}) = -0.0000232008 \delta a$ $\Im \mathfrak{m}(q_{20}) = +0.000073348 \delta a$	$\delta a < 0.214464$	
	0.505424	$-0.0000157305$ $\Im\mathfrak{m}(q_{10}) = -0.000159257$ $\Im\mathfrak{m}(q_{20}) = -0.0000587515$	all values of $\delta a < 1$	
Case 3: $(\epsilon, d) = (0, 0.8)$	1.60852	$\mathfrak{Im}(q_{10}) = -0.0000147439 \delta a$ $\mathfrak{Im}(q_{20}) = 0.0000754663 \delta a$	no values of $\delta a > 0$	
	1.88606	$\Im \mathfrak{m}(q_{10}) = -0.0000256819 \delta a$ $\Im \mathfrak{m}(q_{20}) = 0.0000783412 \delta a$	no values of $\delta a > 0$	
Care 4	2	$\mathfrak{Im}(q_{10}) = 0.000030104 \delta a$ $\mathfrak{Im}(q_{20}) = -0.000090312 \delta a$	no values of $\delta a > 0$	
Case 4: $(\epsilon, d) = (0, 1)$	$\frac{1}{3}\left(3-\sqrt{3}\right)$	$\mathfrak{Im}(q_{10}) = -0.000192253$ $\mathfrak{Im}(q_{20}) = -0.0000892247$	all values of $\delta a < 1$	
	$\frac{1}{3}\left(3+\sqrt{3}\right)$	$\mathfrak{Im}(q_{10}) = -0.0000133328 \delta a$ $\mathfrak{Im}(q_{20}) = 0.0000861845 \delta a$	no values of $\delta a > 0$	

 $\epsilon$  and d lie in Region II. The conditions for the propagation of the quasi-elastic mode of Rayleigh wave fields are derived and are provided in Table 2.2.1.

Case 3 and Case 4 are examined in the context of a micropolar viscoelastic solid and a classical viscoelastic solid, primarily without considering the effects of nonlocal elastic parameters. It can be inferred that nonlocal elasticity effects within the medium lead to the emergence of nonlocal elastic modes. These modes vanish in the absence of nonlocal elasticity. This distinction is important in materials science and mechanics because the presence or absence of nonlocal effects significantly impacts mechanical behavior, particularly in situations where small-scale or long-range effects play a vital role.

Additionally, for further analysis of these quasi-elastic modes, we plot a variety of graphs to visually depict the behavior, thus offering insights into the response of this viscoelastic solid under diverse conditions.

Figure 2.2.8 illustrates the variation in phase velocity of Rayleigh wave fields propagating in the quasi-elastic mode (where  $c < \frac{3}{2}$ ) across varying material parameter values. The velocity pattern resembles that of an incompressible solid, except for the fact that Rayleigh wave fields in this mode propagate with a slightly lower phase velocity compared to those in a Poisson solid. In Figure 2.2.9, a careful graphical analysis is carried out to

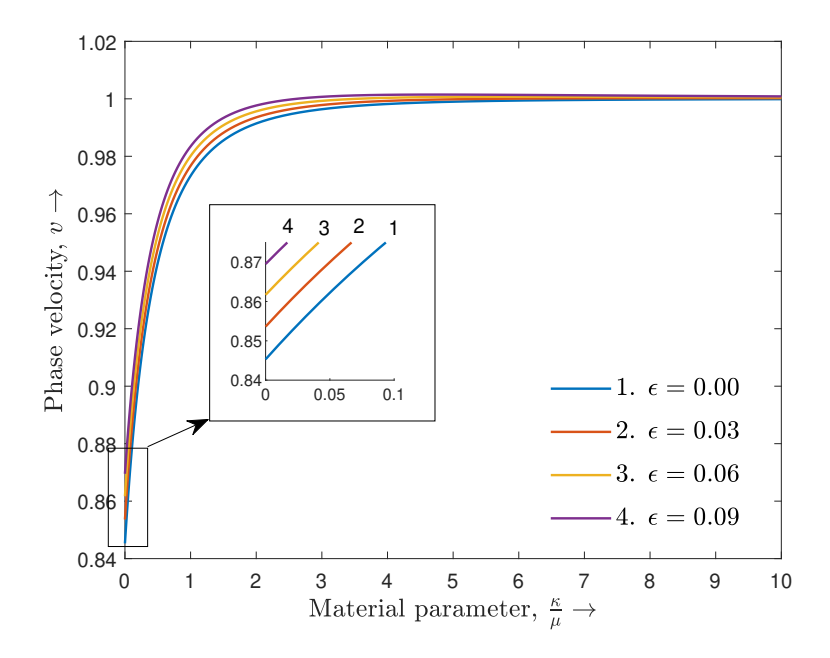


Figure 2.2.8: Variation of phase velocity of Rayleigh waves, v in a quasielastic mode with material parameter  $\frac{\kappa}{\mu}$  for different values of  $\epsilon$ 

comprehend the characteristics of nonlocal elastic modes propagating when parameters

 $\epsilon$  and d lie in Region II of Figure 2.2.7. The two branches obtained for a constant  $\epsilon$  signify the variation in critical values of  $\delta a$  for two nonlocal elastic modes, respectively propagated over the course. It is noteworthy to mention that these two modes exhibit contrasting behaviors and emerge only when the  $\delta a$  for the medium falls below the critical value. Moreover, an increase in the nonlocal elastic parameters of the medium leads to an increase in the critical value  $\delta a$ . Further, Figure 2.2.10 is plotted to understand the

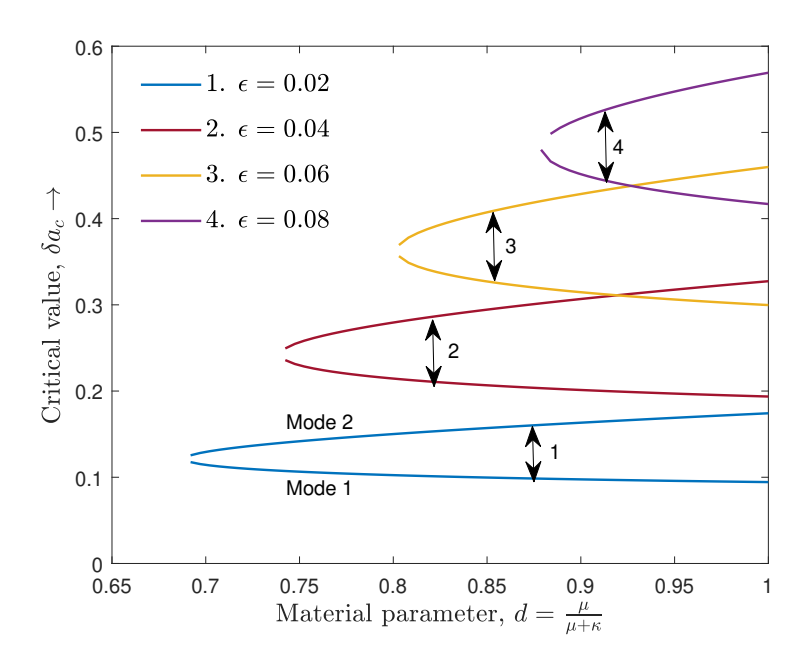


Figure 2.2.9: Variation of critical  $\delta a_c$  with material parameter d for different  $\epsilon$ 

variation of the phase velocity of Rayleigh wave field propagating in a nonlocal elastic mode for different material parameters  $\frac{\kappa}{\mu}$ . A declining trend for the velocity behavior is observed for both modes with the increase in the material parameter for  $\delta a = 0.02$ . Additionally, we observe that one of the nonlocal elastic modes travels faster than the other modes in a particular solid. Figure 2.2.11 presents the Rayleigh waves propagating through a Poisson solid in the quasi-elastic mode wherein the decay of displacement and stress components with depth is noticeably more rapid compared to the incompressible case. This accelerated attenuation results from the Poisson solid's inherent compressibility, which allows for the dissipation of wave energy into volumetric deformations. While the overall amplitude of the displacement and stress components is generally smaller than in the incompressible case, the rapid decay ensures that the wave energy remains confined

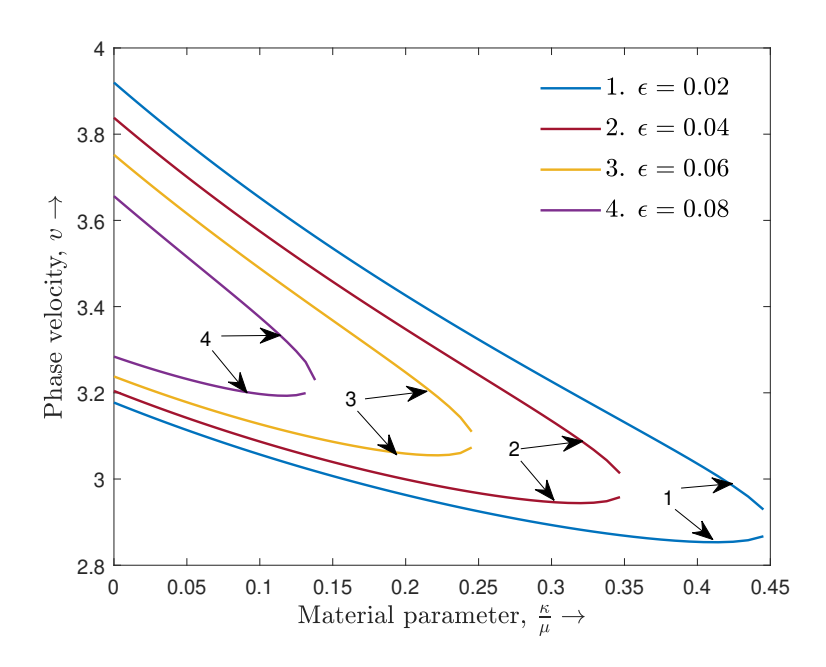


Figure 2.2.10: Variation of phase velocity v with material parameter  $\frac{\kappa}{\mu}$  for different  $\epsilon$ 

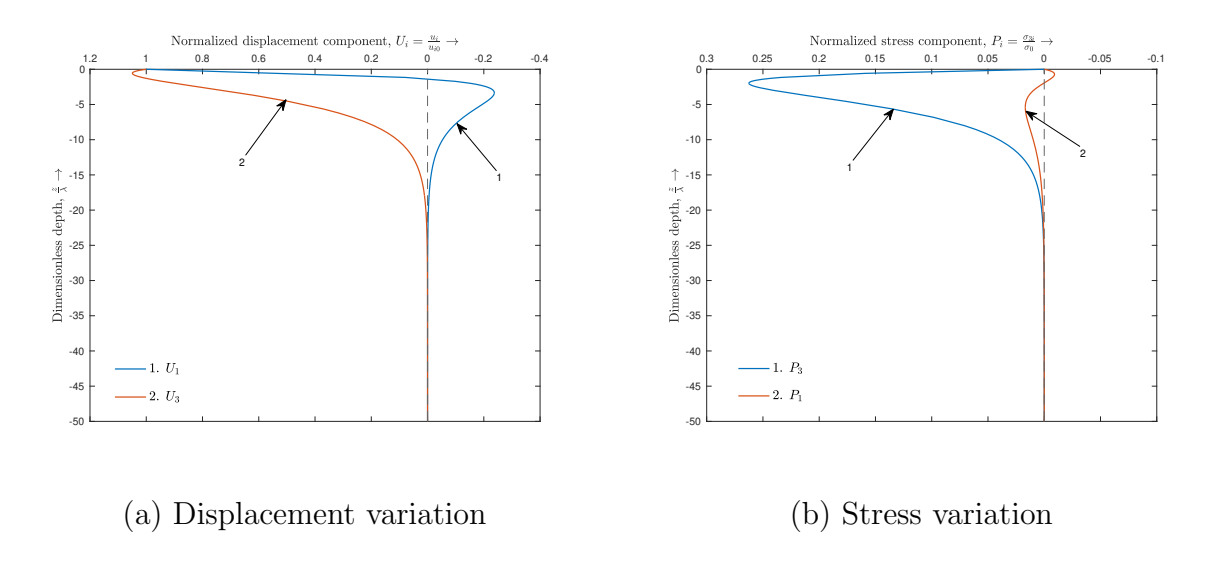


Figure 2.2.11: Normalized (a) displacement components  $(U_i)$  (b) stress components  $(P_i)$  versus dimensionless depth  $\left(\frac{z}{\Lambda}\right)$  for a quasi-elastic mode of Rayleigh waves in a Poisson solid

to a shallow region near the boundary.

Viscoelastic mode: The complex roots of c obtained for the values of  $\epsilon$  and d lying in the Region I are then studied, and the conditions for which these complex roots will

satisfy the dispersion relation is also determined. The overall idea is similar to that followed for the case of incompressible solid semi-infinite medium.

Observe, when  $\epsilon = 0.06$  and d = 0.8, the complex roots of the dispersion relation given in Eq. (2.2.27) are

$$c_1 = 1.71403 - 0.0122788 i,$$
  
 $c_2 = 1.71403 + 0.0122788 i.$ 

Note that, the root  $c_1$  and  $c_2$  satisfy the exact dispersion relation given in Eq. (2.2.11), respectively when

$$0 < \delta a < 0.0501532, \ 0 < \delta a < 0.356779.$$
 (2.2.31)

As a result, there is a possibility of the propagation of two viscoelastic modes of Rayleigh waves when the condition in Eq. (2.2.31) is satisfied.

However, when  $\epsilon = 0.02$  and d = 0.2, the complex roots of Eq. (2.2.27) are

$$c_1 = 1.58115 - 0.232087 i,$$
  
 $c_2 = 1.58115 - 0.232087 i.$ 

Careful observation reveals that only one of the roots among  $c_1$  and  $c_2$  satisfies the exact dispersion relation given in Eq. (2.2.11), provided that  $0.0481324 < \delta a < 1.21068$ .

Therefore, it can be inferred that a specific set of parameters determines the number of possible viscoelastic modes of Rayleigh waves propagating in a nonlocal micropolar viscoelastic medium.

Further, we turn to graphical analysis to deepen our understanding of the problem at hand. By plotting various graphs, we can provide valuable insights into the behavior and trends within the system.

The plot of Figure 2.2.12 determines the range of values for  $\epsilon$  and d for which the viscoelastic modes of the Rayleigh wave fields can propagate. This propagation can take place only when certain conditions on  $\delta a$  are satisfied. The entire plot area is divided into three regions: Region III and Region IV depicting the possible parameter combinations of  $\epsilon$  and d where only one and two viscoelastic modes can propagate, respectively. Region V offers insight into the parameter range where viscoelastic modes are absent and is

equivalent to Region II in Figure 2.2.7. It can also be inferred that the possibility of obtaining two viscoelastic modes increases for larger values of parameter combinations.

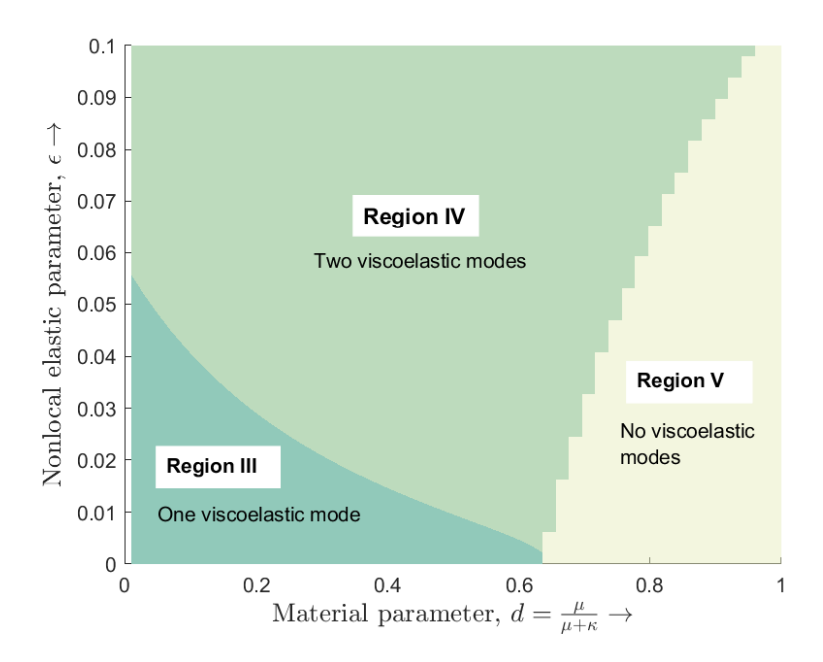


Figure 2.2.12: Regions indicating the range of values of  $\epsilon$  and d for the possible number of viscoelastic modes

While Region III in Figure 2.2.12 provides information on potential parameter combinations of  $\epsilon$  and d, it remains necessary to determine the conditions on  $\delta a$  for which the propagation of only one viscoelastic mode of Rayleigh wave fields can occur. Figure 2.2.13 elaborates on the propagation of this viscoelastic mode by plotting the values of  $\delta a$  against material parameter d for different values of  $\epsilon$ . When  $\epsilon$  and d are fixed, there is a certain minimum and maximum value for  $\delta a$ , and the mode propagation occurs when the value lies within that range. It is also interesting to observe that the range of  $\delta a$  for a constant  $\epsilon$  gradually diminishes with decreasing  $\epsilon$ , and it ceases to exist when the value of d falls out of Region III of Figure 2.2.12.

Figure 2.2.14 is plotted to understand the variation of phase velocity with the material parameter  $\frac{\kappa}{\mu}$  within Region III, where only one viscoelastic mode of Rayleigh wave fields can potentially propagate. By setting a common value of  $\delta a = 0.4$ , it becomes apparent that the phase velocity curve remains nearly consistent across all values of  $\epsilon$ . Although the wave propagates at similar velocities for all  $\epsilon$  values, there exists a limit on the material parameter beyond which propagation is feasible. Magnified images A, B, and C are

provided to distinguish the differences between the curves for different  $\epsilon$ . An intriguing outcome of these findings is that smaller values of the material parameter in the medium can facilitate the propagation of viscoelastic modes with higher velocities, but possible only for smaller values of  $\epsilon$ . In other words, the range of the material parameter for which the propagation is possible decreases with the increase in the value of  $\epsilon$ . Moreover,

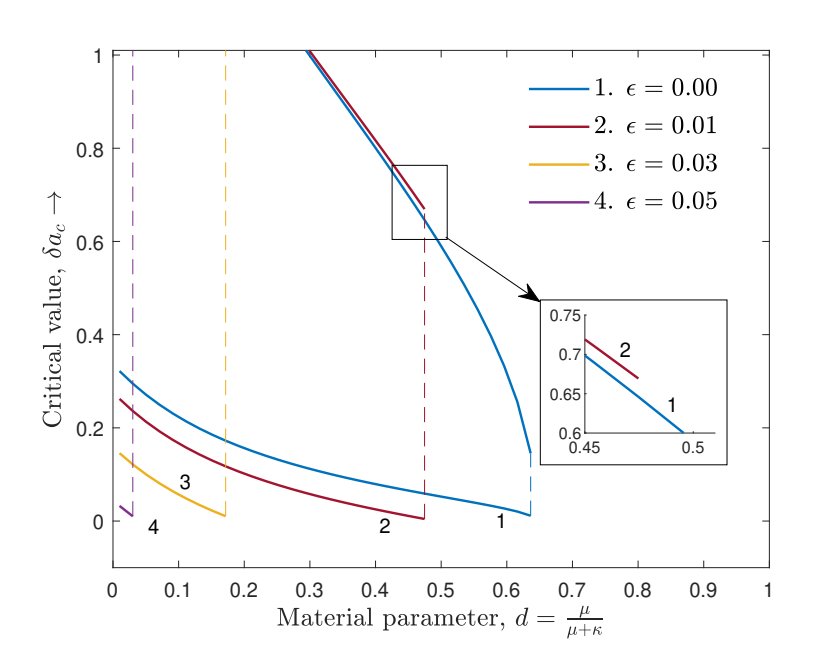


Figure 2.2.13: Variation of values of  $\delta a_c$  with the material parameter d in the Region III (where one viscoelastic mode may propagate)

Figure 2.2.15 is plotted to determine the conditions on  $\delta a$  under which the propagation of the two viscoelastic modes of Rayleigh wave fields may occur. Two distinct intersecting branches of viscoelastic modes are obtained, with one branch corresponding to lower critical values of  $\delta a$  and the other to higher values of  $\delta a$ . Whenever the values of  $\delta a$  fall below this critical value, the viscoelastic mode associated with that specific complex root may propagate. Furthermore, for a fixed d, the critical values of  $\delta a$  corresponding to both the lower and upper branch mode exhibit a significant increase with the increase in the nonlocal parameter,  $\epsilon$ .

To illustrate the relationship between phase velocity and the material parameter  $\frac{\kappa}{\mu}$  for different values of nonlocal parameter,  $\epsilon = 0.03, 0.05, 0.07, 0.09$ . Figure 2.2.16 is plotted while fixing  $\delta a = 0.02$ . This graph offers insights into the propagation of two viscoelastic modes when  $\epsilon$  and d lie within Region IV. Magnified image A describes the variation

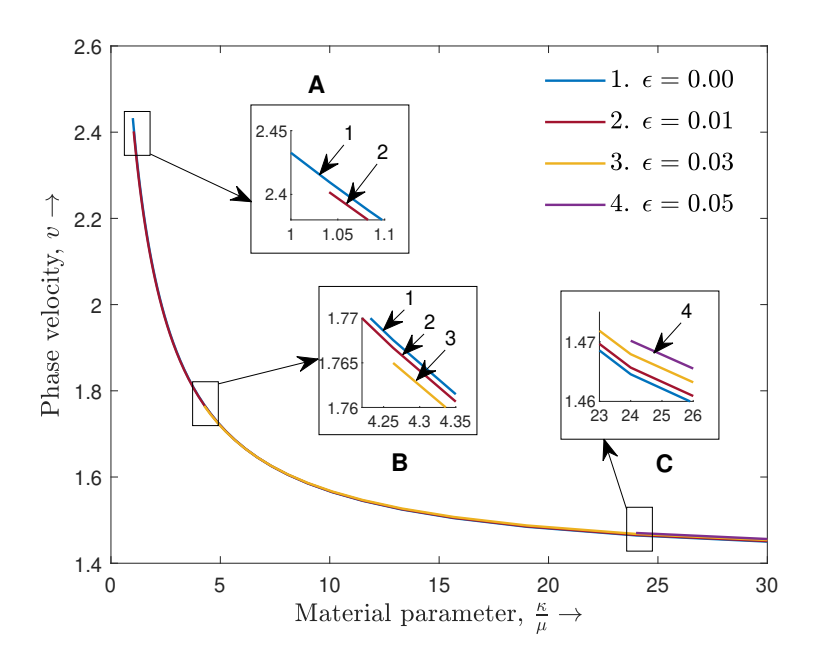


Figure 2.2.14: Variation of phase velocity, v with the material parameter  $\frac{\kappa}{\mu}$  in the Region III (where one viscoelastic mode may propagate)

of phase velocities for the two viscoelastic modes: Mode 1 and Mode 2. Rayleigh wave fields propagating in Mode 2 exhibit slightly higher velocities than Mode 1. Additionally, within each mode, a range of material parameter values  $\frac{\kappa}{\mu}$  exists for every  $\epsilon$  within which propagation occurs. Interestingly, contrary to the behavior observed in Figure 2.2.14, this range of  $\frac{\kappa}{\mu}$  values increases with an increase in values of the nonlocal parameter,  $\epsilon$ . This trend is clearly depicted in magified images B and C.

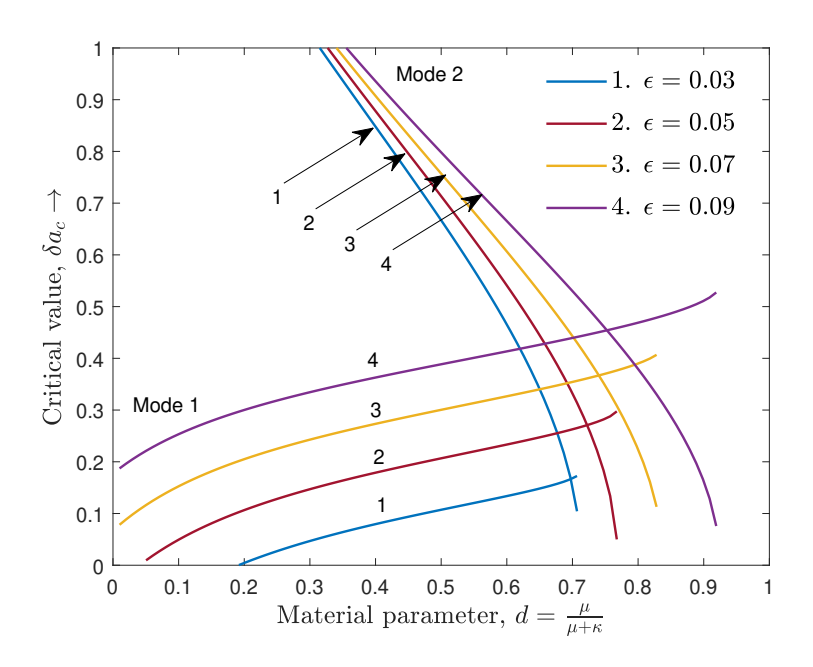


Figure 2.2.15: Variation of values of  $\delta a_c$  with the material parameter d in the Region IV (where two viscoelastic modes may propagate)

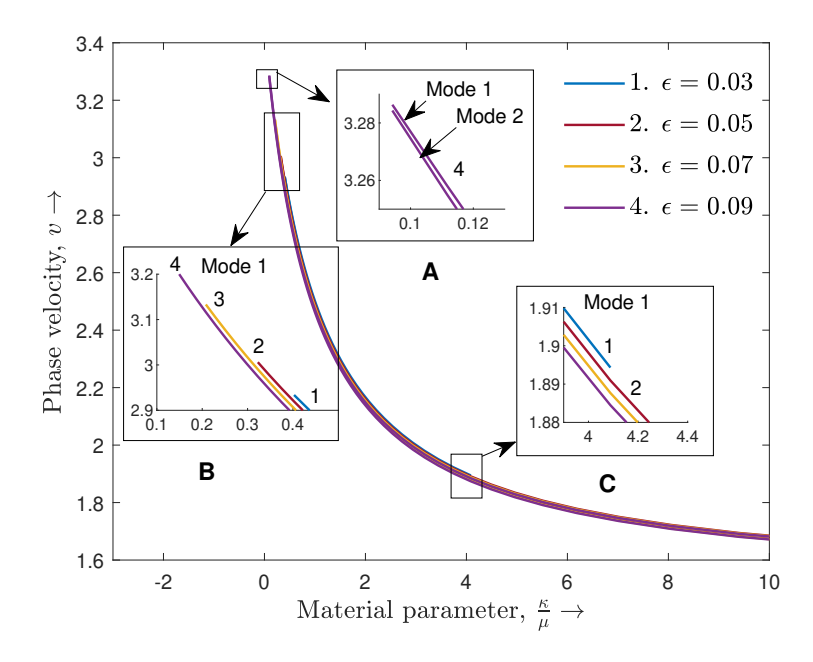
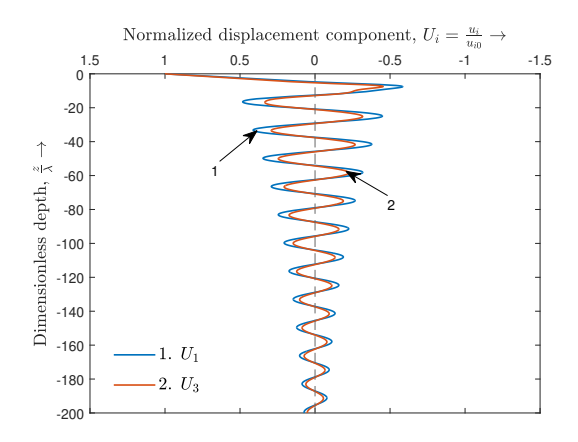
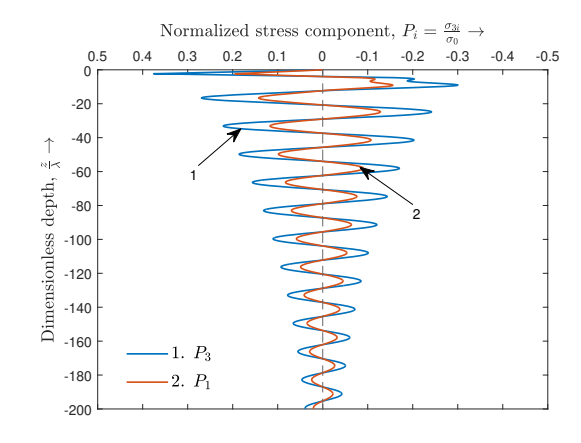


Figure 2.2.16: Variation of phase velocity, v with the material parameter  $\frac{\kappa}{\mu_o}$  in the Region IV (where two viscoelastic modes may propagate)





- (a) Normalized displacement variation
- (b) Normalized stress variation

Figure 2.2.17: Normalized (a) displacement components  $(U_i)$  (b) stress components  $(P_i)$  versus dimensionless depth  $(\frac{z}{\Lambda})$  for a viscoelastic mode of Rayleigh waves in an incompressible solid

Figure 2.2.17 demonstrates that the viscoelastic mode of Rayleigh waves propagating through a Poisson solid exhibit a distinct departure from the previous cases. Unlike the exponential decay observed in the quasi-elastic mode for a Poisson solid, the displacement (Figure 2.2.17a) and stress components (Figure 2.2.17b) in this scenario exhibit a more oscillatory behavior. While the amplitude of these oscillations does diminish with depth, the rate of decay is significantly slower compared to the viscoelastic mode for an incompressible solid. This suggests that the compressibility of the Poisson solid and viscoelastic properties combine to create a more persistent wave field, allowing the oscillations to penetrate deeper into the material.

#### Particle motion

In this section, further analysis will be conducted on the type of particle motion (prograde/retrograde) exhibited by quasi-elastic and viscoelastic modes of Rayleigh wave field particles propagating in a Poisson solid.

The quantities  $A_1(z)$  and  $A_3(z)$  defined in Eq. (2.2.22) are approximated within an error of  $O(\epsilon^2)$  at the surface of a Poisson solid semi-infinite medium to obtain,

$$A_1(0) = A_1 = cs$$
, and  $A_3(0) = A_3 = q_1 - \frac{s^2(c-1)}{q_2}$ . (2.2.32)

Substituting the values of  $q_1$  and  $q_2$  satisfying the exact dispersion relation given in Eq. (2.2.11), we conclude that for Rayleigh waves propagating in a quasi-elastic mode,

$$\mathfrak{Im}(\overline{A_1} A_3) < 0 (> 0)$$
, only when  $1 - c < 0 (> 0)$ .

This indicates that the Rayleigh wave field particles propagating in a nonlocal micropolar Poisson solid exhibit a prograde motion when c > 1 and a retrograde motion when c < 1. Similar to that of an incompressible viscoelastic solid, Rayleigh wave field particles in a nonlocal micropolar Poisson solid exhibit a prograde (retrograde) motion when  $\Re \mathfrak{e}(c) > 1 (< 1)$ , respectively.

#### 2.2.6 Conclusions

This study explores Rayleigh wave propagation in viscoelastic solids under micropolar and nonlocal elastic conditions, revealing multiple wave modes, like, quasi-elastic, viscoelastic, and micropolar—unlike the single mode in classical elasticity. The micropolar mode propagates at higher velocities and exists only due to micropolarity, while nonlocal effects introduce quasi-elastic modes that may not appear otherwise. The study also highlights distinct particle motion behaviors, with quasi-elastic modes exhibiting retrograde motion and viscoelastic modes showing prograde motion. Additionally, viscoelastic modes may travel faster than body waves, whereas quasi-elastic modes propagate at lower velocities. The findings also demonstrate that the number of propagating modes depends on the interplay between nonlocal and material parameters, while surface particle motion remains unaffected. The refined model improves accuracy by addressing boundary layer effects, though its reliance on long-wavelength assumptions limits applicability at shorter wavelengths.

### CHAPTER 3

Rayleigh Wave Propagation in Nonlocal Micropolar Layered  ${\bf Medium}$ 

While nonlocal elasticity theory has enhanced the modeling of wave propagation in homogeneous semi-infinite mediums, extending these formulations to layered media presents significant challenges. This chapter is dedicated to derive refined boundary and interface conditions for Rayleigh waves in layered structures.

# 3.1 Derivation of refined boundary and interface conditions in a nonlocal layered media with an application\*

Here, the focus is on deriving refined boundary and interface conditions for Rayleigh wave propagation in layered media within the framework of nonlocal elasticity and develop effective formulations for nonlocal surface wave propagation.

#### 3.1.1 Mathematical formulations

We analyze a two-layered system as described in Figure 3.1.1 within the framework of nonlocal elasticity. The top layer, a homogeneous, linearly isotropic material of thickness h, occupies the region  $-\infty < x, y < \infty, \ 0 < z \le h$ . Beneath this lies a linearly isotropic semi-infinite medium occupying the region  $-\infty < x, y < \infty, \ -\infty < z \le 0$ , as depicted in Figure 3.1.1

The nonlocal parameters for the lower semi-infinite medium and the upper layer are denoted by  $\aleph_1$  and  $\aleph_2$ , respectively, and are not necessarily the same. The constitutive

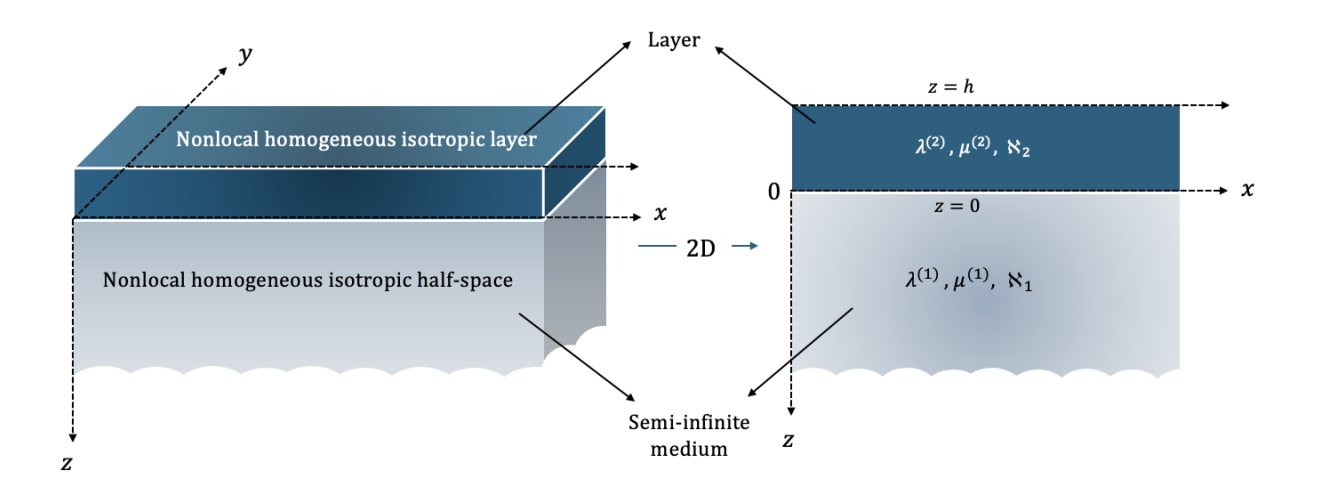


Figure 3.1.1: Geometry of the problem

DOI: 10.1093/imamat/hxaf007

<sup>\*</sup> Published in IMA Journal of Applied Mathematics (Oxford Academic), (2025).

equations (Graff, [2]) describing the elastic behavior of the isotropic, homogeneous layer and semi-infinite medium are given as,

$$\sigma_{jk}^{(n)} = \Lambda^{(n)} \varepsilon_{rr}^{(n)} \delta_{jk} + 2\mu^{(n)} \varepsilon_{jk}^{(n)}, \quad n = 1, 2, \quad j, k, r = 1, 2, 3.$$
 (3.1.1)

In the above expressions, superscripts (1) and (2) refer to the lower semi-infinite medium and upper layer, respectively. The Lamé constants  $\Lambda^{(n)}$ ,  $\mu^{(n)}$  characterize the elastic properties of the respective media, while  $\delta_{jk}$  denotes the Kronecker delta function. Further, the strain tensor  $\varepsilon_{jk}^{(n)}$  is related to the displacement components  $u_k^{(n)}$  through the geometric equation,

$$\varepsilon_{jk}^{(n)} = \frac{1}{2} \left( \frac{\partial u_j^{(n)}}{\partial x_k} + \frac{\partial u_k^{(n)}}{\partial x_j} \right), \quad j, k = 1, 2, 3.$$
 (3.1.2)

To account for nonlocal effects in both the media, the present study adopts the framework of nonlocal elasticity theory. Consequently, the expressions for nonlocal stresses must be established. Following the well-known Eringen's nonlocal elasticity theory [150], the relationship between nonlocal stresses  $\tau_{jk}^{(n)}$  and local stresses  $\sigma_{jk}^{(n)}$  is defined by the singular kernel  $\alpha$  as

$$\tau_{jk}^{(n)}(\vec{x}) = \int_{V} \sigma_{jk}^{(n)}(\vec{x}') \,\alpha(|\vec{x} - \vec{x}'|) \,dV(\vec{x}'), \tag{3.1.3}$$

where V is the volume occupied by the deformed region and  $\alpha$  is the nonlocal kernel that characterizes the material properties and governs the spatial distribution of nonlocal interactions. In this study, a 2D kernel assuming the form of the Bessels function is employed within the framework of Eringen's nonlocal elasticity theory. As a result, the nonlocal stress distributions within both the semi-infinite medium and the layer are expressed through the integral formulations,

$$\tau_{jk}^{(1)} = \frac{1}{2\pi\aleph_1^2} \int_{-\infty}^0 \int_{-\infty}^\infty K_0 \left( \frac{\sqrt{(x-x')^2 + (z-z')^2}}{\aleph_1} \right) \sigma_{jk}^{(1)} (x', z') \, dx' \, dz', \tag{3.1.4}$$

$$\tau_{jk}^{(2)} = \frac{1}{2\pi\aleph_2^2} \int_0^h \int_{-\infty}^\infty K_0 \left( \frac{\sqrt{(x-x')^2 + (z-z')^2}}{\aleph_2} \right) \sigma_{jk}^{(2)} (x', z') \, dx' \, dz'. \tag{3.1.5}$$

It is noteworthy to emphasize the distinct behavior of the lower and upper media despite having identical material properties. This disparity arises from the different integration limits corresponding to the regions occupied by each medium.

Assuming slowly varying local stresses,  $\sigma_{ik}$ , in the x-direction, Eqs. (3.1.4) and (3.1.5)

reduce to the approximate forms derived by Kaplunov et al. [204] as

$$\tau_{jk}^{(1)}(x,z) = \frac{1}{2\aleph_1} \int_{-\infty}^{0} \left\{ \left[ 1 + \frac{\aleph_1^2}{2} \left( 1 + \frac{1}{\aleph_1} |z' - z| \right) \frac{\partial^2}{\partial x^2} \right] \sigma_{jk}^{(1)}(x,z') \right\} e^{-\frac{1}{\aleph_1} |z' - z|} dz', \quad (3.1.6)$$

$$\tau_{jk}^{(2)}(x,z) = \frac{1}{2\aleph_2} \int_0^h \left\{ \left[ 1 + \frac{\aleph_2^2}{2} \left( 1 + \frac{1}{\aleph_2} |z' - z| \right) \frac{\partial^2}{\partial x^2} \right] \sigma_{jk}^{(2)}(x,z') \right\} e^{-\frac{1}{\aleph_2} |z' - z|} dz'. \quad (3.1.7)$$

A differential formulation consistent with the adopted kernel relating nonlocal stresses with local stresses, presented in [60], is as follows:

$$\sigma_{jk}^{(n)} = (1 - \aleph_n^2 \nabla^2) \, \tau_{jk}^{(n)}, \quad n = 1, 2.$$
 (3.1.8)

where  $\nabla^2 = \frac{\partial^2}{\partial x^2} + \frac{\partial^2}{\partial z^2}$  is the Laplacian operator.

For a homogeneous, isotropic elastic medium, the governing equation of motion for non-local elastic wave propagation in the absence of body forces is given by,

$$\tau_{jk,j}^{(n)} - \rho^{(n)} u_{k,tt}^{(n)} = 0, \tag{3.1.9}$$

where  $\rho^{(n)}$ , n = 1, 2 denotes the density of the lower semi-infinite medium and the upper layer, respectively.

#### 3.1.2 Equivalence conditions

This section focuses on deriving the additional boundary conditions required at the interface and the stress-free surface to ensure the equivalence between the integral and differential formulations of the nonlocal elasticity model. By rigorously establishing these conditions, we aim to accurately capture the influence of nonlocal interactions on the elastic behavior of the solid.

#### In the lower nonlocal elastic semi-infinite medium

The nonlocal stresses  $\tau_{jk}^{(1)}$  at the interface z=0 can be given from Eq. (3.1.6) as,

$$\left. \tau_{jk}^{(1)} \right|_{z=0} = \left. \frac{1}{2\aleph_1} \int_{-\infty}^{0} \left\{ \left[ 1 + \frac{\aleph_1^2}{2} \left( 1 - \frac{z'}{\aleph_1} \right) \frac{\partial^2}{\partial x^2} \right] \sigma_{jk}^{(1)}(x, z') \right\} e^{z'/\aleph_1} \, \mathrm{d}z'. \quad (3.1.10)$$

By substituting the differential formulations from Eq. (3.1.8) into Eq. (3.1.10) and subsequently expanding the resulting expressions, we obtain approximate equations under the assumption of a long wavelength relative to the nonlocal elastic parameter of the lower

semi-infinite medium. In other words, we obtain

$$\begin{aligned}
\tau_{jk}^{(1)}\Big|_{z=0} &= \frac{1}{2\aleph_{1}} \int_{-\infty}^{0} \left\{ \left( 1 + \frac{\aleph_{1}^{2}}{2} \left( 1 - \frac{z'}{\aleph_{1}} \right) \frac{\partial^{2}}{\partial x^{2}} \right) \left( 1 - \aleph_{1}^{2} \nabla^{2} \right) \tau_{jk}^{(1)}(x, z') \right\} e^{z'/\aleph_{1}} \, \mathrm{d}z' \\
&= \frac{1}{2\aleph_{1}} \underbrace{\int_{-\infty}^{0} \left\{ \left( 1 - \aleph_{1}^{2} \frac{\partial^{2}}{\partial z^{2}} \right) \tau_{jk}^{(1)}(x, z) \right\} e^{z/\aleph_{1}} \, \mathrm{d}z}_{I_{1}} \\
&+ \frac{1}{2\aleph_{1}} \underbrace{\int_{-\infty}^{0} \left\{ \left( \frac{\aleph_{1}^{3}}{2} \left( z - \aleph_{1} \right) \frac{\partial^{4}}{\partial x^{2} \partial z^{2}} - \frac{\aleph_{1}}{2} \left( z + \aleph_{1} \right) \frac{\partial^{2}}{\partial x^{2}} \right) \tau_{jk}^{(1)}(x, z) \right\} e^{z/\aleph_{1}} \, \mathrm{d}z}.
\end{aligned} \tag{3.1.11}$$

The expansion of the integrals  $I_1$  and  $I_2$  involves lengthy and intricate calculations, ultimately yielding the expressions,

$$I_1 = \left[ \aleph_1 - \aleph_1^2 \frac{\partial}{\partial z} \right] \tau_{jk}^{(1)} \bigg|_{z=0}, \quad I_2 = -\frac{\aleph_1^4}{2} \frac{\partial^3}{\partial x^2 \partial z} \tau_{jk}^{(1)} \bigg|_{z=0}.$$

As a result, Eq. (3.1.11) is simplified to obtain the additional conditions on the nonlocal stresses at the interface z = 0 as,

$$\left[1 + \aleph_1 \frac{\partial}{\partial z} + \frac{\aleph_1^3}{2} \frac{\partial^3}{\partial x^2 \partial z}\right] \left.\tau_{jk}^{(1)}\right|_{z=0} = 0 \tag{3.1.12}$$

#### In the upper nonlocal elastic layer

For the nonlocal elastic layer situated on the top of the nonlocal semi-infinite medium, the equivalence conditions are to be satisfied at both the free surface z = h and the interface z = 0.

Now, at the free surface z = h, the nonlocal stresses  $\tau_{jk}^{(2)}$  can be expressed as,

$$\left. \tau_{jk}^{(2)} \right|_{z=h} = \frac{1}{2\aleph_2} \int_0^h \left\{ \left[ 1 + \frac{\aleph_2^2}{2} \left( 1 - \frac{1}{\aleph_2} \left( z' - h \right) \right) \frac{\partial^2}{\partial x^2} \right] \sigma_{jk}^{(2)}(x, z') \right\} e^{\frac{z' - h}{\aleph_2}} \, \mathrm{d}z'. \tag{3.1.13}$$

Substituting the expressions of differential formulation as given in Eq. (3.1.8) and expanding the integral under the assumption that the nonlocal elastic parameter of the upper

layer is relatively smaller compared to the width of the layer, we obtain the expressions,

$$\begin{aligned}
\tau_{jk}^{(2)}\Big|_{z=h} &= \frac{1}{2\aleph_2} \int_0^h \left\{ \left[ 1 + \frac{\aleph_2^2}{2} \left( 1 - \frac{1}{\aleph_2} \left( z' - h \right) \right) \frac{\partial^2}{\partial x^2} \right] \left( 1 - \aleph_1^2 \nabla^2 \right) \tau_{jk}^{(2)}(x, z') \right\} e^{\frac{z' - h}{\aleph_2}} \, \mathrm{d}z' \\
&= \frac{1}{2\aleph_2} \underbrace{\int_0^h \left\{ \left( 1 - \aleph_2^2 \frac{\partial^2}{\partial z^2} \right) \tau_{jk}^{(2)} \right\} e^{\frac{z - h}{\aleph_2}} \, \mathrm{d}z}_{J_1} \\
&+ \frac{1}{2\aleph_2} \underbrace{\int_0^h \frac{\aleph_2^3}{2} \left( z - \aleph_2 - h \right) \frac{\partial^4 \tau_{jk}^{(2)}}{\partial x^4} e^{\frac{z - h}{\aleph_2}} \, \mathrm{d}z}_{J_2} \\
&+ \frac{1}{2\aleph_2} \underbrace{\int_0^h \left\{ \left( \frac{\aleph_2^3}{2} \left( z - \aleph_2 - h \right) \frac{\partial^4}{\partial x^2 \partial z^2} - \frac{\aleph_2}{2} \left( z + \aleph_2 - h \right) \frac{\partial^2}{\partial x^2} \right) \tau_{jk}^{(2)} \right\} e^{\frac{z - h}{\aleph_2}} \, \mathrm{d}z}.
\end{aligned} \tag{3.1.14}$$

On simplifying and approximating  $J_1$ ,  $J_2$  and  $J_3$ , we obtain the values of these integrals as,

$$\begin{split} J_1 &= \aleph_2 \left[ 1 - \aleph_2 \frac{\partial}{\partial z} \right] \tau_{jk}^{(2)} \bigg|_{z=h} - \aleph_2 \left[ 1 - \aleph_2 \frac{\partial}{\partial z} \right] \tau_{jk}^{(2)} \bigg|_{z=0} e^{-h/\aleph_2}, \\ J_2 &= \left. \frac{\aleph_2^5 h}{4} \frac{\partial^5}{\partial x^4 \partial z} \tau_{jk}^{(2)} \right|_{z=0} e^{-h/\aleph_2}, \\ J_3 &= \left. - \frac{\aleph_2^4}{2} \frac{\partial^3}{\partial x^2 \partial z} \tau_{jk}^{(2)} \right|_{z=h} + \left[ \frac{\aleph_2^3}{2} \left( \aleph_2 + h \right) \frac{\partial^3}{\partial x^2 \partial z} - \frac{\aleph_2^2 h}{2} \frac{\partial^2}{\partial x^2} \right] \tau_{jk}^{(2)} \bigg|_{z=0} e^{-h/\aleph_2}. \end{split}$$

Substituting these expressions into Eq. (3.1.14) results in deriving additional boundary conditions to ensure equivalence. These conditions are thus given by

$$\left[1 + \aleph_2 \frac{\partial}{\partial z} + \frac{\aleph_2^3}{2} \frac{\partial^3}{\partial x^2 \partial z}\right] \tau_{jk}^{(2)} \Big|_{z=h} + \left\{ \left(1 + \frac{\aleph_2 h}{2} \frac{\partial^2}{\partial x^2}\right) \left[1 - \aleph_2 \frac{\partial}{\partial z} - \frac{\aleph_2^3}{2} \frac{\partial^3}{\partial x^2 \partial z}\right] \tau_{jk}^{(2)} \Big|_{z=0} \right\} e^{-h/\aleph_2} = 0.$$
(3.1.15)

Also, the nonlocal stresses in the upper layer at the interface z=0 are given as,

$$\left. \tau_{jk}^{(2)} \right|_{z=0} = \frac{1}{2\aleph_2} \int_0^h \left\{ \left[ 1 + \frac{\aleph_2^2}{2} \left( 1 + \frac{z'}{\aleph_2} \right) \frac{\partial^2}{\partial x^2} \right] \sigma_{jk}^{(2)}(x, z') \right\} e^{-z'/\aleph_2} \, \mathrm{d}z'. \tag{3.1.16}$$

By applying the differential formulation and utilizing an analogous approximation as done previously, additional constraints governing the nonlocal stresses within the upper layer are derived as,

$$\left[1 - \aleph_2 \frac{\partial}{\partial z} - \frac{\aleph_2^3}{2} \frac{\partial^3}{\partial x^2 \partial z}\right] \tau_{jk}^{(2)} \bigg|_{z=0} + \left\{ \left(1 + \frac{\aleph_2 h}{2} \frac{\partial^2}{\partial x^2}\right) \left[1 + \aleph_2 \frac{\partial}{\partial z} + \frac{\aleph_2^3}{2} \frac{\partial^3}{\partial x^2 \partial z}\right] \tau_{jk}^{(2)} \bigg|_{z=h} \right\} e^{-h/\aleph_2} = 0.$$
(3.1.17)

#### 3.1.3 Refined BVP for nonlocally elastic Rayleigh waves

This section focuses on deriving refined boundary and interface conditions for Rayleigh wave propagation in a layered medium composed of an isotropic layer overlying an isotropic elastic semi-infinite medium.

#### Boundary value problem

The governing equations for Rayleigh waves propagating along the x-direction in an isotropic, homogeneous elastic semi-infinite medium and layer characterized with displacement components  $\left(u_1^{(1)}, 0, u_3^{(1)}\right)$  and  $\left(u_1^{(2)}, 0, u_3^{(2)}\right)$ , respectively are expressed as

$$\frac{\partial}{\partial x} \left( \tau_{11}^{(n)} \right) + \frac{\partial}{\partial z} \left( \tau_{31}^{(n)} \right) = \rho^{(n)} \frac{\partial^2 u_1^{(n)}}{\partial t^2}, 
\frac{\partial}{\partial x} \left( \tau_{13}^{(n)} \right) + \frac{\partial}{\partial z} \left( \tau_{33}^{(n)} \right) = \rho^{(n)} \frac{\partial^2 u_3^{(n)}}{\partial t^2},$$
(3.1.18)

subjected to boundary and continuity conditions

Stress-free conditions: 
$$\begin{cases} \tau_{31}^{(2)} = 0, \\ \tau_{33}^{(2)} = 0, \end{cases}$$
 at  $z = h$  (3.1.19)

Continuity conditions: 
$$\begin{cases} \tau_{31}^{(1)} = \tau_{31}^{(2)}, \ \tau_{33}^{(1)} = \tau_{33}^{(2)}, \\ u_1^{(1)} = u_1^{(2)}, \ u_3^{(1)} = u_3^{(2)} \end{cases}$$
 at  $z = 0$  (3.1.20)

It is important to note that not all additional conditions derived for the nonlocal stresses in Eqs. (3.1.12), (3.1.15) and (3.1.17) can be simultaneously satisfied within the problem. Given the pre-existing constraints on  $\tau_{31}^{(n)}$  and  $\tau_{33}^{(n)}$ , we assume that equivalence is established solely for the nonlocal stress component  $\tau_{11}^{(n)}$ . Consequently, the additional conditions imposed on the problem are,

$$\left[1 + \aleph_1 \frac{\partial}{\partial z} + \frac{\aleph_1^3}{2} \frac{\partial^3}{\partial x^2 \partial z}\right] \tau_{11}^{(1)} \bigg|_{z=0} = 0, \tag{3.1.21}$$
 
$$\left[1 + \aleph_2 \frac{\partial}{\partial z} + \frac{\aleph_2^3}{2} \frac{\partial^3}{\partial x^2 \partial z}\right] \tau_{11}^{(2)} \bigg|_{z=h} + \left(1 + \frac{\aleph_2 h}{2} \frac{\partial^2}{\partial x^2}\right) \left[1 - \aleph_2 \frac{\partial}{\partial z} - \frac{\aleph_2^3}{2} \frac{\partial^3}{\partial x^2 \partial z}\right] \tau_{11}^{(2)} \bigg|_{z=0} e^{-h/\aleph_2} = 0, \tag{3.1.22}$$
 
$$\left[1 - \aleph_2 \frac{\partial}{\partial z} - \frac{\aleph_2^3}{2} \frac{\partial^3}{\partial x^2 \partial z}\right] \tau_{11}^{(2)} \bigg|_{z=0} + \left(1 + \frac{\aleph_2 h}{2} \frac{\partial^2}{\partial x^2}\right) \left[1 + \aleph_2 \frac{\partial}{\partial z} + \frac{\aleph_2^3}{2} \frac{\partial^3}{\partial x^2 \partial z}\right] \tau_{11}^{(2)} \bigg|_{z=h} e^{-h/\aleph_2} = 0. \tag{3.1.23}$$

#### Asymptotic analysis

The asymptotic behavior of the solution can be efficiently analyzed by introducing small, naturally occurring parameters

$$\epsilon_1 = \frac{\aleph_1}{\lambda} \ll 1, \quad \epsilon_2 = \frac{\aleph_2}{h} \ll 1,$$

of same orders, where l is the typical wavelength of the propagating wave and h is the thickness of the upper layer.

Also, we define dimensionless variables,

$$\chi = \frac{x}{\lambda}, \ \varkappa_s = \frac{z}{h}, \ \varkappa_f^{(n)} = \frac{z}{\aleph_n}, \ \tau = \frac{c_2^{(1)}}{\lambda}t, \ \eta = \frac{h}{\lambda}, \ \gamma = \left(\frac{c_2^{(2)}}{c_2^{(1)}}\right)^2$$
(3.1.24)

and dimensionless quantities

$$\widetilde{\tau}_{jk}^{(n)} = \frac{\tau_{jk}^{(n)}}{\mu^{(n)}}, \ \widetilde{\sigma}_{jk}^{(n)} = \frac{\sigma_{jk}^{(n)}}{\mu^{(n)}}, \ \widetilde{u}_{1}^{(n)} = \frac{u_{1}^{(n)}}{\lambda}, \ \widetilde{u}_{i}^{(n)} = \frac{u_{i}^{(n)}}{h}, \ i = 1, 3.$$

$$(3.1.25)$$

Here,  $\varkappa_f^{(n)}$  represents the fast variable capturing the rapid oscillations of wave behavior, while  $\varkappa_s$  denotes the slow variable, characterizing the gradual evolution of the wave during propagation. The scales are introduced to capture the effects of the boundary layer on wave behavior.

As a result, the boundary value problem governing the propagation of Rayleigh-like waves in a layered media can be re-written as,

$$\frac{\partial}{\partial \chi} \left( \widetilde{\tau}_{11}^{(n)} \right) + \frac{1}{\eta} \frac{\partial}{\partial \varkappa_{s}} \left( \widetilde{\tau}_{31}^{(n)} \right) + \frac{\eta^{1-n}}{\epsilon_{n}} \frac{\partial}{\partial \varkappa_{f}^{(n)}} \left( \widetilde{\tau}_{31}^{(n)} \right) = \gamma^{(1-n)} \frac{\partial^{2} \widetilde{u}_{1}^{(n)}}{\partial \widetilde{\tau}^{2}}, 
\frac{\partial}{\partial \chi} \left( \widetilde{\tau}_{13}^{(n)} \right) + \frac{1}{\eta} \frac{\partial}{\partial \varkappa_{s}} \left( \widetilde{\tau}_{33}^{(n)} \right) + \frac{\eta^{1-n}}{\epsilon_{n}} \frac{\partial}{\partial \varkappa_{f}^{(n)}} \left( \widetilde{\tau}_{33}^{(n)} \right) = \eta \gamma^{(1-n)} \frac{\partial^{2} \widetilde{u}_{1}^{(n)}}{\partial \widetilde{\tau}^{2}},$$
(3.1.26)

with

$$\left(1 - \epsilon_n^2 \left(\eta^2\right)^{n-1} \left(\frac{\partial^2}{\partial \chi^2} + \frac{1}{\eta^2} \frac{\partial^2}{\partial \varkappa_s^2} + \frac{\left(\eta^2\right)^{1-n}}{\epsilon_n^2} \frac{\partial^2}{\partial \varkappa_f^{(n)^2}} + \frac{2}{\eta^{2-n} \epsilon_n} \frac{\partial^2}{\partial \varkappa_s} \frac{\partial^2}{\partial \varkappa_f^{(n)}}\right)\right) \widetilde{\tau}_{jk}^{(n)} = \widetilde{\sigma}_{jk}^{(n)}, \quad (3.1.27)$$

subjected to boundary and interface conditions,

$$\widetilde{\tau}_{31}^{(2)} = 0, \ \widetilde{\tau}_{33}^{(2)} = 0, \quad \text{at } \varkappa_s = 1, \ \varkappa_f = \frac{1}{\epsilon_2}$$
 (3.1.28)

$$\widetilde{\tau}_{31}^{(1)} = \mu^{-1} \, \widetilde{\tau}_{31}^{(2)}, \ \widetilde{\tau}_{33}^{(1)} = \mu^{-1} \, \widetilde{\tau}_{33}^{(2)}, 
\widetilde{u}_{1}^{(1)} = \widetilde{u}_{1}^{(2)}, \ \widetilde{u}_{3}^{(1)} = \widetilde{u}_{3}^{(2)},$$
at  $\varkappa_{s} = 0, \ \varkappa_{f} = 0$  (3.1.29)

in which  $\mu = \frac{\mu^{(1)}}{\mu^{(2)}}$  along with the additional conditions

$$\begin{bmatrix}
1 + \frac{\partial}{\partial \varkappa_{f}^{(1)}} + \frac{\epsilon_{1}}{\eta} \frac{\partial}{\partial \varkappa_{s}} + \frac{1}{2} \epsilon_{1}^{2} \frac{\partial^{3}}{\partial \chi^{2} \partial \varkappa_{f}^{(1)}} \right] \widetilde{\tau}_{11}^{(1)} \Big|_{\varkappa_{s} = \varkappa_{f} = 0} = 0,$$

$$\begin{bmatrix}
1 + \frac{\partial}{\partial \varkappa_{f}^{(2)}} + \epsilon_{2} \frac{\partial}{\partial \varkappa_{s}} + \frac{1}{2} \eta^{2} \epsilon_{2}^{2} \frac{\partial^{3}}{\partial \chi^{2} \partial \varkappa_{f}^{(2)}} \right] \widetilde{\tau}_{11}^{(2)} \Big|_{\varkappa_{s} = 1, \ \varkappa_{f} = \frac{1}{\epsilon_{2}}}$$

$$+ \left(1 + \frac{\epsilon_{2} \eta^{2}}{2} \frac{\partial^{2}}{\partial \chi^{2}}\right) \left[1 - \frac{\partial}{\partial \varkappa_{f}^{(2)}} - \epsilon_{2} \frac{\partial}{\partial \varkappa_{s}} - \frac{1}{2} \eta^{2} \epsilon_{2}^{2} \frac{\partial^{3}}{\partial \chi^{2} \partial \varkappa_{f}^{(2)}} \right] \widetilde{\tau}_{11}^{(2)} \Big|_{\varkappa_{s} = \varkappa_{f} = 0}$$

$$\begin{bmatrix}
1 - \frac{\partial}{\partial \varkappa_{f}^{(2)}} - \epsilon_{2} \frac{\partial}{\partial \varkappa_{s}} - \frac{1}{2} \eta^{2} \epsilon_{2}^{2} \frac{\partial^{3}}{\partial \chi^{2} \partial \varkappa_{f}^{(2)}} \right] \widetilde{\tau}_{11}^{(2)} \Big|_{\varkappa_{s} = \varkappa_{f} = 0}$$

$$+ \left(1 + \frac{\epsilon_{2} \eta^{2}}{2} \frac{\partial^{2}}{\partial \chi^{2}}\right) \left[1 + \frac{\partial}{\partial \varkappa_{f}^{(2)}} + \epsilon_{2} \frac{\partial}{\partial \varkappa_{s}} + \frac{1}{2} \eta^{2} \epsilon_{2}^{2} \frac{\partial^{3}}{\partial \chi^{2} \partial \varkappa_{f}^{(2)}} \right] \widetilde{\tau}_{11}^{(2)} \Big|_{\varkappa_{s} = 1, \ \varkappa_{f} = \frac{1}{\epsilon_{2}}}$$

$$(3.1.30)$$

Similar to the approach outlined in Chebakov et al. [203], the nonlocal stress components are decomposed into fast and slow components as follows:

$$\widetilde{\tau}_{11}^{(n)} = p_{11}^{(n)} + q_{11}^{(n)}, 
\widetilde{\tau}_{13}^{(n)} = \eta p_{13}^{(n)} + \epsilon_n q_{13}^{(n)}, 
\widetilde{\tau}_{33}^{(n)} = \eta^2 p_{33}^{(n)} + \epsilon_n^2 q_{33}^{(n)}.$$
(3.1.31)

Consequently, the boundary value problem given in Eqs. (3.1.26) and (3.1.27) can be reformulated in terms of slow and fast-varying components, resulting in,

$$\frac{\partial}{\partial \chi} \left( p_{11}^{(n)} \right) + \frac{\partial}{\partial \varkappa_s} \left( p_{31}^{(n)} \right) = \gamma^{1-n} \frac{\partial^2 \tilde{u}_1}{\partial \tilde{\tau}^2}, \quad \frac{\partial}{\partial \chi} \left( q_{11}^{(n)} \right) + \eta^{1-n} \frac{\partial}{\partial \varkappa_f^{(n)}} \left( q_{31}^{(n)} \right) = 0, \\
\frac{\partial}{\partial \chi} \left( p_{13}^{(n)} \right) + \frac{\partial}{\partial \varkappa_s} \left( p_{33}^{(n)} \right) = \gamma^{1-n} \frac{\partial^2 \tilde{u}_3}{\partial \tilde{\tau}^2}, \quad \frac{\partial}{\partial \chi} \left( q_{13}^{(n)} \right) + \eta^{1-n} \frac{\partial}{\partial \varkappa_f^{(n)}} \left( q_{33}^{(n)} \right) = 0,$$
(3.1.32)

together with

$$\left[1 - \epsilon_n^2 \left(\eta^2\right)^{n-1} \left(\frac{\partial^2}{\partial \chi^2} + \frac{1}{\eta^2} \frac{\partial^2}{\partial \varkappa_s^2}\right)\right] p_{11}^{(n)} = \widetilde{\sigma}_{11}^{(n)}, \quad \left[1 - \epsilon_n^2 \left(\eta^2\right)^{n-1} \left(\frac{\partial^2}{\partial \chi^2} + \frac{(\eta^2)^{1-n}}{\epsilon_n^2} \frac{\partial^2}{\partial \varkappa_f^{(n)^2}}\right)\right] q_{11}^{(n)} = 0, \\
\left[1 - \epsilon_n^2 \left(\eta^2\right)^{n-1} \left(\frac{\partial^2}{\partial \chi^2} + \frac{1}{\eta^2} \frac{\partial^2}{\partial \varkappa_s^2}\right)\right] p_{13}^{(n)} = \frac{1}{\eta} \widetilde{\sigma}_{13}^{(n)}, \quad \left[1 - \epsilon_n^2 \left(\eta^2\right)^{n-1} \left(\frac{\partial^2}{\partial \chi^2} + \frac{(\eta^2)^{1-n}}{\epsilon_n^2} \frac{\partial^2}{\partial \varkappa_f^{(n)^2}}\right)\right] q_{13}^{(n)} = 0, \\
\left[1 - \epsilon_n^2 \left(\eta^2\right)^{n-1} \left(\frac{\partial^2}{\partial \chi^2} + \frac{1}{\eta^2} \frac{\partial^2}{\partial \varkappa_s^2}\right)\right] p_{33}^{(n)} = \frac{1}{\eta^2} \widetilde{\sigma}_{33}^{(n)}, \quad \left[1 - \epsilon_n^2 \left(\eta^2\right)^{n-1} \left(\frac{\partial^2}{\partial \chi^2} + \frac{(\eta^2)^{1-n}}{\epsilon_n^2} \frac{\partial^2}{\partial \varkappa_f^{(n)^2}}\right)\right] q_{33}^{(n)} = 0. \right]$$
(3.1.33)

Further, the reformulated constraints in Eqs (3.1.28)–(3.1.30) imposed on the problem are explicitly expressed as

$$\eta \, p_{31}^{(2)} + \epsilon_2 \, q_{31}^{(2)} = 0, 
\eta^2 \, p_{33}^{(2)} + \epsilon_2^2 \, q_{33}^{(2)} = 0.$$
at  $\varkappa_s = 1$ ,  $\varkappa_f = \frac{1}{\epsilon_2}$ 

$$(3.1.34)$$

$$\eta \, p_{31}^{(1)} + \epsilon_1 \, q_{31}^{(1)} = \mu^{-1} \left( \eta \, p_{31}^{(2)} + \epsilon_2 \, q_{31}^{(2)} \right) 
\eta^2 \, p_{33}^{(1)} + \epsilon_1^2 \, q_{33}^{(1)} = \mu^{-1} \left( \eta^2 \, p_{33}^{(2)} + \epsilon_2^2 \, q_{33}^{(2)} \right) 
\widetilde{u}_1^{(1)} = \widetilde{u}_1^{(2)}, \ \widetilde{u}_3^{(1)} = \widetilde{u}_3^{(2)}$$
(3.1.35)

$$\left[1 + \frac{\epsilon_{1}}{\eta} \frac{\partial}{\partial \varkappa_{s}}\right] p_{11}^{(1)} \Big|_{\varkappa_{s}=0} + \left[1 + \frac{\partial}{\partial \varkappa_{f}^{(1)}} + \frac{1}{2} \epsilon_{1}^{2} \frac{\partial^{3}}{\partial \chi^{2} \partial \varkappa_{f}^{(1)}}\right] q_{11}^{(1)} \Big|_{\varkappa_{f}^{(1)}=0} = 0,$$

$$\left[1 + \epsilon_{2} \frac{\partial}{\partial \varkappa_{s}}\right] p_{11}^{(2)} \Big|_{\varkappa_{s}=1} + \left[1 + \frac{\partial}{\partial \varkappa_{f}^{(2)}} + \frac{1}{2} \eta^{2} \epsilon_{2}^{2} \frac{\partial^{3}}{\partial \chi^{2} \partial \varkappa_{f}^{(2)}}\right] q_{11}^{(2)} \Big|_{\varkappa_{f}^{(2)}=\frac{1}{\epsilon_{2}}}$$

$$+ \left(1 + \frac{\epsilon_{2} \eta^{2}}{2} \frac{\partial^{2}}{\partial \chi^{2}}\right) \left[\left(1 - \epsilon_{2} \frac{\partial}{\partial \varkappa_{s}}\right) p_{11}^{(2)} \Big|_{\varkappa_{s}=0} + \left(1 - \frac{\partial}{\partial \varkappa_{f}^{(2)}} - \frac{1}{2} \eta^{2} \epsilon_{2}^{2} \frac{\partial^{3}}{\partial \chi^{2} \partial \varkappa_{f}^{(2)}}\right) q_{11}^{(2)} \Big|_{\varkappa_{f}^{(2)}=0}\right] e^{-1/\epsilon_{2}} = 0,$$

$$\left[1 - \epsilon_{2} \frac{\partial}{\partial \varkappa_{s}}\right] p_{11}^{(2)} \Big|_{\varkappa_{s}=0} + \left[1 - \frac{\partial}{\partial \varkappa_{f}^{(2)}} - \frac{1}{2} \eta^{2} \epsilon_{2}^{2} \frac{\partial^{3}}{\partial \chi^{2} \partial \varkappa_{f}^{(2)}}\right] q_{11}^{(2)} \Big|_{\varkappa_{f}^{(2)}=0}$$

$$+ \left(1 + \frac{\epsilon_{2} \eta^{2}}{2} \frac{\partial^{2}}{\partial \chi^{2}}\right) \left[\left(1 + \epsilon_{2} \frac{\partial}{\partial \varkappa_{s}}\right) p_{11}^{(2)} \Big|_{\varkappa_{s}=1} + \left(1 + \frac{\partial}{\partial \varkappa_{f}^{(2)}} + \frac{1}{2} \eta^{2} \epsilon_{2}^{2} \frac{\partial^{3}}{\partial \chi^{2} \partial \varkappa_{f}^{(2)}}\right) q_{11}^{(2)} \Big|_{\varkappa_{f}^{(2)}=\frac{1}{\epsilon_{2}}}$$

$$(3.1.36)$$

Expanding the following quantities in asymptotic series as,

$$\begin{pmatrix} p_{jk}^{(n)} \\ q_{jk}^{(n)} \\ \tilde{\sigma}_{jk}^{(n)} \\ \tilde{u}_{1}^{(n)} \\ \tilde{u}_{3}^{(n)} \end{pmatrix} = \begin{pmatrix} p_{jk}^{(n,0)} \\ q_{jk}^{(n,0)} \\ \tilde{\sigma}_{jk}^{(n,0)} \\ \tilde{u}_{1}^{(n,0)} \\ \tilde{u}_{3}^{(n,0)} \end{pmatrix} + \epsilon_{n} \begin{pmatrix} p_{jk}^{(n,1)} \\ q_{jk}^{(n,1)} \\ \tilde{\sigma}_{jk}^{(n,1)} \\ \tilde{u}_{1}^{(n,1)} \\ \tilde{u}_{3}^{(n,1)} \end{pmatrix} + \epsilon_{n} \begin{pmatrix} p_{jk}^{(n,2)} \\ q_{jk}^{(n,2)} \\ \tilde{\sigma}_{jk}^{(n,1)} \\ \tilde{u}_{1}^{(n,2)} \\ \tilde{u}_{3}^{(n,2)} \end{pmatrix} + \dots, \text{ for } j, k = 1, 3, \quad (3.1.37)$$

and substituting in the reformulated equations of motion in Eqs. (3.1.32)-(3.1.36), we get

$$\frac{\partial p_{11}^{(n,i)}}{\partial \chi} + \frac{\partial p_{13}^{(n,i)}}{\partial \varkappa_s} = \gamma^{1-n} \frac{\partial^2 \widetilde{u}_1^{(n,i)}}{\partial \widetilde{\tau}^2}, \quad \frac{\partial q_{11}^{(n,i)}}{\partial \chi} + \eta^{1-n} \frac{\partial q_{13}^{(n,i)}}{\partial \varkappa_f^{(n)}} = 0, 
\frac{\partial p_{31}^{(n,i)}}{\partial \chi} + \frac{\partial p_{33}^{(n,i)}}{\partial \varkappa_s} = \gamma^{1-n} \frac{\partial^2 \widetilde{u}_1^{(n,i)}}{\partial \widetilde{\tau}^2}, \quad \frac{\partial q_{31}^{(n,i)}}{\partial \chi} + \eta^{1-n} \frac{\partial q_{33}^{(n,i)}}{\partial \varkappa_f^{(n)}} = 0,$$
(3.1.38)

$$p_{11}^{(n,i)} - \left(\eta^{2}\right)^{n-1} \frac{\partial^{2} p_{11}^{(n,i-2)}}{\partial \chi^{2}} - \left(\eta^{2}\right)^{n-2} \frac{\partial^{2} p_{11}^{(n,i-2)}}{\partial \varkappa_{s}^{2}} = \widetilde{\sigma}_{11}^{(n,i)}, \ q_{11}^{(n,i)} - \frac{\partial^{2} q_{11}^{(n,i)}}{\partial \varkappa_{f}^{(n,i)^{2}}} - \left(\eta^{2}\right)^{n-1} \frac{\partial^{2} q_{11}^{(n,i-2)}}{\partial \chi^{2}} = 0,$$

$$p_{13}^{(n,i)} - \left(\eta^{2}\right)^{n-1} \frac{\partial^{2} p_{13}^{(n,i-2)}}{\partial \chi^{2}} - \left(\eta^{2}\right)^{n-2} \frac{\partial^{2} p_{13}^{(n,i-2)}}{\partial \varkappa_{s}^{2}} = \frac{1}{\eta} \widetilde{\sigma}_{13}^{(n,i)}, \ q_{13}^{(n,i)} - \frac{\partial^{2} q_{13}^{(n,i)}}{\partial \varkappa_{f}^{(n,i)^{2}}} - \left(\eta^{2}\right)^{n-1} \frac{\partial^{2} q_{13}^{(n,i-2)}}{\partial \chi^{2}} = 0,$$

$$p_{33}^{(n,i)} - \left(\eta^{2}\right)^{n-1} \frac{\partial^{2} p_{33}^{(n,i-2)}}{\partial \chi^{2}} - \left(\eta^{2}\right)^{n-2} \frac{\partial^{2} p_{33}^{(n,i-1)}}{\partial \varkappa_{s}^{2}} = \frac{1}{\eta^{2}} \widetilde{\sigma}_{33}^{(n,i)}, \ q_{33}^{(n,i)} - \frac{\partial^{2} q_{33}^{(n,i)}}{\partial \varkappa_{f}^{(n,i)^{2}}} - \left(\eta^{2}\right)^{n-1} \frac{\partial^{2} q_{13}^{(n,i-2)}}{\partial \chi^{2}} = 0,$$

$$(3.1.39)$$

with the local stresses relating to the displacement fields as,

$$\widetilde{\sigma}_{11}^{(n,i)} = \Gamma_n^{-2} \frac{\partial \widetilde{u}_1^{(n,i)}}{\partial \chi} + (\Gamma_n^{-2} - 2) \frac{\partial \widetilde{u}_3^{(n,i)}}{\partial \varkappa_s}, 
\widetilde{\sigma}_{13}^{(n,i)} = \frac{1}{\eta} \frac{\partial \widetilde{u}_1^{(n,i)}}{\partial \varkappa_s} + \eta \frac{\partial \widetilde{u}_3^{(n,i)}}{\partial \chi}, 
\widetilde{\sigma}_{33}^{(n,i)} = (\Gamma_n^{-2} - 2) \frac{\partial \widetilde{u}_1^{(n,i)}}{\partial \chi} + \Gamma_n^{-2} \frac{\partial \widetilde{u}_3^{(n,i)}}{\partial \varkappa_s},$$
(3.1.40)

where  $\Gamma_n = \sqrt{\frac{\mu^{(n)}}{\Lambda^{(n)} + 2\mu^{(n)}}}$  and are subjected to the conditions in asymptotic orders as,

$$\eta \, p_{31}^{(2,i)} + q_{31}^{(2,i-1)} = 0, \ \eta^2 \, p_{33}^{(2,i)} + q_{33}^{(2,i-2)} = 0 \text{ at } \varkappa_s = 1, \ \varkappa_f = \frac{1}{\epsilon_2}$$
(3.1.41)

$$\eta \, p_{31}^{(1,i)} + q_{31}^{(1,i-1)} = \mu^{-1} \left( \eta \, p_{31}^{(2,i)} + q_{31}^{(2,i-1)} \right), 
\eta^{2} \, p_{33}^{(1,i)} + q_{33}^{(1,i-2)} = \mu^{-1} \left( \eta^{2} \, p_{33}^{(2,i)} + q_{33}^{(2,i-2)} \right), 
\widetilde{u}_{1}^{(1,i)} = \widetilde{u}_{1}^{(2,i)}, \ \widetilde{u}_{3}^{(1,i)} = \widetilde{u}_{3}^{(2,i)},$$

$$(3.1.42)$$

$$\left[p_{11}^{(1,i)} + q_{11}^{(1,i)} + \frac{\partial q_{11}^{(1,i)}}{\partial \varkappa_{f}^{(1)}} + \frac{1}{\eta} \frac{\partial p_{11}^{(1,i-1)}}{\partial \varkappa_{s}} + \frac{1}{2} \frac{\partial^{3} q_{11}^{(1,i-2)}}{\partial \chi^{2} \partial \varkappa_{f}^{(1)}}\right]\Big|_{\varkappa_{s} = \varkappa_{f}^{(1)} = 0} = 0,$$

$$\left[p_{11}^{(2,i)} + q_{11}^{(2,i)} + \frac{\partial q_{11}^{(2,i)}}{\partial \varkappa_{f}^{(2)}} + \frac{\partial p_{11}^{(2,i-1)}}{\partial \varkappa_{s}} + \frac{1}{2} \eta^{2} \frac{\partial^{3} q_{11}^{(2,i-2)}}{\partial \chi^{2} \partial \varkappa_{f}^{(2)}}\right]\Big|_{\varkappa_{s} = 1, \ \varkappa_{f}^{(2)} = \frac{1}{\epsilon_{2}}}$$

$$+ \sum_{k=i-1}^{i} \left(\frac{\eta^{2}}{2} \frac{\partial^{2}}{\partial \chi^{2}}\right)^{i-k} \left[p_{11}^{(2,k)} + q_{11}^{(2,k)} - \frac{\partial q_{11}^{(2,k)}}{\partial \varkappa_{f}^{(2)}} - \frac{\partial p_{11}^{(2,k-1)}}{\partial \varkappa_{s}} - \frac{1}{2} \eta^{2} \frac{\partial^{3} q_{11}^{(2,k-2)}}{\partial \chi^{2} \partial \varkappa_{f}^{(2)}}\right]\Big|_{\varkappa_{s} = \varkappa_{f}^{(2)} = 0} e^{-\frac{1}{\epsilon_{2}}} = 0,$$

$$\left[p_{11}^{(2,i)} + q_{11}^{(2,i)} - \frac{\partial q_{11}^{(2,i)}}{\partial \varkappa_{f}^{(2)}} - \frac{\partial p_{11}^{(2,i-1)}}{\partial \varkappa_{s}} - \frac{1}{2} \eta^{2} \frac{\partial^{3} q_{11}^{(2,i-2)}}{\partial \chi^{2} \partial \varkappa_{f}^{(2)}}\right]\Big|_{\varkappa_{s} = \varkappa_{f}^{(2)} = 0}$$

$$+ \sum_{k=i-1}^{i} \left(\frac{\eta^{2}}{2} \frac{\partial^{2}}{\partial \chi^{2}}\right)^{i-k} \left[p_{11}^{(2,k)} + q_{11}^{(2,k)} + \frac{\partial q_{11}^{(2,k)}}{\partial \varkappa_{f}^{(2)}} + \frac{\partial p_{11}^{(2,k-1)}}{\partial \varkappa_{s}} + \frac{1}{2} \eta^{2} \frac{\partial^{3} q_{11}^{(2,k-2)}}{\partial \chi^{2} \partial \varkappa_{f}^{(2)}}\right]\Big|_{\varkappa_{s} = 1, \ \varkappa_{f}^{(2)} = \frac{1}{\epsilon_{2}}}$$

$$(3.1.43)$$

**Leading-order analysis**: Comparing the leading order terms (i = 0) in governing equations, it is easy to obtain

$$q_{jk}^{(1,0)}\left(\chi,\varkappa_f^{(1)}\right) = Q_{jk}^{(1,0)}\left(\chi\right) e^{\varkappa_f^{(1)}},$$
 (3.1.44)

$$q_{jk}^{(2,0)}\left(\chi,\varkappa_{f}^{(2)}\right) = Q_{jk}^{(2,0)}\left(\chi\right) e^{\varkappa_{f}^{(2)}} + \overline{Q}_{jk}^{(2,0)}\left(\chi\right) e^{-\varkappa_{f}^{(2)}}, \tag{3.1.45}$$

where the expressions for  $Q_{jk}^{(n,0)}$ ,  $\overline{Q}_{jk}^{(2,0)}$  are obtained from the conditions in Eq. (3.1.43) as,

$$\begin{split} Q_{11}^{(1,0)} &= -\frac{1}{2} \left. \widetilde{\sigma}_{11}^{(1,0)} \right|_{\varkappa_s = 0}, \; Q_{13}^{(1,0)} &= \frac{1}{2} \left. \frac{\partial}{\partial \chi} \left( \widetilde{\sigma}_{11}^{(1,0)} \right) \right|_{\varkappa_s = 0}, \; Q_{33}^{(1,0)} &= -\frac{1}{2} \left. \frac{\partial^2}{\partial \chi^2} \left( \widetilde{\sigma}_{11}^{(1,0)} \right) \right|_{\varkappa_s = 0} \\ Q_{11}^{(2,0)} &= -\frac{1}{2} \left. \widetilde{\sigma}_{11}^{(2,0)} \right|_{\varkappa_s = 1} e^{-\frac{1}{\epsilon_2}}, \; Q_{13}^{(2,0)} &= \frac{\eta}{2} \left. \frac{\partial}{\partial \chi} \left( \widetilde{\sigma}_{11}^{(2,0)} \right) \right|_{\varkappa_s = 1} e^{-\frac{1}{\epsilon_2}}, \; Q_{33}^{(2,0)} &= -\frac{\eta^2}{2} \left. \frac{\partial^2}{\partial \chi^2} \left( \widetilde{\sigma}_{11}^{(2,0)} \right) \right|_{\varkappa_s = 1} e^{-\frac{1}{\epsilon_2}} \\ \overline{Q}_{11}^{(2,0)} &= -\frac{1}{2} \left. \widetilde{\sigma}_{11}^{(2,0)} \right|_{\varkappa_s = 0}, \; \overline{Q}_{13}^{(2,0)} &= -\frac{\eta}{2} \left. \frac{\partial}{\partial \chi} \left( \widetilde{\sigma}_{11}^{(2,0)} \right) \right|_{\varkappa_s = 0}, \; \overline{Q}_{33}^{(2,0)} &= -\frac{\eta^2}{2} \left. \frac{\partial^2}{\partial \chi^2} \left( \widetilde{\sigma}_{11}^{(2,0)} \right) \right|_{\varkappa_s = 0} \end{split}$$

As a result, the boundary and interface conditions at the leading order become,

$$\widetilde{\sigma}_{31}^{(2,0)} = 0, \ \widetilde{\sigma}_{33}^{(2,0)} = 0 \quad \text{at } \varkappa_s = 1,$$
(3.1.46)

$$\widetilde{\sigma}_{31}^{(1,0)} = \mu^{-1} \, \widetilde{\sigma}_{31}^{(2,0)}, \ \widetilde{\sigma}_{33}^{(1,0)} = \mu^{-1} \, \widetilde{\sigma}_{33}^{(2,0)} 
\widetilde{u}_{1}^{(1,0)} = \widetilde{u}_{1}^{(2,0)}, \ \widetilde{u}_{3}^{(1,0)} = \widetilde{u}_{3}^{(2,0)}$$
at  $\varkappa_{s} = \varkappa_{f} = 0$  (3.1.47)

**First-order analysis**: Similarly, the first-order terms (i = 1) in the governing equations of motion in Eqs. (3.1.38) and (3.1.39) are compared by taking into account Eq. (3.1.43) to obtain

$$q_{jk}^{(1,1)}\left(\chi,\varkappa_f^{(1)}\right) = Q_{jk}^{(1,1)}\left(\chi\right)e^{\varkappa_f^{(1)}},$$
 (3.1.48)

$$q_{jk}^{(2,1)}\left(\chi,\varkappa_{f}^{(2)}\right) = Q_{jk}^{(2,1)}\left(\chi\right) e^{\varkappa_{f}^{(2)}} + \overline{Q}_{jk}^{(2,1)}\left(\chi\right), e^{-\varkappa_{f}^{(2)}}$$
(3.1.49)

where  $Q_{jk}^{(n,1)}$  and  $\overline{Q}_{jk}^{(2,1)}$  attains the value

$$\begin{split} Q_{11}^{(1,1)} &= -\frac{1}{2} \left[ \widetilde{\sigma}_{11}^{(1,1)} + \frac{1}{\eta} \frac{\partial}{\partial \varkappa_s} \left( \widetilde{\sigma}_{11}^{(1,0)} \right) \right] \bigg|_{\varkappa_s = 0}, \\ Q_{13}^{(1,1)} &= \frac{1}{2} \left[ \frac{\partial}{\partial \chi} \left( \widetilde{\sigma}_{11}^{(1,1)} \right) + \frac{1}{\eta} \frac{\partial^2}{\partial \chi \partial \varkappa_s} \left( \widetilde{\sigma}_{11}^{(1,0)} \right) \right] \bigg|_{\varkappa_s = 0}, \\ Q_{33}^{(1,1)} &= -\frac{1}{2} \left[ \frac{\partial^2}{\partial \chi^2} \left( \widetilde{\sigma}_{11}^{(1,1)} \right) + \frac{1}{\eta} \frac{\partial^3}{\partial \chi^2 \partial \varkappa_s} \left( \widetilde{\sigma}_{11}^{(1,0)} \right) \right] \bigg|_{\varkappa_s = 0}, \end{split}$$

$$\begin{split} Q_{11}^{(2,1)} &= -\frac{1}{2} \left[ \widetilde{\sigma}_{11}^{(2,1)} + \frac{\partial}{\partial \varkappa_s} \left( \widetilde{\sigma}_{11}^{(2,0)} \right) \right] \bigg|_{\varkappa_s = 1} e^{-\frac{1}{\epsilon_2}}, \ \ \overline{Q}_{11}^{(2,1)} &= -\frac{1}{2} \left[ \widetilde{\sigma}_{11}^{(2,1)} - \frac{\partial}{\partial \varkappa_s} \left( \widetilde{\sigma}_{11}^{(2,0)} \right) \right] \bigg|_{\varkappa_s = 0}, \\ Q_{13}^{(2,1)} &= \frac{\eta}{2} \left[ \frac{\partial}{\partial \chi} \left( \widetilde{\sigma}_{11}^{(2,1)} \right) + \frac{\partial^2}{\partial \chi \partial \varkappa_s} \left( \widetilde{\sigma}_{11}^{(2,0)} \right) \right] \bigg|_{\varkappa_s = 1} e^{-\frac{1}{\epsilon_2}}, \ \ \overline{Q}_{13}^{(2,1)} &= -\frac{\eta}{2} \left[ \frac{\partial}{\partial \chi} \left( \widetilde{\sigma}_{11}^{(2,1)} \right) - \frac{\partial^2}{\partial \chi \partial \varkappa_s} \left( \widetilde{\sigma}_{11}^{(2,0)} \right) \right] \bigg|_{\varkappa_s = 0}, \\ Q_{33}^{(2,1)} &= -\frac{\eta^2}{2} \left[ \frac{\partial^2}{\partial \chi^2} \left( \widetilde{\sigma}_{11}^{(2,1)} \right) + \frac{\partial^3}{\partial \chi^2 \partial \varkappa_s} \left( \widetilde{\sigma}_{11}^{(2,0)} \right) \right] \bigg|_{\varkappa_s = 0}, \\ &= -\frac{1}{\epsilon_2} \left[ \widetilde{\sigma}_{13}^{(2,1)} \left( \widetilde{\sigma}_{11}^{(2,1)} \right) + \frac{\partial^3}{\partial \chi^2 \partial \varkappa_s} \left( \widetilde{\sigma}_{11}^{(2,0)} \right) \right] \bigg|_{\varkappa_s = 0}, \end{aligned}$$

Consequently, on neglecting the exponentially smaller terms, the boundary and interface conditions for the propagation of Rayleigh waves in a layered medium at the first-order take the form,

$$\widetilde{\sigma}_{31}^{(2,1)} + \frac{\eta}{2} \frac{\partial}{\partial \chi} \left( \widetilde{\sigma}_{11}^{(2,0)} \right) = 0, \ \widetilde{\sigma}_{33}^{(2,1)} = 0 \text{ at } \varkappa_s = 1$$
 (3.1.50)

$$\widetilde{\sigma}_{31}^{(1,1)} + \frac{1}{2} \frac{\partial}{\partial \chi} \left( \widetilde{\sigma}_{11}^{(1,0)} \right) = \mu^{-1} \left( \widetilde{\sigma}_{31}^{(2,1)} - \frac{\eta}{2} \frac{\partial}{\partial \chi} \left( \widetilde{\sigma}_{11}^{(2,0)} \right) \right), 
\widetilde{\sigma}_{33}^{(1,1)} = \mu^{-1} \widetilde{\sigma}_{33}^{(2,1)}, 
\widetilde{u}_{1}^{(1,1)} = \widetilde{u}_{1}^{(2,1)}, \ \widetilde{u}_{3}^{(1,1)} = \widetilde{u}_{3}^{(2,1)}.$$
at  $\varkappa_{s} = 0$  (3.1.51)

**Second-order analysis**: Note that at the second order (i = 2), the equations in Eq. (3.1.39) can be written as,

$$p_{11}^{(n,2)} = \widetilde{\sigma}_{11}^{(n,2)} + (\eta^{2})^{n-1} \frac{\partial^{2}}{\partial \chi^{2}} \left( \widetilde{\sigma}_{11}^{(n,0)} \right) + (\eta^{2})^{n-2} \frac{\partial^{2}}{\partial \varkappa_{s}^{2}} \left( \widetilde{\sigma}_{11}^{(n,0)} \right),$$

$$p_{13}^{(n,2)} = \frac{1}{\eta} \left[ \widetilde{\sigma}_{13}^{(n,2)} + (\eta^{2})^{n-1} \frac{\partial^{2}}{\partial \chi^{2}} \left( \widetilde{\sigma}_{13}^{(n,0)} \right) + (\eta^{2})^{n-2} \frac{\partial^{2}}{\partial \varkappa_{s}^{2}} \left( \widetilde{\sigma}_{13}^{(n,0)} \right) \right],$$

$$p_{33}^{(n,2)} = \frac{1}{\eta^{2}} \left[ \widetilde{\sigma}_{33}^{(n,2)} + (\eta^{2})^{n-1} \frac{\partial^{2}}{\partial \chi^{2}} \left( \widetilde{\sigma}_{33}^{(n,0)} \right) + (\eta^{2})^{n-2} \frac{\partial^{2}}{\partial \varkappa_{s}^{2}} \left( \widetilde{\sigma}_{33}^{(n,0)} \right) \right].$$

$$(3.1.52)$$

Substituting these expressions into the equations of motion in Eq. (3.1.38), we get the second-order refined equations of motion in terms of local stresses as,

$$\frac{\partial}{\partial \chi} \left( \widetilde{\sigma}_{11}^{(n,2)} \right) + \frac{1}{\eta} \frac{\partial}{\partial \varkappa_s} \left( \widetilde{\sigma}_{13}^{(n,2)} \right) = \gamma^{1-n} \left[ \frac{\partial^2 \widetilde{u}_1^{(n,2)}}{\partial \widehat{\tau}^2} - \left( (\eta^2)^{n-2} \frac{\partial^2}{\partial \varkappa_s^2} + (\eta^2)^{n-1} \frac{\partial^2}{\partial \chi^2} \right) \frac{\partial^2 \widetilde{u}_1^{(n,0)}}{\partial \widehat{\tau}^2} \right],$$

$$\frac{\partial}{\partial \chi} \left( \widetilde{\sigma}_{13}^{(n,2)} \right) + \frac{1}{\eta} \frac{\partial}{\partial \varkappa_s} \left( \widetilde{\sigma}_{33}^{(n,2)} \right) = \eta \, \gamma^{1-n} \left[ \frac{\partial^2 \widetilde{u}_3^{(n,2)}}{\partial \widehat{\tau}^2} - \left( (\eta^2)^{n-2} \frac{\partial^2}{\partial \varkappa_s^2} + (\eta^2)^{n-1} \frac{\partial^2}{\partial \chi^2} \right) \frac{\partial^2 \widetilde{u}_1^{(n,0)}}{\partial \widehat{\tau}^2} \right].$$

$$(3.1.53)$$

Further, the second-order refined boundary conditions at the surface  $\varkappa_s = 1$  can be derived as,

$$\widetilde{\sigma}_{31}^{(2,2)} + \frac{\eta}{2} \frac{\partial}{\partial \chi} \left( \widetilde{\sigma}_{11}^{(2,1)} \right) + \frac{\eta}{2} \frac{\partial^{2}}{\partial \chi \partial \varkappa_{s}} \left( \widetilde{\sigma}_{11}^{(2,0)} \right) + \frac{\partial^{2}}{\partial \varkappa_{s}^{2}} \left( \widetilde{\sigma}_{31}^{(2,0)} \right) + \eta^{2} \frac{\partial^{2}}{\partial \chi^{2}} \left( \widetilde{\sigma}_{31}^{(2,0)} \right) = 0, 
\widetilde{\sigma}_{33}^{(2,2)} + \frac{\partial^{2}}{\partial \varkappa_{s}^{2}} \left( \widetilde{\sigma}_{33}^{(2,0)} \right) + \eta^{2} \frac{\partial^{2}}{\partial \chi^{2}} \left( \widetilde{\sigma}_{33}^{(2,0)} \right) - \frac{\eta^{2}}{2} \frac{\partial^{2}}{\partial \chi^{2}} \left( \widetilde{\sigma}_{11}^{(2,0)} \right) = 0,$$

$$(3.1.54)$$

and the refined continuity conditions at the interface  $\varkappa_s = 0$  can be given as,

$$\begin{split} &\widetilde{\sigma}_{31}^{(1,2)} + \frac{1}{2} \frac{\partial}{\partial \chi} \left( \widetilde{\sigma}_{11}^{(1,1)} \right) + \frac{1}{\eta^2} \frac{\partial^2}{\partial \varkappa_s^2} \left( \widetilde{\sigma}_{31}^{(1,0)} \right) + \frac{\partial}{\partial \chi^2} \left( \widetilde{\sigma}_{31}^{(1,0)} \right) + \frac{1}{2\eta} \frac{\partial^2}{\partial \chi \partial \varkappa_s} \left( \widetilde{\sigma}_{11}^{(1,0)} \right) \\ &= \mu^{-1} \left[ \widetilde{\sigma}_{31}^{(2,2)} - \frac{\eta}{2} \frac{\partial}{\partial \chi} \left( \widetilde{\sigma}_{11}^{(2,1)} \right) + \frac{\partial^2}{\partial \varkappa_s^2} \left( \widetilde{\sigma}_{31}^{(2,0)} \right) + \eta^2 \frac{\partial}{\partial \chi^2} \left( \widetilde{\sigma}_{31}^{(2,0)} \right) + \frac{\eta}{2} \frac{\partial^2}{\partial \chi \partial \varkappa_s} \left( \widetilde{\sigma}_{11}^{(2,0)} \right) \right] (3.1.55) \\ &\widetilde{\sigma}_{33}^{(1,2)} - \frac{1}{2} \frac{\partial^2}{\partial \chi^2} \left( \widetilde{\sigma}_{11}^{(1,0)} \right) + \frac{1}{\eta^2} \frac{\partial^2}{\partial \varkappa_s^2} \left( \widetilde{\sigma}_{33}^{(1,0)} \right) + \frac{\partial^2}{\partial \chi^2} \left( \widetilde{\sigma}_{33}^{(1,0)} \right) \\ &= \mu^{-1} \left[ \widetilde{\sigma}_{33}^{(2,2)} - \frac{\eta^2}{2} \frac{\partial^2}{\partial \chi^2} \left( \widetilde{\sigma}_{11}^{(2,0)} \right) + \frac{\partial^2}{\partial \varkappa_s^2} \left( \widetilde{\sigma}_{33}^{(2,0)} \right) + \eta^2 \frac{\partial^2}{\partial \chi^2} \left( \widetilde{\sigma}_{33}^{(2,0)} \right) \right], \end{aligned} \tag{3.1.56}$$

$$\widetilde{u}_1^{(1,2)} = \widetilde{u}_1^{(2,2)}, \ \widetilde{u}_3^{(1,2)} = \widetilde{u}_3^{(2,2)}. \end{split}$$

#### Refined boundary value problem

Using the fact that  $g^{(n,2)} \approx \frac{1}{\epsilon_n^2} g^{(n,0)}$ ,  $g^{(n,1)} \approx \frac{1}{\epsilon_n} g^{(n)}$  for  $g \in \{\widetilde{\sigma}_{jk}, u_k\}$  for j, k = 1, 3, the boundary value problem for Rayleigh waves propagating in a nonlocal layered medium given in Eqs. (3.1.53)-(3.1.57) can rewritten as,

$$\frac{\partial}{\partial \chi} \left( \widetilde{\sigma}_{11}^{(n)} \right) + \frac{1}{\eta} \frac{\partial}{\partial \varkappa_s} \left( \widetilde{\sigma}_{13}^{(n)} \right) = \gamma^{1-n} \left[ 1 - \epsilon_n^2 \left( \eta^2 \right)^{(n-1)} \left( \frac{\partial^2}{\partial \chi^2} + \frac{1}{\eta^2} \frac{\partial^2}{\partial \varkappa_s^2} \right) \right] \frac{\partial^2 \widetilde{u}_1^{(n)}}{\partial \widetilde{\tau}^2}, \\
\frac{\partial}{\partial \chi} \left( \widetilde{\sigma}_{13}^{(n)} \right) + \frac{1}{\eta} \frac{\partial}{\partial \varkappa_s} \left( \widetilde{\sigma}_{33}^{(n)} \right) = \eta \, \gamma^{1-n} \left[ 1 - \epsilon_n^2 \left( \eta^2 \right)^{(n-1)} \left( \frac{\partial^2}{\partial \chi^2} + \frac{1}{\eta^2} \frac{\partial^2}{\partial \varkappa_s^2} \right) \right] \frac{\partial^2 \widetilde{u}_1^{(n)}}{\partial \widetilde{\tau}^2}, \\
\end{cases} (3.1.58)$$

subjected to the boundary conditions at  $\varkappa_s = 1$  as

$$\widetilde{\sigma}_{31}^{(2)} + \epsilon_2 \left[ \frac{\eta}{2} \frac{\partial}{\partial \chi} \left( \widetilde{\sigma}_{11}^{(2)} \right) \right] + \epsilon_2^2 \left[ \frac{\eta}{2} \frac{\partial^2}{\partial \chi \partial \varkappa_s} \left( \widetilde{\sigma}_{11}^{(2)} \right) + \frac{\partial^2}{\partial \varkappa_s^2} \left( \widetilde{\sigma}_{31}^{(2)} \right) + \eta^2 \frac{\partial^2}{\partial \chi^2} \left( \widetilde{\sigma}_{31}^{(2)} \right) \right] = 0, 
\widetilde{\sigma}_{33}^{(2)} + \epsilon_2^2 \left[ \frac{\partial^2}{\partial \varkappa_s^2} \left( \widetilde{\sigma}_{33}^{(2)} \right) + \eta^2 \frac{\partial^2}{\partial \chi^2} \left( \widetilde{\sigma}_{33}^{(2)} \right) - \frac{\eta^2}{2} \frac{\partial^2}{\partial \chi^2} \left( \widetilde{\sigma}_{11}^{(2)} \right) \right] = 0,$$
(3.1.59)

and assuming  $O\left(\epsilon_1^2\right) \sim O\left(\epsilon_2^2\right)$ , the interface conditions at  $\varkappa_s = 0$ ,

$$\widetilde{\sigma}_{31}^{(1)} + \epsilon_{1} \left[ \frac{1}{2} \frac{\partial}{\partial \chi} \left( \widetilde{\sigma}_{11}^{(1)} \right) \right] + \epsilon_{1}^{2} \left[ \frac{1}{\eta^{2}} \frac{\partial^{2}}{\partial \varkappa_{s}^{2}} \left( \widetilde{\sigma}_{31}^{(1)} \right) + \frac{\partial}{\partial \chi^{2}} \left( \widetilde{\sigma}_{31}^{(1)} \right) + \frac{1}{2\eta} \frac{\partial^{2}}{\partial \chi \partial \varkappa_{s}} \left( \widetilde{\sigma}_{11}^{(1)} \right) \right] \\
= \mu^{-1} \left\{ \widetilde{\sigma}_{31}^{(2)} - \epsilon_{2} \left[ \frac{\eta}{2} \frac{\partial}{\partial \chi} \left( \widetilde{\sigma}_{11}^{(2)} \right) \right] + \epsilon_{2}^{2} \left[ \frac{\partial^{2}}{\partial \varkappa_{s}^{2}} \left( \widetilde{\sigma}_{31}^{(2)} \right) + \eta^{2} \frac{\partial}{\partial \chi^{2}} \left( \widetilde{\sigma}_{31}^{(2)} \right) + \frac{\eta}{2} \frac{\partial^{2}}{\partial \chi \partial \varkappa_{s}} \left( \widetilde{\sigma}_{11}^{(2)} \right) \right] \right\}, \quad (3.1.60)$$

$$\widetilde{\sigma}_{33}^{(1)} + \epsilon_{1}^{2} \left[ -\frac{1}{2} \frac{\partial^{2}}{\partial \chi^{2}} \left( \widetilde{\sigma}_{11}^{(1)} \right) + \frac{1}{\eta^{2}} \frac{\partial^{2}}{\partial \varkappa_{s}^{2}} \left( \widetilde{\sigma}_{33}^{(1)} \right) + \frac{\partial^{2}}{\partial \chi^{2}} \left( \widetilde{\sigma}_{33}^{(1)} \right) \right] \\
= \mu^{-1} \left\{ \widetilde{\sigma}_{33}^{(2)} + \epsilon_{2}^{2} \left[ -\frac{\eta^{2}}{2} \frac{\partial^{2}}{\partial \chi^{2}} \left( \widetilde{\sigma}_{11}^{(2)} \right) + \frac{\partial^{2}}{\partial \varkappa_{s}^{2}} \left( \widetilde{\sigma}_{33}^{(2)} \right) + \eta^{2} \frac{\partial^{2}}{\partial \chi^{2}} \left( \widetilde{\sigma}_{33}^{(2)} \right) \right] \right\}, \quad (3.1.61)$$

$$\widetilde{u}_{1}^{(1)} = \widetilde{u}_{1}^{(2)}, \quad \widetilde{u}_{3}^{(1)} = \widetilde{u}_{3}^{(2)}. \quad (3.1.62)$$

In terms of the original variables, we can re-write all the equations from Eq. (3.1.58)-(3.1.62) as,

$$\frac{\partial}{\partial x} \left( \sigma_{11}^{(n)} \right) + \frac{\partial}{\partial z} \left( \sigma_{13}^{(n)} \right) = \rho^{(n)} \left( 1 - \aleph_n^2 \nabla^2 \right) \frac{\partial^2 u_1^{(n)}}{\partial t^2}, 
\frac{\partial}{\partial x} \left( \sigma_{13}^{(n)} \right) + \frac{\partial}{\partial z} \left( \sigma_{33}^{(n)} \right) = \rho^{(n)} \left( 1 - \aleph_n^2 \nabla^2 \right) \frac{\partial^2 u_3^{(n)}}{\partial t^2},$$
(3.1.63)

subjected to the boundary conditions at z = h as

$$(1 + \aleph_2^2 \nabla^2) \,\sigma_{31}^{(2)} + \frac{\aleph_2}{2} \,\frac{\partial}{\partial x} \left(\sigma_{11}^{(2)}\right) + \frac{\aleph_2^2}{2} \,\frac{\partial^2}{\partial x \,\partial z} \left(\sigma_{11}^{(2)}\right) = 0,$$

$$(1 + \aleph_2^2 \nabla^2) \,\sigma_{33}^{(2)} - \frac{\aleph_2^2}{2} \,\frac{\partial^2}{\partial x^2} \left(\sigma_{11}^{(2)}\right) = 0,$$

$$(3.1.64)$$

and at the interface z = 0 underlying conditions,

$$(1 + \aleph_1^2 \nabla^2) \, \sigma_{31}^{(1)} + \frac{\aleph_1}{2} \, \frac{\partial^2}{\partial x \, \partial z} \left( \sigma_{11}^{(1)} \right) + \frac{\aleph_1^2}{2} \, \frac{\partial^2}{\partial x \, \partial z} \left( \sigma_{11}^{(1)} \right) = \mu^{-1} \left\{ \left( 1 + \aleph_2^2 \nabla^2 \right) \sigma_{31}^{(2)} - \frac{\aleph_2}{2} \, \frac{\partial}{\partial x} \left( \sigma_{11}^{(2)} \right) + \frac{\aleph_2^2}{2} \, \frac{\partial^2}{\partial x \, \partial z} \left( \sigma_{11}^{(2)} \right) \right\},$$
(3.1.65)

$$\left(1 + \aleph_1^2 \nabla^2\right) \sigma_{33}^{(1)} - \frac{\aleph_1^2}{2} \frac{\partial^2}{\partial x^2} \left(\sigma_{11}^{(1)}\right)$$

$$= \mu^{-1} \left\{ \left( 1 + \aleph_2^2 \nabla^2 \right) \sigma_{33}^{(2)} - \frac{\aleph_2^2}{2} \frac{\partial^2}{\partial x^2} \left( \sigma_{11}^{(2)} \right) \right\}, \tag{3.1.66}$$

$$u_1^{(1)} = u_1^{(2)}, \ u_3^{(1)} = u_3^{(2)},$$
 (3.1.67)

where  $\nabla^2 = \frac{\partial^2}{\partial x^2} + \frac{\partial^2}{\partial z^2}$  is the well-known Laplacian operator.

#### 3.1.4 Application

In this section, we investigate a two-dimensional problem on the propagation of Rayleigh waves in an isotropic, homogeneous layer of thickness h overlying a homogeneous isotropic semi-infinite medium.

#### Solution to the problem

As mentioned in section 4.1  $u_1^{(n)}$  and  $u_3^{(n)}$  for n = 1, 2 be the horizontal and vertical displacements of Rayleigh waves the semi-infinite medium (n = 1) and the layer (n = 2), respectively.

A coupled system of differential equations are obtained on using the local stress-strain relations in Eqs. (3.1.1) into the refined equation of motion obtained in Eqs. (3.1.63).

Introduce the potentials  $\phi^{(n)}(x, z, t)$  and  $\psi^{(n)}(x, z, t)$  to decompose the displacement components as,

$$u_1^{(n)} = \frac{\partial \phi^{(n)}}{\partial x} - \frac{\partial \psi^{(n)}}{\partial z}, \ u_3^{(n)} = \frac{\partial \phi^{(n)}}{\partial z} + \frac{\partial \psi^{(n)}}{\partial x}.$$

to decouple the coupled differential equations.

As a result, we get

$$\nabla^{2} \phi^{(n)} = \frac{1}{\left(c_{1}^{(n)}\right)^{2}} \left(1 - \aleph_{n}^{2} \nabla^{2}\right) \frac{\partial^{2} \phi^{(n)}}{\partial t^{2}}, 
\nabla^{2} \psi^{(n)} = \frac{1}{\left(c_{2}^{(n)}\right)^{2}} \left(1 - \aleph_{n}^{2} \nabla^{2}\right) \frac{\partial^{2} \psi^{(n)}}{\partial t^{2}}.$$
(3.1.68)

The solution to these systems in Eq. (3.1.68) are evidently,

for the semi-infinite medium: 
$$\phi^{(1)} = A_1 e^{k\alpha_1 z} e^{i(kx-\omega t)},$$

$$\psi^{(1)} = P_1 e^{k\beta_1 z} e^{i(kx-\omega t)},$$

$$(3.1.69)$$

for the layer: 
$$\phi^{(2)} = [A_2 \sinh(k\alpha_2 z) + B_2 \cosh(k\alpha_2 z)] e^{i(kx - \omega t)},$$
$$\psi^{(2)} = [P_2 \sinh(k\beta_2 z) + Q_2 \sinh(k\beta_2 z)] e^{i(kx - \omega t)},$$
 (3.1.70)

where,

$$\alpha_n = \sqrt{1 - \frac{c^2}{\left(c_1^{(n)}\right)^2 - \aleph_n^2 \omega^2}}, \ \beta_n = \sqrt{1 - \frac{c^2}{\left(c_2^{(n)}\right)^2 - \aleph_n^2 \omega^2}}$$
with  $c_1^{(n)} = \sqrt{\frac{\Lambda^{(n)} + 2\mu^{(n)}}{\rho^{(n)}}}$  and  $c_2^{(n)} = \sqrt{\frac{\mu^{(n)}}{\rho^{(n)}}}$ . (3.1.71)

#### Dispersion relation

Define certain quanties,

$$\alpha_n^{(0)} = \sqrt{1 - \frac{c^2}{\left(c_1^{(n)}\right)^2}}, \ \beta_n^{(0)} = \sqrt{1 - \frac{c^2}{\left(c_2^{(n)}\right)^2}},$$
$$\gamma_n = \frac{1}{2} \left(2 \left(\alpha_n^{(0)}\right)^2 - \left(\beta_n^{(0)}\right)^2 + 1\right), \ \Upsilon_n = \left(\beta_n^{(0)}\right)^2 + 1.$$

Now, on substituting the solution forms in Eqs. (3.1.69) and (3.1.70) into the refined boundary conditions derived in Eqs. (3.1.64)-(3.1.67), the dispersion relation obtained

in terms of nondimensionalized variables within an error of  $O(\epsilon_n^2)$  is as follows:

$$\begin{vmatrix} 0 & 0 & \frac{2i\alpha_{2}^{(0)}\cosh\left(\eta\,\alpha_{2}^{(0)}\right)}{-i\gamma_{2}\eta\epsilon_{2}\sinh\left(\eta\,\alpha_{2}^{(0)}\right)} & \frac{2i\alpha_{2}^{(0)}\sinh\left(\eta\,\alpha_{2}^{(0)}\right)}{-i\gamma_{2}\eta\epsilon_{2}\cosh\left(\eta\,\alpha_{2}^{(0)}\right)} & -\gamma_{2}\sinh\left(\eta\,\beta_{2}^{(0)}\right) & \eta\,\beta_{2}^{(0)}\epsilon_{2}\cosh\left(\eta\,\beta_{2}^{(0)}\right) \\ 0 & 0 & \Upsilon_{2}\sinh\left(\eta\,\alpha_{2}^{(0)}\right) & -i\gamma_{2}\eta\epsilon_{2}\cosh\left(\eta\,\alpha_{2}^{(0)}\right) & -\Sigma_{2}\sinh\left(\eta\,\beta_{2}^{(0)}\right) & 2i\beta_{2}^{(0)}\sinh\left(\eta\,\beta_{2}^{(0)}\right) \\ 2i\alpha_{1}^{(0)} - i\gamma_{1}\epsilon_{1} & -\Upsilon_{1} + \epsilon_{1}\beta_{1}^{(0)} & -2i\alpha_{2}^{(0)}\mu^{-1} & -i\gamma_{2}\eta\,\epsilon_{2}\mu^{-1} & \eta\,\beta_{2}^{(0)}\epsilon_{2}\mu^{-1} & \mu^{-1}\Upsilon_{2} \\ \Upsilon_{1} & 2i\beta_{1}^{(0)} & 0 & -\mu^{-1}\Upsilon_{2} & -2i\beta_{2}^{(0)}\mu^{-1} & 0 \\ i & -\beta_{1}^{(0)} & 0 & -i & \beta_{2}^{(0)} & 0 \\ \alpha_{1}^{(0)} & i & -\alpha_{2}^{(0)} & 0 & 0 & -i \end{vmatrix} = 0$$

$$(3.1.72)$$

Note that Eq. (3.1.72) clearly establishes a relationship between the velocity c of Rayleigh waves and their wavenumber k (or wavelength l), indicating the dispersive nature of Rayleigh waves in a nonlocal layered medium.

Let us introduce the following abbreviations to simply our discussions on the dispersion relation.

$$X = 2\mu - \Upsilon_{2}, \quad W = 2(\mu - 1),$$

$$Y = 2 - \mu \Upsilon_{1}, \quad U = \frac{Z - \gamma_{2} Y}{\left(\beta_{2}^{(0)}\right)^{2} - 1},$$

$$Z = \Upsilon_{2} - \mu \Upsilon_{1}, \quad V = \frac{\beta_{1}^{(0)} (\gamma_{2} W - X)}{\left(\beta_{2}^{(0)}\right)^{2} - 1}.$$
(3.1.73)

As a result, the dispersion relation in Eq. (3.1.72) reduces to,

$$(\eta_{1}\xi_{2} - \eta_{2}\xi_{1}) + \mu \epsilon_{1} \left[ \beta_{2}^{(0)} \xi_{3} \left( \beta_{1}^{(0)} \eta_{1} + \gamma_{1} \eta_{2} \right) - \eta_{3} \left( \beta_{1}^{(0)} \xi_{1} + \gamma_{1} \xi_{2} \right) \right] + \eta \epsilon_{2} \left[ \frac{\beta_{2}^{(0)}}{\alpha_{2}^{(0)}} \left( \eta_{2} \xi_{4} + \eta_{1} \xi_{5} \right) - \eta_{3} \left( \xi_{2} U + \xi_{1} V \right) \right] = 0, \quad (3.1.74)$$

where the expressions for  $\xi_1, \xi_2, \xi_3, \xi_4, \xi_5, \eta_1, \eta_2$  and  $\eta_3$  are given in the Appendix B. The leading-order term in Eq. (3.1.74) yields

$$\eta_1 \xi_2 - \eta_2 \xi_1 = 0, \tag{3.1.75}$$

which corresponds to the dispersion relation of Rayleigh waves in a local, elastic, layered isotropic medium. This result aligns precisely with the well-established formulations and results of Love [270] and Fu [271].

#### 3.1.5 Graphical discussions

The dispersion characteristics of surface waves are fundamental to understanding wave propagation in elastic media. In this section, we present and analyze the dispersion curves obtained from the theoretical model, which provide insights into the relationship between wave velocity and wavenumber (or wavelength). These curves serve as a crucial tool for interpreting the effects nonlocal parameters on wave behavior.

Figure 3.1.2 shows the dispersion curve relating wavenumber to wave velocity for Rayleigh waves in a nonlocal isotropic layer overlying a nonlocal isotropic semi-infinite medium. At lower wavenumbers (long-wavelength regime), the Rayleigh waves perceive the medium as effectively homogeneous, with phase velocity approaching that of the stiffer substrate, as the wave motion extends deeper into it. When the wavelength is long relative to the layer thickness, wave motion concentrates in the softer upper layer, reducing the overall phase velocity. This dispersion, where wave velocity decreases with increasing wavenumber, is further influenced by nonlocal elasticity, which further lowers the phase velocity.

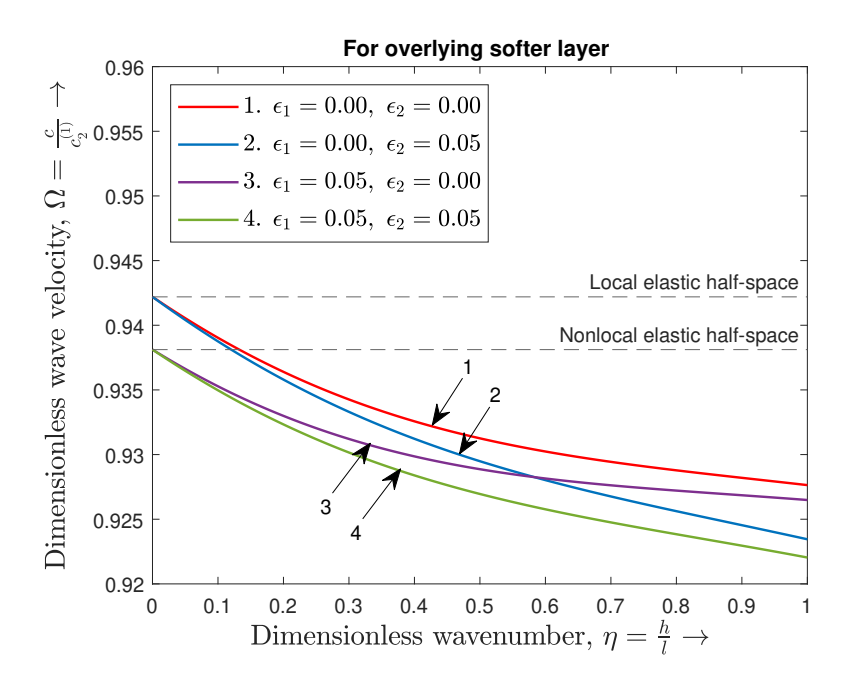


Figure 3.1.2: Dispersion curves for nonlocal elastic Rayleigh waves in an isotropic layered medium

Moreover, the analysis reveals that the nonlocal elasticity effects in the layer are more dominant than those in the semi-infinite medium, a finding that aligns with previous studies. This dominance is likely due to the higher sensitivity of the thinner layer to nonlocal interactions, compared to the more massive semi-infinite medium. The literature corroborates that in layered media, the upper layer's material properties and nonlocal effects have a substantial influence on the overall wave behavior, often overshadowing the contributions from the underlying substrate.

#### 3.1.6 Conclusions

This study derived refined boundary and interface conditions for nonlocal Rayleigh waves in layered media by employing asymptotic analysis and a modified singularly perturbed differential model. The results highlight that nonlocal corrections primarily affect boundary and interface conditions rather than the equations of motion. Refinements in the interface conditions are essential to account for the nonlocal boundary layer developed at the interface. First-order nonlocal corrected dispersion relations were obtained and validated through numerical analysis, demonstrating significant and dominant nonlocal effects in the layer. While the approach aligns well with existing literature, its validity may be limited at scales comparable to the internal size of nonlocal boundary layers, necessitating further advancements in future research.

## 3.2 Extension to nonlocal micropolar elasticity with an application\*

This subsection extends the previous analysis in section 3.1 to analyze the surface wave propagation under the framework of nonlocal micropolar elasticity. Refined boundary and interface conditions, incorporating modifications to couple stress and force stress conditions, are derived to account for boundary and interfacial layer effects.

#### 3.2.1 Mathematical formulation

We examine a two-layer system (provided in Figure 3.2.1) consisting of an isotropic, homogeneous nonlocal micropolar elastic layer of thickness h resting on an isotropic, homogeneous nonlocal micropolar elastic semi-infinite medium. The values in the semi-infinite medium is denoted by script '1', while the values in the layer is denoted by '2'. The z-axis is oriented vertically downwards, with the free surface at z = h and the interface between the two media at z = 0.

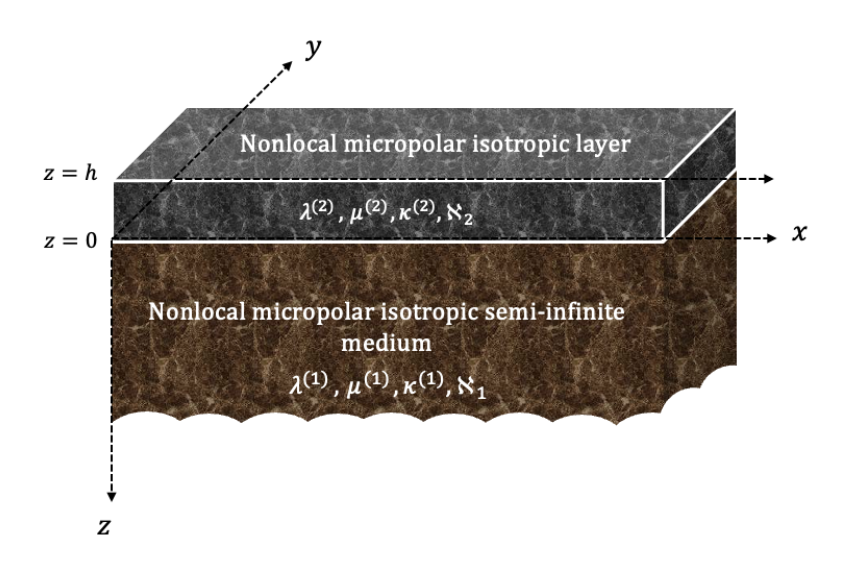


Figure 3.2.1: Geometry of the problem

<sup>\*</sup> Published in Mathematics and Mechanics of Solids (SAGE Publications), (2025).

According to Eringen's theory of nonlocal micropolar elasticity [61], the relationship between nonlocal and local stresses can be expressed through integral equations. Employing kernel of the form given in Eq. (1.3.51), we have,

$$\tau_{mn}^{(i)} = \frac{1}{2\pi\aleph_i^2} \int_{V_i} K_0 \left( \frac{\sqrt{(x-\bar{x})^2 + (z-\bar{z})^2}}{\aleph_i} \right) \sigma_{mn}^{(i)} (\bar{x}, \bar{z}) \, d\bar{x} \, d\bar{z}, 
\pi_{mn}^{(i)} = \frac{1}{2\pi\aleph_i^2} \int_{V_i} K_0 \left( \frac{\sqrt{(x-\bar{x})^2 + (z-\bar{z})^2}}{\aleph_i} \right) \Pi_{mn}^{(i)} (\bar{x}, \bar{z}) \, d\bar{x} \, d\bar{z},$$
(3.2.1)

The superscript i = 1 and i = 2 refers to the quantities for the semi-infinite medium and the upper layer, respectively.

Further, the parameter  $\aleph_i$  denotes the nonlocality parameter for each medium. And the volume where deformation occurs is denoted by  $V_i$ , with i=1,2. Specifically,  $V_1$  corresponds to the region  $-\infty < x < \infty$  and  $-\infty < z \le 0$ , while  $V_2$  corresponds to  $-\infty < x < \infty$  and  $0 \le z \le h$ .

For slowly varying local stresses  $\sigma_{mn}^{(i)}$  and  $\Pi_{mn}^{(i)}$  in the x-direction, Eqs. (3.2.1) reduce to the approximate expressions as presented by Kaplunov et al. [204] for the small nonlocal parameters. As a result, the approximations for the nonlocal force stresses are

$$\tau_{mn}^{(1)}(x,z) = \frac{1}{2\aleph_1} \int_{-\infty}^{0} \left[ 1 + \frac{\aleph_1^2}{2} \left( 1 + \frac{1}{\aleph_1} |\bar{z} - z| \right) \frac{\partial^2}{\partial x^2} \right] \sigma_{mn}^{(1)}(x,\bar{z}) e^{-\frac{1}{\aleph_1} |\bar{z} - z|} d\bar{z}, 
\tau_{mn}^{(2)}(x,z) = \frac{1}{2\aleph_2} \int_{0}^{h} \left[ 1 + \frac{\aleph_2^2}{2} \left( 1 + \frac{1}{\aleph_2} |\bar{z} - z| \right) \frac{\partial^2}{\partial x^2} \right] \sigma_{mn}^{(2)}(x,\bar{z}) e^{-\frac{1}{\aleph_2} |\bar{z} - z|} d\bar{z},$$
(3.2.2)

and for nonlocal couple stresses are given as,

$$\pi_{mn}^{(1)}(x,z) = \frac{1}{2\aleph_1} \int_{-\infty}^{0} \left[ 1 + \frac{\aleph_1^2}{2} \left( 1 + \frac{1}{\aleph_1} |\bar{z} - z| \right) \frac{\partial^2}{\partial x^2} \right] \Pi_{mn}^{(1)}(x,\bar{z}) e^{-\frac{1}{\aleph_1} |\bar{z} - z|} d\bar{z}, 
\pi_{mn}^{(2)}(x,z) = \frac{1}{2\aleph_2} \int_{0}^{h} \left[ 1 + \frac{\aleph_2^2}{2} \left( 1 + \frac{1}{\aleph_2} |\bar{z} - z| \right) \frac{\partial^2}{\partial x^2} \right] \Pi_{mn}^{(2)}(x,\bar{z}) e^{-\frac{1}{\aleph_2} |\bar{z} - z|} d\bar{z}.$$
(3.2.3)

Furthermore, adopting the same two-dimensional kernel as specified in Eq. (3.2.1), the differential model proposed by Eringen [60] establishes the relation between local and non-local stresses as,

$$\begin{aligned}
(1 - \aleph_i^2 \nabla^2) \, \tau_{mn}^{(i)} &= \sigma_{mn}^{(i)}, \\
(1 - \aleph_i^2 \nabla^2) \, \pi_{mn}^{(i)} &= \Pi_{mn}^{(i)},
\end{aligned} \} i = 1, 2.$$
(3.2.4)

Now, the general constitutive equation relating the stress and strain components in a linear micropolar elastic solid are given by,

$$\sigma_{mn}^{(i)} = \mathcal{C}_{mnpq}^{(i)} \, \varepsilon_{pq}^{(i)}, 
\Pi_{mn}^{(i)} = \mathcal{M}_{mnpq}^{(i)} \Gamma_{pq}^{(i)}, 
mathred matrred matrred$$

where  $C_{mnpq}^{(i)}$ ,  $\mathcal{M}_{mnpq}^{(i)}$  are the micropolar elastic stiffness tensors of the corresponding medium.

Also, the strain tensor  $\varepsilon_{pq}^{(i)}$  and the curvature tensor  $\Gamma_{pq}^{(i)}$  are related to the displacement components  $u_j^{(i)}$ , j=1,2,3 and the rotation vector  $\Phi_j$ , j=1,2,3 as,

$$\begin{cases}
\varepsilon_{pq}^{(i)} = u_{q,p}^{(i)} - \epsilon_{qpr} \Phi_r^{(i)}, \\
\Gamma_{pq}^{(i)} = \Phi_{p,q}^{(i)},
\end{cases} p, q, r = 1, 2, 3, \tag{3.2.6}$$

where  $\epsilon_{qpr}$  is the permutation symbol.

In a homogeneous micropolar elastic medium, the governing equation of motion for a nonlocal micropolar elastic wave propagation without body forces is expressed as

$$\tau_{mn,m}^{(i)} - \rho^{(i)} u_{n,tt}^{(i)} = 0, 
\pi_{mn,m}^{(i)} + \epsilon_{npq} \tau_{pq}^{(i)} - j^{(i)} \rho^{(i)} \Phi_{n,tt}^{(i)} = 0,$$
(3.2.7)

in which  $\rho^{(i)}, j^{(i)}$  corresponds to the density and micro-inertia of the each media, respectively.

## 3.2.2 Equivalence conditions

In the next section, we shall derive the additional boundary conditions needed to ensure equivalence between the integral and differential nonlocal micropolar elasticity formulations as described in Eqs. (3.2.2)-(3.2.4). By rigorously establishing these conditions, we aim to accurately model the effects of micropolar and nonlocal elasticity in any layered media.

# In the lower micropolar nonlocal elastic semi-infinite medium

At the interface of the layered media, z=0, the expressions for the nonlocal force and couple stresses,

$$\tau_{mn}^{(1)}\Big|_{z=0} = \frac{1}{2\aleph_{1}} \int_{-\infty}^{0} \left[ 1 + \frac{\aleph_{1}^{2}}{2} \left( 1 - \frac{\bar{z}}{\aleph_{1}} \right) \frac{\partial^{2}}{\partial x^{2}} \right] \sigma_{mn}^{(1)}(x, \bar{z}) e^{\bar{z}/\aleph_{1}} d\bar{z}, 
\pi_{mn}^{(1)}\Big|_{z=0} = \frac{1}{2\aleph_{1}} \int_{-\infty}^{0} \left[ 1 + \frac{\aleph_{1}^{2}}{2} \left( 1 - \frac{\bar{z}}{\aleph_{1}} \right) \frac{\partial^{2}}{\partial x^{2}} \right] \Pi_{mn}^{(1)}(x, \bar{z}) e^{\bar{z}/\aleph_{1}} d\bar{z}.$$
(3.2.8)

Upon substituting the differential formulation given in Eq. (3.2.4), we approximate the first expressions in Eqs. (3.2.2) and (3.2.3) using a methodology similar to that provided in section 3.1 under the assumption of a longer wavelength compared to the nonlocal parameter of the medium, yielding

$$\left[1 + \aleph_1 \frac{\partial}{\partial z} + \frac{\aleph_1^3}{2} \frac{\partial^3}{\partial x^2 \partial z}\right] X^{(1)} \Big|_{z=0} = 0, \tag{3.2.9}$$

for all  $X^{(1)} \in \left\{ \tau_{mn}^{(1)}, \pi_{mn}^{(1)} \right\}$ .

# In the upper micropolar nonlocal elastic layer

It should be noted that for the upper layer of thickness h, the equivalence between the differential and integral nonlocal models must be satisfied at both the surface z = hand the interface z = 0.

Observe that, the nonlocal force and couple stresses at the surface z = h are given as,

$$\begin{aligned}
& \tau_{mn}^{(2)} \Big|_{z=h} = \frac{1}{2\aleph_2} \int_0^h \left[ 1 + \frac{\aleph_2^2}{2} \left( 1 - \frac{1}{\aleph_2} \left( \bar{z} - h \right) \right) \frac{\partial^2}{\partial x^2} \right] \sigma_{mn}^{(2)}(x, \bar{z}) e^{\frac{\bar{z} - h}{\aleph_2}} d\bar{z}, \\
& \pi_{mn}^{(2)} \Big|_{z=h} = \frac{1}{2\aleph_2} \int_0^h \left[ 1 + \frac{\aleph_2^2}{2} \left( 1 - \frac{1}{\aleph_2} \left( \bar{z} - h \right) \right) \frac{\partial^2}{\partial x^2} \right] \Pi_{mn}^{(2)}(x, \bar{z}) e^{\frac{\bar{z} - h}{\aleph_2}} d\bar{z},
\end{aligned} \right\} (3.2.10)$$

and at the interface z = 0 are expressed as,

$$\begin{aligned}
\tau_{mn}^{(2)}\Big|_{z=0} &= \frac{1}{2\aleph_{2}} \int_{0}^{h} \left[ 1 + \frac{\aleph_{2}^{2}}{2} \left( 1 + \frac{\bar{z}}{\aleph_{2}} \right) \frac{\partial^{2}}{\partial x^{2}} \right] \sigma_{mn}^{(2)}(x, \bar{z}) e^{-\bar{z}/\aleph_{2}} d\bar{z}, \\
\pi_{mn}^{(2)}\Big|_{z=0} &= \frac{1}{2\aleph_{2}} \int_{0}^{h} \left[ 1 + \frac{\aleph_{2}^{2}}{2} \left( 1 + \frac{\bar{z}}{\aleph_{2}} \right) \frac{\partial^{2}}{\partial x^{2}} \right] \Pi_{mn}^{(2)}(x, \bar{z}) e^{-\bar{z}/\aleph_{2}} d\bar{z}.
\end{aligned} \right\}$$
(3.2.11)

After rigorous calculations, equivalence conditions are derived at both the surface z = h and the interface z = 0. As a result, we obtain the conditions,

$$\left[1 + \aleph_2 \frac{\partial}{\partial z} + \frac{\aleph_2^3}{2} \frac{\partial^3}{\partial x^2 \partial z}\right] X^{(2)} \bigg|_{z=h} + \left(1 + \frac{\aleph_2 h}{2} \frac{\partial^2}{\partial x^2}\right) \left[1 - \aleph_2 \frac{\partial}{\partial z} - \frac{\aleph_2^3}{2} \frac{\partial^3}{\partial x^2 \partial z}\right] X^{(2)} \bigg|_{z=0} e^{-h/\aleph_2} = 0, \quad (3.2.12)$$

and

$$\left[1 - \aleph_2 \frac{\partial}{\partial z} - \frac{\aleph_2^3}{2} \frac{\partial^3}{\partial x^2 \partial z}\right] X^{(2)} \bigg|_{z=0} + \left(1 + \frac{\aleph_2 h}{2} \frac{\partial^2}{\partial x^2}\right) \left[1 + \aleph_2 \frac{\partial}{\partial z} + \frac{\aleph_2^3}{2} \frac{\partial^3}{\partial x^2 \partial z}\right] X^{(2)} \bigg|_{z=h} e^{-h/\aleph_2} = 0, \quad (3.2.13)$$

which holds good for all  $X^{(2)} \in \left\{ \tau_{mn}^{(2)}, \pi_{mn}^{(2)} \right\}$ .

# 3.2.3 Refined BVP for nonlocally micropolar elastic Rayleigh waves

Consider the propagation of Rayleigh waves along the x-direction, characterized by the displacement components  $\left(u_1^{(i)},0,u_3^{(i)}\right)$  and the microrotation vector components  $\left(0,\Phi_2^{(i)},0\right)$ , where i=1 refers to the semi-infinite medium and i=2 corresponds to the layer.

# Boundary value problem

The boundary value problem is then formulated as follows:

$$\frac{\tau_{1n,x}^{(i)} + \tau_{3n,z}^{(i)} - \rho^{(i)} u_{n,tt}^{(i)} = 0,}{\pi_{12,x}^{(i)} + \pi_{32,z}^{(i)} + \tau_{31}^{(i)} - \tau_{13}^{(i)} - \rho^{(i)} j^{(i)} \Phi_{2,tt}^{(i)} = 0,}$$

$$n = 1, 3$$
(3.2.14)

subjected to the traditional traction-free boundary and continuity conditions, respectively

(i) at the surface 
$$z = h$$
,  $\tau_{31}^{(2)} = 0$ ,  $\tau_{33}^{(2)} = 0$ ,  $\pi_{32}^{(2)} = 0$ ,

(ii) at the interface 
$$z=0,\ \tau_{31}^{(1)}=\tau_{31}^{(2)},\ \tau_{33}^{(1)}=\tau_{33}^{(2)},\ \pi_{32}^{(1)}=\pi_{32}^{(2)},$$
 
$$u_1^{(1)}=u_1^{(2)},\ u_3^{(1)}=u_3^{(2)},\ \Phi_2^{(1)}=\Phi_2^{(2)}.$$

It is noteworthy that not all the equivalence conditions derived in sections 3.2.2 can be simultaneously satisfied, as doing so would render the boundary value problem ill-posed. To ensure a well-posed formulation, we adopt the extra conditions provided in Eqs. (3.2.9), (3.2.12) and (3.2.13) on the nonconstrained stresses  $X^{(1)} \in \left\{\tau_{11}^{(1)}, \pi_{12}^{(1)}\right\}$  and  $X^{(2)} \in \left\{\tau_{11}^{(2)}, \pi_{12}^{(2)}\right\}$ .

# Asymptotic analysis

Introduce two small perturbation parameters of same order,

$$\epsilon_1 = \frac{\aleph_1}{\lambda}, \quad \epsilon_2 = \frac{\aleph_2}{h},$$
(3.2.15)

to address the formulated problem asymptotically. Here  $\lambda$  denotes the wavelength of propagating wave and h is the thickness of upper layer. This results in the different scale of behaviors, which are described as follows:

$$\varkappa_s = \frac{z}{h}, \quad \varkappa_f^{(i)} = \frac{z}{\aleph_i}.$$
(3.2.16)

These scales are introduced to incorporate the influence of the boundary layer on wave dynamics. The variable  $\varkappa_s$  captures the slower variation of the wave during propagation while the rapid oscillations of the wave behavior is captured by the variable  $\varkappa_f^{(i)}$ . Further, we introduces some dimensionless quantities such as,

$$\xi = \frac{x}{\lambda}, \ \widetilde{t} = \frac{c_2^{(1)}}{\lambda} t, \ \zeta = \frac{h}{\lambda}, \ \gamma = \left(\frac{c_2^{(2)}}{c_2^{(1)}}\right)^2, 
\widetilde{\tau}_{mn}^{(i)} = \frac{\tau_{mn}^{(i)}}{\mu^{(i)} + \kappa^{(i)}}, \ \widetilde{\sigma}_{mn}^{(i)} = \frac{\sigma_{mn}^{(i)}}{\mu^{(i)} + \kappa^{(i)}}, \ \widetilde{\pi}_{mn}^{(i)} = \frac{\pi_{mn}^{(i)}}{\mu^{(i)} + \kappa^{(i)}}, \ \widetilde{\Pi}_{mn}^{(i)} = \frac{\Pi_{mn}^{(i)}}{\mu^{(i)} + \kappa^{(i)}}, 
\widetilde{u}_1^{(i)} = \frac{u_1^{(i)}}{\lambda}, \ \widetilde{u}_3^{(i)} = \frac{u_3^{(i)}}{h}, \ J^{(i)} = \frac{j^{(i)}}{\lambda^2}, \ \widetilde{\Phi}_2^{(i)} = \Phi_2^{(i)},$$

$$(3.2.17)$$

where  $c_2^{(i)} = \sqrt{\frac{\mu^{(i)} + \kappa^{(i)}}{\rho^{(i)}}}$  to facilitate the further discussions.

To account for the effects of the boundary layer, the stress components can be decomposed into fast and slow variable components, as done in section 3.1, as follows:

$$\widetilde{\tau}_{11}^{(i)} = p_{11}^{(i)} + q_{11}^{(i)}, \ \widetilde{\tau}_{33}^{(i)} = \zeta^{2} p_{33}^{(i)} + \epsilon_{i}^{2} q_{33}^{(i)}, 
\widetilde{\tau}_{31}^{(i)} = \zeta p_{31}^{(i)} + \epsilon_{i} q_{13}^{(i)}, \ \widetilde{\tau}_{13}^{(i)} = \zeta p_{13}^{(i)} + \epsilon_{i} q_{31}^{(i)} 
\widetilde{\pi}_{12}^{(i)} = r_{12}^{(i)} + s_{12}^{(i)}, \ \widetilde{\pi}_{32}^{(i)} = \zeta r_{32}^{(i)} + \epsilon_{i} s_{32}^{(i)},$$
(3.2.18)

where  $p_{mn}^{(i)}$  and  $r_{mn}^{(i)}$  are the functions of  $\xi, \varkappa_s, \widetilde{t}$ , while  $q_{mn}^{(i)}$  and  $s_{mn}^{(i)}$  are the functions of  $\xi, \varkappa_f, \widetilde{t}$ . This approach allows for a more accurate representation of the stress field near the boundary. It is important to observe that the symmetry of the stress components is preserved for the rapidly varying components, while the symmetry breaks down for the more slowly varying components within a micropolar solid. As a result, we have  $q_{13}^{(i)} = q_{31}^{(i)}$ . Furthermore, we expand the following quantities in an asymptotic series as follows:

$$\mathfrak{F}^{(i)} = \mathfrak{F}^{(i,0)} + \epsilon_i \,\mathfrak{F}^{(i,1)} + \epsilon_i^2 \,\mathfrak{F}^{(i,2)} + \dots$$
 (3.2.19)

where  $\mathfrak{F} \in \left\{ p_{mn}, q_{mn}, \widetilde{\tau}_{mn}, \widetilde{\sigma}_{mn}, r_{mn}, s_{mn}, \widetilde{\pi}_{mn}, \widetilde{\Pi}_{mn}, \widetilde{u}_n, \widetilde{\Phi}_2 \right\}$ .

By decomposing the stress components as outlined in Eq. (3.2.18) and employing the asymptotic expansions from Eq. (3.2.19), the boundary value problem can be reformulated in terms of asymptotic orders as below:

$$\frac{\partial p_{1n}^{(i,r)}}{\partial \xi} + \frac{\partial p_{3n}^{(i,r)}}{\partial z_s} = \gamma^{1-i} \frac{\partial^2 \tilde{u}_n^{(i,r)}}{\partial \tilde{\tau}^2}, 
\frac{\partial q_{1n}^{(i,r)}}{\partial \xi} + \zeta^{1-i} \frac{\partial q_{3n}^{(i,r)}}{\partial z_f^{(i)}} = 0, 
\frac{\partial r_{12}^{(i,r)}}{\partial \xi} + \frac{\partial r_{32}^{(i,r)}}{\partial z_s} + p_{31}^{(i,r)} - p_{13}^{(i,r)} = J^{(i)} \frac{\partial^2 \tilde{\Phi}_2^{(i,r)}}{\partial \tilde{t}^2}, 
\frac{\partial s_{12}^{(i,r)}}{\partial \xi} + \zeta^{1-i} \frac{\partial s_{32}^{(i,r)}}{\partial z_f^{(i)}} = 0,$$
(3.2.20)

together with

$$p_{mn}^{(i,r)} - (\zeta^{2})^{r-1} \frac{\partial^{2} p_{mn}^{(i,r-2)}}{\partial \xi^{2}} - (\zeta^{2})^{r-2} \frac{\partial^{2} p_{mn}^{(i,r-2)}}{\partial \varkappa_{s}^{2}} = (\zeta)^{\frac{2-m+n}{2}} \widetilde{\sigma}_{mn}^{(i,r)},$$

$$q_{mn}^{(i,r)} - \frac{\partial^{2} q_{mn}^{(i,r)}}{\partial \varkappa_{f}^{(i,r)^{2}}} - (\zeta^{2})^{r-1} \frac{\partial^{2} q_{mn}^{(i,r-2)}}{\partial \xi^{2}} = 0,$$

$$r_{mn}^{(i,r)} - (\zeta^{2})^{r-1} \frac{\partial^{2} r_{mn}^{(i,r-2)}}{\partial \xi^{2}} - (\zeta^{2})^{r-2} \frac{\partial^{2} r_{mn}^{(i,r-2)}}{\partial \varkappa_{s}^{2}} = (\zeta)^{\frac{2-m+n}{2}} \widetilde{\Pi}_{mn}^{(i,r)},$$

$$s_{mn}^{(i,r)} - \frac{\partial^{2} s_{mn}^{(i,r)}}{\partial \varkappa_{f}^{(i,r)^{2}}} - (\zeta^{2})^{r-1} \frac{\partial^{2} s_{mn}^{(i,r-2)}}{\partial \xi^{2}} = 0,$$

$$(3.2.21)$$

together with the boundary and interface conditions

(i) at the surface  $\varkappa_s = 1$ ,  $\varkappa_f = \frac{1}{\epsilon_2}$ 

$$\zeta p_{31}^{(2,r)} + q_{31}^{(2,r-1)} = 0,$$

$$\zeta^2 p_{33}^{(2,r)} + q_{33}^{(2,r-2)} = 0,$$

$$\zeta r_{32}^{(2,r)} + s_{32}^{(2,r-2)} = 0,$$
(3.2.22)

(ii) at the interface  $\varkappa_s=\varkappa_f=0$ 

$$\zeta p_{31}^{(1,r)} + q_{31}^{(1,r-1)} = \chi^{-1} \left( \zeta p_{31}^{(2,r)} + q_{31}^{(2,r-1)} \right),$$

$$\zeta^{2} p_{33}^{(1,r)} + q_{33}^{(1,r-2)} = \chi^{-1} \left( \zeta^{2} p_{33}^{(2,r)} + q_{33}^{(2,r-2)} \right),$$

$$\zeta r_{32}^{(1,r)} + s_{32}^{(1,r-2)} = \chi^{-1} \left( \zeta r_{32}^{(2,r)} + s_{32}^{(2,r-2)} \right),$$

$$\widetilde{u}_{1}^{(1,r)} = \widetilde{u}_{1}^{(2,r)}, \ \widetilde{u}_{3}^{(1,r)} = \widetilde{u}_{3}^{(2,r)}, \ \widetilde{\Phi}_{2}^{(1,r)} = \widetilde{\Phi}_{2}^{(2,r)},$$
(3.2.23)

where  $\mu = \frac{\mu^{(1)} + \kappa^{(1)}}{\mu^{(2)} + \kappa^{(2)}}$  and the additional conditions

$$\left[p_{11}^{(1,r)} + q_{11}^{(1,r)} + \frac{\partial q_{11}^{(1,r)}}{\partial \varkappa_{f}^{(1)}} + \frac{1}{\zeta} \frac{\partial p_{11}^{(1,r-1)}}{\partial \varkappa_{s}} + \frac{1}{2} \frac{\partial^{3} q_{11}^{(1,r-2)}}{\partial \xi^{2} \partial \varkappa_{f}^{(1)}}\right]\Big|_{\varkappa_{s} = \varkappa_{f}^{(1)} = 0} = 0,$$

$$\left[p_{11}^{(2,r)} + q_{11}^{(2,r)} + \frac{\partial q_{11}^{(2,r)}}{\partial \varkappa_{f}^{(2)}} + \frac{\partial p_{11}^{(2,r-1)}}{\partial \varkappa_{s}} + \frac{1}{2} \zeta^{2} \frac{\partial^{3} q_{11}^{(2,r-2)}}{\partial \xi^{2} \partial \varkappa_{f}^{(2)}}\right]\Big|_{\varkappa_{s} = 1, \ \varkappa_{f}^{(2)} = \frac{1}{\epsilon_{2}}}$$

$$+ \sum_{k=r-1}^{r} \left(\frac{\zeta^{2}}{2} \frac{\partial^{2}}{\partial \xi^{2}}\right)^{r-k} \left[p_{11}^{(2,k)} + q_{11}^{(2,k)} - \frac{\partial q_{11}^{(2,k)}}{\partial \varkappa_{f}^{(2)}} - \frac{\partial p_{11}^{(2,r-1)}}{\partial \varkappa_{s}} - \frac{\zeta^{2}}{2} \frac{\partial^{3} q_{11}^{(2,r-2)}}{\partial \xi^{2} \partial \varkappa_{f}^{(2)}}\right]\Big|_{\varkappa_{s} = \varkappa_{f}^{(2)} = 0} e^{-\frac{1}{\epsilon_{2}}} = 0,$$

$$\left[p_{11}^{(2,r)} + q_{11}^{(2,r)} - \frac{\partial q_{11}^{(2,r)}}{\partial \varkappa_{f}^{(2)}} - \frac{\partial p_{11}^{(2,r-1)}}{\partial \varkappa_{s}} - \frac{1}{2} \zeta^{2} \frac{\partial^{3} q_{11}^{(2,r-2)}}{\partial \xi^{2} \partial \varkappa_{f}^{(2)}}\right]\Big|_{\varkappa_{s} = \varkappa_{f}^{(2)} = 0}$$

$$+ \sum_{k=r-1}^{r} \left(\frac{\zeta^{2}}{2} \frac{\partial^{2}}{\partial \xi^{2}}\right)^{r-k} \left[p_{11}^{(2,k)} + q_{11}^{(2,k)} + \frac{\partial q_{11}^{(2,k)}}{\partial \varkappa_{f}^{(2)}} + \frac{\partial p_{11}^{(2,k-1)}}{\partial \varkappa_{s}} + \frac{\zeta^{2}}{2} \frac{\partial^{3} q_{11}^{(2,r-2)}}{\partial \xi^{2} \partial \varkappa_{f}^{(2)}}\right]\Big|_{\varkappa_{s} = 1, \ \varkappa_{f}^{(2)} = \frac{1}{\epsilon_{2}}}$$

$$+ \sum_{k=r-1}^{r} \left(\frac{\zeta^{2}}{2} \frac{\partial^{2}}{\partial \xi^{2}}\right)^{r-k} \left[p_{11}^{(2,k)} + q_{11}^{(2,k)} + \frac{\partial q_{11}^{(2,r)}}{\partial \varkappa_{f}^{(2)}} + \frac{\partial p_{11}^{(2,r-1)}}{\partial \varkappa_{s}} + \frac{\zeta^{2}}{2} \frac{\partial^{3} q_{11}^{(2,r-2)}}{\partial \xi^{2} \partial \varkappa_{f}^{(2)}}\right]\Big|_{\varkappa_{s} = 1, \ \varkappa_{f}^{(2)} = \frac{1}{\epsilon_{2}}}$$

$$+ \sum_{k=r-1}^{r} \left(\frac{\zeta^{2}}{2} \frac{\partial^{2}}{\partial \xi^{2}}\right)^{r-k} \left[p_{11}^{(2,k)} + q_{11}^{(2,k)} + \frac{\partial q_{11}^{(2,k)}}{\partial \varkappa_{f}^{(2)}} + \frac{\partial p_{11}^{(2,r-1)}}{\partial \varkappa_{s}} + \frac{\zeta^{2}}{2} \frac{\partial^{3} q_{11}^{(2,r-2)}}{\partial \xi^{2} \partial \varkappa_{f}^{(2)}}\right]\Big|_{\varkappa_{s} = 1, \ \varkappa_{f}^{(2)} = \frac{1}{\epsilon_{2}}}$$

$$+ \sum_{k=r-1}^{r} \left(\frac{\zeta^{2}}{2} \frac{\partial^{2}}{\partial \xi^{2}}\right)^{r-k} \left[p_{11}^{(2,k)} + q_{11}^{(2,k)} + \frac{\partial q_{11}^{(2,k)}}{\partial \varkappa_{f}^{(2)}} + \frac{\partial p_{11}^{(2,r-1)}}{\partial \varkappa_{s}} + \frac{\zeta^{2}}{2} \frac{\partial^{3} q_{11}^{(2,r-2)}}{\partial \xi^{2} \partial \varkappa_{f}^{(2)}}\right]\Big|_{\varkappa_{s} = 1, \ \varkappa_{f}^{(2)} = 0}$$

$$\left[ r_{12}^{(1,r)} + s_{12}^{(1,r)} + \frac{\partial s_{12}^{(1,r)}}{\partial \varkappa_{f}^{(1)}} + \frac{1}{\zeta} \frac{\partial r_{12}^{(1,r-1)}}{\partial \varkappa_{s}} + \frac{1}{2} \frac{\partial^{3} s_{12}^{(1,r-2)}}{\partial \xi^{2} \partial \varkappa_{f}^{(1)}} \right] \Big|_{\varkappa_{s} = \varkappa_{f}^{(1)} = 0} = 0,$$

$$\left[ r_{12}^{(2,r)} + s_{12}^{(2,r)} + \frac{\partial s_{12}^{(2,r)}}{\partial \varkappa_{f}^{(2)}} + \frac{\partial r_{12}^{(2,r-1)}}{\partial \varkappa_{s}} + \frac{1}{2} \zeta^{2} \frac{\partial^{3} s_{12}^{(2,r-2)}}{\partial \xi^{2} \partial \varkappa_{f}^{(2)}} \right] \Big|_{\varkappa_{s} = 1, \ \varkappa_{f}^{(2)} = \frac{1}{\eta_{2}}}$$

$$+ \sum_{k=r-1}^{r} \left( \frac{\zeta^{2}}{2} \frac{\partial^{2}}{\partial \xi^{2}} \right)^{r-k} \left[ r_{12}^{(2,k)} + s_{12}^{(2,k)} - \frac{\partial s_{12}^{(2,k)}}{\partial \varkappa_{f}^{(2)}} - \frac{\partial r_{12}^{(2,k-1)}}{\partial \varkappa_{s}} - \frac{\zeta^{2}}{2} \frac{\partial^{3} s_{12}^{(2,r-2)}}{\partial \xi^{2} \partial \varkappa_{f}^{(2)}} \right] \Big|_{\varkappa_{s} = \varkappa_{f}^{(2)} = 0} e^{-\frac{1}{\eta_{2}}} = 0,$$

$$\left[ r_{12}^{(2,r)} + s_{12}^{(2,r)} - \frac{\partial s_{12}^{(2,r)}}{\partial \varkappa_{f}^{(2)}} - \frac{\partial r_{12}^{(2,r-1)}}{\partial \varkappa_{s}} - \frac{1}{2} \zeta^{2} \frac{\partial^{3} s_{12}^{(2,r-2)}}{\partial \xi^{2} \partial \varkappa_{f}^{(2)}} \right] \Big|_{\varkappa_{s} = \varkappa_{f}^{(2)} = 0}$$

$$+ \sum_{k=r-1}^{r} \left( \frac{\zeta^{2}}{2} \frac{\partial^{2}}{\partial \xi^{2}} \right)^{r-k} \left[ r_{12}^{(2,k)} + s_{12}^{(2,k)} + \frac{\partial s_{12}^{(2,k)}}{\partial \varkappa_{f}^{(2)}} + \frac{\partial r_{12}^{(2,r-1)}}{\partial \varkappa_{s}} + \frac{\zeta^{2}}{2} \frac{\partial^{3} s_{12}^{(2,k-2)}}{\partial \xi^{2} \partial \varkappa_{f}^{(2)}} \right] \Big|_{\varkappa_{s} = 1, \ \varkappa_{f}^{(2)} = \frac{1}{\eta_{2}}} e^{-\frac{1}{\eta_{2}}} = 0.$$

$$(3.2.25)$$

A comparative analysis of the leading order terms (r = 0), first-order terms (r = 1), and second-order terms (r = 2) for the aforementioned system of equations enables a refinement of the boundary and interface conditions. By ignoring exponentially smaller terms, the refined boundary and interface conditions for different asymptotic orders are summarized below:

**Leading order analysis:** Comparing the first-order terms, we obtain the conditions (i) at the surface  $\varkappa_s = 1$ ,

$$\widetilde{\sigma}_{31}^{(2,0)} = 0, \ \widetilde{\sigma}_{33}^{(2,0)} = 0, \ \widetilde{\Pi}_{32}^{(2,0)} = 0.$$

(ii) at the interface  $\varkappa_s = 0$ ,

$$\begin{split} \widetilde{\sigma}_{31}^{(1,0)} &= \chi^{-1} \, \widetilde{\sigma}_{31}^{(2,0)}, \ \widetilde{\sigma}_{33}^{(1,0)} &= \chi^{-1} \, \widetilde{\sigma}_{33}^{(2,0)}, \ \widetilde{\Pi}_{32}^{(1,0)} &= \chi^{-1} \, \widetilde{\Pi}_{32}^{(2,0)} \\ \widetilde{u}_{1}^{(1,0)} &= \widetilde{u}_{1}^{(2,0)}, \ \widetilde{u}_{3}^{(1,0)} &= \widetilde{u}_{3}^{(2,0)}, \ \widetilde{\Phi}_{2}^{(1,0)} &= \widetilde{\Phi}_{2}^{(2,0)}. \end{split}$$

First-order analysis: Comparing the first-order terms, we obtain the conditions

(i) at the surface  $\varkappa_s = 1$ ,

$$\begin{split} \widetilde{\sigma}_{31}^{(2,1)} + \frac{\eta}{2} \, \frac{\partial}{\partial \xi} \left( \widetilde{\sigma}_{11}^{(2,0)} \right) &= 0, \ \, \widetilde{\sigma}_{33}^{(2,1)} &= 0, \\ \widetilde{\Pi}_{32}^{(2,1)} + \frac{\eta}{2} \, \frac{\partial}{\partial \xi} \left( \widetilde{\Pi}_{12}^{(2,0)} \right) &= 0. \end{split}$$

(ii) at the interface  $\varkappa_s = 0$ ,

$$\begin{split} \widetilde{\sigma}_{31}^{(1,1)} + \frac{1}{2} \, \frac{\partial}{\partial \xi} \left( \widetilde{\sigma}_{11}^{(1,0)} \right) &= \chi^{-1} \left( \widetilde{\sigma}_{31}^{(2,1)} - \frac{\eta}{2} \, \frac{\partial}{\partial \xi} \left( \widetilde{\sigma}_{11}^{(2,0)} \right) \right), \\ \widetilde{\sigma}_{33}^{(1,1)} &= \chi^{-1} \, \widetilde{\sigma}_{33}^{(2,1)}, \\ \widetilde{\Pi}_{32}^{(1,1)} + \frac{1}{2} \, \frac{\partial}{\partial \xi} \left( \widetilde{\Pi}_{12}^{(1,0)} \right) &= \chi^{-1} \left( \widetilde{\Pi}_{32}^{(2,1)} - \frac{\eta}{2} \, \frac{\partial}{\partial \xi} \left( \widetilde{\Pi}_{12}^{(2,0)} \right) \right), \\ \widetilde{u}_{1}^{(1,1)} &= \widetilde{u}_{1}^{(2,1)}, \ \ \widetilde{u}_{3}^{(1,1)} &= \widetilde{u}_{3}^{(2,1)}, \ \ \widetilde{\Phi}_{2}^{(1,1)} &= \widetilde{\Phi}_{2}^{(2,1)}. \end{split}$$

**Second-order analysis:** We rewrite the equations of motion in Eq. (3.2.7) as,

$$\frac{\partial}{\partial \xi} \left( \widetilde{\sigma}_{11}^{(i,2)} \right) + \frac{1}{\zeta} \frac{\partial}{\partial \varkappa_{s}} \left( \widetilde{\sigma}_{13}^{(i,2)} \right) = \gamma^{1-i} \left[ \frac{\partial^{2} \widetilde{u}_{1}^{(i,2)}}{\partial t^{2}} - \left( \left( \zeta^{2} \right)^{i-2} \frac{\partial^{2}}{\partial \varkappa_{s}^{2}} + \left( \zeta^{2} \right)^{i-1} \frac{\partial^{2}}{\partial \xi^{2}} \right) \frac{\partial^{2} \widetilde{u}_{1}^{(i,0)}}{\partial t^{2}} \right],$$

$$\frac{\partial}{\partial \xi} \left( \widetilde{\sigma}_{13}^{(i,2)} \right) + \frac{1}{\zeta} \frac{\partial}{\partial \varkappa_{s}} \left( \widetilde{\sigma}_{33}^{(i,2)} \right) = \zeta \gamma^{1-i} \left[ \frac{\partial^{2} \widetilde{u}_{3}^{(i,2)}}{\partial t^{2}} - \left( \left( \zeta^{2} \right)^{i-2} \frac{\partial^{2}}{\partial \varkappa_{s}^{2}} + \left( \zeta^{2} \right)^{i-1} \frac{\partial^{2}}{\partial \xi^{2}} \right) \frac{\partial^{2} \widetilde{u}_{3}^{(i,0)}}{\partial t^{2}} \right].$$

$$\frac{\partial}{\partial \xi} \left( \widetilde{\Pi}_{12}^{(i,2)} \right) + \frac{1}{\zeta} \frac{\partial}{\partial \varkappa_{s}} \left( \widetilde{\Pi}_{32}^{(i,2)} \right) + \widetilde{\sigma}_{31}^{(i,2)} - \widetilde{\sigma}_{13}^{(i,2)} = \gamma^{1-i} \left[ \frac{\partial^{2} \widetilde{u}_{1}^{(i,2)}}{\partial t^{2}} - \left( \left( \zeta^{2} \right)^{i-2} \frac{\partial^{2}}{\partial \varkappa_{s}^{2}} + \left( \zeta^{2} \right)^{i-1} \frac{\partial^{2}}{\partial \xi^{2}} \right) \frac{\partial^{2} \widetilde{u}_{3}^{(i,0)}}{\partial t^{2}} \right],$$

$$(3.2.26)$$

subjected to refined boundary and interface conditions,

(i) at the surface  $\varkappa_s = 1$ ,

$$\widetilde{\sigma}_{31}^{(2,2)} + \frac{\zeta}{2} \frac{\partial}{\partial \xi} \left( \widetilde{\sigma}_{11}^{(2,1)} \right) + \frac{\zeta}{2} \frac{\partial^2}{\partial \xi \partial \varkappa_s} \left( \widetilde{\sigma}_{11}^{(2,0)} \right) + \frac{\partial^2}{\partial \varkappa_s^2} \left( \widetilde{\sigma}_{31}^{(2,0)} \right) + \zeta^2 \frac{\partial^2}{\partial \xi^2} \left( \widetilde{\sigma}_{31}^{(2,0)} \right) = 0, \tag{3.2.27}$$

$$\widetilde{\sigma}_{33}^{(2,2)} + \frac{\partial^2}{\partial \varkappa_s^2} \left( \widetilde{\sigma}_{33}^{(2,0)} \right) + \zeta^2 \frac{\partial^2}{\partial \xi^2} \left( \widetilde{\sigma}_{33}^{(2,0)} \right) - \frac{\zeta^2}{2} \frac{\partial^2}{\partial \xi^2} \left( \widetilde{\sigma}_{11}^{(2,0)} \right) = 0, \tag{3.2.28}$$

$$\widetilde{\Pi}_{32}^{(2,2)} + \frac{\zeta}{2} \frac{\partial}{\partial \xi} \left( \widetilde{\Pi}_{12}^{(2,1)} \right) + \frac{\zeta}{2} \frac{\partial^2}{\partial \xi \partial \varkappa_s} \left( \widetilde{\Pi}_{12}^{(2,0)} \right) + \frac{\partial^2}{\partial \varkappa_s^2} \left( \widetilde{\Pi}_{32}^{(2,0)} \right) + \zeta^2 \frac{\partial^2}{\partial \xi^2} \left( \widetilde{\Pi}_{32}^{(2,0)} \right) = 0, \tag{3.2.29}$$

(ii) at the interface  $\varkappa_s = 0$ ,

$$\begin{split} &\widetilde{\sigma}_{31}^{(1,2)} + \frac{1}{2} \frac{\partial}{\partial \xi} \left( \widetilde{\sigma}_{11}^{(1,1)} \right) + \frac{1}{\zeta^{2}} \frac{\partial^{2}}{\partial \varkappa_{s}^{2}} \left( \widetilde{\sigma}_{31}^{(1,0)} \right) + \frac{\partial}{\partial \xi^{2}} \left( \widetilde{\sigma}_{31}^{(1,0)} \right) + \frac{1}{2\zeta} \frac{\partial^{2}}{\partial \xi \partial \varkappa_{s}} \left( \widetilde{\sigma}_{11}^{(1,0)} \right) \\ &= \chi^{-1} \left[ \widetilde{\sigma}_{31}^{(2,2)} - \frac{\zeta}{2} \frac{\partial}{\partial \xi} \left( \widetilde{\sigma}_{11}^{(2,1)} \right) + \frac{\partial^{2}}{\partial \varkappa_{s}^{2}} \left( \widetilde{\sigma}_{31}^{(2,0)} \right) + \zeta^{2} \frac{\partial}{\partial \xi^{2}} \left( \widetilde{\sigma}_{31}^{(2,0)} \right) + \frac{\zeta}{2} \frac{\partial^{2}}{\partial \xi \partial \varkappa_{s}} \left( \widetilde{\sigma}_{11}^{(2,0)} \right) \right], (3.2.30) \\ &\widetilde{\sigma}_{33}^{(1,2)} - \frac{1}{2} \frac{\partial^{2}}{\partial \xi^{2}} \left( \widetilde{\sigma}_{11}^{(1,0)} \right) + \frac{1}{\zeta^{2}} \frac{\partial^{2}}{\partial \varkappa_{s}^{2}} \left( \widetilde{\sigma}_{33}^{(1,0)} \right) + \frac{\partial^{2}}{\partial \xi^{2}} \left( \widetilde{\sigma}_{33}^{(1,0)} \right) \right) \\ &= \chi^{-1} \left[ \widetilde{\sigma}_{33}^{(2,2)} - \frac{\zeta^{2}}{2} \frac{\partial^{2}}{\partial \xi^{2}} \left( \widetilde{\sigma}_{11}^{(2,0)} \right) + \frac{\partial^{2}}{\partial \varkappa_{s}^{2}} \left( \widetilde{\sigma}_{33}^{(2,0)} \right) + \zeta^{2} \frac{\partial^{2}}{\partial \xi^{2}} \left( \widetilde{\sigma}_{33}^{(2,0)} \right) \right], \\ &\widetilde{\Pi}_{32}^{(1,2)} + \frac{1}{2} \frac{\partial}{\partial \xi} \left( \widetilde{\Pi}_{12}^{(1,1)} \right) + \frac{1}{\zeta^{2}} \frac{\partial^{2}}{\partial \varkappa_{s}^{2}} \left( \widetilde{\Pi}_{32}^{(1,0)} \right) + \frac{\partial}{\partial \xi^{2}} \left( \widetilde{\Pi}_{32}^{(1,0)} \right) + \frac{1}{2\zeta} \frac{\partial^{2}}{\partial \xi \partial \varkappa_{s}} \left( \widetilde{\Pi}_{12}^{(1,0)} \right) \\ &= \chi^{-1} \left[ \widetilde{\Pi}_{32}^{(2,2)} - \frac{\zeta}{2} \frac{\partial}{\partial \xi} \left( \widetilde{\Pi}_{12}^{(2,1)} \right) + \frac{\partial^{2}}{\partial \varkappa_{s}^{2}} \left( \widetilde{\Pi}_{32}^{(2,0)} \right) + \zeta^{2} \frac{\partial}{\partial \xi^{2}} \left( \widetilde{\Pi}_{32}^{(2,0)} \right) + \frac{\zeta}{2} \frac{\partial^{2}}{\partial \xi \partial \varkappa_{s}} \left( \widetilde{\Pi}_{12}^{(2,0)} \right) \right] (3.2.32) \\ &\widetilde{u}_{1}^{(1,2)} &= \widetilde{u}_{1}^{(2,2)}, \ \widetilde{u}_{3}^{(1,2)} &= \widetilde{u}_{3}^{(2,2)}, \ \widetilde{\Phi}_{2}^{(1,2)} &= \widetilde{\Phi}_{2}^{(2,2)}, \end{aligned}$$

where  $\chi = \frac{\mu^{(1)} + \kappa^{(1)}}{\mu^{(2)} + \kappa^{(2)}}$ .

# Refined boundary value problem

Utilizing the approximation that

$$\mathfrak{F}^{(i,r)} pprox rac{1}{\aleph_i^r} \, \mathfrak{F}^{(i)}$$

for r = 1, 2 and  $\mathfrak{F} \in \left\{ \widetilde{\sigma}_{31}, \widetilde{\sigma}_{11}, \widetilde{\sigma}_{33}, \widetilde{\Pi}_{32}, \widetilde{\Pi}_{12}, \widetilde{u}_1, \widetilde{u}_3, \widetilde{\Phi}_2 \right\}$ , the refined equations of motion for the propagation of Rayleigh waves in a micropolar layered medium can be reformulated in terms of original variables as,

$$\frac{\partial}{\partial x} \left( \sigma_{11}^{(i)} \right) + \frac{\partial}{\partial z} \left( \sigma_{13}^{(i)} \right) = \rho^{(i)} \left( 1 - \aleph_i^2 \nabla^2 \right) \frac{\partial^2 u_1^{(i)}}{\partial t^2},$$

$$\frac{\partial}{\partial x} \left( \sigma_{13}^{(i)} \right) + \frac{\partial}{\partial z} \left( \sigma_{33}^{(i)} \right) = \rho^{(i)} \left( 1 - \aleph_i^2 \nabla^2 \right) \frac{\partial^2 u_3^{(i)}}{\partial t^2},$$

$$\frac{\partial}{\partial x} \left( \Pi_{12}^{(i)} \right) + \frac{\partial}{\partial z} \left( \Pi_{32}^{(i)} \right) + \sigma_{31}^{(i)} - \sigma_{13}^{(i)} = \rho^{(i)} j^{(i)} \left( 1 - \aleph_i^2 \nabla^2 \right) \frac{\partial^2 \Phi_2}{\partial t^2},$$
(3.2.34)

with the refined traction-free boundary conditions at the surface z = h as

$$(1 + \aleph_{2}^{2} \nabla^{2}) \, \sigma_{31}^{(2)} + \frac{\aleph_{2}}{2} \, \frac{\partial}{\partial x} \left( \sigma_{11}^{(2)} \right) + \frac{\aleph_{2}^{2}}{2} \, \frac{\partial^{2}}{\partial x \, \partial z} \left( \sigma_{11}^{(2)} \right) = 0,$$

$$(1 + \aleph_{2}^{2} \nabla^{2}) \, \sigma_{33}^{(2)} - \frac{\aleph_{2}^{2}}{2} \, \frac{\partial^{2}}{\partial x^{2}} \left( \sigma_{11}^{(2)} \right) = 0,$$

$$(1 + \aleph_{2}^{2} \nabla^{2}) \, \Pi_{32}^{(2)} + \frac{\aleph_{2}}{2} \, \frac{\partial}{\partial x} \left( \Pi_{12}^{(2)} \right) + \frac{\aleph_{2}^{2}}{2} \, \frac{\partial^{2}}{\partial x \, \partial z} \left( \Pi_{12}^{(2)} \right) = 0,$$

$$(3.2.35)$$

and the continuity conditions at the interface z = 0 as,

$$\left(1 + \aleph_1^2 \nabla^2\right) \sigma_{31}^{(1)} + \frac{\aleph_1}{2} \frac{\partial^2 \sigma_{11}^{(1)}}{\partial x \partial z} + \frac{\aleph_1^2}{2} \frac{\partial^2 \sigma_{11}^{(1)}}{\partial x \partial z} = \chi^{-1} \left\{ \left(1 + \aleph_2^2 \nabla^2\right) \sigma_{31}^{(2)} - \frac{\aleph_2}{2} \frac{\partial \sigma_{11}^{(2)}}{\partial x} + \frac{\aleph_2^2}{2} \frac{\partial^2 \sigma_{11}^{(2)}}{\partial x \partial z} \right\}, \qquad (3.2.36)$$

$$(1 + \aleph_1^2 \nabla^2) \, \sigma_{33}^{(1)} - \frac{\aleph_1^2}{2} \, \frac{\partial^2 \sigma_{11}^{(1)}}{\partial x^2} = \chi^{-1} \, \left\{ \left( 1 + \aleph_2^2 \nabla^2 \right) \sigma_{33}^{(2)} - \frac{\aleph_2^2}{2} \, \frac{\partial^2 \sigma_{11}^{(2)}}{\partial x^2} \right\},$$
 (3.2.37)

$$\left(1 + \aleph_1^2 \nabla^2\right) \Pi_{32}^{(1)} + \frac{\aleph_1}{2} \frac{\partial^2 \Pi_{12}^{(1)}}{\partial x \partial z} + \frac{\aleph_1^2}{2} \frac{\partial^2 \Pi_{12}^{(1)}}{\partial x \partial z} = \chi^{-1} \left\{ \left(1 + \aleph_2^2 \nabla^2\right) \Pi_{32}^{(2)} - \frac{\aleph_2}{2} \frac{\partial \Pi_{12}^{(2)}}{\partial x} + \frac{\aleph_2^2}{2} \frac{\partial^2 \Pi_{12}^{(2)}}{\partial x \partial z} \right\}, \quad (3.2.38)$$

$$u_1^{(1)} = u_1^{(2)}, \ u_3^{(1)} = u_3^{(2)}, \ \Phi_2^{(1)} = \Phi_2^{(2)},$$
 (3.2.39)

where  $\nabla^2$  is the two-dimensional Laplacian operator, defined as  $\nabla^2 = \frac{\partial^2}{\partial x^2} + \frac{\partial^2}{\partial z^2}$ .

# 3.2.4 Application

In this section, we investigate the propagation and dispersion of Rayleigh waves in an isotropic nonlocal micropolar layer of thickness h overlying an isotropic nonlocal micropolar semi-infinite medium.

## Solution to the problem

The constitutive relations relating local stresses with the strain components for an isotropic micropolar structure are given by:

$$\frac{\sigma_{mn}^{(i)} = \Lambda^{(i)} \,\varepsilon_{pp}^{(i)} \,\delta_{mn} + \left(\mu^{(i)} + \kappa^{(i)}\right) \,\varepsilon_{mn}^{(i)} + \mu^{(i)} \,\varepsilon_{nm}^{(i)},}{\Pi_{mn}^{(i)} = \alpha^{(i)} \,\Gamma_{pp}^{(i)} \,\delta_{mn} + \beta^{(i)} \,\Gamma_{mn}^{(i)} + \gamma^{(i)} \,\Gamma_{nm}^{(i)},}\right\} m, n = 1, 2, 3.$$
(3.2.40)

Here, the strain tensor  $\varepsilon_{mn}^{(i)}$  and curvature tensor  $\Gamma_{mn}^{(i)}$  are defined as previously described. Additionally,  $\Lambda^{(i)}$  and  $\mu^{(i)}$  represent the Lamé elastic constants, while  $\kappa^{(i)}$ ,  $\alpha^{(i)}$  and  $\beta^{(i)}$  denote the micropolar constants.

Substituting the constitutive relations from Eq. (3.2.40) into the equations of motion presented in Eq. (3.2.7) yields a coupled system of equations involving  $u_1^{(i)}, u_3^{(i)}$  and  $\Phi_2^{(i)}$ . To decouple this system, we employ Helmholtz decomposition technique that expresses the displacement components as a sum of scalar and vector potentials as follows:

$$u_1^{(i)} = \frac{\partial \phi^{(i)}}{\partial x} - \frac{\partial \psi^{(i)}}{\partial z}, \ u_3^{(i)} = \frac{\partial \phi^{(i)}}{\partial z} + \frac{\partial \psi^{(i)}}{\partial x}.$$
 (3.2.41)

The resulting decoupled equations can be readily solved, yielding solutions to the displacement, micro-rotation components of the semi-infinite medium and the layer in the following form (the detailed derivation is left to the reader),

$$u_{1}^{(1)}(x,z,t) = ik \left[ \mathcal{A}_{1}e^{k\mathbf{v}_{1}^{(1)}z} + i\left(\mathcal{B}_{1}\mathbf{v}_{2}^{(1)}e^{k\mathbf{v}_{2}^{(1)}z} + \mathcal{D}_{1}\mathbf{v}_{3}^{(1)}e^{k\mathbf{v}_{3}^{(1)}z}\right) \right] e^{i(kx-\omega t)},$$

$$u_{3}^{(1)}(x,z,t) = k \left[ \mathcal{A}_{1}\mathbf{v}_{1}^{(1)}e^{k\mathbf{v}_{1}^{(1)}z} + i\left(\mathcal{B}_{1}e^{k\mathbf{v}_{2}^{(1)}z} + \mathcal{D}_{1}e^{k\mathbf{v}_{3}^{(1)}z}\right) \right] e^{i(kx-\omega t)},$$

$$\Phi_{2}^{(1)}(x,z,t) = \mathfrak{s}^{(1)}k^{2}\mathcal{D}_{1}e^{k\mathbf{v}_{3}^{(1)}z}e^{i(kx-\omega t)},$$

$$u_{1}^{(2)}(x,z,t) = k \left[ i\left(\mathcal{A}_{2}\sinh\left(k\mathbf{v}_{1}^{(2)}z\right) + \mathcal{P}_{2}\cosh\left(k\mathbf{v}_{1}^{(2)}z\right)\right) - \mathbf{v}_{2}^{(2)}\left(\mathcal{B}_{2}\sinh\left(k\mathbf{v}_{2}^{(2)}z\right) + \mathcal{Q}_{2}\cosh\left(k\mathbf{v}_{2}^{(2)}z\right)\right) - \mathbf{v}_{3}^{(2)}\left(\mathcal{D}_{2}\cosh\left(k\mathbf{v}_{3}^{(2)}z\right) + \mathcal{R}_{2}\sinh\left(k\mathbf{v}_{3}^{(2)}z\right)\right) \right] e^{i(kx-\omega t)},$$

$$u_{3}^{(2)}(x,z,t) = k \left[ \mathbf{v}_{1}^{(2)}\left(\mathcal{A}_{2}\cosh\left(k\mathbf{v}_{1}^{(2)}z\right) + \mathcal{P}_{2}\sinh\left(k\mathbf{v}_{1}^{(2)}z\right)\right) + i\left(\mathcal{B}_{2}\sinh\left(k\mathbf{v}_{2}^{(2)}z\right) + \mathcal{Q}_{2}\cosh\left(k\mathbf{v}_{2}^{(2)}z\right)\right) + i\left(\mathcal{D}_{2}\sinh\left(k\mathbf{v}_{3}^{(2)}z\right) + \mathcal{R}_{2}\cosh\left(k\mathbf{v}_{3}^{(2)}z\right)\right) \right] e^{i(kx-\omega t)},$$

$$\Phi_{2}^{(2)}(x,z,t) = k^{2}\mathfrak{s}^{(2)}\left[\mathcal{D}_{2}\sinh\left(k\mathbf{v}_{3}^{(2)}z\right) + \mathcal{R}_{2}\cosh\left(k\mathbf{v}_{3}^{(2)}z\right)\right] e^{i(kx-\omega t)},$$

where  $k = \frac{1}{\lambda}$ ,  $\omega$  are the wavelength and frequency of the propagating wave, respectively. And,

(3.2.43)

$$\left(\mathbf{v}_{1}^{(i)}\right)^{2} = 1 - \frac{v^{2}}{\left(c_{1}^{(i)}\right)^{2} - \aleph_{i}^{2}v^{2}}, \ \left(\mathbf{v}_{2}^{(i)}\right)^{2} = 1 - \frac{v^{2}}{\left(c_{2}^{(i)}\right)^{2} - \aleph_{i}^{2}v^{2}}, \ \left(\mathbf{v}_{3}^{(i)}\right)^{2} = 1 - \frac{v^{2}}{\left(c_{4}^{(i)}\right)^{2} - \aleph_{i}^{2}v^{2}} \left(1 - \frac{2\left(c_{3}^{(i)}\right)^{2}}{j^{(i)}\omega^{2}}\right),$$
 
$$\mathbf{s}^{(i)} = \frac{v^{2}}{\left(c_{3}^{(i)}\right)^{2}} \left[1 - \frac{\left(c_{2}^{(i)}\right)^{2} - \aleph_{i}^{2}v^{2}}{\left(c_{4}^{(i)}\right)^{2} - \aleph_{i}^{2}v^{2}} \left(1 - \frac{2\left(c_{3}^{(i)}\right)^{2}}{j^{(i)}\omega^{2}}\right)\right].$$

It is necessary that  $\text{Re}(\mathbf{v}_m^{(i)}) > 0$  for m = 1, 2, 3 to guarantee the exponential decay of the waves from the surface. Also,

$$c_1^{(i)} = \sqrt{\frac{\Lambda^{(i)} + 2\mu^{(i)} + \kappa^{(i)}}{\rho^{(i)}}}, \ c_2^{(i)} = \sqrt{\frac{\mu^{(i)} + \kappa^{(i)}}{\rho^{(i)}}}, \ c_3^{(i)} = \sqrt{\frac{\kappa^{(i)}}{\rho^{(i)}}}, \ c_4^{(i)} = \sqrt{\frac{\gamma}{\rho^{(i)}j^{(i)}}},$$

are the velocities associated with the micropolar media.

## Dispersion relations

Now, substituting the expressions for the displacement and micro-rotation components of both the semi-infinite medium and the layer, as given in Eqs. (3.2.42) and (3.2.43), into the refined boundary conditions derived in Eqs. (3.2.35)-(3.2.39), we obtain a  $9 \times 9$  system of equations. Solving this system for a nontrivial solution yields the dispersion relations. For computational efficiency, we evaluate the first-order corrected dispersion relations. Two dispersion relations are obtained out of which one is entirely due to the

micropolarity in the media and vanishes in its absence.

Define the quantities in their leading order expressions as,

$$\left(\mathbf{v}_{10}^{(i)}\right)^{2} = 1 - \frac{v^{2}}{\left(c_{1}^{(i)}\right)^{2}}, \ \left(\mathbf{v}_{20}^{(i)}\right)^{2} = 1 - \frac{v^{2}}{\left(c_{2}^{(i)}\right)^{2}}, \ \left(\mathbf{v}_{30}^{(i)}\right)^{2} = 1 - \frac{v^{2}}{\left(c_{4}^{(i)}\right)^{2}} \left(1 - \frac{2\left(c_{3}^{(i)}\right)^{2}}{j^{(i)}\omega^{2}}\right) (3.2.44)$$

As a result, the dispersion relation corresponding to the Rayleigh surface wave mode that counterparts with the purely elastic solid can be given explicitly as,

$$\Delta_0 + \epsilon_1 \Delta_1 + \epsilon_2 \Delta_2 = 0, \tag{3.2.45}$$

where

$$\Delta_{0} = 2 \left( \prod_{1}^{(2)} + \prod_{3}^{(2)} \right) \nu_{10}^{(2)} \left( \varpi_{1} \xi_{2} - \varpi_{2} \xi_{1} \right), 
\Delta_{1} = 2G_{2} \left( \nu_{20}^{(2)} \varpi_{2} \xi_{3} - \varpi_{3} \xi_{2} \right) + G_{1} \nu_{20}^{(1)} \left( \varpi_{3} \xi_{1} - \nu_{20}^{(2)} \varpi_{1} \xi_{3} \right), 
\Delta_{2} = \eta \left( \nu_{20}^{(2)} \left( \varpi_{2} \xi_{4} + \varpi_{1} \xi_{5} \right) - \varpi_{3} \nu_{10}^{(2)} \left( \xi_{2} U + \nu_{20}^{(1)} \xi_{1} V \right) \right)$$

is the first-order corrected dispersion relation for Rayleigh waves propagating in a nonlocal micropolar layered medium. Further, the expressions for  $\varpi_j$ , j = 1, 2, 3 and  $\xi_j$ , j = 1, 2, ... 5 are as follows:

$$\begin{array}{lll} \varpi_1 & = & \prod_{1}^{(2)} \mathsf{v}_{10}^{(2)} \left( \mathsf{v}_{10}^{(1)} \mathsf{v}_{20}^{(2)} W \sinh \left( \zeta \mathsf{v}_{20}^{(2)} \right) + Z \cosh \left( \zeta \mathsf{v}_{20}^{(2)} \right) \right) + \prod_{3}^{(2)} \left( \mathsf{v}_{10}^{(1)} X \sinh \left( \zeta \mathsf{v}_{10}^{(2)} \right) + \mathsf{v}_{10}^{(2)} Y \cosh \left( \zeta \mathsf{v}_{10}^{(2)} \right) \right), \\ \varpi_2 & = & \prod_{3}^{(2)} \left( \mathsf{v}_{10}^{(2)} \mathsf{v}_{20}^{(1)} W \cosh \left( \zeta \mathsf{v}_{10}^{(2)} \right) + Z \sinh \left( \zeta \mathsf{v}_{10}^{(2)} \right) \right) + \prod_{1}^{(2)} \mathsf{v}_{10}^{(2)} \left( \mathsf{v}_{20}^{(1)} X \cosh \left( \zeta \mathsf{v}_{20}^{(2)} \right) + \mathsf{v}_{20}^{(2)} Y \sinh \left( \zeta \mathsf{v}_{20}^{(2)} \right) \right), \\ \varpi_3 & = & \prod_{3}^{(2)} \sinh \left( \zeta \mathsf{v}_{10}^{(2)} \right) + \prod_{1}^{(2)} \mathsf{v}_{10}^{(2)} \mathsf{v}_{20}^{(2)} \sinh \left( \zeta \mathsf{v}_{20}^{(2)} \right) \\ & \left( \zeta \mathsf{v}_{20}^{(2)} \right) + \prod_{1}^{(2)} \mathsf{v}_{10}^{(2)} \mathsf{v}_{20}^{(2)} \sinh \left( \zeta \mathsf{v}_{20}^{(2)} \right) \\ & & \left( \zeta \mathsf{v}_{20}^{(2)} \right) + \prod_{1}^{(2)} \mathsf{v}_{10}^{(2)} \mathsf{v}_{20}^{(2)} \sinh \left( \zeta \mathsf{v}_{20}^{(2)} \right) \\ & & \left( \zeta \mathsf{v}_{20}^{(2)} \right) + \prod_{1}^{(2)} \mathsf{v}_{10}^{(2)} \mathsf{v}_{20}^{(2)} \sinh \left( \zeta \mathsf{v}_{20}^{(2)} \right) \\ & & \left( \zeta \mathsf{v}_{20}^{(2)} \right) + \prod_{1}^{(2)} \mathsf{v}_{10}^{(2)} \mathsf{v}_{20}^{(2)} \sinh \left( \zeta \mathsf{v}_{20}^{(2)} \right) \\ & & \left( \zeta \mathsf{v}_{20}^{(2)} \right) + \prod_{1}^{(2)} \mathsf{v}_{10}^{(2)} \mathsf{v}_{20}^{(2)} \sinh \left( \zeta \mathsf{v}_{20}^{(2)} \right) \\ & & \left( \zeta \mathsf{v}_{20}^{(2)} \right) + \prod_{1}^{(2)} \mathsf{v}_{20}^{(2)} \sinh \left( \zeta \mathsf{v}_{20}^{(2)} \right) \\ & \left( \zeta \mathsf{v}_{20}^{(2)} \right) + \prod_{1}^{(2)} \mathsf{v}_{20}^{(2)} \sinh \left( \zeta \mathsf{v}_{20}^{(2)} \right) \\ & \left( \zeta \mathsf{v}_{20}^{(2)} \right) + \prod_{1}^{(2)} \mathsf{v}_{20}^{(2)} \sinh \left( \zeta \mathsf{v}_{20}^{(2)} \right) \\ & \left( \zeta \mathsf{v}_{20}^{(2)} \right) + \prod_{1}^{(2)} \mathsf{v}_{20}^{(2)} \sinh \left( \zeta \mathsf{v}_{20}^{(2)} \right) \\ & \left( \zeta \mathsf{v}_{20}^{(2)} \right) + \prod_{1}^{(2)} \mathsf{v}_{20}^{(2)} \sinh \left( \zeta \mathsf{v}_{20}^{(2)} \right) \\ & \left( \zeta \mathsf{v}_{20}^{(2)} \right) + \prod_{1}^{(2)} \mathsf{v}_{20}^{(2)} \sinh \left( \zeta \mathsf{v}_{20}^{(2)} \right) \\ & \left( \zeta \mathsf{v}_{20}^{(2)} \right) + \prod_{1}^{(2)} \mathsf{v}_{20}^{(2)} \sinh \left( \zeta \mathsf{v}_{20}^{(2)} \right) \\ & \left( \zeta \mathsf{v}_{20}^{(2)} \right) + \prod_{1}^{(2)} \mathsf{v}_{20}^{(2)} \sinh \left( \zeta \mathsf{v}_{20}^{(2)} \right) \\ & \left( \zeta \mathsf{v}_{20}^{(2)} \right) + \prod_{1}^{(2)} \mathsf{v}_{20}^{(2)} \det \left( \zeta \mathsf{v}_{20}^{(2)} \right) \\ & \left( \zeta \mathsf{v}_{20}^{(2)} \right) + \prod_{1}^{(2)} \mathsf{v}_{20}^{(2)} \det \left( \zeta \mathsf{v}_{20}^{(2)} \right) \\ & \left( \zeta \mathsf{v}_{20}^{(2)} \right) + \prod_{1}^{(2)} \mathsf{v}_{20}^{(2)} \det \left( \zeta \mathsf{v}_{20$$

and

$$\begin{split} \xi_{1} &= \prod_{3}^{(2)} \left( \mathbf{v}_{10}^{(1)} \mathbf{v}_{20}^{(2)} W \cosh \left( \zeta \mathbf{v}_{20}^{(2)} \right) + Z \sinh \left( \zeta \mathbf{v}_{20}^{(2)} \right) \right) + \prod_{1}^{(2)} \mathbf{v}_{10}^{(1)} \mathbf{v}_{20}^{(2)} X \cosh \left( \zeta \mathbf{v}_{10}^{(2)} \right) + \prod_{1}^{(2)} \mathbf{v}_{10}^{(2)} \mathbf{v}_{20}^{(2)} Y \sinh \left( \zeta \mathbf{v}_{10}^{(2)} \right), \\ \xi_{2} &= \prod_{1}^{(2)} \mathbf{v}_{20}^{(2)} \left( \mathbf{v}_{10}^{(2)} \mathbf{v}_{20}^{(1)} W \sinh \left( \zeta \mathbf{v}_{10}^{(2)} \right) + Z \cosh \left( \zeta \mathbf{v}_{10}^{(2)} \right) \right) + \prod_{3}^{(2)} \left( \mathbf{v}_{20}^{(1)} X \sinh \left( \zeta \mathbf{v}_{20}^{(2)} \right) + \mathbf{v}_{20}^{(2)} Y \cosh \left( \zeta \mathbf{v}_{20}^{(2)} \right) \right), \\ \xi_{3} &= \prod_{1}^{(2)} \cosh \left( \zeta \mathbf{v}_{10}^{(2)} \right) + \prod_{3}^{(2)} \cosh \left( \zeta \mathbf{v}_{20}^{(2)} \right), \\ \xi_{4} &= -\left( \mathbf{v}_{10}^{(2)} \left( \left( \prod_{1}^{(2)} \left( \prod_{1}^{(2)} + \prod_{3}^{(2)} \right) Z - \prod_{3}^{(2)} U \right) \cosh \left( \zeta \mathbf{v}_{20}^{(2)} \right) + \prod_{1}^{(2)} \left( \left( \prod_{1}^{(2)} + \prod_{3}^{(2)} \right) \mathbf{v}_{10}^{(1)} \mathbf{v}_{20}^{(2)} W \sinh \left( \zeta \mathbf{v}_{20}^{(2)} \right) \right) \\ &+ \mathbf{v}_{10}^{(2)} \left( 2 \prod_{2}^{(2)} \left( \prod_{1}^{(2)} + \prod_{3}^{(2)} \right) Y - \prod_{1}^{(2)} U \right) \cosh \left( \zeta \mathbf{v}_{10}^{(2)} \right) + 2 \prod_{2}^{(2)} \left( \left( \prod_{1}^{(2)} + \prod_{3}^{(2)} \right) \mathbf{v}_{10}^{(1)} X \sinh \left( \zeta \mathbf{v}_{10}^{(2)} \right) \right), \\ \xi_{5} &= \mathbf{v}_{10}^{(2)} \mathbf{v}_{20}^{(1)} \left( \prod_{1}^{(2)} Y + 2 \prod_{2}^{(2)} \left( \prod_{1}^{(2)} + \prod_{3}^{(2)} \right) W \right) \cosh \left( \zeta \mathbf{v}_{10}^{(2)} \right) + \mathbf{v}_{10}^{(2)} \left( \mathbf{v}_{10}^{(2)} + \prod_{1}^{(2)} \left( \prod_{1}^{(2)} + \prod_{3}^{(2)} \right) X \right) \cosh \left( \zeta \mathbf{v}_{20}^{(2)} \right) \\ &+ \prod_{1}^{(2)} \left( \prod_{1}^{(2)} + \prod_{3}^{(2)} \right) \mathbf{v}_{20}^{(2)} Y \sinh \left( \zeta \mathbf{v}_{20}^{(2)} \right) + 2 \prod_{2}^{(2)} \left( \prod_{1}^{(2)} + \prod_{3}^{(2)} \right) Z \sinh \left( \zeta \mathbf{v}_{10}^{(2)} \right), \end{aligned}$$

while the expressions for the rest of the unknown terms are provided in the Appendix C for reference.

Also, the dispersion relation corresponding to the micropolar surface wave that vanishes in the absence of the micropolarity in its first-order correction is given as,

$$\nabla_0 + \epsilon_1 \nabla_1 + \epsilon_2 \nabla_2 = 0, \tag{3.2.46}$$

where,

$$\begin{split} \nabla_0 &= 2\zeta \mathbf{v}_3^{(2)} \left[ \left( \Theta_3^{(1)} \right)^2 \mathbf{v}_{30}^{(1)} \chi \cosh \left( \zeta \mathbf{v}_{30}^{(2)} \right) + \left( \Theta_3^{(2)} \right)^2 \frac{j^{(2)}}{j^{(1)}} \mathbf{v}_{30}^{(2)} \sinh \left( \zeta \mathbf{v}_{30}^{(2)} \right) \right], \\ \nabla_1 &= -\left( \Theta_3^{(1)} \right)^2 \mathbf{v}_{30}^{(2)} \chi \cosh \left( \zeta \mathbf{v}_{30}^{(2)} \right), \\ \nabla_3 &= -\zeta \left[ \left( \Theta_3^{(1)} \right)^2 \mathbf{v}_{30}^{(1)} \chi \sinh \left( \zeta \mathbf{v}_{30}^{(2)} \right) + 2 \left( \Theta_3^{(2)} \right)^2 \frac{j^{(2)}}{j^{(1)}} \mathbf{v}_{30}^{(2)} \cosh \left( \zeta \mathbf{v}_{30}^{(2)} \right) \right], \end{split}$$

where  $\Theta_3^{(i)}$ , i = 1, 2 are defined in Appendix C.

# 3.2.5 Graphical discussions

To gain deeper insights into the influence of nonlocal elasticity and micropolarity on Rayleigh wave propagation within a layered medium, a series of graphical representations are presented. These figures elucidate the dispersive nature of Rayleigh waves and the variations in phase velocities with respect to wavenumber and micropolar parameters. To facilitate a comprehensive understanding of the graphical results, we introduce the following non-dimensional parameters: Poisson's ratio  $(\nu)$ , micropolar ratio (d) and characteristic length ratio (l). For the semi-infinite medium (i = 1) and the layer (i = 2), these parameters are defined as:

$$\nu^{(i)} = \frac{\lambda^{(i)}}{2\lambda^{(i)} + 2\mu^{(i)} + \kappa^{(i)}}, \ d^{(i)} = \frac{\kappa^{(i)}}{\mu^{(i)}}, \ l^{(i)} = \frac{\gamma^{(i)}}{j^{(i)}\mu^{(i)}}.$$

Throughout the graphical analysis, we assume the following values for the non-dimensional parameters:  $\nu^{(1)} = 0.1$ ,  $\nu^{(2)} = 0.4$ ,  $\ell^{(1)} = 0.2$ ,  $\ell^{(2)} = 0.8$ , unless otherwise specified.

The graphical analysis presented in Figure 3.2.2 provides a comprehensive comparison of Rayleigh wave propagation in four distinct scenarios: local elastic, nonlocal elastic, incorrect nonlocal results, local micropolar, nonlocal micropolar media and incorrect nonlocal micropolar results. We deliberately include incorrect dispersion curves to demonstrate the inaccuracies present in past literature compared to the refined boundary condition

results presented in this study. The introduction of micropolarity, characterized by additional rotational degrees of freedom, results in an increase in phase velocity. Conversely, nonlocality, which accounts for long-range interactions, leads to a decrease in phase velocity. The interplay between these two effects shapes the overall dispersion behavior. Micropolar media (both local and nonlocal case) exhibit a concave downward dispersion curve, indicating a positive dispersion relation. This means that that lower frequency components travel faster than higher frequency components, leading to a compression of the wave packet. Purely elastic materials (both local and nonlocal case), on the other hand, exhibit concave upwards dispersion curve indicating a negative dispersion, where higher frequency components travel faster than lower frequency components. This leads to a spreading of the wave packet over time. It is important to note that the limit  $hk \to 0$  corresponds to an infinitely long wavelength relative to the layer thickness. Our analysis reveals that even for small hk, where the wavelength is significantly larger than h, nonlocal effects persist, influencing wave propagation. This observation highlights the crucial role of layer thickness in governing nonlocal behavior.

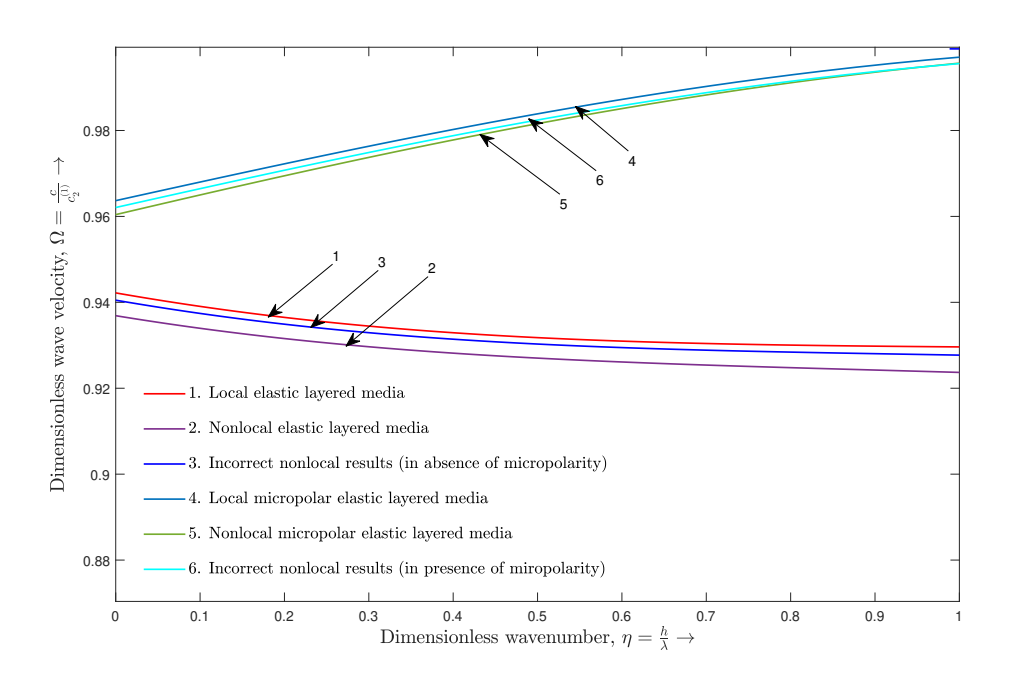


Figure 3.2.2: Comparision of Rayleigh wave dispersion curves under the influence of micropolarity and nonlocality in a layered medium

The provided dispersion curve in Figure 3.2.3 illustrates the influence of the micropolar ratio  $d_2$  in the layer on the phase velocity of Rayleigh waves. As the micropolar ratio  $d_2$  of the layer increases, the phase velocity curves increases with the increase in the wavenumber. This indicates that a higher micropolar ratio leads to a faster propagation of Rayleigh waves at the higher wavenumbers. However, beyond a certain value of  $d_2$ , the dispersion curve shows a concave upward trend in the phase velocity with the increasing wavenumber. This complex behavior is attributed to the interplay between the micropolar effects and the geometric properties of the layer.

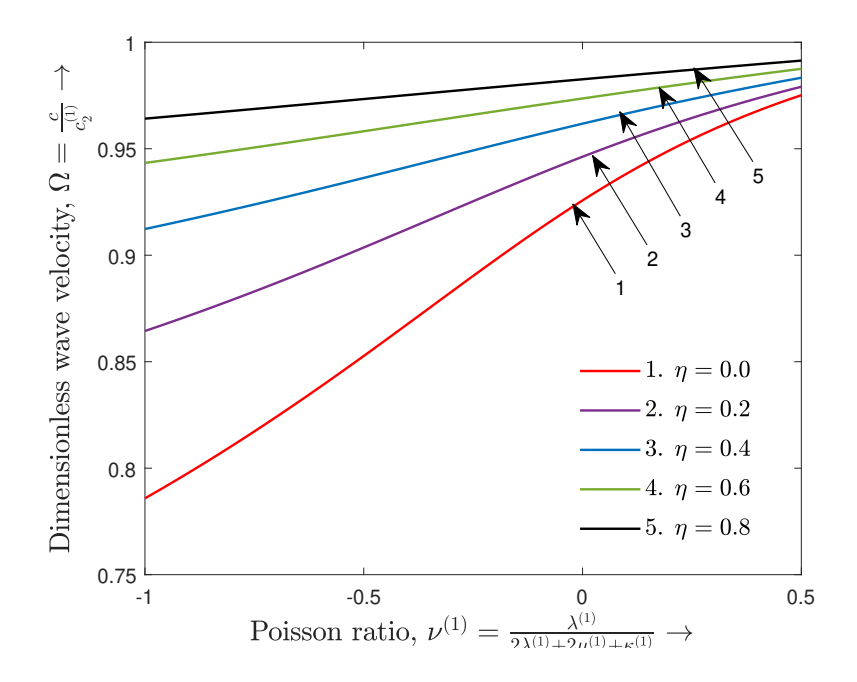


Figure 3.2.3: Dispersion curves of nonlocal micropolar Rayleigh waves for different values of micropolar ratio  $d^{(2)}$ 

The graph plotted in Figure 3.2.4 illustrate the impact of Poisson's ratio  $\nu^{(1)}$  in the semi-infinite medium on the phase velocity of Rayleigh waves. As  $\nu^{(1)}$  increases, the phase velocity also increases for a given wavenumber, indicating a positive correlation between material stiffness and wave propagation speed. Also at a higher value of  $\nu^{(1)}$ , the variation in phase velocity with respect to wavenumber becomes less significant. A higher Poisson's ratio in the semi-infinite medium corresponds to a stiffer material. This increased stiffness leads to faster propagation of Rayleigh waves, resulting in higher phase velocities. However, as the material stiffness increases, the dispersive nature of the Rayleigh waves becomes less pronounced.

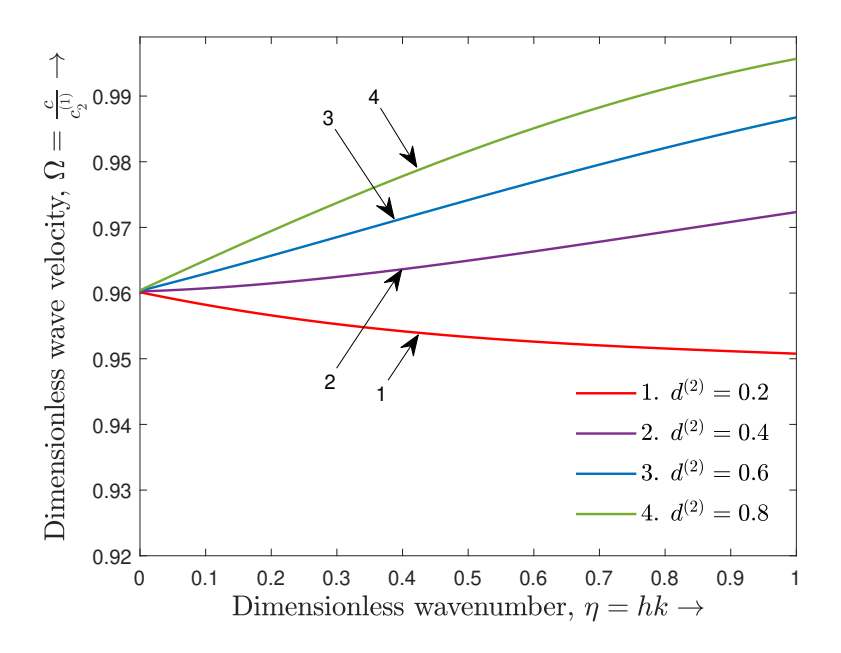


Figure 3.2.4: Variation of dimensionless phase velocity against Poisson's ratio of the semi-infinite medium  $\nu^{(1)}$ 

The dispersion curve in Figure 3.2.5 illustrates the behavior of micropolar surface waves as a function of the micropolar parameter  $l^{(2)}$ . As  $l^{(2)}$  increases, the frequency of the micropolar surface wave also increases, especially at higher wavenumbers. This indicates that the micropolar effect enhances the wave propagation frequency for the newer mode of Rayleigh waves, particularly for shorter wavelengths. Moreover, the dispersion curve exhibits a rapid increase in frequency at lower wavenumbers, followed by a plateau at higher wavenumbers. This suggests that the micropolar surface wave experiences significant dispersion at shorter wavelengths, while the dispersion effect diminishes at longer wavelengths.

Figure 3.2.6 provides a comparative analysis in a reduced model of Rayleigh wave dispersion in a nonlocal micropolar half-space, highlighting the evolution of modeling accuracy. The black dotted line, representing classical micropolar elasticity, shows a non-dispersive wave behavior, serving as a baseline. When Eringen's nonlocal boundary conditions [60] are applied, the dispersion curves reveal a notable deviation, indicating the introduction of dispersive characteristics. Pham and Vu's approach (see, [275,276]) which incorporates an additional condition on  $\tau_{11}$  further demonstrates this dispersion, showing a substantial decrease in phase velocity with increasing nonlocal parameters. In contrast,

the asymptotic approach presented in this research which accounts for boundary layer effects, explicitly captures the dispersive nature of Rayleigh waves. The plotted first-order corrected dispersion relation demonstrates a distinct representation of this phenomenon compared to previous models. This comparison underscores the importance of considering boundary layer effects and refined boundary conditions in accurately modeling Rayleigh wave propagation in nonlocal micropolar media.

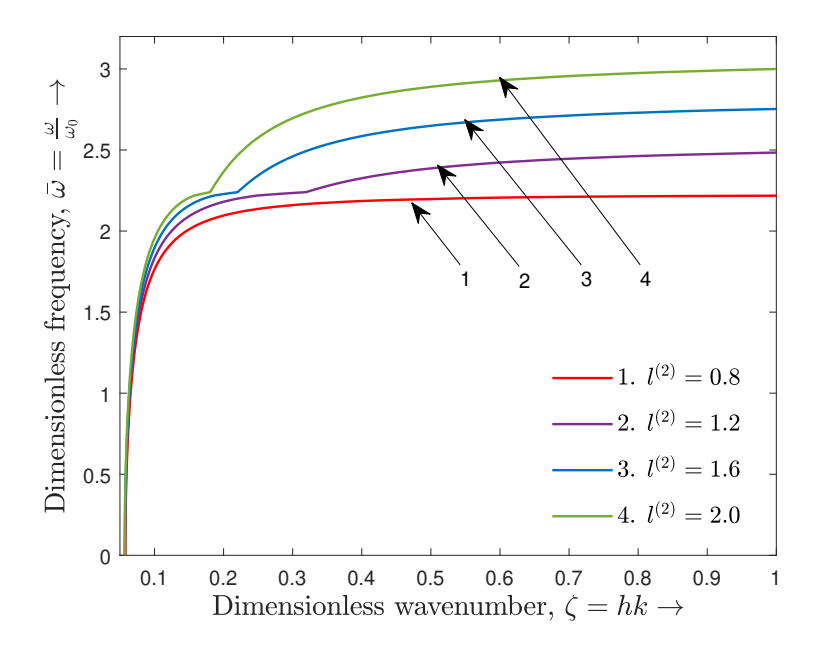


Figure 3.2.5: Dispersion curves of a new micropolar surface wave for different values of  $l^{(2)}$ 

## 3.2.6 Conclusions

Assuming that the wavelength of the propagating wave and the thickness of the layer are significantly larger than the nonlocal parameter in both the lower semi-infinite medium and the layer, respectively the original double integral formulations of the nonlocal stresses are reduced to asymptotic expansions involving single integrals. Specifically, an infinite integral is obtained for the nonlocal stresses in the lower semi-infinite medium, while a finite integral is derived for the stresses within the layer.

To ensure equivalence between the differential and integral formulations of nonlocal elasticity, additional conditions are introduced. These conditions impose constraints

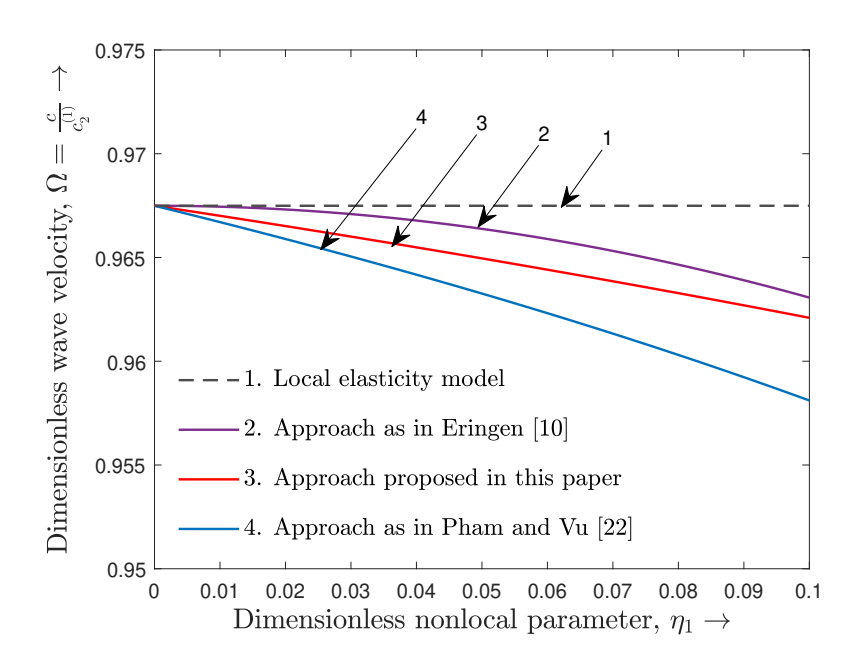


Figure 3.2.6: Comparision of nonlocal dispersion curves of Rayleigh waves in a micropolar half-space via different approaches

on the normal force stresses and shear couple stresses, leading to the development of a modified singularly perturbed differential model.

Using this framework, an asymptotic solution is obtained, and refined boundary and interface conditions are derived within the context of nonlocal and micropolar elasticity. Applying these refined conditions yields first-order nonlocal corrected dispersion relations, which clearly demonstrate the influence of the nonlocal parameters in both media.

The graphical results further reveal that micropolar media exhibit a concave downward dispersion curve, signifying positive dispersion. In contrast, purely elastic materials display a concave upward dispersion curve, indicating negative dispersion. Also, as the material stiffness increases, the dispersive nature of Rayleigh waves becomes less pronounced. Additionally, significant dispersion effects are observed in micropolar surface waves at shorter wavelengths, while these effects diminish at longer wavelengths.

# CHAPTER 4 Rayleigh Wave Propagation and Control by Metasurfaces

The insights gained from the investigation of Rayleigh wave propagation in microstruc-

tural frameworks pave the way for exploring active surface wave control strategies. In this

chapter, we transition our studies from understanding the fundamental behavior of these

waves to manipulating their propagation using resonating structures, alternatively termed

as metasurfaces.

4.1 Nonlinear metasurface with dual spring-mass resonators<sup>\*</sup>

A novel metasurface design comprising an array of dual spring-mass resonators sit-

uated on a nonlocal host substrate to manipulate the surface wave propagation. This

subchapter combines the concepts of nonlocal elasticity, nonlinearity, and double reso-

nance to analyze Rayleigh wave dispersion characteristics.

Description of the proposed model 4.1.1

The configuration for the proposed model is given in Figure 4.1.1. The nonlinear

metasurface is placed around the target structure to protect it from seismic damage. This

metasurface consists of an array of spring-mass systems and is mounted on the surface of

a nonlocal elastic substrate (cf. Figure 4.1.1(a)). Each resonant unit cell of the spring-

mass system is further described in Figure 4.1.1(b). The reference system is introduced

in Figure 4.1.1.

Mathematical formulation and solution 4.1.2

Description of the host nonlocal elastic substrate

The present investigation deals with a simplest material model composed of a lin-

ear isotropic material, say soil as a substrate exhibiting nonlocal elastic properties. This

homogeneous, isotropic nonlocal elastic substrate is characterized by its nonlocal elastic

parameter  $\aleph$ , mass density  $\rho_s$  and longitudinal and transverse shear wave velocities  $\beta_1$ 

and  $\beta_2$ , respectively.

Practically soil could be described as a medium exhibiting both elastic-platic behavior.

On the other hand, it can act as a fully elastic material at much smaller deformations.

The intricate and complex nature of the soil justifies its nonlocal elastic behavior. The

\* Published in European Journal of Mechanics-A/Solids (Elsevier), (2024).

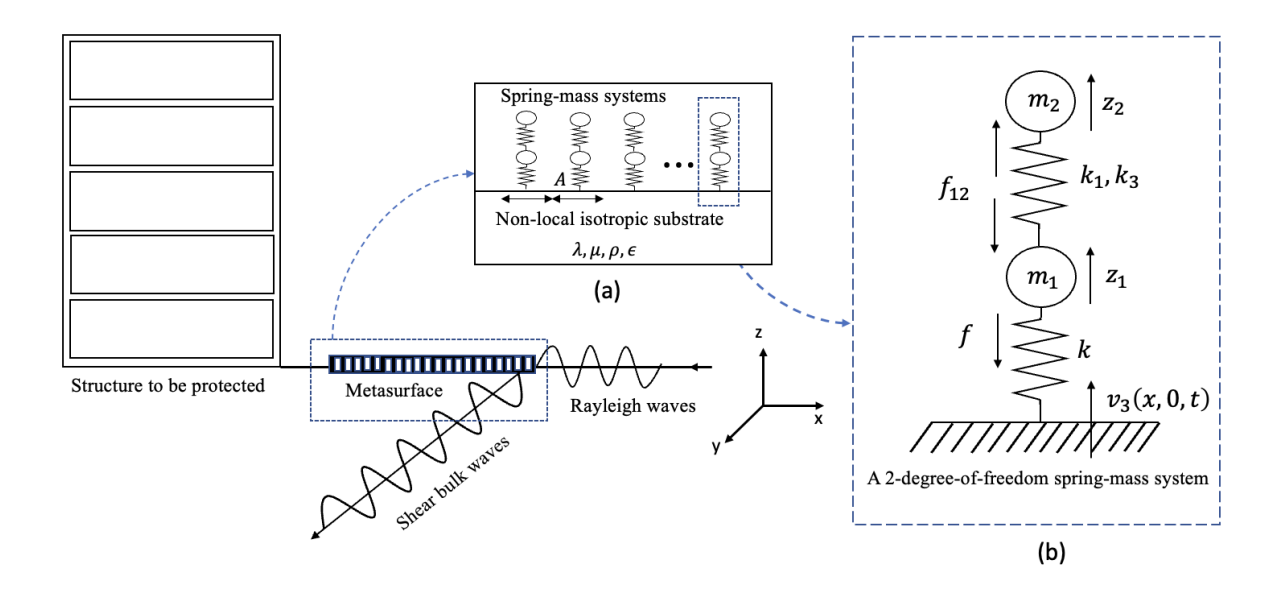


Figure 4.1.1: Schematics of the proposed model (a) design of metasurface (b) a resonant unit cell

existence of an array of spring-mass resonators on the surface could lead to smaller deformation or redistribution of stress among neighboring soil particles. In certain instances, stress distribution might not be uniform, resulting in strain localization in specific areas. Consequently, to account for these long-range interactions, strain localization, and the size-dependent behavior of the soil substrate, we have applied the principles of nonlocal elasticity theory to the soil. Nonlocal models help in interpreting the experimental results accurately. The nonlocal elastic effects are introduced into the model through Eringen's nonlocal elasticity theory, see section 1.3.3 for details.

## Wave propagation in the nonlocal elastic substrate

The seismic waves are characterized by high frequencies, they act on the ground for shorter durations, resulting in inducing smaller strains and smaller deformations. As a result, the soil typically exhibits predominantly elastic behavior due to the relatively shorter duration of seismic ground motion. Also, the seismic events impose short-term loading conditions that are insufficient to cause any significant plastic deformation. Consequently, the soil response is primarily elastic, with particle displacement and strain values remaining within the elastic range during such loading conditions. Although localized plastic deformation and liquefaction can occur under specific circumstances, the overall seismic response of the soil is often reasonably approximated as elastic. Thereby we consider

elastic constitutive assumption for soil during seismic engineering analyses and structural design.

Consider the propagation of Rayleigh waves in a nonlocal elastic substrate (soil), which is a host to an array of nonlinear spring-mass systems. The kinematic equations relating nonlocal elastic stress  $(\tau_{ij})$  in the host substrate with the strains  $(\varepsilon_{ij})$  are given as:

$$(1 - \aleph^2 \nabla^2) \tau_{ij} = \Lambda \, \delta_{ij} \, \varepsilon_{kk} + 2 \, \mu \, \varepsilon_{ij} = \sigma_{ij}, \ i, j = 1, 2, 3 \tag{4.1.1}$$

in which  $\nabla^2 = \frac{\partial^2}{\partial x^2} + \frac{\partial}{\partial z^2}$  is the the usual Laplacian in 2D co-ordinates and  $\delta_{ij}$  stands for Kronecker delta operator;  $\lambda$  and  $\mu$  are the Lame's constants.

Also, the equation relating the strains  $(\varepsilon_{ij})$  to the displacement components  $(u_i)$  is as follows:

$$\varepsilon_{ij} = \frac{1}{2} (u_{i,j} + u_{j,i}), \ i, j = 1, 2, 3$$
 (4.1.2)

Now, the governing equations of motion for Rayleigh waves in a nonlocal elastic substrate and in the absence of body forces can be written as,

$$\tau_{ij,j} - \rho_s u_{i,tt} = 0. (4.1.3)$$

Using Helmholtz decomposition theorem, we decompose the displacement vector  $\vec{u}(x, z, t) = (u_1, 0, u_3)$  into the sum of a scalar potential  $\Phi$  and a vector potential  $\vec{\Psi} = (\Psi_1, \Psi_2, \Psi_3)$ . i.e.,

$$\vec{u} = \nabla \Phi + \nabla \times \vec{\Psi} \tag{4.1.4}$$

As a result, the displacement components can be expressed as,

$$u_1 = \frac{\partial \Phi}{\partial x} - \frac{\partial \Psi_2}{\partial z}, \ u_3 = \frac{\partial \Phi}{\partial z} + \frac{\partial \Psi_2}{\partial x}.$$
 (4.1.5)

On substituting the constitutive relations given in Eq. (4.1.2) into the equation of motion provided in Eq. (4.1.3) and using Eq. (4.1.5), we obtain two decoupled equations in  $\Phi$  and  $\Psi_2$  as

$$\nabla^2 \Phi = \frac{1 - \aleph^2 \nabla^2}{\beta_t^2} \Phi_{tt}, \ \nabla^2 \Psi_2 = \frac{1 - \aleph^2 \nabla^2}{\beta_2^2} \Psi_{tt}, \tag{4.1.6}$$

in which

$$\beta_1 = \sqrt{\frac{\Lambda + 2\mu}{\rho_s}}, \ \beta_2 = \sqrt{\frac{\mu}{\rho_s}}.$$

Assume the time-harmonic Rayleigh waves propagating in x-direction with the wavenumber k, angular frquency  $\omega$  and phase velocity  $c = \frac{\omega}{k}$ .

Let the potential functions be of the form,

$$\Phi(x,z,t) = (A_1 e^{-r_1 z} + A_2 e^{r_1 z}) e^{i(kx-\omega t)}, 
\Psi_2(x,z,t) = (A_3 e^{-r_2 z} + A_4 e^{r_2 z}) e^{i(kx-\omega t)}.$$
(4.1.7)

Here  $A_1$ ,  $A_2$ ,  $A_3$  and  $A_4$  are the amplitudes of the potential functions.

Simple algebraic substitutions of Eqs. (4.1.7) into Eq. (4.1.6) gives the value of  $r_1$  and  $r_2$ as,

$$r_1 = \sqrt{k^2 - \frac{\omega^2}{\beta_1^2 - \aleph^2 \omega^2}}, \ r_2 = \sqrt{k^2 - \frac{\omega^2}{\beta_2^2 - \aleph^2 \omega^2}}.$$

An exponential decay in the amplitudes of Rayleigh waves along positive z-direction suggests the value of constants  $A_2 = A_4 = 0$ . This gives the displacement components as

$$u_1(x,z,t) = \left(i \, p \, A_1 e^{-r_1 z} + r_2 \, A_3 e^{-r_2 z}\right) e^{i(kx - \omega t)},\tag{4.1.8}$$

$$u_3(x,z,t) = \left(-r_1 A_1 e^{-r_1 z} + i p A_3 e^{-r_2 z}\right) e^{i(kx - \omega t)}, \tag{4.1.9}$$

and the corresponding stress vector components acting on a plane normal to z-direction as

$$(1 - \aleph^2 \nabla^2) \, \tau_{31} = \mu \left[ -2 \, i \, p \, r_1 \, A_1 e^{-r_1 z} - (r_2^2 + k^2) \, A_3 e^{-r_2 z} \right] e^{i(kx - \omega t)} = \sigma_{31},$$

$$(1 - \aleph^2 \nabla^2) \, \tau_{32} = 0 = \sigma_{32},$$

$$(1 - \aleph^2 \nabla^2) \, \tau_{33} = \left[ \left\{ (\Lambda + 2\mu) \, r_1^2 - \Lambda \, k^2 \right\} \, A_1 e^{-r_1 z} - 2 \, i \, p \, r_2 \, \mu \, A_3 e^{-r_2 z} \right] \, e^{i(kx - \omega t)} = \sigma_{33}.$$

$$(4.1.10)$$

# Description of the nonlinear metasurface

The metasurface is placed on the free-surface of nonlocal elastic substrate is to control the Rayleigh wave dispersion. To comprehend fully the physics of metasurface, consider the typical configuration of metasurface made up of an array of nonlinear two-degrees-of-freedom spring-mass systems of identical height, arranged with a lattice distance 'a' between each of them. They are spaced apart in order to avoid contact forces between any two resonators. Since our interest lies in analysing the dispersive properties of Rayleigh waves, we treat the metasurface as an effective continuum model via classical homogenization theory.

A simplified variant of classical homogenization theory, known as effective medium theory [272], has been employed to characterize the dynamics of an array of spring-mass resonators placed on a substrate. According to this theory, the resonators, which have subwavelength dimensions, are assumed to be evenly distributed across the surface of the medium, applying uniform normal stress to the elastic medium. Consequently, the normal stresses exerted by the resonators on the surface can be estimated as the averaged elastic force exerted by the resonators over an area that is much larger than the spacing between them but considerably smaller than the wavelength. It is important to note that, in this specific scenario of interest, the wavelengths of surface waves (denoted as  $\lambda$ ) are significantly larger than the average distance 'a' between the resonators, and the dimensions of the area 'A' defined by the regular spatial arrangement of the resonators are larger than 'a' but smaller than  $\lambda$  (for example, a quadratic lattice arrangement has an area,  $A = a^2$ ). This circumstance allows for the practical use of an effective medium approximation, which introduces modified homogenized boundary conditions that relate stress and displacement at the surface.

Each resonant unit cell consists of two masses  $m_1$  and  $m_2$  coupled to each other by means of a nonlinear elastic spring. The main mass  $m_1$  is attached to the nonlocal elastic substrate by an intertialess linear elastic spring of force constant k. We resort to the fact that the surface Rayleigh wave could excite only the vertical motion of the two masses in this two-degree-of-freedom system. The frequency of the torsional mode associated with the rotational motion of the spring-mass system is lower than the frequency associated with vertical oscillations of the spring-mass system excited by the Rayleigh waves. Further, due to this fact, the mass rotation in the z-direction is ignored as the contribution of the torsional mode of the resonators is not significant in the context of generating a local resonance bandgap [70].

## Dynamics of the nonlinear resonators

The free-body diagram representing the direction of displacements and the forces acting on each masses of spring-mass system is as described in Figure 4.1.1(b).

We compute the equation of motion for each masses in the spring-mass system by balancing the forces as per Newton's second law of motion. As we are dealing with a twodegree-of-freedom system here, there are two equations in the form of a coupled differential equations (precisely one written for each mass). It is interesting to note that this system is subjected to an external excitation by Rayleigh waves propagating on the free-surface of the host substrate. Hence, this excitation is primarily due to the displacement component  $u_3(x, 0, t)$  of the Rayleigh waves.

From Eq. (4.1.9), we can write

$$u_3(x,0,t) = B_r e^{i(kx-\omega t)}$$
 where  $B_r = (-r_1 A_1 + i p A_3)$ . (4.1.11)

Let  $z_1$  and  $z_2$  be the displacement of masses  $m_1$  and  $m_2$  respectively. Without loss of generality, let us assume  $z_2 > z_1$ . Let f be the force exerted by the linear spring on the mass  $m_1$  and  $f_{12}$  be the force-displacement function describing the coupling due to the nonlinear spring. i.e.,

$$f = k_0 z_1, (4.1.12)$$

$$f_{12} = \phi(z_1 - z_2), \tag{4.1.13}$$

in which  $\phi$  denotes the restoring force function for the nonlinear spring.

The coupled differential equations for this 2-DOF spring-mass system can be written by balancing the forces on the mass  $m_1$  and  $m_2$ . This gives the equations of motion as,

$$m_{1} \frac{d^{2}z_{1}}{dt^{2}} + k_{0} [z_{1} - u_{3}(x, 0, t)] + f_{12} = 0,$$

$$m_{2} \frac{d^{2}z_{2}}{dt^{2}} + f_{21} = 0.$$
(4.1.14)

For our convenience, define the dimensionless variables

$$u_1 = \frac{z_1}{B_r}, \ u_2 = \frac{z_2 - z_1}{B_r}, \ \tau = \omega t,$$
 (4.1.15)

and specialize the nonlinear spring as the complex duffing oscillator whose force function takes the form,

$$\phi(r) = k_1 r + k_3 r \left| r^2 \right|,$$

where  $k_1$  and  $k_3$  represent the linear and nonlinear stiffness of the spring, respectively. This force function can further be modified by introducing the new dimensionless parameters  $\mu_1$ ,  $\lambda_1$  and  $\nu$ . Hence on introducing  $\mu_1 = \frac{m_2}{m_1}$ ,  $\lambda_1^2 = \frac{k_1}{k_0 \mu_1}$  as the coefficient of linear part of force function  $\frac{\phi}{\mu_1}$  of the nonlinear spring and  $\nu = \frac{k_3|B_r|^2}{k_0}$  as the coefficient of the nonlinear part of the force function, we can write the force function as,

$$\phi(u_i) = k_0 B_r \left( \mu_1 \lambda_1^2 u_i + \nu u_i |u_i|^2 \right).$$

A hardening nonlinearity corresponds to positive values of  $\nu$ , while a softening nonlinearity corresponds to negative values of  $\nu$ . As a result, the system of equations given in Eq. (4.1.14) can be re-written as

$$\Omega_R^2 \frac{d^2 u_1}{d\tau^2} + u_1 - \mu_1 \lambda_1^2 u_2 - \nu u_2 |u_2|^2 - e^{i(kx - \tau)} = 0, 
\mu \Omega_R^2 \left( \frac{d^2 u_1}{d\tau^2} + \frac{d^2 u_2}{d\tau^2} \right) + \mu_1 \lambda_1^2 u_2 + \nu u_2 |u_2|^2 = 0,$$
(4.1.16)

in which  $\Omega_R = \frac{\omega}{\omega_R}$  and  $\omega_R = \sqrt{\frac{k}{m_1}}$ .

On further inserting the parameters,

$$\bar{\Lambda}^2 = \mu_1 \, \lambda_1^2 \text{ and } M = 1 + \frac{1}{\mu_1}.$$

and supposing a time-harmonic form to the dimensionless displacement components given in Eq. (4.1.15) as,

$$u_1 = U_1 e^{i(kx-\tau)}$$
 and  $u_2 = U_2 e^{i(kx-\tau)}$ , (4.1.17)

As a result, the system of differential equations given in Eqs. (4.1.16) can be re-written as

$$\left(\Omega_R^2 - 1\right) U_1 + \bar{\Lambda}^2 U_2 + \nu U_2 |U_2|^2 + 1 = 0, 
\left(\Omega_R^2 - M \bar{\Lambda}^2\right) U_2 + U_1 - \nu M U_2 |U_2|^2 - 1 = 0.$$
(4.1.18)

Simple algebraic manipulations of equations in Eq. (4.1.18) yields the value of  $U_1$  in terms of magnitude of  $U_2$ . Thus, we obtain

$$U_{1} = \frac{1 + \bar{\Lambda}^{2} \zeta + \nu \zeta |U_{2}|^{2}}{1 - \Omega_{R}^{2} + (M + \zeta) (\bar{\Lambda}^{2} + \nu |U_{2}|^{2})}, \text{ where } \zeta = \frac{1 - M}{\Omega_{R}^{2}}.$$
 (4.1.19)

Since resonators facilitate the dispersion of Rayleigh waves, it is feasible to customize their dynamic response to create the metamaterials with desired properties. Moreover, the motion of the mass  $m_1$  in the system can be controlled by tuning the magnitude  $|U_2|$  and  $B_r$  to the required value as the displacement for the mass  $m_1$  can be sought in the form,

$$z_{1} = Z_{1} e^{i(kx - \omega t)} \text{ in which } Z_{1} = \frac{\left(1 + \bar{\Lambda}^{2} \zeta + \nu \zeta |U_{2}|^{2}\right)}{1 - \Omega_{R}^{2} + (M + \zeta) \left(\bar{\Lambda}^{2} + \nu |U_{2}|^{2}\right)} B_{r}. \tag{4.1.20}$$

# 4.1.3 Refined nonlocal boundary conditions

Following from Eqs.(1.3.94), the refined boundary conditions accounting nonlocal boundary layer effects are given as,

1. at 
$$z = 0$$
,

$$(1 + \aleph^2 \nabla^2) \sigma_{31} - \frac{\aleph}{2} \frac{\partial \sigma_{11}}{\partial x} + \frac{\aleph^2}{2} \frac{\partial^2 \sigma_{11}}{\partial x \partial z} = 0$$
 (4.1.21)

2. at 
$$z = 0$$
,

$$(1 + \aleph^2 \nabla^2) \,\sigma_{33} - \frac{\aleph^2}{2} \frac{\partial^2 \sigma_{11}}{\partial x^2} = -\frac{k_0 \, z_1}{A}. \tag{4.1.22}$$

# 4.1.4 Dispersion relation

Substituting the expressions given in Eqs. (4.1.7)-(4.1.9) and (4.1.20) in the boundary conditions given in Eqs. (4.1.21) and (4.1.22) and further rearrangement gives the system of equations with the coefficients  $A_1$ ,  $A_3$ ,  $U_1$  and  $B_r$ .

The prerequisite for this system of equations to have a non-trivial solution is that the determinant of the coefficient matrix must vanish. This solvability criterion yields a first-order nonlocal corrected dispersion relation for hybrid Rayleigh waves as,

$$-4k^{2}r_{10}r_{20} + \left(r_{20}^{2} + k^{2}\right)^{2} - \left(\frac{m_{1}\omega_{R}^{2}}{\rho_{s} A \beta_{2}^{2}}\right)r_{10}\left(r_{20}^{2} - k^{2}\right)Z_{1}$$

$$+\aleph\left[2\left(\gamma^{2} - 1\right)k^{2}r_{20}\left(k^{2} - r_{10}^{2}\right) + \frac{1}{2}k^{2}\left(\frac{m_{1}\omega_{R}^{2}}{\rho_{s} A \beta_{2}^{2}}\right)\left(\gamma^{2}\left(-k^{2}\right) + \left(\gamma^{2} - 2\right)r_{10}^{2} + 2r_{10}r_{20}\right)Z_{1}\right] = 0$$

$$(4.1.23)$$

where  $\gamma = \frac{\beta_1}{\beta_2}$  is the material parameter determining mechanical property of the host nonlocal elastic substrate. Also,  $r_{10}$ ,  $r_{20}$  are the leading order expressions for the quantities  $r_1$ ,  $r_2$  and are given by,

$$r_{10} = \sqrt{k^2 - \frac{\omega^2}{\beta_1^2}}, \qquad r_{20} = \sqrt{k^2 - \frac{\omega^2}{\beta_2^2}}.$$

Dispersion equation for the linear 2-DOF spring-mass resonators

To understand better the impact of nonlinearity on the dispersion curves, we shall initially analyse the effect of linearity of metasurface on the dispersion relation of local hybrid Rayleigh waves. The model is thereby investigated in the context of local elasticity theory. A linear spring (instead of a nonlinear one) is deviced to couple the two masses in every resonant unit cell of the spring-mass system constituting the metasurface. This

reduces the magnitude of the normalized displacement of the spring-mass system given in Eq. (4.1.19) to,

$$U_1 = \frac{1 + \bar{\Lambda}^2 \zeta}{1 - \Omega_R^2 + (M + \zeta) \bar{\Lambda}^2}, \text{ where } \zeta = \frac{1 - M}{\Omega_R^2}.$$

It is natural to obtain two resonant frequencies due to the presence of two-degree-of-freedom spring-mass resonators. These resonant frequencies correspond to the horizontal asymptotes in the dispersion curves whereas the threshold frequencies for each branch can be determined by examining the local hybrid Rayleigh wave dispersion relation. Interestingly, these dispersion curves lie on the shear wave dispersion curve and as a result, the threshold frequencies can be obtained by setting  $c = \beta_2$  along with  $\aleph = 0$  and  $\nu = 0$  in Eq. (4.1.23). This gives,

$$\omega_t^5 - \omega_R^2 \left( 1 + M\bar{\Lambda}^2 \right) \omega_t^3 - \left( \frac{m_1 \, \omega_R^4}{\rho_s \, A \, \beta_2} \right) \sqrt{1 - \frac{\beta_2^2}{\beta_1^2}} \, \omega_t^2 + \omega_R^4 \, \bar{\Lambda}^2 \left( M - 1 \right) \omega_t$$
$$+ \omega_R^4 \, \bar{\Lambda}^2 \left( \frac{m_1 \, \omega_R^2}{\rho_s \, A \, \beta_2} \right) \sqrt{1 - \frac{\beta_2^2}{\beta_1^2}} \left( M - 1 \right) = 0. \tag{4.1.24}$$

As the coefficients in the Eq. (4.1.24) are all positive, we can deduce that this equation has exactly two positive real roots by the Descartes's rule of signs. And these positive real roots corresponds to the cut-off frequencies or the terminating frequencies for the dispersion branch.

### Dispersion equation for the linear 1-DOF spring-mass resonators

In this section, we shall outline the dispersive features of the Rayleigh waves propagating on a linear metasurface consisting of only one mass attached to the local elastic substrate ( $\aleph = 0$ ) by the means of an elastic linear spring. If the second mass  $m_2$  is absent in the spring-mass system, then  $\mu_1 = 0$  and consequently M = 1 and  $\zeta = 0$ . Thus, the expression  $U_1$  given in Eq. (4.1.19) can be re-written as,

$$U_1 = \frac{1}{1 - \Omega_R^2 + \bar{\Lambda}^2}.$$

As discussed in the last section, we can obtain the cut-off frequencies for the dispersion branch curves by substituting  $c = \beta_2$  along with  $\aleph = 0$  in the dispersion equation [see, Eq. (4.1.23)]. Therefore, the cut-off frequencies are the positive real solutions to the cubic

equation,

$$\omega_t^3 - \omega_R^2 \left( 1 + \bar{\Lambda}^2 \right) \, \omega_t - \frac{m_1 \omega_R^4}{\rho_s \, A \, \beta_2} \sqrt{1 - \frac{\beta_2^2}{\beta_1^2}} = 0. \tag{4.1.25}$$

Similar observations of this cubic equation suggests that there is exactly one positive real solution. This indicates that there exists only one high-frequency dispersion branch whose threshold (cut-off) frequency is the positive real root of the Eq. (4.1.25).

## Dispersion equation in the absence of metasurface

To derive the dispersion equation for Rayleigh waves in the absence of the metasurface on the host nonlocal elastic substrate, we substitute  $m_1 = 0$  in Eq. (4.1.23). This provides,

$$-4k^{2}r_{10}r_{20} + (r_{20}^{2} + k^{2})^{2} + \aleph \left[2(\gamma^{2} - 1)k^{2}r_{20}(k^{2} - r_{10}^{2})\right]. \tag{4.1.26}$$

which matches with the results in Eq. (1.3.95).

Under the local elastic conditions, a secular equation is obtained by inserting  $\aleph = 0$  in Eq. (4.1.26):

$$\left(2 - \frac{c^2}{\beta_2^2}\right)^2 - 4\sqrt{1 - \frac{c^2}{\beta_1^2}}\sqrt{1 - \frac{c^2}{\beta_2^2}} = 0.$$
(4.1.27)

In fact, the frequency relation obtained above is exactly the same as that of the well-known secular Rayleigh wave equation [14]. This shows the validity of the proposed model.

# 4.1.5 Graphical discussions

The presence of harmonic spring-mass resonators over the host substrate induces local resonance bandgaps and can be visualized by plotting the dispersion curves. In this section, we describe numerically and graphically the dispersive behavior of Rayleigh waves associated with the different spring nonlinearity, relative amplitude inputs, nonlocal elastic parameters and the mechanical characteristics of the substrate.

The details of normalized parameters used while plotting the graphs in this section are given in the table below (unless otherwise specified):

The dispersion curves shown in Figure 4.1.2 are plotted to describe the surface wave propagation in three different configurations of resonators constituting the metasurface: (a) linear spring-mass resonators ( $\nu = 0$ ) (b) soft nonlinear spring-mass resonators ( $\nu = -1$ ) (c) hard nonlinear spring-mass resonators ( $\nu = +1$ ). These harmonic resonators prevent the occurrence of pure Rayleigh waves, but instead the waves attenuating at certain regions are discovered. These waves differ from the typical Rayleigh waves and

Table 4.1.1: Values of some normalized paramteres

Normalized parameters	Values
Material parameter, $\gamma = \frac{\beta_1}{\beta_2}$	1.5
Nonlocal elastic parameter, $\epsilon = \aleph k$	0.1
Mass ratio, $\mu_1 = \frac{m_1}{m_2}$	0.5
$ar{\Lambda}$	0.75
$ U_2 $	0.8
$w = \frac{m \omega_R}{\rho_s A \beta_2}$	0.7

exists because of the presence of an array of spring-mass resonators embedded on the free-surface of host substrate; it is therefore termed as, 'hybrid Rayleigh waves'. An initial observation of dispersion curves indicates that the local resonances of the spring-mass systems couple with the propagating Rayleigh wave, thereby yielding dispersion branch curves near the resonant frequencies. A spectral bandgap separates these repelling dispersion branch curves. More importantly, it is this frequency region where the mode-conversion takes place and the Rayleigh waves diverge deeply into the earth as bulk shear waves, thereby protecting the structures from seismic damage.

The parameters  $\gamma$ ,  $\epsilon = \aleph k$ ,  $\mu_1$ ,  $\bar{\Lambda}$ ,  $|U_2|$  and w are fixed to the values given in the table. The dispersion curves for hybrid Rayleigh waves, pure Rayleigh waves and bulk shear waves are denoted by the solid black lines, dotted black lines and dotted red lines, respectively. The dispersion curves creates two resonance bandgaps in Figures 4.1.2(a) and 4.1.2(c), where as Figure 4.1.2(b) representing the configuration of soft nonlinear spring-mass systems creates only one spectral bandgap. Amazingly, despite the fact that there are varying numbers of bandgaps in each of the three configurations, the sum of the bandwidths still remains the same. The hybrid Rayleigh waves propagate with a velocity of  $c_{hR} < c_{pR}$  in the dispersion branch I of Figures 4.1.2(a), 4.1.2(b) and 4.1.2(c), where the curve asymptotically reaches the resonant frequencies. In addition, the dispersion branch II of Figure 4.1.2(a) and 4.1.2(c) also approach the second resonant frequency asymptotically. In this branch, the phase velocity of hybrid Rayleigh waves increases with the decrease in the wavenumber and finally becomes equivalent to  $c_{pR}$  at a particular wavenumber. When  $c_{hR} > c_{pR}$  below this wavenumber, the branch terminates at

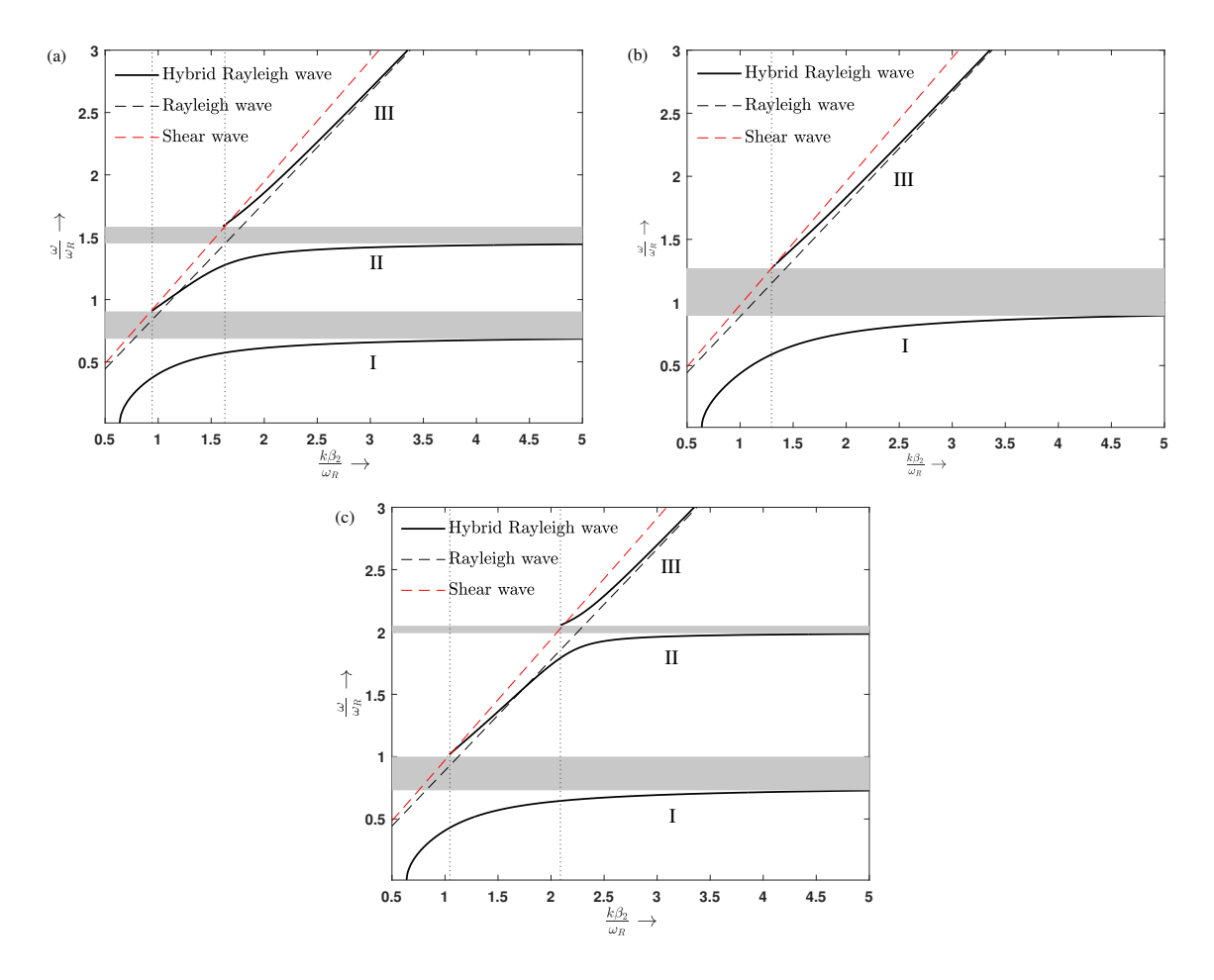


Figure 4.1.2: Dispersion curves for three different configurations in springmass systems. (a) Linear resonators ( $\nu = 0$ ) (b) Soft nonlinear resonators ( $\nu = -1$ ) (c) Hard nonlinear resonators ( $\nu = +1$ )

a frequency where  $c_{hR} = c_s$ . This is because of the fact that the surface waves cannot exist for  $c_{hR} > c_s$ . As a consequence, the dispersion relation cannot have any surface solutions, leading to an effective bandgap. In addition to this, the dispersion branches III of Figures 4.1.2(a), 4.1.2(b) and 4.1.2(c) also terminates at a frequency where  $c_{hR} = c_s$ , resulting in the mode-conversion of Rayleigh waves producing another bandgap. These terminating frequencies, in other words are the cut-off frequencies described in section 3. Waves can cross the metasurface at this frequency, but they are able to accomplish this only by transforming themselves into shear waves.

One might also infer that the metasurface with hard springs can even attenuate more high-frequency Rayleigh waves, making it more beneficial than the linear metasurface. Besides, a metasurface with soft springs could also be preferred over the linear metasurface as this configuration provides a broader bandgap at a certain relative amplitude than the rest. In brief, the nonlinearity in the spring-mass systems has a crucial positive impact on the dispersive nature of the Rayleigh waves.

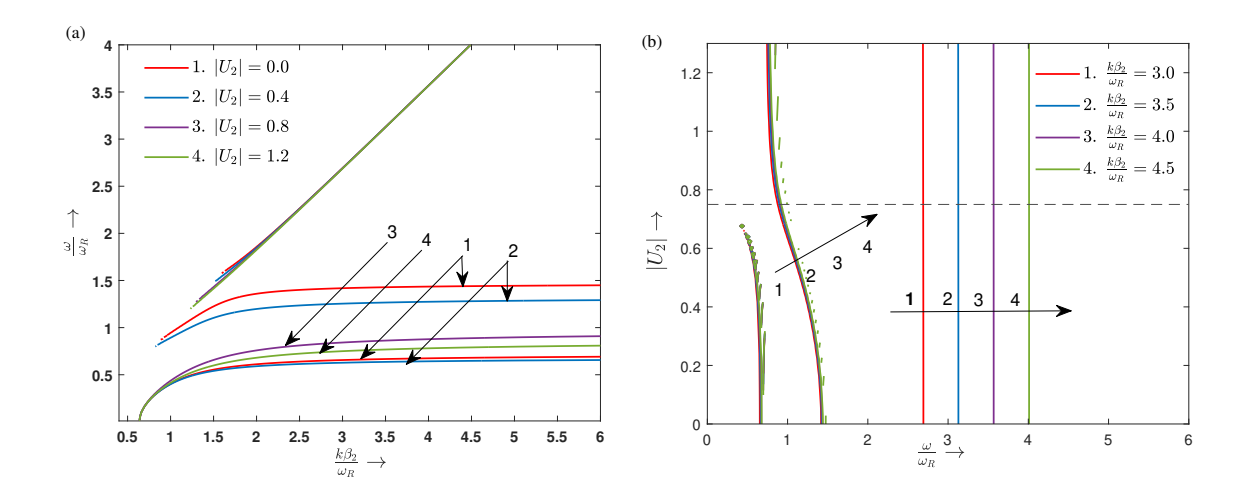


Figure 4.1.3: Effect of relative amplitude input on dispersion curves in a soft nonlinear spring. (a) Dispersion curves showing spectral bandgaps (b) Variation of relative amplitude input with dimensionless frequency

Figure 4.1.3 depicts the effect of relative amplitude  $|U_2|$  on the dispersive behavior of hybrid Rayleigh waves propagating on a soft nonlinear metasurface. The design of the nonlinear metasurface involves the setting up of this parameter as a prerequisite for interpreting the characteristics of the dispersion curves. Figure 4.1.3(a) is plotted to demonstrate the bandgaps produced as a result of varying  $|U_2|$ . It can be clearly seen that when  $|U_2| = 0$  and  $|U_2| = 0.4$ , two spectral bandgaps are created, whereas for  $|U_2| = 0.8$  and  $|U_2| = 1.2$ , the dispersion curves produces a single bandgap. This suggests that a certain limiting point on the magnitude  $|U_2|$  exists beyond which a single spectral bandgap is achieved. To interpret clearly this limiting value, we plot a graph in Figure 4.1.3(b) showing the variation of  $|U_2|$  with the dimensionless frequency. A limiting value exists around  $|U_2| = 0.75$ , below which the soft spring-mass systems resonates with two natural frequencies resulting in two bandgaps. Moreover, the frequency at which the Rayleigh wave propagates for a particular wavenumber decreases with the increase in the values of  $|U_2|$  upto 0.75. Beyond this value, the propagating wave frequency increase with the increase in  $|U_2|$ . In brief, a significant effect in the spectral bandgaps is observed with

the variation in relative amplitude input. A single bandgap observed in the case of soft spring splits into two with the decrease in the input amplitude.

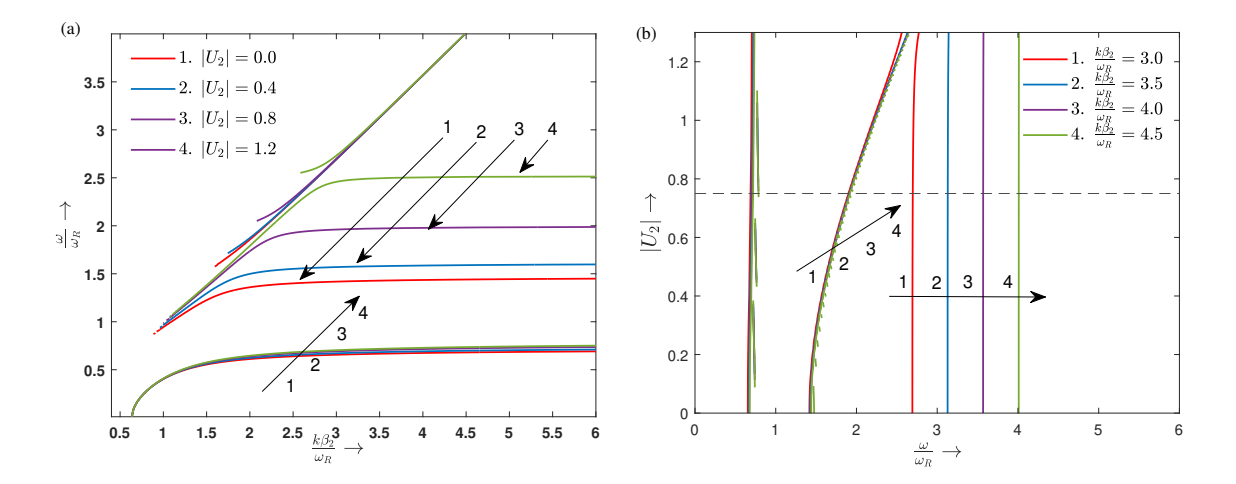


Figure 4.1.4: Effect of relative amplitude input on dispersion curves in a hard nonlinear spring. (a) Dispersion curves showing spectral bandgaps (b) Variation of relative amplitude input with dimensionless frequency

Similarly, Figure 4.1.4 is plotted to demonstrate the effects of relative amplitude ratio  $|U_2|$  in a hard spring. The dispersion curves creates two bandgaps corresponding to two resonant frequencies for all the values of  $|U_2|$  (refer Figure 4.1.4(b)). A careful observation of Figure 4.1.4(a) shows that the lower frequency bandgap remains the same for all increasing values of  $|U_2|$ ; while the frequency bandgaps corresponding to second resonant frequency occur at higher frequency region with the increase in the values of  $|U_2|$ . This indicates that the metasurface designed with hard springs and higher input relative amplitude ratio can shield the structure from Rayleigh waves propagating even at a higher frequency.

The red solid line in Figure 4.1.5 represents the Rayleigh waves propagating in the absence of metasurface. The effect of k (or  $\omega_R$ ) on the dispersion curves are analysed in Figure 4.1.5 for both the soft (Figure 4.1.5(a)) and hard (Figure 4.1.5(b)) springs. The phase velocity and the cut-off frquency of the hybrid Rayleigh waves decrease and increase, respectively with the increasing linear stiffness of the spring.

Figures 4.1.6 and 4.1.7 shows the variation of behavior of Rayleigh waves with the various nonlocal elastic parameters and material properties of the host substrate, respectively. The effect of increasing nonlocal elastic parameters on the dispersion curves for

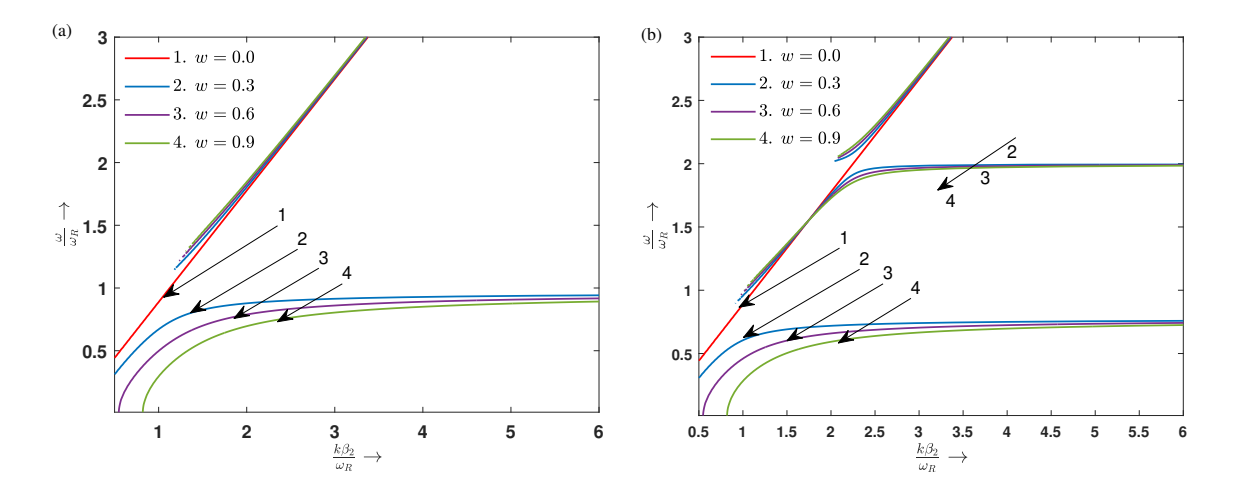


Figure 4.1.5: Dispersion curves showing the effect of linear stiffness  $(k/\omega_R)$  of the spring on the spectral bandgaps of (a) soft nonlinear spring-mass systems (b) hard nonlinear spring-mass systems

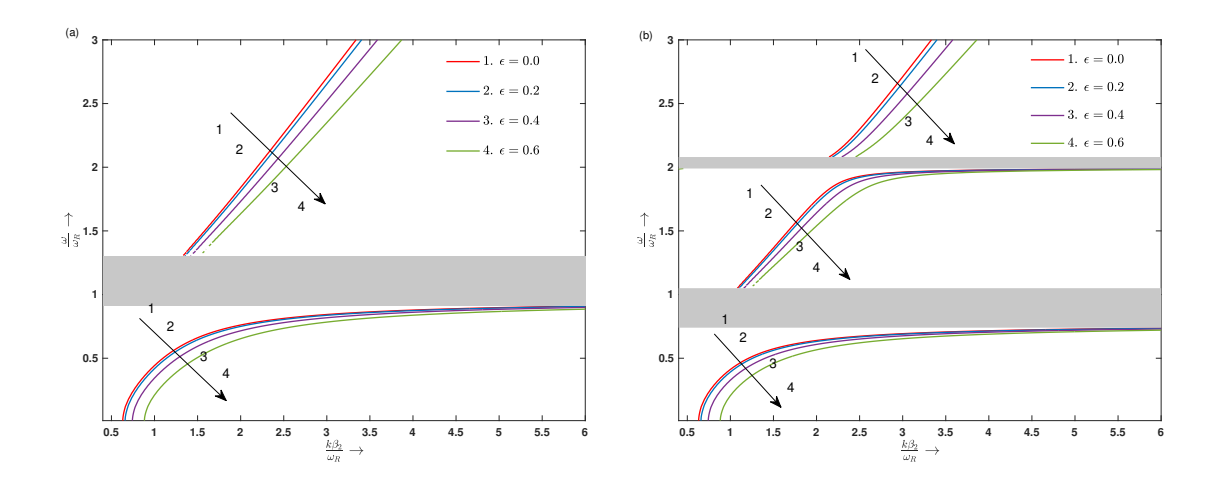


Figure 4.1.6: Dispersion curves showing the effect of nonlocal elastic parameter  $(\epsilon)$  of the substrate on the spectral bandgaps of (a) soft nonlinear spring-mass systems (b) hard nonlinear spring-mass systems

soft and hard springs are presented in Figure 4.1.6(a) and 4.1.6(b), respectively. While the bandgaps are unchanged by changes in the nonlocal elastic parameters of the substrate, the nonlocal elasticity in the substrate has a substantial effect on the phase velocity of the hybrid Rayleigh waves. Furthermore, the increase in the nonlocal elastic parameter of the substrate reduces the phase velocity of the hybrid Rayleigh waves.

Figure 4.1.7 shows the influence of the material parameter  $\gamma$  on the dispersion curves. An increase in this material parameter increases the phase velocity of hybrid Rayleigh wave propagating in every dispersion branch curves. However, the resonant frequency and the cut-off frequency have the same values for every material taken under the study. The spectral bandgaps too occupy the same frequency region indicating that there is a negligible influence of material property on the width of the bandgaps.

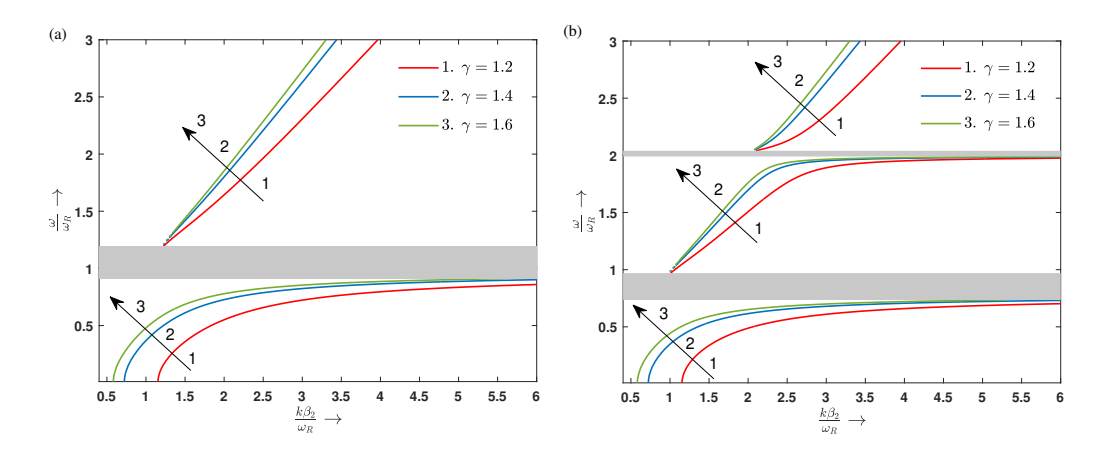


Figure 4.1.7: Dispersion curves showing the effect of material parameter  $(\gamma)$  of the substrate property on the spectral bandgaps of (a) soft nonlinear spring-mass systems (b) hard nonlinear spring-mass systems

## 4.1.6 Conclusions

This study demonstrates the existence of cut-off frequencies at which surface waves transform into shear waves and are visualized through dispersion curves. Notably, dual spring-mass metasurfaces exhibit two distinct frequency bandgaps. Nonlinearities significantly influence bandgap characteristics with hard springs confining higher frequency Rayleigh waves, while soft springs yielding broader bandgaps than linear designs. Input amplitude variations also induce substantial spectral bandgap changes, including the splitting of single bandgaps in soft spring systems. Furthermore, increased linear spring stiffness and nonlocal elastic parameters in the substrate reduce Rayleigh wave phase velocity. While substrate material parameter increases also reduce phase velocity, their impact on spectral bandgap width is negligible. In essence, this research reveals the critical role of resonator design, nonlinearity, input amplitude, and material properties in controlling Rayleigh wave propagation and bandgap formation.

# 4.2 A multiple scattering formulation in a nonlinear metasur- $face^*$

Developing further the previous chapter, this section incorporates inter-resonator coupling effects, which are crucial for accurate metasurface modeling. Recognizing that each resonator acts as a secondary wave source, leading to multiple scattering events, we employ a multiple scattering formulation to investigate Rayleigh wave control in nonlinear metasurfaces. Specifically, we focus on manipulating Rayleigh wave disturbances generated by an interior source through detailed analysis.

## 4.2.1 Description of the proposed model

Consider a metasurface consisting of an array of nonlinear spring-mass systems of mass m placed on the surface of a homogeneous, isotropic elastic medium occupying the region  $z \geq 0$  (see Figure 4.2.1). Let z- direction be positively downwards. An interior source located along the line z=h produces disturbances, thereby inducing Rayleigh waves at the surface.

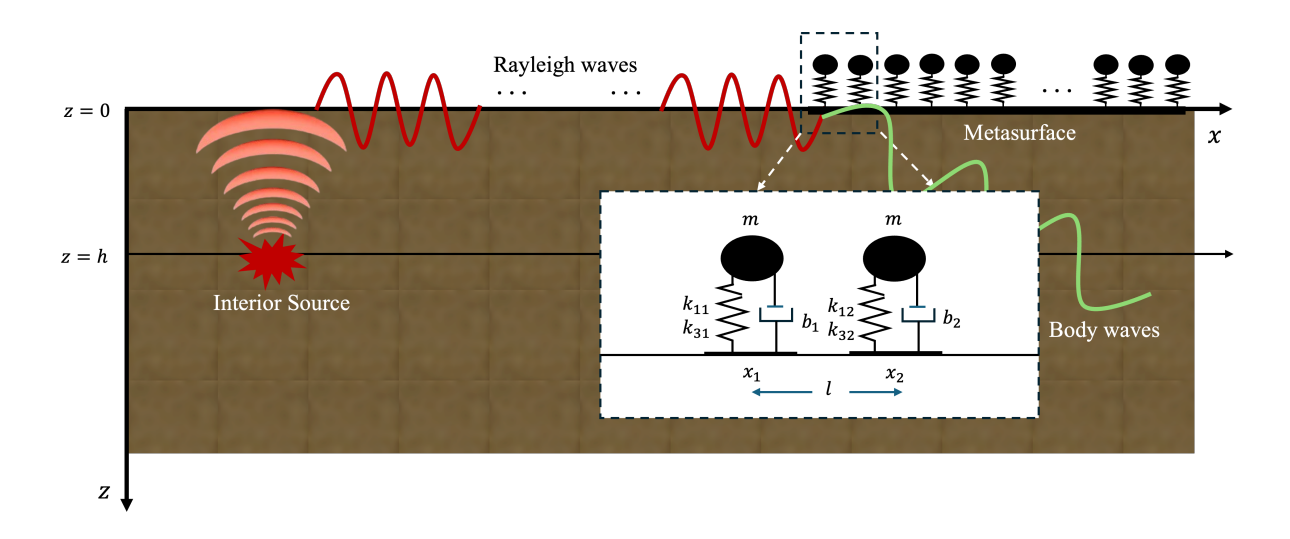


Figure 4.2.1: Description of the metasurface model

<sup>\*</sup> Ready to submit

## 4.2.2 Mathematical formulation and solution

The constitutive stress-strain relations for a homogeneous, isotropic elastic medium are given by,

$$\sigma_{ij} = \Lambda \epsilon_{kk} \delta_{ij} + 2\mu \epsilon_{ij}, \tag{4.2.1}$$

where  $\epsilon_{ij}$  denotes the stress tensor given by  $\epsilon_{ij} = \frac{1}{2} (u_{i,j} + u_{j,i})$  and  $\Lambda$ ,  $\mu$  are the Lamé elastic moduli,  $\delta_{ij}$  denotes the Kronecker delta,  $u_i$  represents the displacement components.

Also, using Eq. (4.2.1), the equation of motion of a two-dimensional isotropic elastic medium with the material density  $\rho$  and in the absence of body forces can be given as

$$(\Lambda + 2\mu) \frac{\partial^{2} u_{1}}{\partial x^{2}} + (\Lambda + \mu) \frac{\partial^{2} u_{3}}{\partial x \partial z} + \mu \frac{\partial^{2} u_{1}}{\partial z^{2}} = \rho \frac{\partial^{2} u_{1}}{\partial t^{2}},$$

$$(\Lambda + 2\mu) \frac{\partial^{2} u_{3}}{\partial z^{2}} + (\Lambda + \mu) \frac{\partial^{2} u_{1}}{\partial x \partial z} + \mu \frac{\partial^{2} u_{3}}{\partial x^{2}} = \rho \frac{\partial^{2} u_{3}}{\partial t^{2}},$$

$$(4.2.2)$$

On Helmholtz decomposition of the displacement vector  $\mathbf{u}(x, z, t)$  in terms of a scalar potential  $\Phi(x, z, t)$  and a vector potential  $\Psi(x, z, t) = (\Psi_1, \Psi, \Psi_3)$  as  $\mathbf{u} = \nabla \Phi + \nabla \times \Psi$ , or specifically,

$$u_1(x,z,t) = \frac{\partial \Phi}{\partial x} - \frac{\partial \Psi}{\partial z}, \qquad u_3(x,z,t) = \frac{\partial \Phi}{\partial z} + \frac{\partial \Psi}{\partial x},$$
 (4.2.3)

decouples the coupled equations of motion given in Eq. (4.2.2) into,

$$\nabla^2 \Phi = \frac{1}{c_L^2} \frac{\partial^2 \Phi}{\partial t^2}, \qquad \nabla^2 \Psi = \frac{1}{c_T^2} \frac{\partial^2 \Psi}{\partial t^2}, \tag{4.2.4}$$

where  $c_L = \sqrt{\frac{\Lambda + 2\mu}{\rho}}$  and  $c_T = \sqrt{\frac{\mu}{\rho}}$  are the longitudinal and transverse wave velocities, respectively.

The time-harmonic potentials assumed of the form,

$$\Phi(x,z,t) = \phi(x,z) e^{i\omega t}, \qquad \Psi(x,z,t) = \psi(x,z) e^{i\omega t},$$

simplifies the wave equations in Eq. (4.2.4) as,

$$(\nabla^2 + k_L^2) \phi = 0, \qquad (\nabla^2 + k_T^2) \psi = 0,$$
 (4.2.5)

where  $\omega = \frac{k}{c}$  is the angular frequency; k is the wavenumber and c is the wave velocity;  $k_L = \frac{\omega}{c_L}$  and  $k_T = \frac{\omega}{c_T}$ .

Applying the Fourier transformation in x to Eq. (4.2.5), the resulting equations can be

solved to obtain expressions for the potentials that exhibit the appropriate behavior. This gives,

$$\overline{\Phi}(\xi, z, t) = c_1 e^{-p_L z} e^{i\omega t}, \qquad \overline{\Psi}(\xi, z, t) = c_2 e^{-p_T z} e^{i\omega t},$$
(4.2.6)

where  $p_L = \sqrt{\xi^2 - k_L^2}$  and  $p_T = \sqrt{\xi^2 - k_T^2}$ .

## Green's functions for prescribed stresses at the surface

In this section, the fundamental steps involved in deriving Green's functions for Lamb's problem [273] are expressed in terms of the displacement components,  $u_1$  and  $u_3$ , for prescribed surface stresses. In essence, we aim to determine the displacement components of wavefields generated by surface stresses  $P_1$  and  $P_2$ . To this end, the wave equation in Eq. (4.2.4) is subjected to boundary conditions at the surface z = 0,

$$\sigma_{31}|_{z=0} = P_1(x,t), \qquad \sigma_{33}|_{z=0} = P_2(x,t).$$
 (4.2.7)

The Fourier transformed normal stress and tangential stress components, expressed in terms of the potentials, are given by

$$\overline{\sigma}_{31} = \mu \left[ -2i\xi p_L \overline{\Phi} - (2\xi^2 - k_L^2) \overline{\Psi} \right],$$

$$\overline{\sigma}_{33} = \mu \left[ (2\xi^2 - k_L^2) \overline{\Psi} - 2i\xi p_T \overline{\Phi} \right].$$
(4.2.8)

Utilizing the Fourier transformed displacement potentials provided in Eq. (4.2.6), a system of equations involving  $c_1$  and  $c_2$  can be formulated as,

$$-2i\xi \, p_L \, c_1 - (2\xi^2 - k_L^2) \, c_2 = \frac{\overline{p}_1}{\mu} \, e^{-i\omega t},$$

$$(2\xi^2 - k_L^2) \, c_1 - 2i\xi \, p_T \, c_2 = \frac{\overline{p}_2}{\mu} \, e^{-i\omega t}.$$

$$(4.2.9)$$

Solving for  $c_1$  and  $c_2$  in Eqs. (4.2.9) gives the values,

$$c_1 = \frac{(2\xi^2 - k_T^2) \,\overline{P}_2 - 2i\,\xi\,p_T\,\overline{P}_1}{\mu\,R(\xi)} \,e^{-i\omega t}, \quad c_2 = \frac{(2\xi^2 - k_T^2)\,\overline{P}_1 + 2\,i\xi\,p_L\,\overline{P}_2}{\mu\,R(\xi)} \,e^{-i\omega t},$$

where  $R(\xi) = (2\xi^2 - k_T^2)^2 - 4\xi^2 p_L p_T$  is known as a Rayleigh function.

This yields the potentials,

$$\overline{\Phi}(\xi, z, t) = \left[ \frac{-2i\xi \, p_T \, \overline{P}_1 + \left(2\xi^2 - k_T^2\right) \, \overline{P}_2}{\mu \, R(\xi)} \right] e^{-p_L z}, 
\overline{\Psi}(\xi, z, t) = -\left[ \frac{\left(2\xi^2 - k_T^2\right) \, \overline{P}_1 + 2i\xi \, p_L \, \overline{P}_2}{\mu \, R(\xi)} \right] e^{-p_T z}.$$
(4.2.10)

Consequently, utilizing Eq. (4.2.3), the displacement components of wavefields can be determined as,

$$u_{1}(x,z,t) = \int_{-\infty}^{\infty} \left[ \frac{2\xi^{2} p_{T} e^{-p_{L}z} - (2\xi^{2} - k_{T}^{2}) p_{T} e^{-p_{T}z}}{\mu R(\xi)} \overline{P}_{1}(\xi,t) + \frac{i \xi (2\xi^{2} - k_{T}^{2}) e^{-p_{L}z} - 2i \xi p_{L} p_{T} e^{-p_{T}z}}{\mu R(\xi)} \overline{P}_{2}(\xi,t) \right] e^{i\xi x} d\xi, (4.2.11)$$

$$u_{3}(x,z,t) = \int_{-\infty}^{\infty} \left[ \frac{2i \xi p_{L} p_{T} e^{-p_{L}z} - i \xi (2\xi^{2} - k_{T}^{2}) e^{-p_{T}z}}{\mu R(\xi)} \overline{P}_{1}(\xi,t) + \frac{-(2\xi^{2} - k_{T}^{2}) p_{L} e^{-p_{L}z} + 2\xi^{2} p_{L} e^{-p_{T}z}}{\mu R(\xi)} \overline{P}_{2}(\xi,t) \right] e^{i\xi x} d\xi$$

$$(4.2.12)$$

These Green's functions are specifically tailored to model two distinct types of stress distributions encountered in this work: (a) those originating from internal sources of disturbance and (b) those generated by the vertical motion of surface resonators.

## Internal source of disturbance

Consider the simplest source within this infinite elastic solid that generates symmetrical radial motion in two dimensions. This source, located along the line z = h, acts as an internal disturbance and takes the form:

$$\Phi_s(x,z,t) = \frac{i}{2k^2} H_0^{(2)}(k_L r) e^{i\omega t}, \qquad \Psi_s(x,z,t) = 0, \tag{4.2.13}$$

where  $H_0^{(2)}(\cdot)$  is the Hankel function of the zeroth order, and the second kind,  $r = \sqrt{x^2 + (z - h)^2}$  denotes the distance from the source. To account for the reflection, we assume an imaginary equal source in the line z = -h. This takes the form,

$$\Phi_r(x, z, t) = \frac{i}{2k^2} H_0^{(2)}(k_L \overline{r}) e^{i\omega t}, \qquad \Psi_r(x, z, t) = 0, \tag{4.2.14}$$

where  $\overline{r} = \sqrt{x^2 + (z+h)^2}$ .

Superposing the waveforms obtained in Eqs. (4.2.13) and (4.2.14) yields

$$\Phi(x,z,t) = \frac{i}{2k^2} \left( H_0^{(2)}(k_L r) + H_0^{(2)}(k_L \overline{r}) \right) e^{i\omega t}, \qquad \Psi(x,z,t) = 0.$$
 (4.2.15)

It can be further noted that the value of  $\Phi(x, z, t)$  is equivalent to (see, Lapwood [277]),

$$\Phi(x, z, t) = \left[ \frac{1}{2\pi k^2} \int_{-\infty}^{\infty} \frac{e^{p_L(z-h)}}{p_L} e^{i\xi x} \, d\xi + \frac{1}{2\pi} \int_{-\infty}^{\infty} \frac{e^{-p_L(z+h)}}{p_L} e^{i\xi x} \, d\xi \right] e^{i\omega t} 
= \left[ \frac{1}{2\pi k^2} \int_{-\infty}^{\infty} \frac{2\cosh(p_L z)}{p_L} e^{-p_L h} e^{i\xi x} \, d\xi \right] e^{i\omega t}.$$
(4.2.16)

As a result, the stresses induced at the surface z = 0 by these internal source of disturbance is,

$$P_1^{(s)} = \sigma_{13}\big|_{z=0} = 0, \ P_2^{(s)} = \sigma_{33}\big|_{z=0} = \left[\frac{\mu}{2\pi k^2} \int_{-\infty}^{\infty} \frac{2\xi^2 - k_T^2}{p_L} e^{-p_L h} e^{i\xi x} d\xi\right] e^{i\omega t}. (4.2.17)$$

The subscript 's' is used to designate stress components originating from an internal source of disturbance.

Equivalently, the Fourier transformation of the above stress components yields,

$$\overline{P}_1^{(s)} = 0, \qquad \overline{P}_2^{(s)} = \frac{\mu}{k^2} \frac{2\xi^2 - k_T^2}{p_L} e^{-p_L h} e^{i\omega t}.$$
 (4.2.18)

For the sake of brevity, we have omitted the time-harmonic term in further analysis. As a result, the Green's functions modelling the stress-distributions generated by an internal source of disturbance can be given by,

$$G_{1(s)}(x,z) = \frac{1}{2\pi k^2} \int_{-\infty}^{\infty} \left[ \frac{i\,\xi\,\left(2\xi^2 - k_T^2\right)\,e^{-p_L z} - 2i\,\xi\,p_L\,p_T\,e^{-p_T z}}{p_L\,R(\xi)} \right] \left(2\xi^2 - k_T^2\right)\,e^{i\xi x}\,\mathrm{d}\xi,$$
(4.2.19)

$$G_{3(s)}(x,z) = -\frac{1}{2\pi k^2} \int_{-\infty}^{\infty} \left[ \frac{(2\xi^2 - k_T^2) e^{-p_L z} - 2\xi^2 e^{-p_T z}}{R(\xi)} \right] (2\xi^2 - k_T^2) e^{i\xi x} d\xi. \quad (4.2.20)$$

At the surface z = 0, these Green's functions modelling the interior source become,

$$G_{1(s)}(x,0) = \frac{1}{2\pi k^2} \int_{-\infty}^{\infty} \frac{i\xi \left(2\xi^2 - k_T^2\right) \left(2\xi^2 - k_T^2 - 2p_L p_T\right)}{p_L R(\xi)} e^{-p_L h} e^{i\xi x} d\xi, (4.2.21)$$

$$G_{3(s)}(x,0) = \frac{1}{2\pi k^2} \int_{-\infty}^{\infty} \frac{k_T^2 (2\xi^2 - k_T^2)}{R(\xi)} e^{-p_L h} e^{i\xi x} d\xi.$$
 (4.2.22)

#### Dynamics of surface resonators

We investigate the steady-state dynamics of a system comprising nonlinear massspring-dashpot resonators with mass m that are situated on top of an elastic substrate. Let  $\mathcal{O} = \{x_1, x_2, \dots, x_N | N \in \mathbb{N}\}$  denote the set of x-coordinates for these resonators. These resonators are arranged with a uniform spacing of l along x-direction, and each resonator covers an area of A.

Furthermore, we consider the case where  $\frac{l}{2} \ll \lambda$ , implying that the distance between the resonators is much smaller than the wavelength  $\lambda$  of the propagating wave.

Now, the equation of motion describing the displacement of each resonator is,

$$m \ddot{y_n} + f_R(y_n) = -m \ddot{\tilde{u}}(x_n, 0, t),$$
 (4.2.23)

where

 $-\widetilde{u}(x_n,0,t)$  is the average vertical displacement of the base of the resonator and is given by the expression,

$$\widetilde{u}(x_n, 0, t) = \frac{1}{l} \left[ \int_{x_n - \frac{l}{2}}^{x_n + \frac{l}{2}} u(x, 0, t) \, \mathrm{d}x \right], \text{ where } x \in \left( x_n - \frac{l}{2}, x_n + \frac{l}{2} \right). \tag{4.2.24}$$

For the displacement solution of the form  $u(x,0,t) = U e^{i(kx-\omega t)}$ , consider the case when  $\frac{l}{2} << \lambda$  or  $\frac{kl}{2} << 1$ . This evaluates the expression in Eq. (4.2.24) as,

$$\widetilde{u}(x_n, 0, t) = \frac{e^{i\omega t}}{l} \left[ \int_{x_n - \frac{l}{2}}^{x_n + \frac{l}{2}} U e^{ikx} dx \right]$$

$$= U e^{ikx_n} \left( \frac{2}{kl} \right) \sin \left( \frac{kl}{2} \right) e^{i\omega t}. \tag{4.2.25}$$

Using the fact that  $\sin\left(\frac{kl}{2}\right) \approx \frac{kl}{2}$  for  $\frac{kl}{2} << 1$ , we obtain the approximate expression of  $\widetilde{u}(x_n, 0, t)$  in Eq. (4.2.25) as,

$$\widetilde{u}(x_n, 0, t) \approx u(x_n, 0, t). \tag{4.2.26}$$

-  $y_n$  stands for the relative displacement between the absolute vertical displacement of the  $n^{\text{th}}$  mass  $u_R(x_n, 0, t)$  and the average base displacement of the resonator  $\widetilde{u}(x_n, 0, t)$ , i.e.,

$$y_n(x_n, 0, t) = u_R(x_n, 0, t) - \widetilde{u}(x_n, 0, t). \tag{4.2.27}$$

- The function  $f_R(\cdot)$  represents the force exerted by the nonlinear spring. For a damped Duffing oscillator, the nonlinear complex spring force is given by

$$f_R(\cdot) = k_1(\cdot) + b \frac{d(\cdot)}{dt} + k_3(\cdot)|(\cdot)|^2.$$
 (4.2.28)

Here,  $k_1, k_3$  denote the linear and nonlinear stiffness coefficients, respectively, while b represents the damping parameter.

Consequently, for the specific problem under consideration, we have,

$$f_R(y_n) = k_{1n} y_n + b_n \frac{\mathrm{d}y_n}{\mathrm{d}t} + k_{3n} y_n |y_n|^2, \tag{4.2.29}$$

where  $k_{1n}$ ,  $k_{3n}$  and  $b_n$  represent the linear stiffness, nonlinear stiffness, and damping parameter for the  $n^{\text{th}}$  resonator.

Assuming a time-harmonic variation in the displacements of the spring of the form, say

$$(y_n, u_{Rn}) \equiv (y(x_n, 0, t), u_R(x_n, 0, t)) = (Y_n, U_{Rn}) e^{ikx_n} e^{i\omega t},$$

$$\widetilde{u}_n \equiv \widetilde{u}(x_n, 0, t) = \widetilde{U} e^{ikx_n} e^{i\omega t},$$

$$(4.2.30)$$

where the amplitudes of the expressions  $Y_n, U_{Rn}$  depends on the resonator properties and the amplitude  $\widetilde{U}$  is independent of any resonator properties.

Substituting Eqs. (4.2.30) in equations of motion given in Eq. (4.2.23) gives,

$$-m\omega^{2} Y_{n} + i\omega b_{n} Y_{n} + k_{1n} Y_{n} + k_{3n} Y_{n} |Y_{n}|^{2} = m\omega^{2} \widetilde{U}.$$
(4.2.31)

Further, we define some additional variables,

$$\omega_{Rn} = \sqrt{\frac{k_{1n}}{m}}, \ r_n = \frac{\omega}{\omega_{Rn}}, \ \nu_n = \frac{k_{3n}}{k_{1n}}, \ \zeta_n = \frac{b_n}{m \,\omega_{Rn}}.$$

Dropping all the n's, the equation of motion in Eq. (4.2.31) can be further simplified to obtain the relation,

$$Y = \frac{r^2}{1 - r^2 + 2i \, r \, \zeta + \nu \, |Y|^2} \, \widetilde{U}. \tag{4.2.32}$$

As a result, for a known amplitude  $\widetilde{U}$ , the frequency amplitude response of the nonlinear spring-mass system can be given by,

$$s = \frac{r^2}{\sqrt{\left(1 - r^2 + \nu \left|\widetilde{U}\right|^2 s^2\right)^2 + 4r^2 \zeta^2}}, \text{ where } s = \left|\frac{Y}{\widetilde{U}}\right|. \tag{4.2.33}$$

Alternatively, Eq. (4.2.33) can further be simplified to obtain a polynomial equation of the form,

$$r^{4} - \left(4s^{2}\zeta^{2}\right) r^{2} - s^{2} \left(1 - r^{2} + \nu \left|\widetilde{U}\right|^{2} s^{2}\right)^{2} = 0.$$
 (4.2.34)

Notably, by employing Eq. (4.2.27), we can derive a linear relationship from Eq. (4.2.32) that connects the amplitudes  $U_{Rn}$  and  $\widetilde{U}_n$  as,

$$U_{Rn} = \left[ 1 + \frac{r_n^2}{1 - r_n^2 + \nu_n \, s_n^2 \, \left| \widetilde{U}_n \right|^2 + 2i \, r_n \, \zeta_n} \right] \, \widetilde{U}_n. \tag{4.2.35}$$

In addition, a motion transmissibility ratio,  $\mathcal{T}_n$ , can be determined for the surface resonators. It is defined as the ratio of the absolute value of the resonator's amplitude,  $|U_{Rn}|$ ,

to that of the absolute value of the base displacement amplitude,  $\widetilde{U}_n$ .

$$\mathcal{T}_{Rn} = \frac{\sqrt{\left(1 + \nu_n \, s_n^2 \, |\widetilde{U}_n|^2\right)^2 + (2r_n \, \zeta_n)^2}}{\sqrt{\left(1 - r_n^2 + \nu_n \, s_n^2 \, |\widetilde{U}_n|^2\right)^2 + (2r_n \, \zeta_n)^2}}.$$
(4.2.36)

This ratio provides a measure of how effectively vibrations are transmitted to the resonator.

Consequently, omitting the time-harmonic terms, the normal force exerted by the nonlinear resonator on the substrate can be expressed as,

$$F_n = -m \, \ddot{u}_R(x_n, 0, t) = \varpi_n \, \widetilde{u}(x_n, 0), \text{ for } x_n \in \mathcal{O}, \tag{4.2.37}$$

where the parameter  $\varpi_n$  is given as,

$$\varpi_n = m \,\omega^2 \left[ 1 + \frac{r_n^2}{1 - r_n^2 + \nu_n \,s_n^2 \left| \widetilde{U}_n \right|^2 + 2i \,r_n \,\zeta_n} \right]. \tag{4.2.38}$$

As a result, we can now evaluate the uniform stress exerted by each resonator over the contact area A,

$$\sigma_{13}^{(n)}(x,0) = 0, 
\sigma_{33}^{(n)}(x,0) = -\frac{F_n}{A} = -\frac{\varpi_n}{A} \widetilde{u}(x_n,0)$$
 for  $x \in \left(x_n - \frac{l}{2}, x_n + \frac{l}{2}\right), x_n \in \mathcal{O}$ . (4.2.39)

The presence of these harmonic stresses gives rise to additional wavefields within the half-space. These newly generated wavefields subsequently interact with the free-field wave motions originating from the interior source.

Analogously, let  $L_x^{(n)}$  represent the magnitude of the amplitude of the stress distributed at the surface due to the resonator vibrations. We can model this scenario by assuming a uniform normal stress distribution. This distribution can be written in the form,

$$P_1^{(r)} = \sigma_{13}(x,0) = 0 \text{ or } \sigma_{13}^{(n)}(x,0) = 0$$
 (4.2.40)

$$P_2^{(r)} = \sigma_{33}(x,0) = \begin{cases} L_x^{(n)}, & \text{if } |x - x_n| \le \frac{l}{2} \\ 0, & \text{otherwise} \end{cases}$$
 or  $\sigma_{33}^{(n)}(x,0) = L_x^{(n)}$  (4.2.41)

Taking the Fourier transform to Eqs. (4.2.40) and (4.2.41), we get

$$\overline{P}_1^{(r)} = 0, \qquad \overline{P}_2^{(r)} = \frac{2L_x^{(n)}}{\xi} \sin\left(\frac{\xi l}{2}\right) e^{-i\xi x_n}.$$
 (4.2.42)

Consequently, using Eq. (4.2.42), the Green's functions that model the uniform normal unitary stress distributions generated by resonator vibrations can be expressed as,

$$G_{1(r)}^{(n)}(x,z) = \frac{1}{\pi\mu} \int_{-\infty}^{\infty} \left[ \frac{i \left( 2\xi^2 - k_T^2 \right) e^{-p_L z} - 2i p_L p_T e^{-p_T z}}{R(\xi)} \right] \sin\left(\frac{\xi l}{2}\right) e^{i\xi(x-x_n)} d\xi,$$
(4.2.43)

$$G_{3(r)}^{(n)}(x,z) = -\frac{1}{\pi\mu} \int_{-\infty}^{\infty} \left[ \frac{(2\xi^2 - k_T^2) e^{-p_L z} - 2\xi^2 e^{-p_T z}}{\xi R(\xi)} \right] \sin\left(\frac{\xi l}{2}\right) e^{i\xi(x-x_n)} d\xi. \quad (4.2.44)$$

At the surface z = 0, these Green's functions modelling the scattered wavefields are given as,

$$G_{1(r)}^{(n)}(x,0) = \frac{1}{\pi\mu} \int_{-\infty}^{\infty} \frac{i \left(2\xi^2 - k_T^2 - 2i p_L p_T\right)}{R(\xi)} \sin\left(\frac{\xi l}{2}\right) e^{i\xi(x-x_n)} d\xi, \quad (4.2.45)$$

$$G_{3(r)}^{(n)}(x,0) = \frac{1}{\pi\mu} \int_{-\infty}^{\infty} \frac{k_T^2 p_L}{\xi R(\xi)} \sin\left(\frac{\xi l}{2}\right) e^{i\xi(x-x_n)} d\xi.$$
 (4.2.46)

## Coupling of surface resonators to the half-space

As previously described, the system comprises N resonators coupled to the half-space. The total wavefield in the system arises from the wavefield induced by the interior source and the additional wavefields generated by the base excitation of the coupled resonators. To determine these wavefields, we employ a multiple scattering approach. This involves utilizing Green's functions for both the generated and scattered wavefields, which allows us to solve the resulting problem and determine the unknown amplitudes of the scattered wavefields.

A multiple scattering formulation provides a quantitative framework for modeling the destructive and constructive interference effects arising from the interior source acting at the surface and those induced by the vertical motion of the N resonators.

This gives the complete displacement of the wavefield as,

$$u_{1(c)}(x,z) = u_{1(s)}(x,z) + \sum_{n=1}^{n=N} L_x^{(n)} G_{1(r)}^{(n)}(x,z),$$
 (4.2.47)

$$u_{3(c)}(x,z) = u_{3(s)}(x,z) + \sum_{n=1}^{n=N} L_x^{(n)} G_{3(r)}^{(n)}(x,z),$$
 (4.2.48)

where the expressions for  $u_{1(s)}(x,z)$  and  $u_{3(s)}(x,z)$  are the Green's functions obtained in Eqs. (4.2.19) and (4.2.20).

Now, on comparing Eqs. (4.2.39) and (4.2.41), we get

$$L_x^{(m)} = -Q_m \, \widetilde{u}(x_m, 0) \qquad \text{or} \qquad \widetilde{u}(x_m, 0) = -Q_m^{-1} \, L_x^{(m)},$$
 (4.2.49)

where  $Q_m = \frac{\varpi_m}{A}$  is defined as the impedance factor.

Further on imposing the continuity conditions,  $u(x, 0, t) = u_{3(c)}(x, 0, t)$  between the resonators and the half-space, we have

$$\widetilde{u}(x_m, 0) = \frac{1}{l} \int_{x_m - \frac{l}{2}}^{x_m + \frac{l}{2}} u_{3(c)}(x, 0) dx$$

$$= \frac{1}{l} \int_{x_m - \frac{l}{2}}^{x_m + \frac{l}{2}} \left( G_{3(s)}(x, 0) + \sum_{n=1}^{n=N} L_x^{(n)} G_{3(r)}^{(n)}(x, 0) \right) dx.$$
(4.2.50)

Assuming the conditions for interchanging the order of integration are satisfied, Eq. (4.2.50) can be simplified to yield,

$$\widetilde{u}(x_m, 0) = \frac{1}{l} \left[ J_{3(s)}(x_m, 0) + \sum_{n=1}^{n=N} L_x^{(n)} J_{3(r)}^{(n)}(x_m, 0) \right], \tag{4.2.51}$$

where

$$J_{3(s)}(x_m, 0) = \frac{1}{\pi k^2} \int_{-\infty}^{\infty} \frac{k_T^2 (2\xi^2 - k_T^2)}{\xi R(\xi)} e^{-p_L h} \sin\left(\frac{\xi l}{2}\right) e^{i\xi x_m} d\xi, \qquad (4.2.52)$$

$$J_{3(r)}^{(n)}(x_m, 0) = \frac{1}{\pi \mu} \int_{-\infty}^{\infty} \frac{2 k_T^2 p_L}{\xi^2 R(\xi)} \sin^2 \left(\frac{\xi l}{2}\right) e^{i\xi(x_m - x_n)} d\xi. \tag{4.2.53}$$

Substituting the value of Eq. (4.2.49) in Eq. (4.2.53), we get

$$J_{3(s)}(x_m, 0) = -l Q_m^{-1} L_x^{(m)} - \sum_{n=1}^{n=N} L_x^{(n)} J_{3(r)}^{(n)}(x_m, 0), \text{ for } x_m \in \mathcal{O}$$

$$(4.2.54)$$

Expanding Eq. (4.2.54) for different values of m yields,

$$J_{3(s)}(x_1,0) = \left(-lQ_1^{-1} - J_{3(r)}^{(1)}(x_1,0)\right) L_x^{(1)} - J_{3(r)}^{(2)}(x_1,0) L_x^{(2)} - J_{3(r)}^{(3)}(x_1,0) L_x^{(3)} - \dots - J_{3(r)}^{(N)}(x_1,0) L_x^{(N)},$$

$$J_{3(s)}(x_2,0) = -J_{3(r)}^{(1)}(x_2,0) L_x^{(1)} + \left(-lQ_2^{-1} - J_{3(r)}^{(2)}(x_2,0)\right) L_x^{(2)} - J_{3(r)}^{(3)}(x_2,0) L_x^{(3)} - \dots - J_{3(r)}^{(N)}(x_2,0) L_x^{(N)},$$

$$J_{3(s)}(x_3,0) = -J_{3(r)}^{(1)}(x_3,0) L_x^{(1)} - J_{3(r)}^{(2)}(x_3,0) L_x^{(2)} + \left(-lQ_3^{-1} - J_{3(r)}^{(3)}(x_3,0)\right) L_x^{(3)} - \dots - J_{3(r)}^{(N)}(x_3,0) L_x^{(N)},$$

$$\vdots$$

$$J_{3(s)}(x_N,0) = -J_{3(r)}^{(1)}(x_N,0) L_x^{(1)} - J_{3(r)}^{(2)}(x_N,0) L_x^{(2)} - J_{3(r)}^{(3)}(x_N,0) L_x^{(3)} - \dots + \left(-lQ_N^{-1} - J_{3(r)}^{(N)}(x_N,0)\right) L_x^{(N)}.$$

This can be further written in the matrix form as,

$$AX = B, (4.2.55)$$

where

$$A = \begin{bmatrix} -lQ_1^{-1} - J_{3(r)}^{(1)}(x_1, 0) & -J_{3(r)}^{(2)}(x_1, 0) & -J_{3(r)}^{(3)}(x_1, 0) & \cdots & -J_{3(r)}^{(N)}(x_1, 0) \\ -J_{3(r)}^{(2)}(x_2, 0) & -lQ_2^{-1} - J_{3(r)}^{(2)}(x_2, 0) & -J_{3(r)}^{(3)}(x_2, 0) & \cdots & -J_{3(r)}^{(N)}(x_2, 0) \\ -J_{3(r)}^{(1)}(x_3, 0) & -J_{3(r)}^{(2)}(x_3, 0) & -lQ_3^{-1} - J_{3(r)}^{(3)}(x_3, 0) & \cdots & -J_{3(r)}^{(N)}(x_3, 0) \\ \vdots & \vdots & \vdots & \ddots & \vdots \\ -J_{3(r)}^{(1)}(x_N, 0) & -J_{3(r)}^{(2)}(x_N, 0) & -J_{3(r)}^{(3)}(x_N, 0) & \cdots & -lQ_N^{-1} - J_{3(r)}^{(N)}(x_N, 0) \end{bmatrix}$$

$$(4.2.56)$$

$$X = \begin{bmatrix} L_x^{(1)} \\ L_x^{(2)} \\ L_x^{(3)} \\ \vdots \\ L_x^{(n)} \end{bmatrix}, B = \begin{bmatrix} J_{3(s)}(x_1, 0) \\ J_{3(s)}(x_2, 0) \\ J_{3(s)}(x_3, 0) \\ \vdots \\ J_{3(s)}(x_N, 0) \end{bmatrix}$$

$$(4.2.57)$$

By solving Eq. (4.2.55) for X, we obtain the solution for the amplitude of the scattered wavefield, which is given by the expression,

$$X = A^{-1}B$$
 or  $L_x^{(m)} = (A^{-1}B)_m$  (4.2.58)

Hence, the complete displacement of the wavefield can be expressed using Eqs. (4.2.47) and (4.2.48) as,

$$u_{1(c)}(x,z) = u_{1(s)}(x,z) + \sum_{n=1}^{n=N} (A^{-1}B)_n G_{1(r)}^{(n)}(x,z)$$
 (4.2.59)

$$u_{3(c)}(x,z) = u_{3(s)}(x,z) + \sum_{n=1}^{n=N} (A^{-1}B)_n G_{3(r)}^{(n)}(x,z)$$
 (4.2.60)

And at the surface z = 0, the complete wavefield becomes,

$$u_{1(c)}(x,0) = u_{1(s)}(x,0) + \sum_{n=1}^{n=N} (A^{-1}B)_n G_{1(r)}^{(n)}(x,0),$$
 (4.2.61)

$$u_{3(c)}(x,0) = u_{3(s)}(x,0) + \sum_{n=1}^{n=N} (A^{-1}B)_n G_{3(r)}^{(n)}(x,0).$$
 (4.2.62)

It is worth mentioning that the contribution of Rayleigh wavefields can be readily determined by evaluating the pole contributions within the infinite integrands in Eqs. (4.2.61) and (4.2.62).

## 4.2.3 Dispersion relation

We now consider an infinite array of equally spaced (at a distance l) identical nonlinear resonators arranged on the top of an elastic substrate. Let us assume that the steady state is obtained, say at  $x_m = 0$ . It is also important to note that at this position  $x_m = 0$ , the effect of the incident wavefield is nil. As a result, we can write from Eq. (4.2.54) that,

$$lQ^{-1}L_x = -\sum_{n=-\infty}^{n=\infty} L_x^{(n)} J_r(x_n), \qquad (4.2.63)$$

where  $L_x^{(n)} \equiv L(x_n)$  and  $J_r(x_n)$  is equivalent form of  $J_{3(r)}^{(n)}(0,0)$ . In other words,

$$J_r(x_n) = \frac{1}{\pi \mu} \int_{-\infty}^{\infty} \frac{2 k_T^2 p_L}{\xi^2 R(\xi)} \sin^2 \left(\frac{\xi l}{2}\right) e^{-i\xi x_n} d\xi.$$
 (4.2.64)

An effective medium approach is employed, which is based on the assumption that the lattice spacing l is much smaller than the wavelength  $\lambda$  of the propagating wave. Further, the discretization is modelled rather continuously by taking the average values that give,

$$lQ^{-1}L_x = -\frac{1}{l} \sum_{n=-\infty}^{n=\infty} \int_{x_n - \frac{l}{2}}^{x_n + \frac{l}{2}} L(x) J_r(x) dx.$$
 (4.2.65)

Note that, due to the identical resonator properties, we can write  $L(x) = L_x e^{i\xi x}$ . Using this fact and the assumption of an effective medium approach, Eq. (4.2.65) can be reduced to,

$$Q^{-1} + \frac{k_T^2 p_L}{\mu R(\xi)} = 0. (4.2.66)$$

Utilizing the expression of the Rayleigh function  $R(\xi)$  and replacing  $\xi$  by k, we obtain the dispersion relation for Rayleigh waves in the presence of an infinite array of resonators as

$$\left(2k^2 - \frac{\omega^2}{c_T^2}\right)^2 - 4k^2 \sqrt{\left(k^2 - \frac{\omega^2}{c_L^2}\right)\left(k^2 - \frac{\omega^2}{c_T^2}\right)} + \frac{\omega^2 \overline{\omega}}{\rho A c_T^4} \sqrt{k^2 - \frac{\omega^2}{c_L^2}} = 0,$$
(4.2.67)

where

$$\varpi = m\,\omega^2 \left[ 1 + \frac{r^2}{1 - r^2 + \nu\,s^2 \left| \widetilde{\boldsymbol{U}} \right|^2 + 2i\,r\,\zeta} \right].$$

Clearly note that, in the absence of resonators, the dispersion relation for Rayleigh waves reduces to,

$$\left(2k^2 - \frac{\omega^2}{c_T^2}\right)^2 - 4k^2 \sqrt{\left(k^2 - \frac{\omega^2}{c_L^2}\right)\left(k^2 - \frac{\omega^2}{c_T^2}\right)} = 0$$
(4.2.68)

which matches exactly with the Rayleigh wave secular equation [14].

## 4.2.4 Graphical results and discussions

This section presents a comprehensive analysis of Rayleigh wave phenomena in nonlinear resonating structures, utilizing the theoretical framework established in the preceding sections. We delve into three distinct scenarios: (1) the dynamics of the single nonlinear resonator excited by the Rayleigh waves induced by the interior source (2) the coupled dynamics of a pair of nonlinear spring-mass resonators, showcasing the results of our analytical formulation in capturing their mutual interplay (3) the dispersion curve of Rayleigh waves interacting with an infinite length metasurface consisting of an array of identical nonlinear damped spring-mass system.

To facilitate this analysis, we first introduce several key parameters that will organize our calculations and discussions.

- Normalized source depth (H): This is defined as the ratio of the source depth (h) to the characteristic wavelength  $(\lambda)$  of the propagating wave and expressed as,  $H = \frac{h}{\lambda}$ .
- Normalized mass parameter (M): This dimensionless quantity characterizes the inertial influence of the resonator relative to the surrounding medium. It is given by,  $M = \frac{m\omega_{R1}}{\rho Ac_T}$ , where,
  - $\rho$  is the density of the half-space
  - $\omega_{R1} = \sqrt{\frac{k_{11}}{m}}$  represents the natural frequency of the first resonator of mass m, with  $k_{11}$  being the corresponding linear stiffness coefficient.
- Nonlinearity parameter ( $\nu_n$ ): This parameter characterizes the nature of the nonlinearity in the system with
  - $\nu_n > 0$  implying hardening nonlinearity.
  - $\nu_n = 0$  implying linear behavior.
  - $\nu_n < 0$  implying softening nonlinearity.

A limiting case is discussed in the following cases for which  $\Lambda = \mu$ . Table 4.2.1 below provides the parameter values adopted in the three cases under investigation.

Table 4.2.1: Values of the mechanical parameters used in the study

Parameter	Expression	Definition	Values used*
Н	$\frac{h}{\lambda}$ or $kh$	Normalized source depth	3.5
$ \widetilde{U} $	_	Base input amplitude	0.2
M	$rac{m\omega_{R1}}{ ho Ac_T}$	Normalized mass parameter	0.6
$ u_n$	$rac{k_{3n}}{k_{1n}}$	Nonlinearity parameter	+1
L	$\frac{l}{h}$	Normalized distance between the resonators	0.02
$\zeta_n$	$rac{b_n}{m\omega_{Rn}}$	Dimensionless damping parameter	0.17

<sup>\*</sup> whenever needed and unless specified

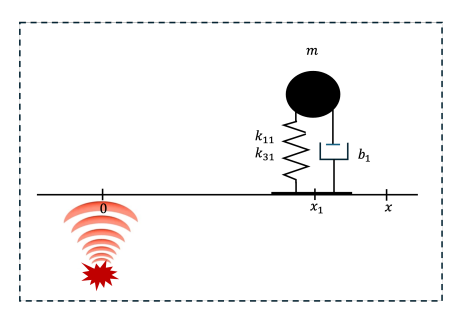
To further characterize the influence of the surface resonators on wave propagation, we introduce the parameter transmittance or transmission ratio,  $|A_R|$  defined as,

$$|A_R| = \left| \frac{u_{3(c)}(x,0)}{u_{3(s)}(x,0)} \right|, \text{ where } u_{3(s)}(x,0) \equiv G_{3(s)}(x,0),$$
 (4.2.69)

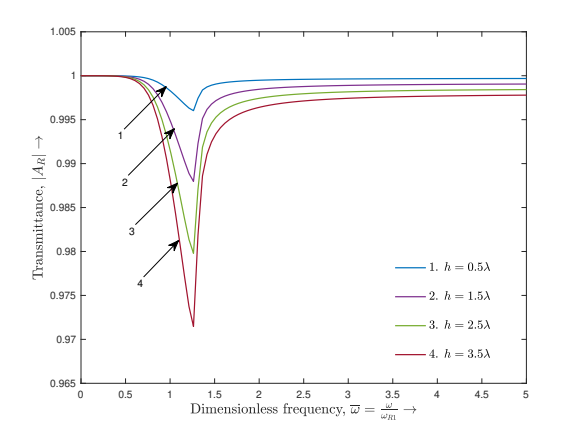
and  $|A_R| < 1$  indicates the efficacy of the resonators in attenuating Rayleigh wave vibrations.

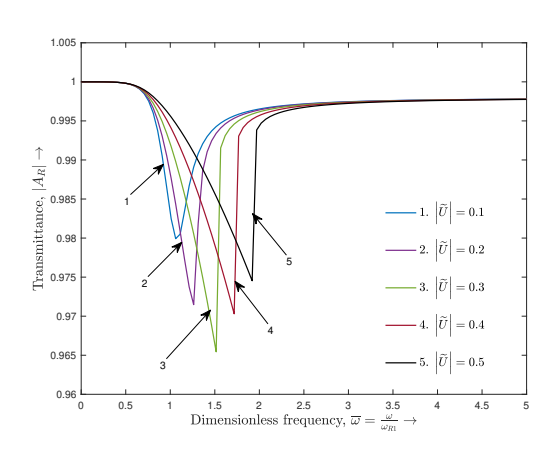
## Single resonator scenario:

We investigate the scenario depicted in Figure 4.2.2a, where a single nonlinear resonator interacts with Rayleigh waves generated by an interior source. The receiver is positioned at  $x = 3\lambda$ , and the resonator is located at  $x_1 = \lambda$ . We generate four plots to analyze the impact of various parameters on the transmittance ( $|A_R|$ ) vs frequency ( $\bar{\omega}$ ) curve. Recall that a lower  $|A_R|$  value corresponds to a greater reduction in the transmitted wave amplitude, indicating enhanced attenuation of ground-borne vibrations. The values of the parameters used in the analysis are provided in Table 4.2.1 unless otherwise specified.



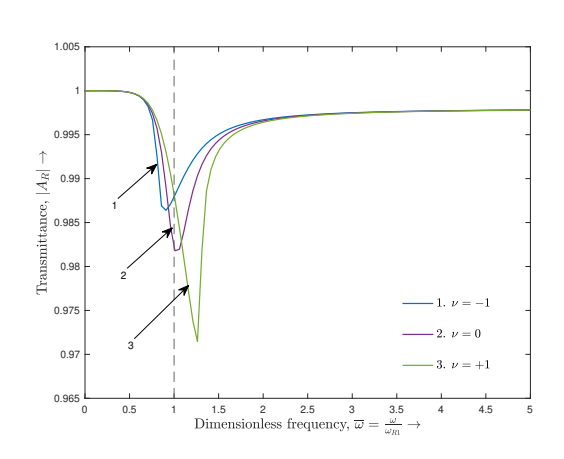
(a) Schematics of single resonator scenario

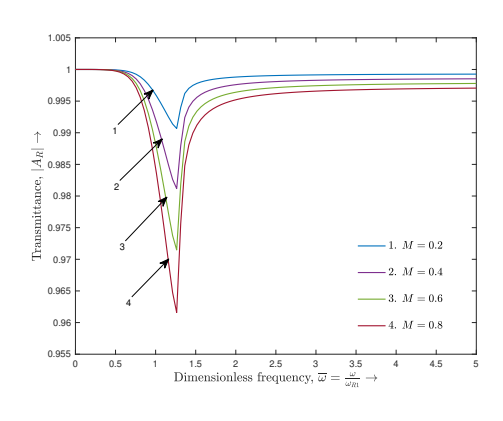




(b) Effect of the normalized source depth







(e) Effect of the normalized mass of the

(d) Effect of the nonlinearity of resonators

system

Figure 4.2.2: Transmittance  $|A_R|$  versus dimensionless frequency in a single resonator scenario

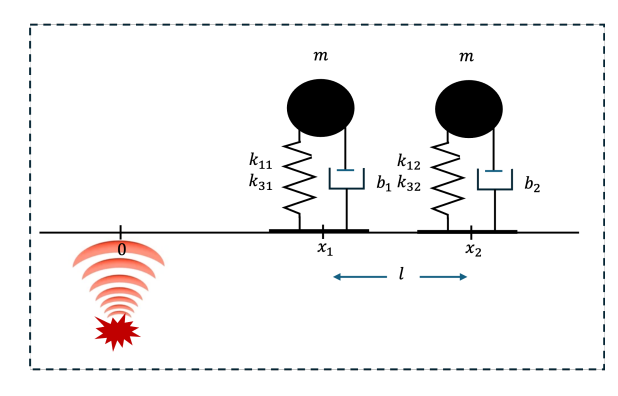
Figure 4.2.2b illustrates the influence of source depth on the transmittance ( $|A_R|$ ) vs dimensionless frequency ( $\bar{\omega}$ ) curve. As the normalized source depth H increases, the peak  $|A_R|$  value decreases. This indicates that a deeper source leads to greater attenuation of ground-borne vibrations by the resonators. Conversely, a shallower source results in less effective Rayleigh wave attenuation. This behavior can likely be attributed to the decay of waves as they propagate through the medium. A deeper source means the waves have to travel a larger distance to reach the resonator, leading to greater attenuation before they even interact with the resonator. These findings underscore the importance of considering source location relative to the resonator when designing systems for mitigating ground-borne vibrations.

The plot in Figure 4.2.2c reveals that the effectiveness of the resonators in reducing wave transmission increases with the base input amplitude, but only up to a certain point. Beyond this threshold, further increase in amplitude actually lead to less effective attenuation. This suggests an optimal range of excitation amplitudes where the resonators perform best at mitigating vibrations.

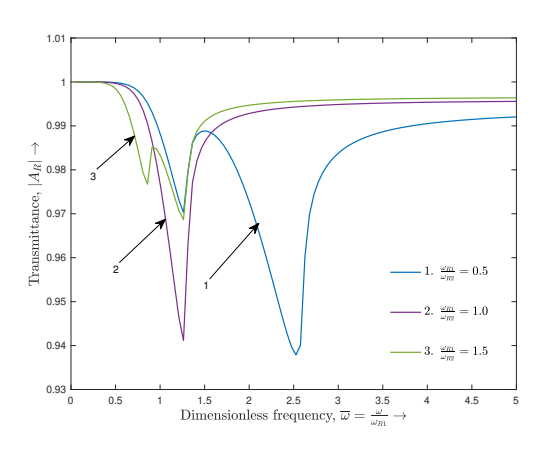
The influence of nonlinearity on the transmittance characteristics is illustrated in Figure 4.2.2d, where the response curves for hardening, softening, and linear cases are presented. Hardening nonlinearity ( $\nu = +1$ ) results in a shift of the transmittance peak towards higher frequencies  $\omega > \omega_{R1}$ , accompanied by a reduction in the peak transmittance value. Conversely, softening nonlinearity ( $\nu = -1$ ) shifts the peak to lower frequencies ( $\omega < \omega_{R1}$ ) with a slight increase in peak transmittance. The linear case ( $\nu = 0$ ) exhibits a peak at the resonant frequency ( $\omega_{R1}$ ) of the spring-mass system, as expected. This behavior can be attributed to the frequency-dependent nature of the nonlinearity, where hardening effects stiffen the system and shift the resonance to higher frequencies while softening effects lead to a decrease in stiffness and a corresponding shift to lower frequencies. In other words, the hardening nonlinearity in the resonators can be beneficial for achieving enhanced vibration mitigation at higher frequencies.

The plot in Figure 4.2.2e shows that increasing the dimensionless mass parameter M leads to lower transmittance, meaning better vibration reduction. This is because a heavier resonator creates a larger impedance mismatch with the ground, causing more wave reflection and less transmission. Essentially, a heavier resonator acts as a better barrier for ground-borne vibrations.

## A pair of resonators scenario:



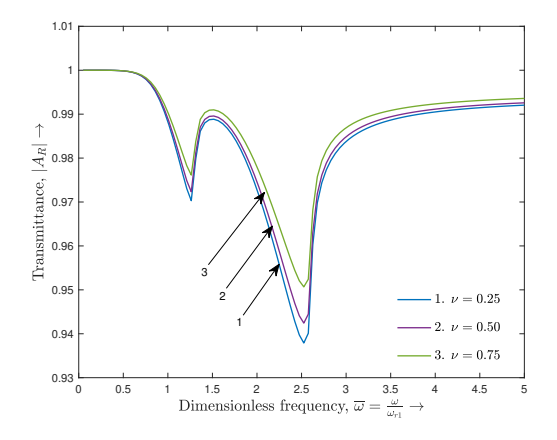
(a) Schematics of the a pair of resonators scenario

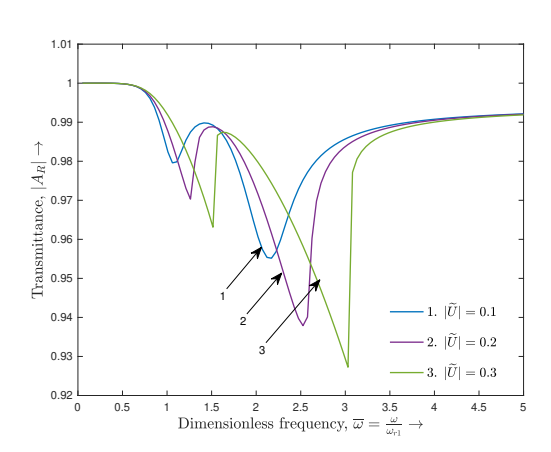


 $\begin{array}{c} \uparrow 0.98 \\ \hline 0.92 \\ \hline 0.92 \\ \hline 0.92 \\ \hline 0.92 \\ \hline 0.05 \\ \hline 1 \\ \hline 1.5 \\ \hline 2 \\ \hline 2.5 \\ \hline 2.5 \\ \hline 0.92 \\ \hline -2. \ L = 0.04 \\ \hline -3. \ L = 0.06 \\ \hline 0.88 \\ \hline 0 \\ \hline 0.5 \\ \hline 1 \\ \hline 0.5 \\ 0.5 \\ \hline 0$ 

(b) Effect of the linear stiffness of the resonator

(c) Effect of the normalized distance between the resonators





(d) Effect of the poisson ratio of the half-space

(e) Effect of the base input amplitude

Figure 4.2.3: Transmittance  $|A_R|$  versus dimensionless frequency  $\frac{\omega}{\omega_{R1}}$  in a pair of resonators scenario

165

This section examines the interaction of Rayleigh waves, generated by an interior source, with two nonlinear resonators spaced a distance l apart, as depicted in Figure 4.2.3a.

Figure 4.2.3b shows that the frequencies of the two resonators significantly affect wave transmission. When the second resonator has a higher frequency, stronger attenuation occurs at higher frequencies. Conversely, a lower-frequency second resonator leads to weaker attenuation at lower frequencies. This is due to the interaction between the resonators, creating either constructive or destructive interference depending on their frequencies.

In Figure 4.2.3c, the decreasing transmittance with larger resonator separation arises from reduced near-field coupling effects and increased independent scattering. Most likely, as the resonators move apart, they act more like individual scatterers, disrupting any interference that might have aided wave transmission when they were closer. This leads to more effective wave attenuation and, thus, lower transmittance.

Figure 4.2.3d shows the effect of Poisson's ratio ( $\nu$ ) of the half-space, where three different values (0.25, 0.50, and 0.75) produce distinct transmission characteristics, with all curves exhibiting multiple resonance dips at specific frequencies though the depth and sharpness of these dips vary significantly with Poisson's ratio. Figure 4.2.3e illustrates how the base input amplitude  $|\tilde{U}|$  affects transmission, with three amplitude levels (0.1, 0.2, and 0.3) showing that higher input amplitudes generally lead to deeper transmission minima and more pronounced nonlinear effects, particularly visible in the shifting and broadening of the resonance dips. Both graphs reveal that the system exhibits strong frequency-dependent behavior with multiple resonance frequencies where transmission is significantly reduced, and these resonant characteristics are sensitive to both the material properties of the substrate and the amplitude of the base excitation.

Figure 4.2.4 illustrates the relationship between the number of surface resonators and the effective attenuation of Rayleigh waves. The plot reveals that as the number of resonators increases, the frequency range over which significant attenuation occurs also expands. This trend can be attributed to the broader range of resonant frequencies introduced by the addition of more resonators. Each resonator contributes its own resonant frequency, and the collective response of multiple resonators effectively widens the frequency band over which attenuation is achieved. Essentially, a larger number of

resonators provides a more comprehensive barrier to Rayleigh wave propagation, leading to enhanced attenuation over a wider range of frequencies.

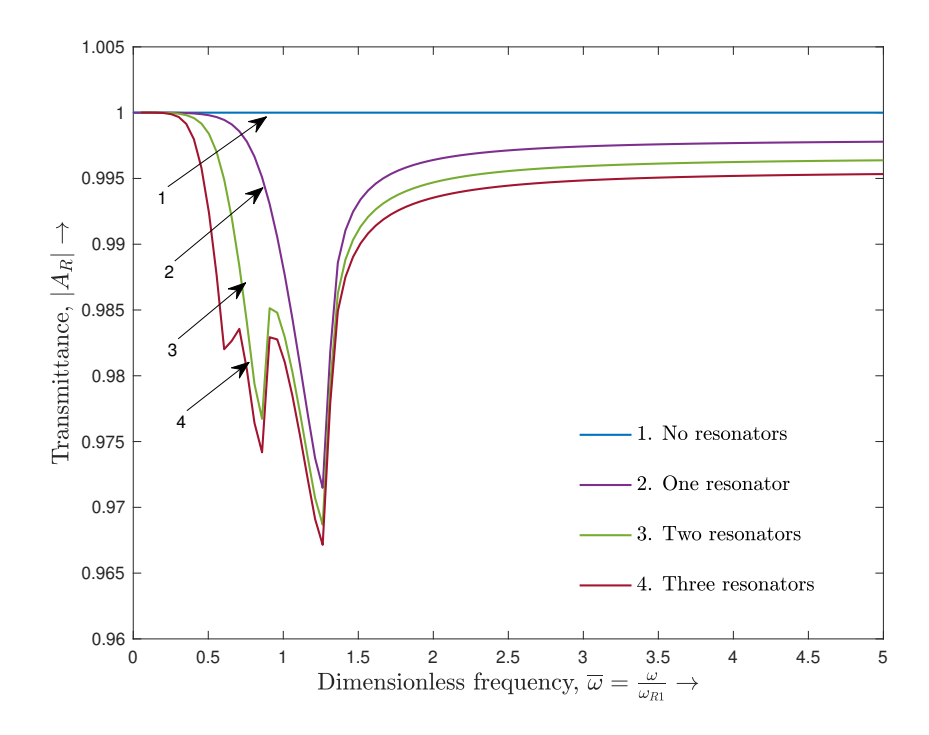


Figure 4.2.4: Effect of number of resonators on the transmittance  $|A_R|$  versus dimensionless frequency  $\frac{\omega}{\omega_{R1}}$  curve

## Infinite resonators scenario:

This section investigates the dispersion characteristics of Rayleigh waves propagating along a surface covered with an infinite array of resonators, effectively forming a metasurface. The analysis reveals the emergence of frequency bandgaps, where wave propagation is significantly attenuated. Notably, the nonlinearity of the resonators plays a crucial role in determining the location of these bandgaps as depicted in Figure 4.2.5. Hardening nonlinearity shifts the bandgaps to higher frequencies while softening nonlinearity results in bandgaps at lower frequencies. This behavior is consistent with the expected stiffening and softening effects of the respective nonlinearities. Importantly, within these bandgaps, there is a possibility of mode conversion from surface Rayleigh waves to body waves, which propagate into the bulk medium. This mode conversion offers a potential mechanism for protecting structures from incoming surface waves by diverting the wave energy away from the surface.

In Figure 4.2.6a, the effect of base input amplitude is shown through three curves with different  $\widetilde{U}$  values (0, 0.1, and 0.2), where increasing the base input amplitude causes Rayleigh waves to deviate more significantly from their linear dispersion relationship, particularly in the frequency range between 1.0 and 1.5.

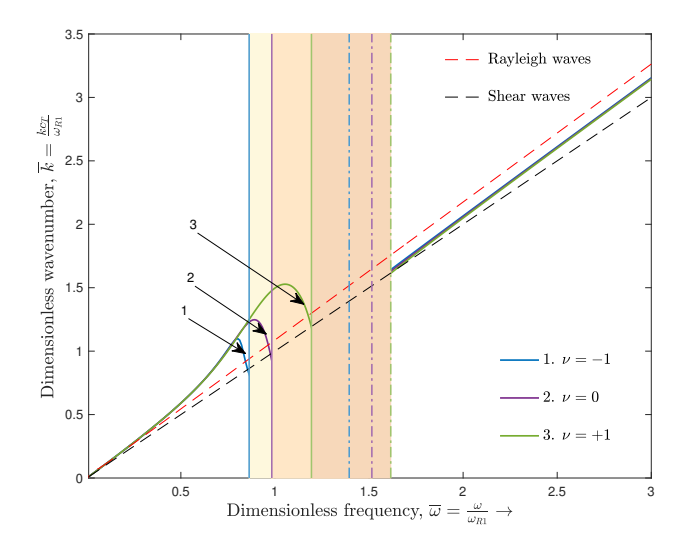
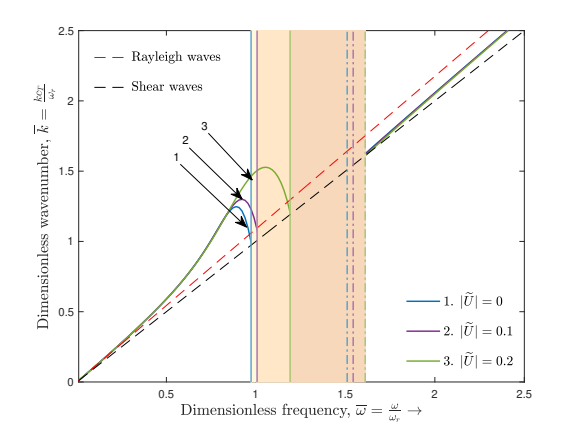
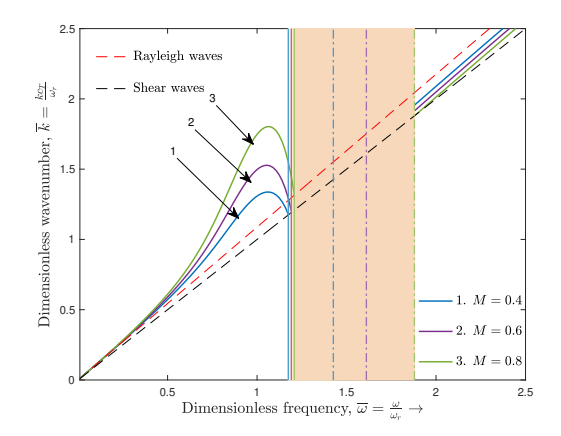


Figure 4.2.5: Effect of nonlinearity on frequency bandgaps in the dispersion curve





- (a) Effect of the base input amplitude
- (b) Effect of normalized mass parameter

Figure 4.2.6: Dispersion curves showing the variation of dimensionless wavenumber  $\bar{k}$  with dimensionless frequency  $\bar{\omega}$ 

Figure 4.2.6b demonstrates the effect of the normalized mass parameter M (0.4, 0.6, and 0.8), where higher mass values create more pronounced nonlinear behavior and

stronger coupling between the wave modes, leading to a larger frequency band-gaps. Both graphs show that nonlinear effects become more prominent at intermediate frequencies, with the shaded regions likely indicating zones of wave interaction or mode conversion, and the vertical dashed lines marking critical frequency values where significant changes in wave behavior occur.

#### 4.2.5 Conclusions

The multiple scattering formulation, by accurately capturing inter-resonator interactions and near-field effects, emerges as a crucial tool for analyzing seismic metasurfaces. Its flexibility in handling diverse resonator configurations and types allows for effective design optimization. This study reveals that deeper source locations significantly enhance ground-borne vibration attenuation, highlighting the importance of source depth. Furthermore, the proposed metasurface design demonstrates tunability; hardening nonlinearity in resonators effectively mitigates higher-frequency vibrations, while increasing normalized mass increases overall attenuation efficiency. Importantly, incorporating a larger number of resonators broadens frequency bandgaps and promotes the mode conversion of surface waves into bulk waves, significantly improving vibration mitigation capabilities. This comprehensive approach provides valuable insights for designing effective seismic metasurfaces.

# CHAPTER 5

Rayleigh Waves Generation and Propagation due to External Sources

Beyond the propagation and control of Rayleigh waves, this chapter addresses their generation, which can be modeled as either an initial value problem or a boundary value problem. Subchapter 5.1 employs Laplace transforms and an asymptotic model for interior source generation, while Subchapter 5.2 uses Hankel transforms and a matrix approach for seismic surface loading in micropolar media.

# 5.1 Interior initial value problem in a semi-infinite medium\*

#### 5.1.1 Mathematical formulation

We investigate the Rayleigh wave field over a linearly isotropic, elastic half-plane occupying the region  $-\infty < x < \infty$  and  $0 < z < \infty$ . It is assumed that the wave motion is due to initial conditions prescribed along the line z = h, see Figure. 5.1.1.

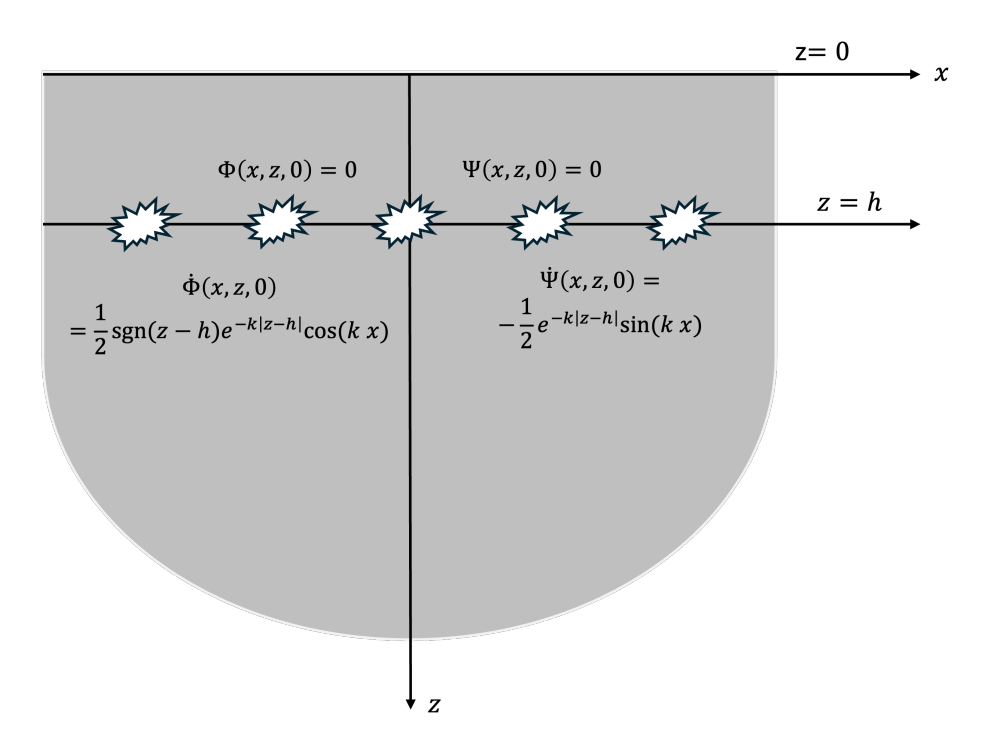


Figure 5.1.1: Geometry of the problem

The plane-strain equations of motion in absence of external forces can be written as

$$\sigma_{ij,j} = \rho \, u_{i,tt}. \tag{5.1.1}$$

Here  $u_i(x, z, t)$  are the components of displacement vector  $\vec{u}$  of the elastic wave;  $\rho$  is the volume density; and  $\sigma_{ij}$  (i, j = 1, 2) are components of the Cauchy stress tensor.

<sup>\*</sup> Ready to submit

Also, for a homogeneous, isotropic solid, the stress-strain relations are defined by

$$\sigma_{ij} = \lambda \epsilon_{kk} \delta_{ij} + 2\mu \epsilon_{ij}, \tag{5.1.2}$$

where  $\lambda$  and  $\mu$  are the Lamé elastic moduli,  $\delta_{ij}$  denotes the Kronecker delta, and  $\epsilon_{ij}$  denotes the strain tensor.

The kinematic relation to express the components of strain tensor  $\epsilon_{ij}$  in terms of displacement components  $u_i$  is given as

$$\epsilon_{ij} = \frac{1}{2} \left( \frac{\partial u_i}{\partial x_j} + \frac{\partial u_j}{\partial x_i} \right).$$

As a result, the governing equation of motion for Rayleigh waves propagating along x-direction with the displacement components  $\mathbf{u} = (u_1(x, z, t), u_3(x, z, t), 0)$  can be given as,

$$\mu \nabla^2 \mathbf{u} + (\lambda + \mu) \nabla \nabla \cdot \mathbf{u} = \rho \ddot{\mathbf{u}}. \tag{5.1.3}$$

Employing Helmholtz decomposition, the displacement field  $\mathbf{u}$  can be represented as the sum of a scalar potential  $\Phi(x, z, t)$  and a vector potential  $\vec{\Psi}(x, z, t) = (0, 0, \Psi)$  as,

$$u_1(x,z,t) = \frac{\partial \Phi}{\partial x} - \frac{\partial \Psi}{\partial z}, \qquad u_3(x,z,t) = \frac{\partial \Phi}{\partial z} + \frac{\partial \Psi}{\partial x}.$$
 (5.1.4)

Upon substitution of expressions given in Eq. (5.1.4) into equations of motion, the system in Eq. (5.1.3) decouples into,

$$\nabla^2 \Phi = \frac{1}{\beta_1^2} \frac{\partial^2 \Phi}{\partial t^2}, \qquad \nabla^2 \Psi = \frac{1}{\beta_2^2} \frac{\partial^2 \Psi}{\partial t^2}, \tag{5.1.5}$$

where  $\beta_1 = \sqrt{\frac{\lambda + 2\mu}{\rho}}$  and  $\beta_2 = \sqrt{\frac{\mu}{\rho}}$  are the body wave velocities.

The above equations are subjected to **initial interior conditions**, which are given below:

$$u_1(x, z, 0) = u_3(x, z, 0) \equiv 0,$$

$$\frac{\partial u_1}{\partial t}\Big|_{t=0} = 0, \ \frac{\partial u_3}{\partial t}\Big|_{t=0} = \delta(z - h) \sin(kx)$$

In terms of potentials, these conditions can be rewritten as,

$$\Phi(x, z, 0) = \Psi(x, z, 0) \equiv 0,$$

$$\frac{\partial \Phi}{\partial t}\big|_{t=0} = \frac{1}{2}\operatorname{sgn}(z - h)\operatorname{exp}(-k|z - h|)\operatorname{cos}(kx),$$

$$\frac{\partial \Psi}{\partial t}\big|_{t=0} = -\frac{1}{2}\operatorname{exp}(-k|z - h|)\operatorname{sin}(kx)$$
(5.1.6)

Further, an asymptotic hyperbolic-elliptic model developed by Kaplunov and Prikazchikov [87] accounts for the contributions of Rayleigh wave fields. According to this model, the decay of Rayleigh waves from the surface towards the interior is governed by the following quasi-static elliptic equations for the potentials,

$$\frac{\partial^2 \Phi}{\partial z^2} + \alpha^2 \frac{\partial^2 \Phi}{\partial x^2} = 0, \quad \frac{\partial^2 \Psi}{\partial z^2} + \beta^2 \frac{\partial^2 \Psi}{\partial x^2} = 0, \tag{5.1.7}$$

in which

$$\alpha^2 = 1 - \frac{c_R^2}{\beta_1^2}, \ \beta^2 = 1 - \frac{c_R^2}{\beta_2^2},$$

with  $c_R$  denoting the velocity of Rayleigh waves.

In contrast to the interior behavior, the wave propagation along the surface z = 0 is governed by a hyperbolic wave equation for one potential, coupled with a differential relation between two potentials, see section 1.3.2 for details. For the case of horizontal loading  $P_1$  and vertical loading  $P_2$ , the equations at the surface z = 0 become

$$\left[ \frac{\partial^2 \Phi}{\partial x^2} - \frac{1}{v^2} \frac{\partial^2 \Phi}{\partial t^2} \right] \Big|_{y=0} = \frac{1+\beta^2}{2\mu B} \left( P_2 + \nu^{-1} P_1^* \right), \tag{5.1.8}$$

where the superscript \* on  $P_2$  denotes, in the sense, its Hilbert transform and the constant B,  $\nu$  assumes the value

$$B = \frac{\alpha}{\beta} \left( 1 - \beta^2 \right) + \frac{\beta}{\alpha} \left( 1 - \alpha^2 \right) - 1 + \beta^4, \quad \nu = \frac{2\alpha}{1 + \beta^2},$$

and the relation between the potentials is given as,

$$\Psi = \frac{2\alpha}{1+\beta^2} \Phi^c, \tag{5.1.9}$$

where the superscript 'c' denotes the harmonic conjugate of the corresponding function. We employ this asymptotic model to assess the Rayleigh wave contributions arising from initial interior conditions. The solution for these initial interior sources is derived in the following section and is then integrated into the asymptotic model to approximate the resulting Rayleigh wave field.

#### 5.1.2 Solution for the interior source problem

Let the solutions to Eq. (5.1.5) takes the form

$$\Phi(x, z, t) = \phi(z, t) \cos(kx), 
\Psi(x, z, t) = \psi(z, t) \sin(kx),$$
(5.1.10)

This will reduce the equations of motion given in Eq. (5.1.5) as,

$$\frac{\partial^2 \phi}{\partial z^2} - k^2 \phi = \frac{1}{\beta_1^2} \frac{\partial^2 \phi}{\partial t^2}, 
\frac{\partial^2 \psi}{\partial z^2} - k^2 \psi = \frac{1}{\beta_2^2} \frac{\partial^2 \psi}{\partial t^2}.$$
(5.1.11)

Defining the non-dimensional parameters,

$$\xi = \frac{x}{h}, \ \chi = \frac{z}{h}, \ \tau = \frac{\beta_2}{h}t, \ \kappa = kh, \ \text{and} \ \gamma = \frac{\beta_1}{\beta_2},$$

the governing equations of motion in Eq. (5.1.11) can be re-written as

$$\frac{\partial^2 \phi}{\partial \chi^2} - \kappa^2 \phi = \frac{1}{\gamma^2} \frac{\partial^2 \phi}{\partial \tau^2}, 
\frac{\partial^2 \psi}{\partial \chi^2} - \kappa^2 \psi = \frac{\partial^2 \psi}{\partial \tau^2},$$
(5.1.12)

subjected to the non-dimensional interior initial conditions,

$$\phi(\chi,0) = 0, \ \psi(\chi,0) = 0$$

$$\frac{\partial \phi}{\partial \tau}\big|_{\tau=0} = \frac{1}{2}\operatorname{sgn}(\chi - 1) \exp(-\kappa|\chi - 1|),$$

$$\frac{\partial \psi}{\partial \tau}\big|_{\tau=0} = -\frac{1}{2}\exp(-\kappa|\chi - 1|).$$
(5.1.13)

A Laplace integral transformation is employed on the variable ' $\tau$ ' according to the definition, see Debnath and Bhatta [274],

$$f^{L}(z,s) = \int_{0}^{\infty} f(z,\tau) e^{-s\tau} d\tau,$$

where s is the complex transform variable with Re(s) > 0.

Further, the inverse Laplace transformation is defined as,

$$f(z,\tau) = \frac{1}{2\pi i} \int_{C-i\infty}^{C+i\infty} f^L(z,s) e^{s\tau} ds,$$

where C > 0 is larger than all the real parts of singularities of  $f^L(z, s)$ .

As a result, application of Laplace transformation to Eq. (5.1.12) gives the following decoupled system of ordinary differential equations,

$$\frac{d^2\phi^L}{d\chi^2} - r_1^2 \phi^L = -\frac{1}{2\gamma^2} \operatorname{sgn}(\chi - 1) \exp(-\kappa |\chi - 1|),$$

$$\frac{d^2\phi^L}{d\chi^2} - r_2^2 \psi^L = \frac{1}{2} \exp(-\kappa |\chi - 1|),$$
(5.1.14)

where 
$$r_1 = \sqrt{\kappa^2 + \frac{s^2}{\gamma^2}}, \ r_2 = \sqrt{\kappa^2 + s^2}.$$

Since the modelling of the interior source is carried in an unbounded medium, we also employ Fourier transforms. Specifically, we apply the Fourier transform, defined as,

$$f^{F}(p,t) = \int_{-\infty}^{\infty} f(\chi,t) e^{-ip\chi} d\chi,$$

and its inverse,

$$f(\chi, t) = \int_{-\infty}^{\infty} f^{F}(p, t) e^{ip\chi} d\xi,$$

to both sides of Eq. (5.1.13). This transformation leads to the following Laplace-Fourier transformed potential components as,

$$\phi^{LF}(p,s) = \frac{-1}{\gamma^2} \left[ \frac{ip \exp(ip)}{(p^2 + r_1^2)(p^2 + \kappa^2)} \right],$$

$$\psi^{LF}(p,s) = \frac{-\kappa \exp(ip)}{(p^2 + r_2^2)(p^2 + \kappa^2)}.$$
(5.1.15)

Taking inverse Fourier transformation in Eqs. (5.1.15) yields,

$$\phi^{L}(\chi, s) = \frac{1}{2s^{2}} \left[ \exp(-\kappa |\chi - 1|) - \exp(-r_{1}|\chi - 1|) \right] \operatorname{sgn}(\chi - 1),$$

$$\psi^{L}(\chi, s) = -\frac{1}{2s^{2}} \left[ \exp(-\kappa |\chi - 1|) - \frac{\kappa}{r_{2}} \exp(-r_{2}|\chi - 1|) \right].$$
(5.1.16)

As a result, the associated stress components  $\sigma_{21}$  and  $\sigma_{22}$  at  $\chi = 0$  can be calculated using Eq. (5.1.2).

As a consequence of the superposition principle, we can now formulate the initial value problem for the elastic half-space with

$$P_1(x,t) = -\sigma_{21}\big|_{y=0}, \qquad P_2(x,t) = -\sigma_{22}\big|_{y=0}.$$
 (5.1.17)

Define the dimensionless loading terms  $\widetilde{P}_1 = \frac{P_1(x,\tau)}{\mu}, \ \widetilde{P}_2 = \frac{P_2(x,\tau)}{\mu}.$ 

Thus, applying the Laplace transformation to both sides of Eq. (5.1.17) and utilizing Eqs.

(5.1.16), we obtain,

$$\begin{split} \widetilde{P}_{1}^{L}(\xi,s) &= -\widetilde{\sigma}_{21}^{L} \big|_{\chi=0} &= -\frac{\kappa}{2s^{2}} \left[ \frac{e^{-r_{2}} \left( 2\kappa^{2} + s^{2} \right)}{r_{2}} - 2r_{1} e^{-r_{1}} \right] \sin\left(\kappa\xi\right) \\ &= -\frac{\kappa}{2s^{2}} \left[ \frac{e^{-\sqrt{\kappa^{2} + s^{2}}} \left( 2\kappa^{2} + s^{2} \right)}{\sqrt{\kappa^{2} + s^{2}}} - 2e^{-\sqrt{\kappa^{2} + \frac{s^{2}}{\gamma^{2}}}} \sqrt{\kappa^{2} + \frac{s^{2}}{\gamma^{2}}} \right] \sin\left(\kappa\xi\right) \end{split}$$

$$(5.1.18)$$

$$\widetilde{P}_{2}^{L}(\xi, s) = -\widetilde{\sigma}_{22}^{L}\big|_{\chi=0} = -\frac{1}{2s^{2}} \left[ e^{-r_{1}} \left( 2\kappa^{2} + s^{2} \right) - 2\kappa^{2} e^{-r_{2}} \right] \cos\left(\kappa\xi\right) 
= -\frac{1}{2s^{2}} \left[ e^{-\sqrt{\kappa^{2} + \frac{s^{2}}{\gamma^{2}}}} \left( 2\kappa^{2} + s^{2} \right) - 2\kappa^{2} e^{-\sqrt{\kappa^{2} + s^{2}}} \right] \cos\left(\kappa\xi\right). (5.1.19)$$

Observe that  $\widetilde{P}_1^L$  and  $\widetilde{P}_2^L$  are the stress disturbances produced at the surface of the halfplane due to the interior initial conditions.

## 5.1.3 Asymptotic solution

On defining  $c = \frac{v}{\beta_2}$  and non-dimensionalizing Eq. (5.1.7), we obtain

$$\left[ \frac{\partial^2 \Phi}{\partial \xi^2} - \frac{1}{c^2} \frac{\partial^2 \Phi}{\partial \tau^2} \right] \bigg|_{\chi=0} = \frac{1+\beta^2}{2B} \left( \widetilde{P}_2 + \nu^{-1} \widetilde{P}_1^* \right).$$
(5.1.20)

Assuming a cossinusoidal form as given in Eq. (5.1.10) followed by the application of Laplace transformation and utilizing the stress components obtained in Eqs. (5.1.18) and (5.1.19), we get

$$\phi^{L}(0,s) = -\frac{c^{2}(1+\beta^{2})}{2B(s^{2}+\kappa^{2}c^{2})}H(s),$$
(5.1.21)

where

$$H(s) = -\frac{1}{2s^2} \left[ e^{-r_1} \left( 2\kappa^2 + s^2 \right) - 2\kappa^2 e^{-r_2} \right] + \nu^{-1} \left\{ \frac{\kappa}{2s^2} \left[ \frac{e^{-r_2} \left( 2\kappa^2 + s^2 \right)}{r_2} - 2r_1 e^{-r_1} \right] \right\}.$$

This gives,

$$\phi(0,\tau) = \frac{c^2 (1+\beta^2) I(\tau)}{2B}$$
 (5.1.22)

where

$$I(\tau) = -\frac{1}{2\pi i} \int_{C-i\infty}^{C+i\infty} \frac{1}{s^2 + \kappa^2 c^2} H(s) \exp(s\tau) ds,$$
 (5.1.23)

is the Bromwich integral to be evaluated to obtain the inverse Laplace of  $\phi^L$ . Note that  $C \in \mathbb{R}$  is considered larger than any real part of the poles in the integrand.

The complex integral given in Eq. (5.1.23) contains integrand with singularities in the form of poles and branch cuts. There are two poles  $s = \pm i\kappa c$ , generally known as Rayleigh poles, and two branch points at  $s = \pm i\kappa$ . The residue theorem can be employed to evaluate

the contribution of the Rayleigh poles to the integral, thereby determining the Rayleigh wave contribution. Additionally, the model also predicts bulk wave contributions, which can be understood by analyzing the local behavior of the integral around the branch points.

As a result, we can write

$$I(\tau) = I_B(\tau) + I_P(\tau),$$
 (5.1.24)

where  $I_B(\tau)$  and  $I_P(\tau)$  are the contributions from the branch cuts for larger  $\tau$  and Rayleigh poles, respectively.

We shall now chose the contour paths and branch cuts for the integral in Eq. (5.1.23) as indicated in the Figure 5.1.2.

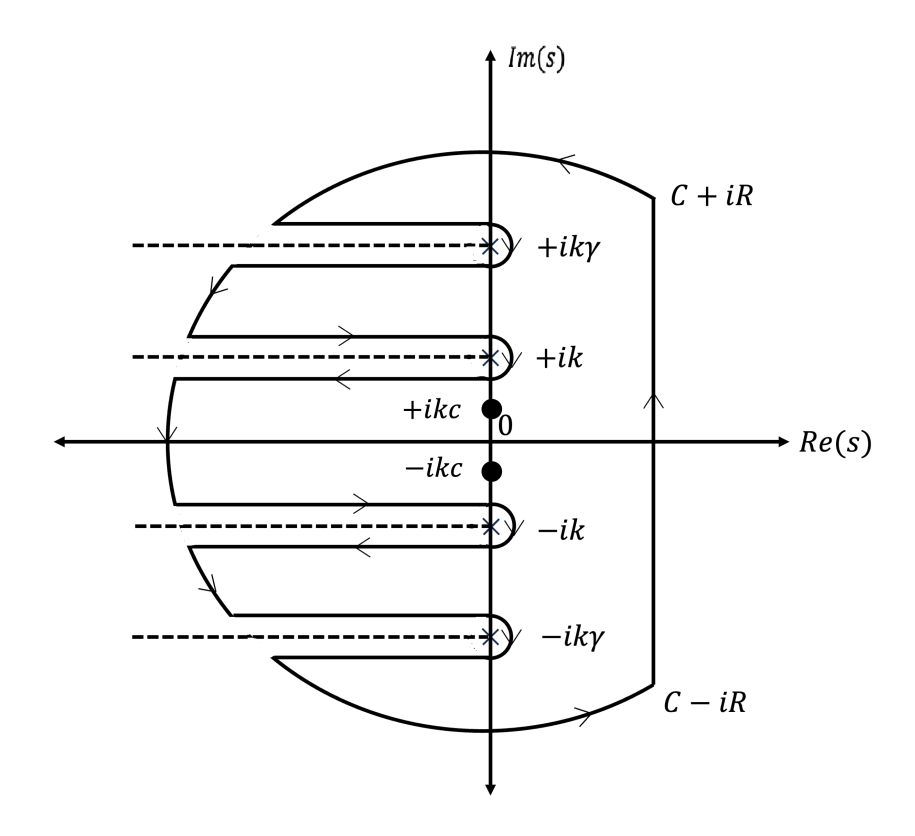


Figure 5.1.2: Choice of contour paths and branch cuts for the integral encountered in asymptotic model of Rayleigh waves

By expanding Eq. (5.1.23) locally around each branch point  $s = \pm ik$ , the total contribution of the branch cuts to the integral can be evaluated as,

$$I_{B}(\tau) \sim \frac{1}{\kappa^{2}\pi\tau} \left[ \frac{(2-\gamma^{2})-2\nu^{-1}}{\gamma^{2}(\gamma^{2}-c^{2})} \sin(\kappa\gamma\tau) - \frac{\nu^{-1}(\gamma^{2}-2)}{\gamma^{2}\sqrt{\gamma^{2}-1}(\gamma^{2}-c^{2})} \cos\left(\kappa\gamma\tau - \kappa\sqrt{\gamma^{2}-1}\right) \right] + \frac{1}{\kappa^{2}\pi\tau(1-c^{2})} \left[ -2 + \left(1 + 2\nu^{-1}\sqrt{1 - \frac{1}{\gamma^{2}}}\right) e^{-\kappa\sqrt{1 - \frac{1}{\gamma^{2}}}} \right] \sin(\kappa\tau) - \frac{\nu^{-1}}{\sqrt{2\pi\kappa^{3}\tau}(1-c^{2})} \cos\left(\kappa\tau - \frac{\pi}{4}\right).$$
(5.1.25)

It is worth mentioning that the asymptotic behavior of the integrand at larger time scales, evaluated using the saddle point method, aligns perfectly with the solution obtained. As a result, we conclude that the asymptotic hyperbolic-elliptic model predicts the existence of a transient bulk wave solution associated with branch cuts. For large values of  $\tau$ , we have,

$$\phi_{B}(0,\tau) \sim \frac{c^{2}(1+\beta^{2})}{2B} \left\{ \frac{1}{\kappa^{2}\pi\tau} \left[ \frac{(2-\gamma^{2})-2\nu^{-1}}{\gamma^{2}(\gamma^{2}-c^{2})} \sin(\kappa\gamma\tau) - \frac{\nu^{-1}(\gamma^{2}-2)}{\gamma^{2}\sqrt{\gamma^{2}-1}(\gamma^{2}-c^{2})} \cos\left(\kappa\gamma\tau-\kappa\sqrt{\gamma^{2}-1}\right) \right] + \frac{1}{\kappa^{2}\pi\tau(1-c^{2})} \left[ -2 + \left(1+2\nu^{-1}\sqrt{1-\frac{1}{\gamma^{2}}}\right) e^{-\kappa\sqrt{1-\frac{1}{\gamma^{2}}}} \right] \sin(\kappa\tau) - \frac{\nu^{-1}}{\sqrt{2\pi\kappa^{3}\tau}(1-c^{2})} \cos\left(\kappa\tau-\frac{\pi}{4}\right) \right\}.$$
(5.1.26)

Hence, the scalar potential can be given as,

$$\Phi_{B}(\xi, 0, \tau) \sim \frac{c^{2} (1 + \beta^{2})}{2B} \left\{ \frac{1}{\kappa^{2} \pi \tau} \left[ \frac{(2 - \gamma^{2}) - 2\nu^{-1}}{\gamma^{2} (\gamma^{2} - c^{2})} \sin(\kappa \gamma \tau) \right. \right. \\
\left. - \frac{\nu^{-1} (\gamma^{2} - 2)}{\gamma^{2} \sqrt{\gamma^{2} - 1} (\gamma^{2} - c^{2})} \cos\left(\kappa \gamma \tau - \kappa \sqrt{\gamma^{2} - 1}\right) \right] \\
+ \frac{1}{\kappa^{2} \pi \tau (1 - c^{2})} \left[ -2 + \left( 1 + 2\nu^{-1} \sqrt{1 - \frac{1}{\gamma^{2}}} \right) e^{-\kappa \sqrt{1 - \frac{1}{\gamma^{2}}}} \right] \sin(\kappa \tau) \\
- \frac{\nu^{-1}}{\sqrt{2\pi \kappa^{3} \tau} (1 - c^{2})} \cos\left(\kappa \tau - \frac{\pi}{4}\right) \right\} \cos(\kappa \xi). \tag{5.1.27}$$

Additionally, the residue theorem is employed to evaluate the pole contribution, zielding

$$I_{P}(\tau) = \left\{ \frac{\left(-2\nu^{-1}\sqrt{1 - \frac{c^{2}}{\gamma^{2}}} + (c^{2} - 2)\right)}{2\kappa c^{3}} \exp\left(-\kappa\sqrt{1 - \frac{c^{2}}{\gamma^{2}}}\right) + \frac{\left(2\sqrt{1 - c^{2}} - \nu^{-1}(c^{2} - 2)\right)}{2\kappa c^{3}\sqrt{1 - c^{2}}} \exp\left(-\kappa\sqrt{1 - c^{2}}\right) \right\} \sin(\kappa c\tau). \quad (5.1.28)$$

This gives the expression for scalar potential of Rayleigh waves propagating on the surface  $\chi = 0$  as,

$$\phi_P(0,\tau) = \frac{c(1+\beta^2)}{2B} \left\{ \frac{\left(-2\nu^{-1}\sqrt{1-\frac{c^2}{\gamma^2}} + (c^2 - 2)\right)}{2\kappa c^3} \exp\left(-\kappa\sqrt{1-\frac{c^2}{\gamma^2}}\right) + \frac{\left(2\sqrt{1-c^2} - \nu^{-1}(c^2 - 2)\right)}{2\kappa c^3\sqrt{1-c^2}} \exp\left(-\kappa\sqrt{1-c^2}\right) \right\} \sin(\kappa c\tau).$$
 (5.1.29)

This gives, the scalar potential,

$$\Phi_{P}(\xi, 0, \tau) = \frac{c(1+\beta^{2})}{2B} \left\{ \frac{\left(-2\nu^{-1}\sqrt{1-\frac{c^{2}}{\gamma^{2}}} + (c^{2}-2)\right)}{2\kappa c^{3}} \exp\left(-\kappa\sqrt{1-\frac{c^{2}}{\gamma^{2}}}\right) + \frac{\left(2\sqrt{1-c^{2}} - \nu^{-1}(c^{2}-2)\right)}{2\kappa c^{3}\sqrt{1-c^{2}}} \exp\left(-\kappa\sqrt{1-c^{2}}\right) \right\} \sin(\kappa c\tau) \cos(\kappa\xi) (5.1.30)$$

Further, solving for the quasi-elliptic equation of the form given in Eq. (5.1.7),

$$\frac{d^2\Phi}{d\chi^2} + \alpha^2 \frac{d^2\Phi}{d\xi^2} = 0, (5.1.31)$$

subjected to the boundary condition given in Eq. (5.1.30) yields,

$$\Phi(\xi, \alpha \chi, \tau) = \{ \Phi_B(\xi, 0, \tau) + \Phi_P(\xi, 0, \tau) \} \exp(-\kappa \alpha \chi) \cos(\kappa \xi).$$
 (5.1.32)

Also, the transverse potential  $\Psi$  can be easily restored by using Eq. (5.1.9) as,

$$\Psi(\xi, \beta \chi, \tau) = \frac{2\alpha}{1 + \beta^2} \left\{ \Phi_B(\xi, 0, \tau) + \Phi_P(\xi, 0, \tau) \right\} \exp\left(-\kappa \beta \chi\right) \sin\left(\kappa \xi\right). \tag{5.1.33}$$

Thus, the total wave field displacement components can be expressed in terms of the potential  $\psi$  as,

$$u_1(\xi, \chi, \tau) = \frac{\partial \Phi(\xi, \alpha \chi, \tau)}{\partial \xi} + \frac{1 + \beta^2}{2} \frac{\partial \Phi(\xi, \beta \chi, \tau)}{\partial \xi}, \tag{5.1.34}$$

$$u_3(\xi, \chi, \tau) = \frac{\partial \Phi(\xi, \alpha \chi, \tau)}{\partial \chi} + \frac{2}{1 + \beta^2} \frac{\partial \Phi(\xi, \beta \chi, \tau)}{\partial \chi}.$$
 (5.1.35)

## 5.1.4 Exact solution

Now, we shall produce the exact expressions for the displacements at the free surface due to the prescribed surface stresses  $\widetilde{P}_1^L$  and  $\widetilde{P}_2^L$ .

If  $\Phi$  and  $\vec{\Psi} = (0, \Psi, 0)$  are the dimensionless scalar and vector potentials of the wave generated due to the surface stresses, then the equations of motion could be re-written as,

$$\frac{\partial^2 \Phi}{\partial \xi^2} + \frac{\partial^2 \Phi}{\partial \chi^2} = \frac{1}{\gamma^2} \frac{\partial^2 \Phi}{\partial \tau^2}, \qquad \frac{\partial^2 \Psi}{\partial \xi^2} + \frac{\partial^2 \Psi}{\partial \chi^2} = \frac{\partial^2 \Psi}{\partial \tau^2}. \tag{5.1.36}$$

The relevant stress-strain relations are written in terms of potentials as,

$$\tau_{21} = \mu \left( 2 \frac{\partial^2 \Phi}{\partial \xi \partial \chi} + \frac{\partial^2 \Psi}{\partial \xi^2} - \frac{\partial^2 \Psi}{\partial \chi^2} \right), \tag{5.1.37}$$

$$\tau_{22} = \lambda \left( \frac{\partial^2 \Phi}{\partial \xi^2} + \frac{\partial^2 \Phi}{\partial \chi^2} \right) + 2\mu \left( \frac{\partial^2 \Phi}{\partial \chi^2} - \frac{\partial^2 \Psi}{\partial \xi \partial \chi} \right). \tag{5.1.38}$$

Assuming the potentials of the form,

$$\Phi(\xi, \chi, \tau) = \phi(\chi, t) \cos(\kappa \xi), 
\Psi(\xi, \chi, \tau) = \psi(\chi, t) \sin(\kappa \xi),$$
(5.1.39)

and subsequently applying the Laplace transform, we obtain the following system of ordinary differential equations as,

$$\frac{d^2\phi^L}{d\chi^2} - r_1^2 \phi^L = 0, \qquad \frac{d^2\psi^L}{d\chi^2} - r_2^2 \psi^L = 0, \tag{5.1.40}$$

where  $r_1$  and  $r_2$  are defined previously. Solutions to Eq. (5.1.36) that show appropriate behavior for larger values of  $\chi$  are,

$$\Phi^L(\xi,\chi,\tau) = A \exp\left(-r_1 \chi\right) \cos(\kappa \xi), \qquad \Psi^L(\xi,\chi,\tau) = B \exp\left(-r_2 \chi\right) \sin(\kappa \xi). \tag{5.1.41}$$

Defining  $\tilde{\tau}_{21} = \frac{\tau_{21}}{\mu}$  and  $\tilde{\tau}_{22} = \frac{\tau_{22}}{\mu}$ , the boundary conditions at  $\chi = 0$  can be transformed as,

$$\widetilde{\tau}_{21}^L\big|_{\gamma=0} = \widetilde{P}_1^L, \qquad \widetilde{\tau}_{22}^L\big|_{\gamma=0} = \widetilde{P}_2^L.$$
 (5.1.42)

Substituting the expressions for  $\Phi^L$  and  $\Psi^L$  and using Eqs. (5.1.42), the following equations for A and B are obtained:

$$2\kappa r_1 A - (2\kappa^2 + s^2) B = \widetilde{P}_1^L, (s^2 + 2\kappa^2) A - 2\kappa r_2 B = \widetilde{P}_2^L.$$
(5.1.43)

This system is solved to obtain the values of A and B. As a result, the expression for the transformed potentials are given as,

$$\Phi^{L}(\xi, \chi, s) = \left\{ -\frac{4\kappa^{2}r_{1}r_{2} + (2\kappa^{2} + s^{2})^{2}}{2s^{2}R(s)} \exp(-r_{1}) + \frac{2\kappa^{2}(2\kappa^{2} + s^{2})}{s^{2}R(s)} \exp(-r_{2}) \right\} \exp(-r_{1}\chi) \cos(\kappa\xi), \qquad (5.1.44)$$

$$\Psi^{L}(\xi, \chi, s) = \left\{ \frac{2\kappa r_{1}(2\kappa^{2} + s^{2})}{s^{2}R(s)} \exp(-r_{1}) - \frac{\kappa\left(4\kappa^{2}r_{1}r_{2} + (2\kappa^{2} + s^{2})^{2}\right)}{2r_{2}s^{2}R(s)} \exp(-r_{2}) \right\} \exp(-r_{2}\chi) \sin(\kappa\xi), \quad (5.1.45)$$

where 
$$R(s) = (2\kappa^2 + s^2)^2 - 4\kappa^2 r_1 r_2$$
.

On taking the inverse Laplace transform for the displacement potentials, we get

$$\Phi(\xi, \chi, \tau) = \frac{\cos(\kappa \xi)}{2\pi i} \int_{C-i\infty}^{C+i\infty} \left\{ -\frac{4\kappa^2 r_1 r_2 + (2\kappa^2 + s^2)^2}{2s^2 R(s)} \exp(-r_1) + \frac{2\kappa^2 (2\kappa^2 + s^2)}{s^2 R(s)} \exp(-r_2) \right\} \exp(-r_1 \chi) \exp(s\tau) ds, \qquad (5.1.46)$$

$$\Psi(\xi, \chi, \tau) = \frac{\sin(\kappa \xi)}{2\pi i} \int_{C-i\infty}^{C+i\infty} \left\{ \frac{2\kappa r_1 (2\kappa^2 + s^2)}{s^2 R(s)} \exp(-r_1) - \frac{\kappa \left(4\kappa^2 r_1 r_2 + (2\kappa^2 + s^2)^2\right)}{2r_2 s^2 R(s)} \exp(-r_2) \right\} \exp(-r_2 \chi) \exp(s\tau) ds. \quad (5.1.47)$$

The integrands in Eqs. (5.1.46) and (5.1.47) contain both poles and branch points as singularities.

The poles are located at the zeroes of the Rayleigh-wave dispersion equation R(s) = 0. Additionally, branch points exist at  $s = \pm ik$  and  $s = \pm ik\gamma$ .

To evaluate the integral explicitly, the contour paths and branch cuts are chosen as depicted in Figure 5.1.3.

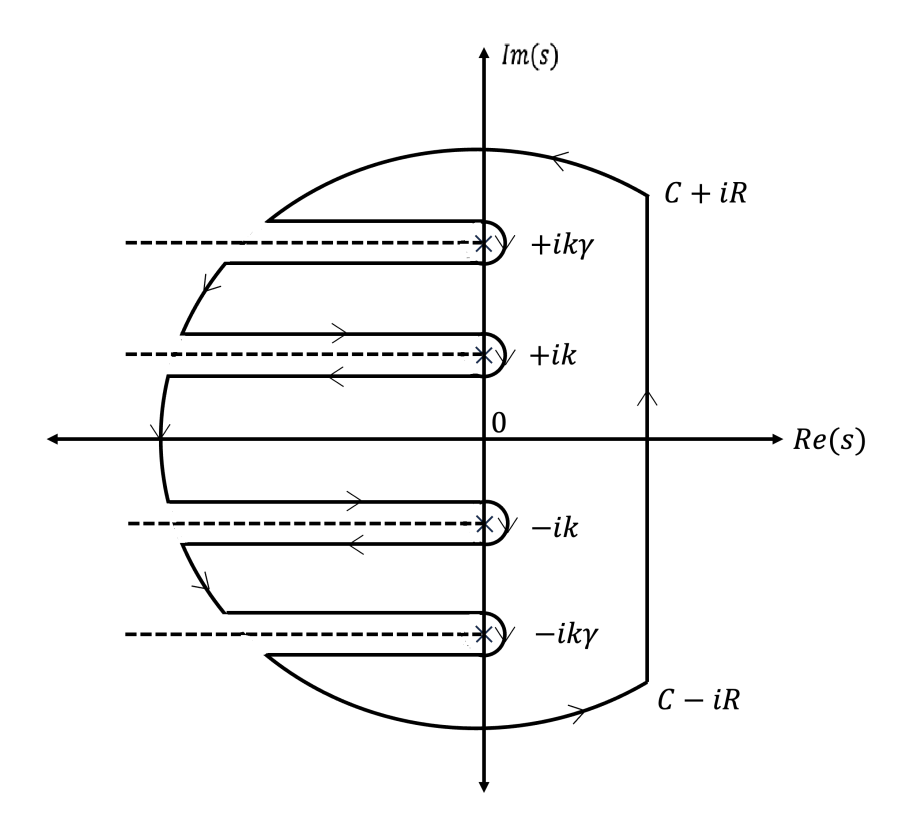


Figure 5.1.3: Choice of contour paths and branch cuts for the integral encountered in exact solution for Rayleigh waves

Now, let  $s = \pm i\kappa c$  be the roots of the Rayleigh-wave equation.

Rewriting R(s) as a function  $G\left(\frac{s^2}{\kappa^2}\right)$  as,

$$G\left(\frac{s^2}{\kappa^2}\right) = \kappa^4 \left(4\sqrt{\frac{s^2}{\kappa^2} + 1}\sqrt{\frac{s^2}{\kappa^2\gamma^2} + 1} - \left(2 + \frac{s^2}{\kappa^2}\right)^2\right),\,$$

and approximating the expression about its roots using Taylor series expansion as,

$$G\left(\frac{s^2}{\kappa^2}\right) \approx G'(-c^2)\left(\frac{s^2}{\kappa^2} + c^2\right),$$

allows us to determine the Rayleigh wave displacement potentials as,

$$\Phi_{P}(\xi,\chi,\tau) = \begin{cases}
-\frac{\kappa^{3} \left(c^{4} + 4\sqrt{1 - c^{2}}\sqrt{1 - \frac{c^{2}}{\gamma^{2}}} - 4c^{2} + 4\right) e^{-\kappa(\chi+1)\sqrt{1 - \frac{c^{2}}{\gamma^{2}}}}}{2 c^{3} G'(-c^{2})} \\
-\frac{2 (2 - c^{2}) \kappa^{3} e^{-\kappa\left(\chi\sqrt{1 - \frac{c^{2}}{\gamma^{2}}} + \sqrt{1 - c^{2}}\right)}}{c^{3} G'(-c^{2})} \\
\end{cases} \sin(\kappa c \tau) \cos(\kappa \xi), \quad (5.1.48)$$

$$\psi_{P}(\xi,\chi,\tau) = \begin{cases} -\frac{2(2-c^{2})\kappa^{3}\sqrt{1-\frac{c^{2}}{\gamma^{2}}}e^{-k\left(\sqrt{1-\frac{c^{2}}{\gamma^{2}}}+\sqrt{1-c^{2}}z\right)}}{c^{3}G'(-c^{2})} \\ +\frac{\kappa^{3}\left(c^{4}+4\sqrt{1-c^{2}}\sqrt{1-\frac{c^{2}}{\gamma^{2}}}-4c^{2}+4\right)e^{-\sqrt{1-c^{2}}\kappa(\chi+1)}}{2c^{3}\sqrt{1-c^{2}}G'(-c^{2})} \end{cases} \sin(\kappa c\tau) \sin(\kappa \xi).$$

$$(5.1.49)$$

For larger timescales  $\tau$ , the contribution from the branch cuts can be approximated by focusing on the dominant contribution near the branch points. This involves expanding the integral locally around each branch point. As a result,

$$\Phi_{B}(\xi,\chi,\tau) \sim \frac{1}{\kappa^{2}\pi\tau} \left\{ \frac{1}{2\gamma^{2}} \sin(\kappa\gamma\tau) + \frac{1}{\gamma^{2} (\gamma^{2} - 2)} \cos\left(\kappa\gamma\tau - \kappa\sqrt{\gamma^{2} - 1}\right) + \left[ \frac{e^{-\kappa(\chi+1)\frac{\sqrt{\gamma^{2} - 1}}{\gamma}}}{2} - 2e^{-\kappa\chi\frac{\sqrt{\gamma^{2} - 1}}{\gamma}} \right] \sin(\kappa\tau) \right\} \cos(\kappa\xi), \qquad (5.1.50)$$

$$\Psi_{B}(\xi,\chi,\tau) \sim \left\{ -\frac{1}{2\pi\kappa^{2}\gamma^{2}\sqrt{\gamma^{2} - 1}} \cos\left(\kappa\gamma\tau - \kappa(\chi+1)\sqrt{\gamma^{2} - 1}\right) - \frac{2\sqrt{\gamma^{2} - 1}e^{-\frac{\kappa\sqrt{\gamma^{2} - 1}}{\gamma}}}{\kappa^{2}\pi\gamma} \sin(\kappa\tau) - \frac{1}{2\sqrt{\pi\kappa^{3}\tau}} \cos\left(\kappa\tau - \frac{\pi}{4}\right) \right\} \sin(\kappa\xi). \qquad (5.1.51)$$

Thus, the total wavefield can be easily determined by combining the contributions from both the branch points and the poles.

#### 5.1.5 Graphical discussions

To elucidate the characteristics of the exact and asymptotic solutions and facilitate a comparative analysis, a series of graphical representations is presented. These figures depict the larger time-dependent behavior of total wavefield induced by interior sources. By visualizing the discrepancies between the two solution approaches, we aim to assess the efficiency of the asymptotic model in capturing the essential wave phenomenon.

Figure 5.1.4 presents a comparative analysis of the total wave contributions at the surface of the half-space ( $\chi = 0$ ) and at a depth of ( $\chi = 10$ ), as computed using both the exact and asymptotic approaches. As expected, the wave potential amplitudes at  $\chi = 10$  are significantly lower compared to those at the surface. The results highlight

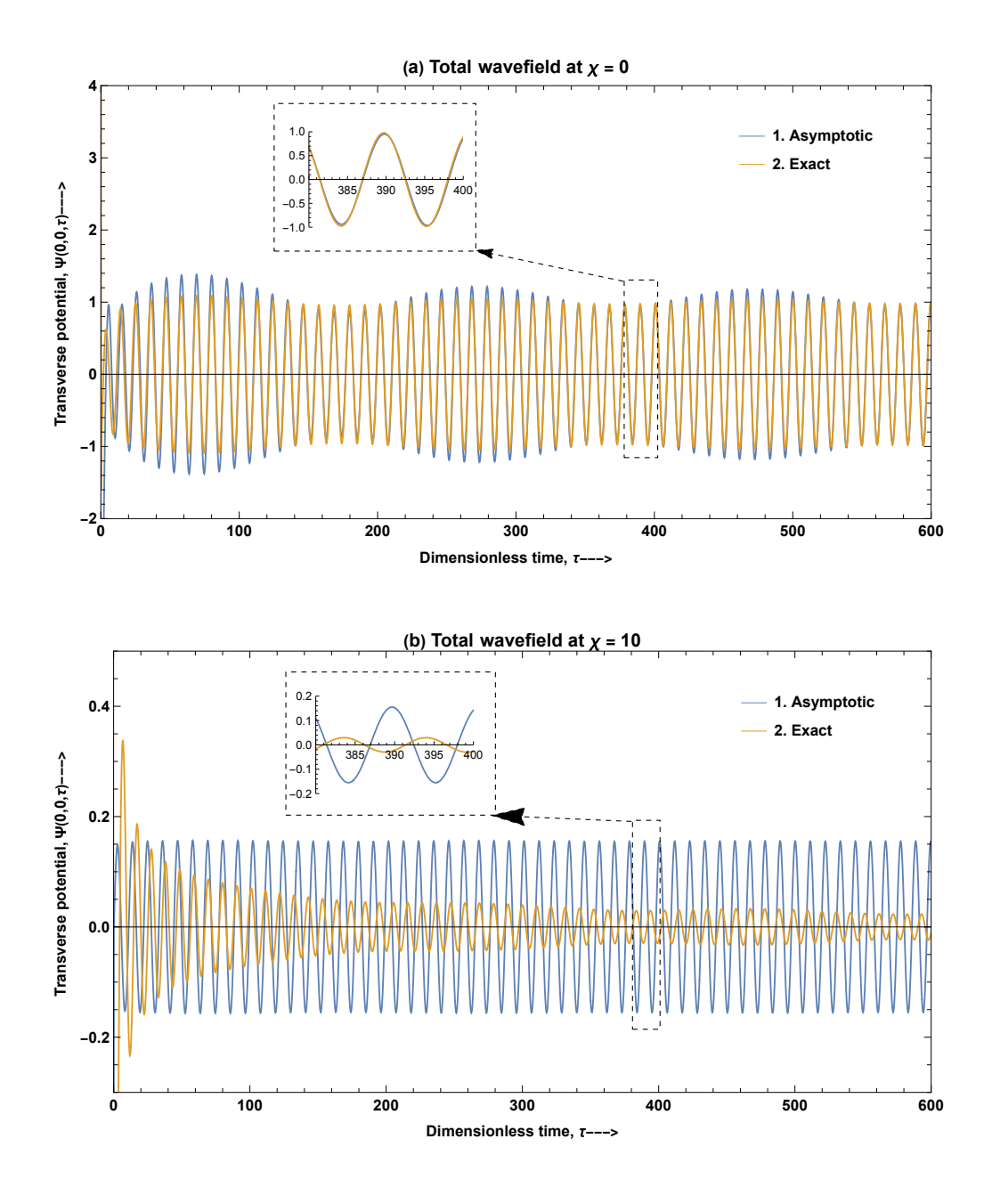


Figure 5.1.4: Comparison of total wave behavior at a larger time for both asymptotic and exact methods at dimensionless depth (a)  $\chi = 0$  (b)  $\chi = 10$ 

a noticeable discrepancy between the asymptotic and exact models, particularly at early times and deep below the surface. This discrepancy is attributed to the limitations of the asymptotic model in accurately capturing bulk wave phenomena. It is further important to point out that while the asymptotic and exact approaches agree well in capturing Rayleigh wave contributions, they exhibit significant discrepancies in predicting bulk wave

contributions. However, at the surface, as time progresses, the results from the two models converge, with the asymptotic predictions aligning closely with the exact solution.

#### 5.1.6 Conclusions

This study investigated the generation of wave fields within an elastic half-space due to prescribed initial displacement potential and velocity patterns. These initial conditions were employed to simulate a wave source. By applying Laplace transformation in time and utilizing an eigenvalue approach, the solution to the interior initial value problem was obtained. An image-source technique was incorporated to account for reflected wave fields from the surface. The superposition of the generated and reflected wave fields allowed for the calculation of surface stresses. These surface stresses, in turn, act as the loading mechanism for the generation of Rayleigh waves within the half-space.

The solution was analyzed from both asymptotic and exact perspectives. The explicit asymptotic hyperbolic-elliptic model was employed to elucidate the contribution from Rayleigh waves (represented by the residues arising from the Rayleigh poles). Additionallz, the local dominant contributions from the branch points were utilized to capture the bulk wave contribution within the asymptotic model. The resulting displacement potential was then compared with the exact solution. The exact solution was obtained by Laplace transforming the equations of motion, followed by a Taylor series expansion centered at the Rayleigh pole to isolate the Rayleigh wave contribution. Similar to the asymptotic approach, the local dominant contributions from the branch-cut were used to account for the bulk-wave contributions in the exact solution.

Graphical analysis revealed that a significant discrepancy was observed between the asymptotically derived and exact solutions for the behavior of displacement potentials of total wavefield. This disparity suggests that the asymptotic hyperbolic-elliptic model is highly effective in capturing the behavior of Rayleigh waves but exhibits limitations in representing the behavior of bulk waves.

# 5.2 Surface boundary value problem in a multi-layered micropolar media\*

This chapter investigates the generation and propagation of Rayleigh waves due to surface seismic impacts, formulated as a boundary value problem. We model two surface pulse scenarios, a point load and a vertical line load, through boundary conditions within the frameowrk of micropolar elasticity. The analysis is further extended to multilayered micropolar structures to examine dispersion characteristics. Various mathematical tools, like method of displacement potentials, Hankel transformation and a matrix approach is employed to analyze the problem efficiently.

#### 5.2.1 Description of the model

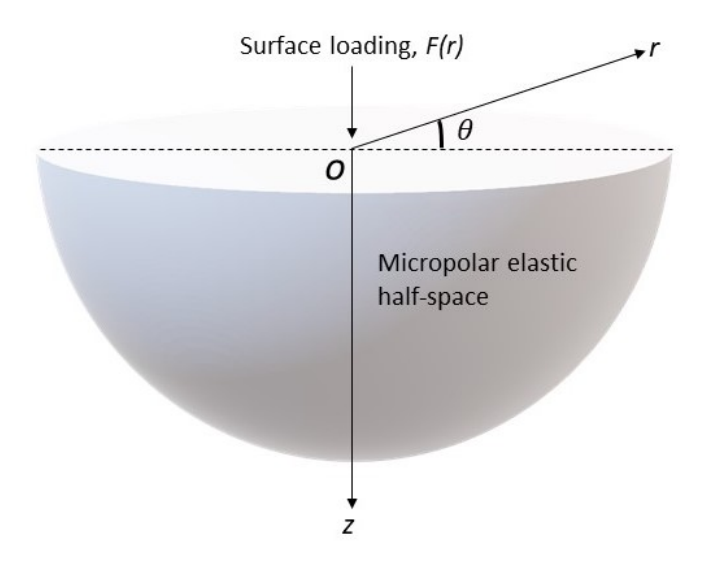


Figure 5.2.1: Geometry of the problem

Consider the propagation of Rayleigh waves in a homogeneous isotropic micropolar half-space occupying a region  $z \geq 0$  as depicted in Figure 5.2.1. A cylindrical co-ordinate system  $(r, \theta, z)$  is used to obtain the solution for the displacement components of Rayleigh waves produced by a source situated on the surface z = 0 of the micropolar half-space. To maintain the consistency with the usual notations, z-axis is now considered to be

DOI: 10.1061/IJGNAI.GMENG-8725

<sup>\*</sup> Published in International Journal of Geomechanics (ASCE), (2024).

pointing vertically downwards. Also, this problem of seismic surface pulse can also be viewed as the surface loading problem wherein the surface of the half-space is loaded by a concentrated time-harmonic force in the axial direction. Let  $(\hat{e}_r, \hat{e}_\theta, \hat{e}_z)$  be the basis vectors for the cylindrical system of co-ordinates. Also, let  $(u_r, u_\theta, u_z)$  and  $(\varphi_r, \varphi_\theta, \varphi_z)$  be the displacement components and microrotation vector components along  $(r, \theta, z)$  directions, respectively.

#### 5.2.2 Mathematical formulation and solution

#### Constitutive relations and balance laws

In any linear micropolar elastic continuum possessing a centre of symmetry, the deformation in the body is described by the displacement vector  $\vec{u}$  and the microrotation vector  $\vec{\varphi}$ . As a result, the force stresses (i.e.,  $\tau_{ij}$ ) and the couple (moment) stresses  $(m_{ij})$  are developed in the body. These stress tensors are defined in terms of the antisymmetric deformation (strain) tensor  $\epsilon_{ij}$  and torsional flexural (curvature) tensor  $\gamma_{ij}$  as,

$$\begin{cases}
\epsilon_{ij} = u_{j,i} - \varepsilon_{ijk}\varphi_k, \\
\gamma_{ij} = \varphi_{i,j}.
\end{cases}$$
(5.2.1)

Following Eringen [117] and Nowacki [122], the stresses in a homogeneous, isotropic, micropolar elastic half-space can be expressed linearly by using strain and curvature tensors as,

$$\tau_{ij} = \Lambda \epsilon_{kk} \delta_{ij} + (\mu + \kappa) \epsilon_{ij} + \mu \epsilon_{ij}, 
m_{ij} = \alpha \gamma_{kk} \delta_{ij} + \beta \gamma_{ij} + \nu \gamma_{ji},$$
(5.2.2)

where  $\Lambda$  and  $\mu$  are Lame's constants, and  $\kappa$ ,  $\alpha$ ,  $\beta$  and  $\nu$  are micropolar constants;  $\delta_{ij}$  is the Kronecker delta and  $\varepsilon_{ijk}$  is the permutation tensor. Throughout the paper, a comma in the subscript represents the partial derivative.

To describe any physical phenomenon associated with the dynamic problems of micropolar elasticity theory, it is essential to compute the displacement components and microrotation vector components satisfying the constitutive relations, equations of motion and boundary and initial conditions. Eringen [51] derived the equation of motion for the wave propagating in a micropolar elastic half-space and in absence of body forces, this equation

of motion can be written as,

$$(\Lambda + 2\mu + \kappa)\nabla(\nabla \cdot \vec{u}) - (\mu + \kappa)\nabla \times (\nabla \times \vec{u}) + \kappa\nabla \times \vec{\varphi} = \rho \frac{\partial^2 \ddot{\vec{u}}}{\partial t^2},$$

$$\nu\nabla^2 \vec{\varphi} + \kappa\nabla \times \vec{u} - 2\kappa \vec{\varphi} = j\rho \frac{\partial^2 \ddot{\vec{\varphi}}}{\partial t^2},$$

$$(5.2.3)$$

where  $\rho$  is the density, j is the micro-inertia co-efficient and  $\nabla$  is the usual del operator. The above form of the equation of motion has a larger advantage because this result is valid in any curvilinear coordinate system.

#### Formulation of the problem

Owing to the propagation of Rayleigh waves in this problem, the displacement component  $u_{\theta} = 0$  and the microrotation vector components  $\varphi_r = \varphi_z = 0$ . Thus, we write

$$u_r = u_r(r, z, t), \ u_\theta = 0, \ u_z = u_z(r, z, t),$$
  
$$\varphi_r = 0, \ \varphi_\theta = \varphi_\theta(r, z, t), \ \varphi_z = 0.$$

so that

$$\vec{u}(r,z,t) = u_r(r,z,t)\hat{e_r} + u_z(r,z,t)\hat{e_z}.$$
 (5.2.4)

The given problem assumes an antiplane strain state in the  $\theta$ -direction, which means that all field variables are independent of  $\theta$ -direction, i.e.,  $\frac{\partial}{\partial \theta} = 0$ .

#### Method of displacement potentials

The method of displacement potentials is one of the powerful technique in obtaining the solution to an axisymmetrical wave equation. Consider the Helmholtz resolution of the displacement vector field in cylindrical co-ordinates. According to the Helmholtz's theorem [2], a rapidly decaying displacement vector field  $\vec{u}$  can be resolved into sum of a scalar potential  $\phi$  and a vector potential  $\vec{H}$ , which provides

$$\vec{u} = \nabla \Phi + \nabla \times \vec{H},\tag{5.2.5}$$

where the components of displacement vector  $\vec{u}$  and vector potential  $\vec{H}$  are given by

$$\vec{u} = u_r(r, z, t)\hat{e_r} + u_z(r, z, t)\hat{e_z}, 
\vec{H} = H_{\theta}(r, z, t)\hat{e_{\theta}}.$$
(5.2.6)

Appropriate substitutions of  $\vec{u}$  given in Eq. (5.2.5) in equation of motion given in Eq. (5.2.4) gives

$$(\Lambda + 2\mu + \kappa)\nabla^{2}\Phi = \rho \frac{\partial^{2}\Phi}{\partial t^{2}},$$

$$(\mu + \kappa)\left(\nabla^{2} - \frac{1}{r^{2}}\right)H_{\theta} + \kappa\varphi_{\theta} = \rho \frac{\partial^{2}H_{\theta}}{\partial t^{2}},$$

$$\nu\left(\nabla^{2} - \frac{1}{r^{2}}\right)\varphi_{\theta} - \kappa\left(\nabla^{2} - \frac{1}{r^{2}}\right)H_{\theta} - 2\kappa\varphi_{\theta} = \rho j \frac{\partial^{2}\varphi_{\theta}}{\partial t^{2}}.$$

$$(5.2.7)$$

Here  $\nabla^2 = \frac{1}{r} \frac{\partial}{\partial r} \left( r \frac{\partial}{\partial r} \right) + \frac{\partial^2}{\partial z^2}$  denotes the Laplacian operator in cylindrical coordinates. In order to reduce further the second and third equations of Eq. (5.2.7) to scalar wave equation, define the function  $\Psi$  and  $\phi$  as,

$$H_{\theta} = -\frac{\partial \Psi}{\partial r},$$
$$\varphi_{\theta} = -\frac{\partial \phi}{\partial r}.$$

Then Eq. (5.2.7) can be re-written as,

$$(\Lambda + 2\mu + \kappa)\nabla^{2}\Phi = \rho \frac{\partial^{2}\Phi}{\partial t^{2}},$$

$$(\mu + \kappa)\nabla^{2}\Psi + \kappa\phi = \rho \frac{\partial^{2}\Psi}{\partial t^{2}},$$

$$\nu\nabla^{2}\phi - \kappa\nabla^{2}\Psi - 2\kappa\phi = \rho j \frac{\partial^{2}\phi}{\partial t^{2}}.$$

$$(5.2.8)$$

Assuming the time harmonic fields with the time factor  $e^{i\omega t}$ , where  $\omega = kc$  is the angular velocity of the Rayleigh wave propgating with wave velocity c and wave number k, the displacement potentials and the quantity  $\phi(r, z, t)$  may be expressed in the form,

$$\Phi(r, z, t) = \Phi(r, z)e^{i\omega t},$$

$$\Psi(r, z, t) = \Psi(r, z)e^{i\omega t},$$

$$\phi(r, z, t) = \phi(r, z)e^{i\omega t}.$$
(5.2.9)

Inserting Eqs. (5.2.9) in Eqs. (5.2.8), we get

$$\left(\nabla^{2} + \frac{k^{2} c^{2}}{c_{1}^{2} + c_{2}^{2}}\right) \Phi = 0,$$

$$\left(\nabla^{2} + \frac{k^{2} c^{2}}{c_{2}^{2} + c_{4}^{2}}\right) \Psi + \frac{c_{2}^{2}}{c_{2}^{2} + c_{4}^{2}} \phi = 0,$$

$$\left(\nabla^{2} + \frac{-2c_{2}^{2} + jk^{2} c^{2}}{jc_{3}^{2}}\right) \phi - \frac{c_{2}^{2}}{jc_{3}^{2}} \nabla^{2} \Psi = 0,$$
(5.2.10)

where the quantities  $c_1$ ,  $c_2$ ,  $c_3$  and  $c_4$  are defined as,

$$c_1 = \sqrt{\frac{\Lambda + 2\mu}{\rho}}, \ c_2 = \sqrt{\frac{\kappa}{\rho}}, \ c_3 = \sqrt{\frac{\nu}{j\rho}}, \ c_4 = \sqrt{\frac{\mu}{\rho}}$$

It is understood that the system of equations obtained in Eq. (5.2.10) involves a coupled differential equations of second order. To further uncouple these equations, we begin with defining the parameters,

$$r_1^2 = \frac{k^2 \, c^2}{c_1^2 + c_2^2}, \ p_1^2 = \frac{k^2 \, c^2}{c_2^2 + c_4^2}, \ p_2^2 = \frac{-2c_2^2 + jk^2 \, c^2}{jc_3^2}, \ p_3^2 = \frac{c_2^4}{j \, c_3^2 \, (c_2^2 + c_4^2)},$$

and by regrouping the terms, Eqs. (5.2.10) can be reduced to

$$(\nabla^2 + r_1^2) \Phi = 0, (5.2.11)$$

$$\nabla^4 \Psi + \left( p_1^2 + p_2^2 + p_3^2 \right) \nabla^2 \Psi + p_1^2 p_2^2 \Psi = 0. \tag{5.2.12}$$

The Eq. (5.2.12) can be further simplified to give

$$(\nabla^2 + r_2^2) (\nabla^2 + r_3^2) \Psi = 0,$$

where  $r_2$  and  $r_3$  are the roots having values,

$$r_{2,3}^2 = \frac{-(p_1^2 + p_2^2 + p_3^2) \pm \sqrt{(p_1^2 + p_2^2 + p_3^2)^2 - 4p_1^2p_2^2}}{2}.$$
 (5.2.13)

To solve explicity the equations given in Eqs. (5.2.11) and (5.2.12), the Hankel transformation technique [274] is employed naturally in view of the geometry of the model. Define the zeroth order Hankel transformation of  $\Phi$  as

$$\bar{\Phi}(\xi,z) = \int_0^\infty r J_0(\xi r) \,\Phi(r,z) \,dr,$$

whose inverse transformation is

$$\Phi(r,z) = \int_0^\infty \xi J_0(\xi r) \,\bar{\Phi}(\xi,z) \,d\xi,$$

Here  $\xi$  is the transformed parameter. We note that the similar definitions are adopted for the quantities  $\bar{\Psi}$ .

Now, application of the zeroth order Hankel transformation to Eqs. (5.2.10) and (5.2.11) reduces the set of partial differential equations to a set of ordinary differential equations. Thus

$$\frac{d^2\bar{\Phi}}{dz^2} - (\xi^2 - r_1^2)\,\Phi = 0,$$

$$\frac{d^4\bar{\Psi}}{dz^4} - (2\xi^2 - r_2^2 - r_3^2)\,\frac{d^2\bar{\Psi}}{dz^2} + (\xi^2 - r_2^2)\,(\xi^2 - r_3^2)\,\bar{\Psi} = 0.$$
(5.2.14)

The solutions to these equations takes the form,

$$\bar{\Phi}(\xi, z) = A_1 e^{-\alpha z} + A_2 e^{\alpha z}, 
\bar{\Psi}(\xi, z) = B_1 e^{-\beta z} + B_2 e^{-\zeta z} + B_3 e^{\beta z} + B_4 e^{\zeta z},$$
(5.2.15)

where  $A_1$ ,  $A_2$ ,  $B_1$ ,  $B_2$ ,  $B_3$  and  $B_4$  are all functions of  $\xi$  and are determined from the boundary conditions applied on the problem. Here,

$$\alpha^2 = \xi^2 - r_1^2, \ \beta^2 = \xi^2 - r_2^2, \ \zeta^2 = \xi^2 - r_3^2.$$

Note that  $\Psi(r,z)$  and  $\phi(r,z)$  are the solutions to the coupled differential equations given in Eq. (5.2.10). As a result, assume the solution to  $\bar{\phi}(\xi,z)$  to be of the form,

$$\bar{\phi}(\xi, z) = s_1 B_1 e^{-\beta z} + s_2 B_2 e^{-\zeta z} + s_3 B_3 e^{\beta z} + s_4 B_4 e^{\zeta z}, \tag{5.2.16}$$

where  $s_1$ ,  $s_2$ ,  $s_3$  and  $s_4$  are the unknowns to be determined.

Substituting the explicit solutions of  $\bar{\Psi}(\xi,z)$  and  $\bar{\phi}(\xi,z)$  in Eq. (5.2.9), we get

$$s_1 = \frac{c_2^2 + c_4^2}{c_2^2} \left( r_2^2 - p_1^2 \right), \ s_2 = \frac{c_2^2 + c_4^2}{c_2^2} \left( r_3^2 - p_1^2 \right), \ s_3 = s_1 \text{ and } s_4 = s_2.$$
 (5.2.17)

In brief, the transformed displacement vector potentials and microrotation vector takes the form,

$$\bar{\Phi}(\xi, z) = A_1 e^{-\alpha z} + A_2 e^{\alpha z},$$

$$\bar{\Psi}(\xi, z) = B_1 e^{-\beta z} + B_2 e^{-\zeta z} + B_3 e^{\beta z} + B_4 e^{\zeta z},$$

$$\bar{\phi}(\xi, z) = s_1 B_1 e^{-\beta z} + s_2 B_2 e^{-\zeta z} + s_3 B_3 e^{\beta z} + s_4 B_4 e^{\zeta z},$$
(5.2.18)

where the value of  $s_1$ ,  $s_2$ ,  $s_3$  and  $s_4$  are given in Eq. (5.2.17).

#### 5.2.3 Analytical solution for the elastic micropolar half-space

In order for the solution to be compatible with the half-space considered, the solution to Eq. (5.2.18) must be bounded as z approaches infinity. Due to this radiation condition, we must have  $A_2 = 0$  and  $B_3 = B_4 = 0$  in Eq. (5.2.18). Thus,

$$\bar{\Phi}(\xi, z) = A_1 e^{-\alpha z}, 
\bar{\Psi}(\xi, z) = B_1 e^{-\beta z} + B_2 e^{-\zeta z}, 
\bar{\phi}(\xi, z) = s_1 B_1 e^{-\beta z} + s_2 B_2 e^{-\zeta z}.$$
(5.2.19)

#### Boundary conditions

To determine the unknown parameters  $A_1$ ,  $B_1$  and  $B_2$  in Eq. (5.2.19), suitable boundary conditions are imposed on the above equations.

• The force stress component in the axial direction on the free surface assumes the value,

$$\tau_{zz} = F(r)e^{i\omega t} \text{ at } z = 0, \tag{5.2.20}$$

where F(r) is taken to be an arbitrary function. We note that as a result of surface seismic pulsations, a time-harmonic force function  $F(r)e^{i\omega t}$  is assumed in the axial direction.

• The mechanically stress free condition on the free surface in radial direction for the half-plane indicates,

$$\tau_{zr} = 0$$
, at  $z = 0$ . (5.2.21)

• Also, the couple stress in  $\theta$ -direction is unaffected due to the surface loading. This implies,

$$m_{z\theta} = 0 \text{ at } z = 0.$$
 (5.2.22)

By using the stress-strain relation given in Eq. (5.2.2), the force stress component  $\tau_{zr}$  and  $\tau_{zz}$  can be expressed as,

$$\tau_{zz} = (\Lambda + 2\mu + \kappa) \frac{\partial u_z}{\partial z} + \Lambda \left( \frac{\partial u_r}{\partial r} + \frac{u_r}{r} \right), 
\tau_{zr} = (\mu + \kappa) \frac{\partial u_r}{\partial z} + \mu \frac{\partial u_z}{\partial r} - \kappa \varphi_{\theta}.$$
(5.2.23)

On further substituting the introduced Helmholtz representation of displacement vector using scalar and vector potential given in Eq. (5.2.5), we get

$$\tau_{zz} = \Lambda \nabla^2 \Phi + (2\mu + \kappa) \frac{\partial}{\partial z} \left( \frac{\partial \Phi}{\partial z} + \frac{\partial^2 \Psi}{\partial z^2} + \frac{c_2^2}{c_2^2 + c_4^2} \phi + p_1^2 \Psi \right),$$

$$\tau_{zr} = \frac{\partial}{\partial r} \left[ (2\mu + \kappa) \left( \frac{\partial \Phi}{\partial z} + \frac{\partial^2 \Psi}{\partial z^2} \right) + \left( \frac{\mu c_2^2}{c_2^2 + c_4^2} + \kappa \right) \phi + \mu p_1^2 \Psi \right].$$
(5.2.24)

The above representation of the force stress components is a consequence of using the Eq. (5.2.9) and appropriate identitities related to the del ( $\nabla$ ) operator in cylindrical coordinates.

Now, we may apply the Hankel transformation on these stress components according to

$$\bar{\tau}_{zz} = \int_0^\infty r \, \tau_{zz} J_0(\xi r) \, dr,$$

$$\bar{\tau}_{zr} = \int_0^\infty r \, \tau_{zr} J_1(\xi r) \, dr,$$

which gives

$$\bar{\tau}_{zz} = -\Lambda r_1^2 \bar{\Phi} + (2\mu + \kappa) \frac{d}{dz} \left( \frac{d\Phi}{dz} + \frac{d^2 \Psi}{dz^2} + \frac{c_2^2}{c_2^2 + c_4^2} \bar{\phi} + p_1^2 \bar{\Psi} \right),$$

$$\bar{\tau}_{zr} = -\xi \left[ (2\mu + \kappa) \left( \frac{d\bar{\Phi}}{dz} + \frac{d^2 \bar{\Psi}}{dz^2} \right) + \left( \frac{\mu c_2^2}{c_2^2 + c_4^2} + \kappa \right) \bar{\phi} + \mu p_1^2 \bar{\Psi} \right].$$

Under these circumstances, the boundary conditions in Eqs. (5.2.20) and (5.2.21) reduces to

$$-\Lambda r_1^2 \bar{\Phi} + (2\mu + \kappa) \frac{d}{dz} \left( \frac{d\bar{\Phi}}{dz} + \frac{d^2 \bar{\Psi}}{dz^2} + \frac{c_2^2}{c_2^2 + c_4^2} \bar{\phi} + p_1^2 \bar{\Psi} \right) = \bar{F}(\xi) \text{ at } z = 0, \\ -\xi \left[ (2\mu + \kappa) \left( \frac{d\bar{\Phi}}{dz} + \frac{d^2 \bar{\Psi}}{dz^2} \right) + \left( \frac{\mu c_2^2}{c_2^2 + c_4^2} + \kappa \right) \bar{\phi} + \mu p_1^2 \bar{\Psi} \right] = 0 \text{ at } z = 0, \end{cases}$$
 (5.2.25)

where  $\bar{F}(\xi)$  is the zeroth order Hankel tranformation of the force function F(r), i.e.,

$$\bar{F}(\xi) = \int_0^\infty r \, J_0(\xi r) \, dr.$$

Now, substitution of Eq. (5.2.19) in the transformed boundary conditions given in Eq. (5.2.25) gives

$$\left[-\Lambda r_{1}^{2}+\left(2\mu+\kappa\right)\alpha^{2}\right]A_{1}-\beta\left(2\mu+\kappa\right)\left(\beta^{2}+p_{1}^{2}+\frac{c_{2}^{2}\,s_{1}}{c_{2}^{2}+c_{4}^{2}}\right)B_{1}-\zeta\left(2\mu+\kappa\right)\left(\zeta^{2}+p_{1}^{2}+\frac{c_{2}^{2}\,s_{2}}{c_{2}^{2}+c_{4}^{2}}\right)B_{2}=\bar{F}(\xi),\;(5.2.26)$$

$$\alpha\,\xi\left(2\mu+K\right)A_{1}-\xi\left[\left(2\mu+\kappa\right)\beta^{2}+\left(\frac{\mu\,c_{2}^{2}}{c_{2}^{2}+c_{4}^{2}}+\kappa\right)s_{1}+\mu\,p_{1}^{2}\right]B_{1}-\xi\left[\left(2\mu+\kappa\right)\zeta^{2}+\left(\frac{\mu\,c_{2}^{2}}{c_{2}^{2}+c_{4}^{2}}+\kappa\right)s_{2}+\mu\,p_{1}^{2}\right]B_{2}=0.\;(5.2.27)$$

The third boundary condition in Eq. (5.2.22) is transformed according to

$$\bar{m}_{z\theta} = \int_0^\infty r \, m_{z\theta} J_1(\xi r) \, dr,$$

where

$$m_{z\theta} = -\nu \, \frac{\partial^2 \phi}{\partial r \, \partial z}.$$

Then the transformed couple stress component  $\bar{m}_{z\theta}$  takes the form

$$\bar{m}_{z\theta} = \nu \, \xi \, \frac{d\bar{\phi}}{dz}.$$

Therefore, the resulting third boundary condition may be written immediately as

$$\beta \, s_1 \, B_1 + \zeta \, s_2 \, B_2 = 0. \tag{5.2.28}$$

Defining  $\eta = \frac{2\mu + \kappa}{\mu + \kappa}$ , the boundary conditions in Eqs. (5.2.26), (5.2.27) and (5.2.28) may be re-written using the matrix notations as,

$$\begin{bmatrix} b_{11} & b_{12} & b_{13} \\ b_{21} & b_{22} & b_{23} \\ 0 & b_{32} & b_{33} \end{bmatrix} \begin{bmatrix} A_1 \\ B_1 \\ B_2 \end{bmatrix} = \begin{bmatrix} \frac{\bar{F}(\xi)}{\mu + \kappa} \\ 0 \\ 0 \end{bmatrix}$$
 (5.2.29)

where,  $b_{11} = \eta \xi^2 - p_1^2$ ,  $b_{12} = -\eta \beta \xi^2$ ,  $b_{13} = -\eta \zeta \xi^2$ ,  $b_{21} = -\eta \alpha$ ,  $b_{22} = \eta \xi^2 - p_1^2$ ,  $b_{23} = \eta \xi^2 - p_1^2$ ,  $b_{32} = \beta s_1$ ,  $b_{33} = \zeta s_2$ .

The system of equations obtained above in Eq. (5.2.29) is solved to determine the unknown quantities,  $A_1$ ,  $B_1$  and  $B_2$ . Unique solutions to these unknown quantities are obtained for the non-zero determinant of the co-efficient matrix.

Let  $\Theta$  be the determinant of the co-efficient matrix, i.e.,

$$\Theta = \begin{vmatrix} \eta \, \xi^2 - p_1^2 & -\eta \beta \, \xi^2 & -\eta \zeta \, \xi^2 \\ -\eta \alpha & \eta \, \xi^2 - p_1^2 & \eta \, \xi^2 - p_1^2 \\ 0 & \beta \, s_1 & \zeta \, s_2 \end{vmatrix}$$
$$= (\eta \xi^2 - p_1^2)^2 (\zeta s_2 - \beta s_1) - \eta^2 \, \alpha \, \beta \, \zeta \, \xi^2 (s_2 - s_1). \tag{5.2.30}$$

Tranforming the parameter  $\xi$  as the wave number k in Eq. (5.2.30), we get the dispersion relation for Rayleigh waves propagating in a micropolar media as,

$$(\eta k^2 - p_1^2)^2 (\zeta s_2 - \beta s_1) - \eta^2 \alpha \beta \zeta k^2 (s_2 - s_1) = 0.$$
 (5.2.31)

Then by Cramers rule,

$$A_{1} = \frac{\bar{F}(\xi)}{\mu + \kappa} \frac{\left(\eta \xi^{2} - p_{1}^{2}\right)(\zeta s_{2} - \beta s_{1})}{\Theta},$$

$$B_{1} = \frac{\bar{F}(\xi)}{\mu + \kappa} \frac{\eta \alpha \zeta s_{2}}{\Theta},$$

$$B_{2} = -\frac{\bar{F}(\xi)}{\mu + \kappa} \frac{\eta \alpha \beta s_{1}}{\Theta}.$$

$$(5.2.32)$$

The transformed displacement components of Rayleigh waves are determined by applying the Hankel transformation according to,

$$\bar{u}_r(\xi, z) = \int_0^\infty r \, u_r(r, z) \, J_1(\xi r) \, dr,$$

$$\bar{u}_z(\xi, z) = \int_0^\infty r \, u_z(r, z) \, J_0(\xi r) \, dr,$$

which gives

$$\begin{split} \bar{u}_r(\xi,z) &= -\xi \left( \bar{\Phi} + \frac{d\bar{\Psi}}{dz} \right), \\ \bar{u}_z(\xi,z) &= \frac{d\bar{\Phi}}{dz} + \frac{d^2\bar{\Psi}}{dz^2} + \frac{c_2^2 \bar{\phi}}{c_2^2 + c_1^2} + p_1^2 \bar{\Psi}. \end{split}$$

Using the expressions for the potentials in the elastic half-space, the displacement components are obtained for two different cases (depending on the load on the free surface) by taking the inverse of transformed displacement components.

#### Case 1:

When F(r) is a point load, i.e., we write,  $F(r) = \frac{\delta(r)}{2\pi r} Z$ , where Z is the magnitude of the applied force, then we have,  $\bar{F}(\xi) = \frac{Z}{2\pi}$ . Substituting this value of  $\bar{F}(\xi)$  in Eqs. (5.2.32), the displacement components are expressed as,

$$u_{r}(r,z) = \frac{-Z}{2\pi (\mu + \kappa)} \int_{0}^{\infty} \frac{X \xi^{2} J_{1}(\xi r)}{\Theta} d\xi, \qquad (5.2.33)$$
where,  $X = (\eta \xi^{2} - p_{1}^{2}) (\zeta s_{2} - \beta s_{1}) e^{-\alpha z} - \eta \alpha \beta \zeta (s_{2} e^{-\beta z} + s_{1} e^{-\zeta z}),$ 

$$u_{z}(r,z) = \frac{Z}{2\pi (\mu + \kappa)} \int_{0}^{\infty} \frac{Y \xi J_{0}(\xi r)}{\Theta} d\xi \qquad (5.2.34)$$
where,  $Y = -\alpha (\eta \xi^{2} - p_{1}^{2}) (\zeta s_{2} - \beta s_{1}) e^{-\alpha z} + \eta \alpha \xi^{2} (\zeta s_{2} e^{-\beta z} + \beta s_{1} e^{-\zeta z}).$ 

#### Case 2:

When a uniformly distributed vertical load, F(r) is applied along z-direction, i.e.,

$$F(r) = \begin{cases} \frac{Z}{2\pi a^2}, & \text{when } 0 < r < a \\ 0, & \text{when } r \ge a \end{cases},$$

where Z is the magnitude of the load applied and a is the radius of the circular region on which the uniform distribution of the load takes place, then  $\bar{F}(\xi, z) = \frac{Z J_1(\xi a)}{2\pi a \xi}$ . This gives the expressions for displacement components as,

$$u_r(r,z) = \frac{-Z}{2\pi a (\mu + \kappa)} \int_0^\infty \frac{X\xi J_1(\xi a) J_1(\xi r)}{\Theta} d\xi,$$
 (5.2.35)

$$u_z(r,z) = \frac{Z}{2\pi a (\mu + \kappa)} \int_0^\infty \frac{Y J_1(\xi a) J_0(\xi r)}{\Theta} d\xi,$$
 (5.2.36)

where X and Y have same values as that given in case 1.

#### 5.2.4 Analytical solution to a multi-layered elastic micropolar layers

Utilizing the expressions for potentials given in Eqs. (5.2.18), the force stress and couple stress can be given by,

$$\begin{split} &\bar{u}_r(\xi,z) = -\xi \left( A_1 e^{-\alpha z} + A_2 e^{\alpha z} - \beta B_1 e^{-\beta z} - B_2 e^{-\zeta z} + \beta B_3 e^{\beta z} + B_4 e^{\zeta z} \right), \\ &\bar{u}_z(\xi,z) = -\alpha A_1 e^{-\alpha z} + \alpha A_2 e^{\alpha z} + \xi^2 \left( B_1 e^{-\beta z} + B_2 e^{-\zeta z} + B_3 e^{\beta z} + B_4 e^{\zeta z} \right), \\ &\bar{\varphi}_{\theta}(\xi,z) = \xi \left( s_1 B_1 e^{-\beta z} + s_2 B_2 e^{-\zeta z} + s_1 B_3 e^{\beta z} + s_2 B_4 e^{\zeta z} \right), \\ &\bar{\tau}_{zz}(\xi,z) = (\mu + \kappa) \left( b_{11} (A_1 e^{-\alpha z} + A_2 e^{\alpha z}) + b_{12} (B_1 e^{-\beta z} - B_2 e^{\beta z}) + b_{13} (B_3 e^{-\zeta z} - B_4 e^{\zeta z}) \right), \\ &\bar{\tau}_{zr}(\xi,z) = (\mu + \kappa) \left( b_{21} A_1 (e^{-\alpha z} - A_2 e^{\alpha z}) + b_{22} (B_1 e^{-\beta z} + B_2 e^{\beta z} + B_3 e^{-\zeta z} + B_4 e^{\zeta z}) \right), \\ &\bar{m}_{z\theta}(\xi,z) = \nu \xi \left( b_{32} (B_1 e^{-\beta z} - B_2 e^{-\beta z}) + b_{33} (B_3 e^{-\zeta z} - B_4 e^{-\zeta z}) \right). \end{split}$$

Define the generalised displacement vector and stress vector as,

$$\bar{\boldsymbol{U}}(\xi,z) = \begin{bmatrix} \bar{u}_r(\xi,z) & \bar{u}_z(\xi,z) & \bar{\varphi}_{\theta}(\xi,z) \end{bmatrix} \text{ and } \bar{\boldsymbol{T}}(\xi,z) = \begin{bmatrix} \frac{\bar{\tau}_{zz}(\xi,z)}{\mu+\kappa} & \frac{\bar{\tau}_{zr}(\xi,z)}{\mu+\kappa} & \frac{\bar{m}_{z\theta}(\xi,z)}{\nu} \end{bmatrix}$$

. Then the matrix equations can be written as,

$$\begin{bmatrix} \bar{\boldsymbol{U}}(\xi,0) \\ \bar{\boldsymbol{U}}(\xi,z) \end{bmatrix} = \boldsymbol{P} \cdot \begin{bmatrix} A_1 & A_2 & B_1 & B_2 & B_3 & B_4 \end{bmatrix}^T$$
 (5.2.37)

$$\begin{bmatrix} -\bar{\boldsymbol{T}}(\xi,0) \\ \bar{\boldsymbol{T}}(\xi,z) \end{bmatrix} = \boldsymbol{Q} \cdot \begin{bmatrix} A_1 & A_2 & B_1 & B_2 & B_3 & B_4 \end{bmatrix}^T$$
 (5.2.38)

where  $\mathbf{P} = [p_{ij}]$  and  $\mathbf{Q} = [q_{ij}]$  are  $6 \times 6$  matrix whose elements are provided in Appendix D. Thus, the expression relating the displacement vectors and stress vectors for a single layer element can be given of the form,

$$\begin{bmatrix} -\bar{\boldsymbol{T}}(\xi,0) \\ \bar{\boldsymbol{T}}(\xi,z) \end{bmatrix} = (\boldsymbol{Q}\boldsymbol{P}^{-1}) \begin{bmatrix} \bar{\boldsymbol{U}}(\xi,0) \\ \bar{\boldsymbol{U}}(\xi,z) \end{bmatrix} = \boldsymbol{M} \begin{bmatrix} \bar{\boldsymbol{U}}(\xi,0) \\ \bar{\boldsymbol{U}}(\xi,z) \end{bmatrix}$$
(5.2.39)

Let us consider N isotropic micropolar elastic layers situated one above the other. Let these layers be numbered in such a way that the layer at the top is given the number 1 and the layer at the bottom is numbered as N. Also, the  $i^{th}$  layer is bounded by the  $i^{th}$ interface at the bottom and  $(i-1)^{th}$  interface at the top. Let  $d_i$  defines the thickness of each layer and  $d_i = h_i - h_{i-1}$ , where  $h_i$  and  $h_{i-1}$  denotes the distance from the surface to the bottom and the top of the  $i^{th}$  layer, respectively. Let  $z = z_i$  be the position of the interface between  $(i+1)^{th}$  and  $i^{th}$  layer. Also,  $z = z_0$  and  $z = z_N$  represents the free surface and the bottom of the  $N^{th}$  layer respectively. Based on the calculations made for the single layer element, the expression relating the displacement vector and stress vectors for multi-layers can be extended by considering the interfacial continuity conditions on displacements and stresses. Thus, for any layer

$$\begin{bmatrix} -\bar{\boldsymbol{T}}(\xi, z_{i-1}) \\ \bar{\boldsymbol{T}}(\xi, z_{i}) \end{bmatrix} = \begin{bmatrix} \boldsymbol{M}_{1}^{(i)} & \boldsymbol{M}_{2}^{(i)} \\ \boldsymbol{M}_{3}^{(i)} & \boldsymbol{M}_{4}^{(i)} \end{bmatrix} \begin{bmatrix} \bar{\boldsymbol{U}}(\xi, z_{i-1}) \\ \bar{\boldsymbol{U}}(\xi, z_{i}) \end{bmatrix} = \boldsymbol{M}^{(i)} \begin{bmatrix} \bar{\boldsymbol{U}}(\xi, z_{i-1}) \\ \bar{\boldsymbol{U}}(\xi, z_{i}) \end{bmatrix}$$
(5.2.40)

The stress and displacement continuity conditions at the interface of the closely contacted layers without any external force are mathematically expressed as,

$$\bar{T}(\xi, z_i) = \bar{T}(\xi, z_{i+1}),$$
 (5.2.41)

$$\bar{U}(\xi, z_i) = \bar{U}(\xi, z_{i+1}).$$
 (5.2.42)

Using Eqs. (5.2.41) and (5.2.42), the stiffness matrix associated with N-layered micropolar system is,

where  $-\bar{\boldsymbol{T}}(\xi,0)$  represents the surface loading at the free surface and  $\boldsymbol{M}_{j}^{(i)}$ , for i=1,2,...,N and j=1,2,3,4 denotes the block matrix of size  $3\times 3$ . Assuming the external surface loading at the free surface and the fixed bottom of the  $N^{th}$  layer, the additional boundary conditions to the above multi-layered problem are,

$$\frac{\bar{\tau}_{zz}(\xi,0)}{\mu+\kappa} = \bar{F}(\xi), \ \frac{\bar{\tau}_{zr}(\xi,0)}{\mu+\kappa} = 0, \ \frac{\bar{m}_{z\theta}(\xi,0)}{\nu} = 0, 
\bar{u}_r(\xi,z_N) = 0, \ \bar{u}_z(\xi,z_N) = 0, \ \bar{\varphi}_{\theta}(\xi,z_N) = 0.$$

#### Case 1:

When a point load,  $F(r) = \frac{\delta(r)}{2\pi r} Z$  is applied on the free surface, where Z is the magnitude of the applied force, then

$$\bar{\boldsymbol{T}}(\xi,0) = \begin{bmatrix} \frac{Z}{2\pi} & 0 & 0 \end{bmatrix}. \tag{5.2.44}$$

The real solutions for  $\left[\bar{\boldsymbol{U}}(\xi,0)\ \bar{\boldsymbol{U}}(\xi,z_1)\ \bar{\boldsymbol{U}}(\xi,z_2)\ \dots\ \bar{\boldsymbol{U}}(\xi,z_{N-1})\ \bar{\boldsymbol{U}}(\xi,z_N)\right]$  are obtained using Eq. (5.2.44) and by taking the inverse Hankel transformation of the unknown variables given in Eq. (5.2.43).

#### Case 2:

If a vertical load,  $F(r) = \begin{cases} \frac{Z}{2\pi a^2}, & \text{when } 0 < r < a \\ 0, & \text{when } r \geq a \end{cases}$ , is uniformly distributed on the free surface, where Z is the magnitude of the applied force, then

$$\bar{\boldsymbol{T}}(\xi,0) = \begin{bmatrix} \frac{Z}{2\pi} \frac{J_1(\xi a)}{a\,\xi} & 0 & 0 \end{bmatrix}. \tag{5.2.45}$$

The real solutions for  $\left[\bar{\boldsymbol{U}}(\xi,0) \ \bar{\boldsymbol{U}}(\xi,z_1) \ \bar{\boldsymbol{U}}(\xi,z_2) \ \dots \ \bar{\boldsymbol{U}}(\xi,z_{N-1}) \ \bar{\boldsymbol{U}}(\xi,z_N)\right]$  are obtained similarly by taking the inverse Hankel transformation of the unknown variables.

#### 5.2.5 Validation of the model

#### Case 1:

A set of approximate roots can be obtained for  $r_2$  and  $r_3$  in Eq. (5.2.13) by assuming the quantity  $\frac{c_2^4}{c_4^4} \to 0$ . This gives the approximation,  $r_2 = p_1$  and  $r_3 = p_2$ . As a result, the elastic counterpart of the dispersion equation given in Eq. (5.2.31) reduces to,

$$\left(\eta - \frac{c^2}{c_2^2 + c_4^2}\right)^2 = \eta^2 \sqrt{1 - \frac{c^2}{c_1^2 + c_2^2}} \sqrt{1 - \frac{c^2}{c_2^2 + c_4^2}}.$$
 (5.2.46)

On further simplification, the dispersion relation in Eq. (5.2.46) reduces to,

$$\left(2 + \frac{c_2^2 - c^2}{c_4^2}\right)^2 = \left(2 + \frac{c_2^2}{c_4^2}\right)^2 \sqrt{1 - \frac{c^2}{c_1^2 + c_2^2}} \sqrt{1 - \frac{c^2}{c_2^2 + c_4^2}}.$$
(5.2.47)

This Eq. (5.2.47) coincides with the particular results obtained from Mondal and Acharya [278] where the different notations are being used.

#### Case 2:

In the absence of the micropolarity,  $\kappa = j = 0$ , the dispersion relation in Eq. (5.2.31) for Rayleigh waves propagating in elastic media becomes,

$$\left(2 - \frac{c^2}{c_4^2}\right)^2 = 4\sqrt{1 - \frac{c^2}{c_1^2}}\sqrt{1 - \frac{c^2}{c_4^2}}.$$
(5.2.48)

This is the exact secular equation for Rayleigh waves as derived by Rayleigh [14] in 1885. These two different cases provides the validity of the proposed model.

#### 5.2.6 Graphical discussions

The integrals obtained in Eqs. (5.2.30)-(5.2.33) are complicated to solve analytically because of the presence of exponential, radical and Bessel functions. As a result, we try to plot the graphs describing the relation between the displacement components with the r- and z-direction numerically using MATLAB. It can be observed that due to the presence of Bessel functions, the convergence rate of the oscillatory integral is very slow. The following values of physical constants are considered for the plotting purposes: The

Table 5.2.1: Values of parameters used in the study

Parameters	Values		
Λ	$7.59 \times 10^{11} \text{ dyne/cm}^2$		
$\mu$	$1.89\times10^{11}~\mathrm{dyne/cm}^2$		
$\rho$	$2.19~\mathrm{gm/cm}^3$		
$\kappa$	$0.0149 \times 10^{11} \text{ dyne/cm}^2$		
ν	$0.268 \times 10^{11} \text{ dyne}$		
j	$0.0196 \text{ cm}^2$		
$\frac{\rho c^2}{\Lambda + 2\mu}$	0.4		
$\frac{Z}{\mu + \kappa}$	2		
$\begin{bmatrix} -1 & -1 & -1 & -1 & -1 & -1 & -1 & -1 $	0.2		
ka	0.9		

integrand in the Eqs. (5.2.30)-(5.2.33) has poles and branch points as its singularity. In the absence of micropolarity, these singular points include a point that is related to Rayleigh wave number. Because of the presence of micropolarity in the medium, the roots of the denominator are all in conjugate pairs, i.e., the poles and the branch points have a non-zero imaginary part. Since, the inverse Hankel transformation involves only the real axis (i.e.,  $\xi \in [0, \infty)$ ) as the path of integration, the numerical integration is carried out easily using MATLAB along the real path.

Figure 5.2.2 depicts the normalized displacement of Rayleigh wave fields at the surface (z=0) along the r-direction produced due to the delta variation in surface loading (case 1). As observed from the figure, the amplitudes of propagating Rayleigh waves decreases with the increase in r, and finally reaches zero, thus coinciding with the well-known decay behaviour of Rayleigh waves. It is interesting to note a larger change in amplitude occurring near the surface at the origin. This is mainly because of the presence of a sudden (delta) impact at the surface that induces wave fields and thus causing a great deal of change in the amplitude behavior of Rayleigh waves. Also, due to the presence of delta function in r- direction, the displacement component  $(u_r)$  undergoes a larger change in amplitude while compared to that of displacement component  $(u_z)$ .

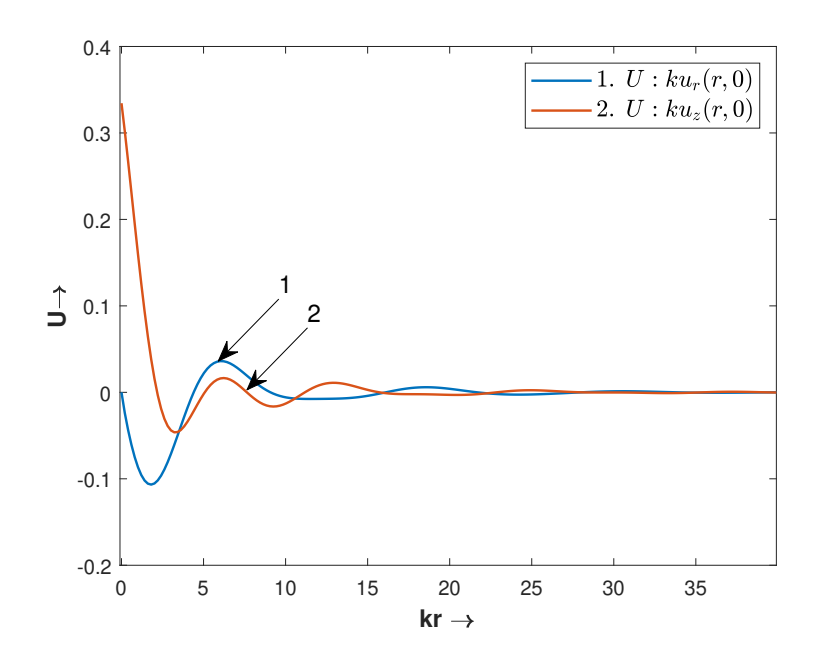


Figure 5.2.2: Variation of normalised displacement components (U) of Rayleigh wave fields produced due to case 1 with r-direction for z = 0

Figure 5.2.3 shows the variation of displacement components  $(u_r \text{ and } u_z)$  with z-direction at r=0 for case 1. Since the displacement component  $u_r$  depends on the Bessel function of order 1,  $J_1(\xi r)$  and since  $J_1(0)=0$ , we obtain  $u_r(0,z)=0$ . This means that displacement component of Rayleigh waves produced during the sudden surface loading at r=0 vanishes along r-direction. However, a steep change in the amplitude is observed for the displacement along z-direction due to the impact of a seismic load applied in the form

of delta function,  $\delta(r)$ . These Rayleigh waves produced due to sudden seismic loading decays with the depth, thus verifying the nature of decay of Rayleigh waves with depth.

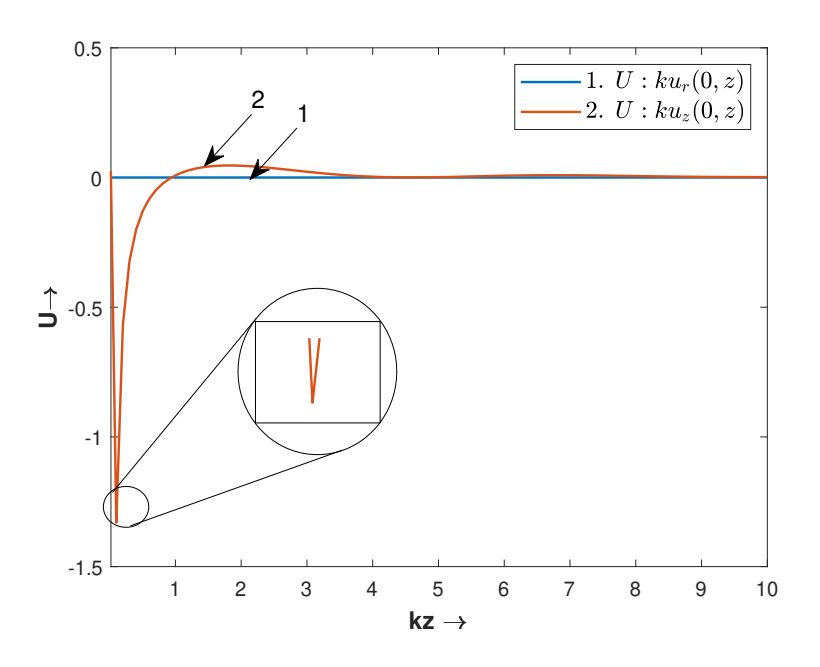


Figure 5.2.3: Variation of normalised displacement components (U) of Rayleigh wave fields produced due to case 1 with z-direction for r=0

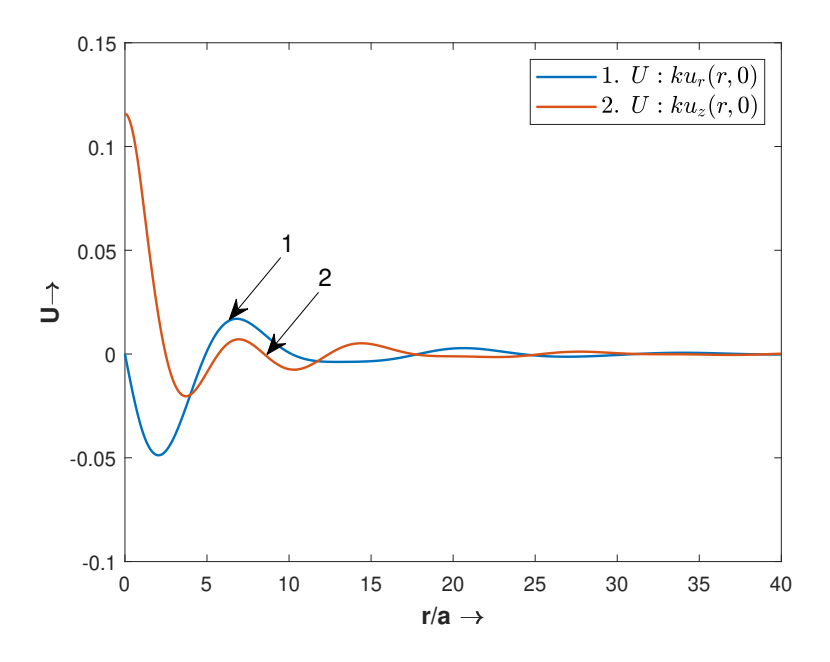


Figure 5.2.4: Variation of normalised displacement components (U) of Rayleigh wave fields produced due to case 2 with r-direction for z=0

Similarly, Figures 5.2.4 and 5.2.5 are plotted for the describing the nature of normalised displacement components along r-direction for z=0 and z-direction for r=0 respectively when a uniformly distributed vertical load is applied on the surface of the half-space along a circular region having radius a. The amplitudes decreases with the increase in the  $\frac{r}{a}$  and  $\frac{z}{a}$ , indicating the decay of Rayleigh waves in both z- and r- direction. The observation of a single larger amplitude sinusoidal-type curve in Figure 5.2.5 represents the effect of uniformly distributed load impact on the surface of the micropolar half-space.

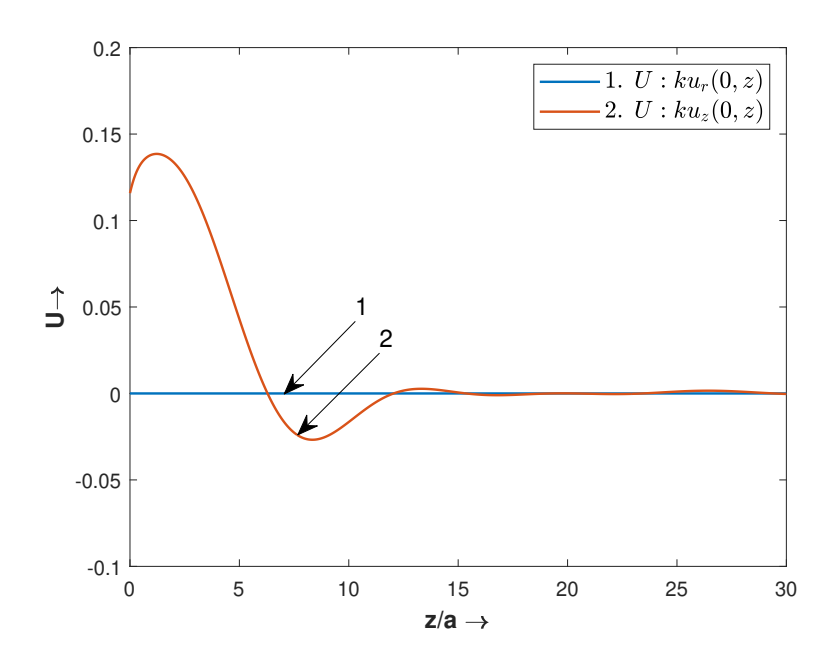


Figure 5.2.5: Variation of normalised displacement components (U) of Rayleigh wave fields produced due to case 2 with z-direction for r=0

Some surface plots have been plotted for case 1 in Figures 5.2.6 and 5.2.7 describing the motion of Rayleigh waves along r- and z- direction for  $u_r(r,z)$  and  $u_z(r,z)$  in an elastic micropolar half-space respectively. Simlar surface plots have been described for case 2 in Figures 5.2.8 and 5.2.9.

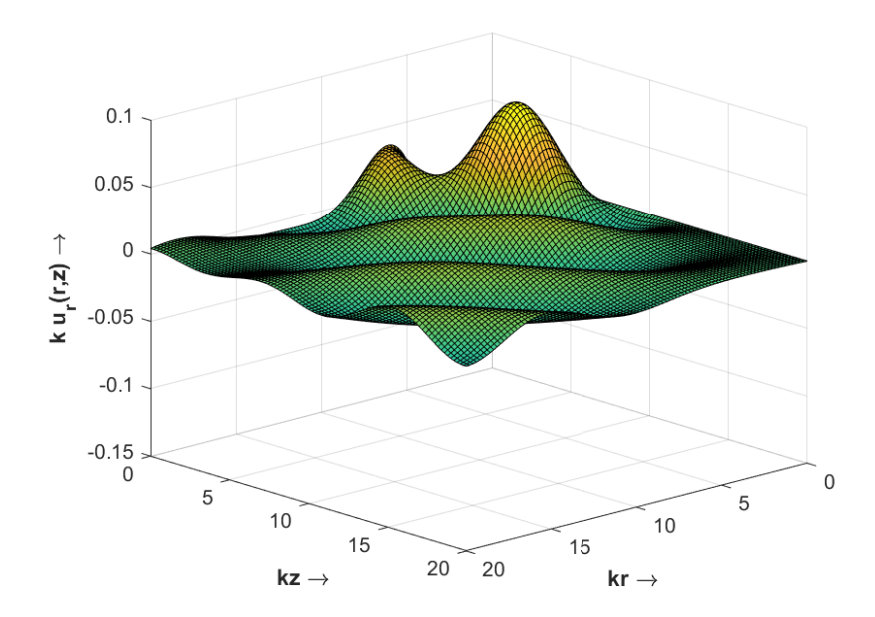


Figure 5.2.6: Surface plot showing the variation of normalized displacement components of Rayleigh wave fields with dimensionless r- and z-direction for case 1

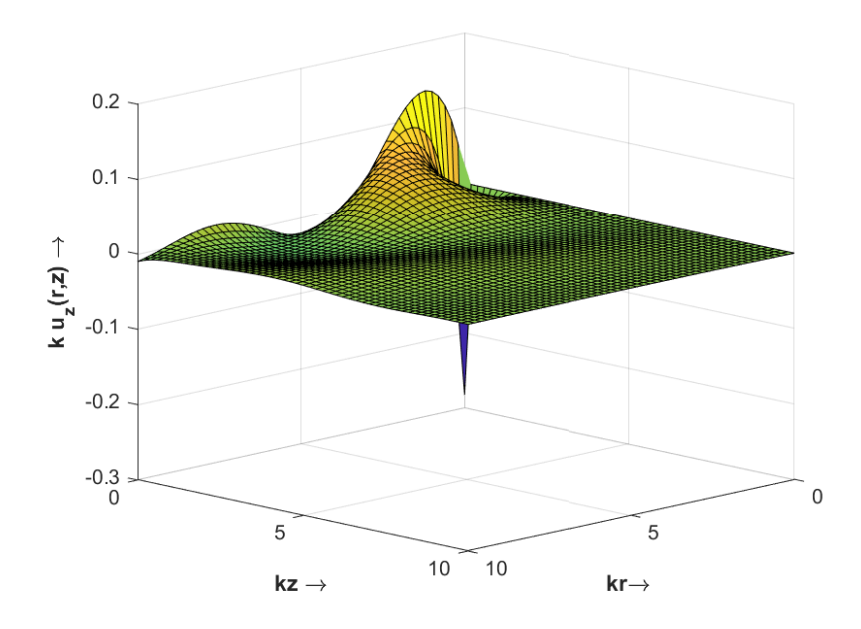


Figure 5.2.7: Surface plot showing the variation of normalized displacement components of Rayleigh wave fields with dimensionless r- and z-direction for case 1

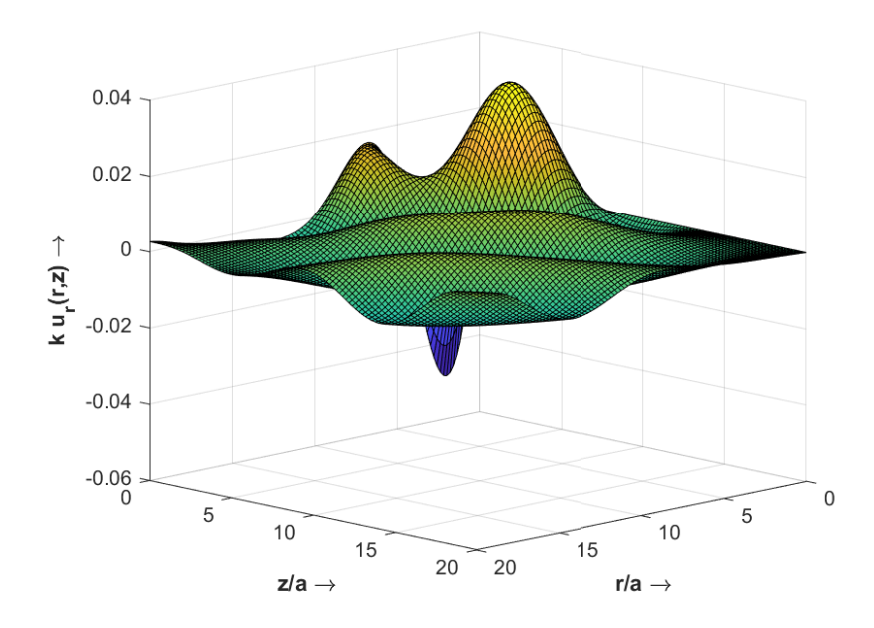


Figure 5.2.8: Surface plot showing the variation of normalized displacement components of Rayleigh wave fields with dimensionless r- and z-direction for case 2

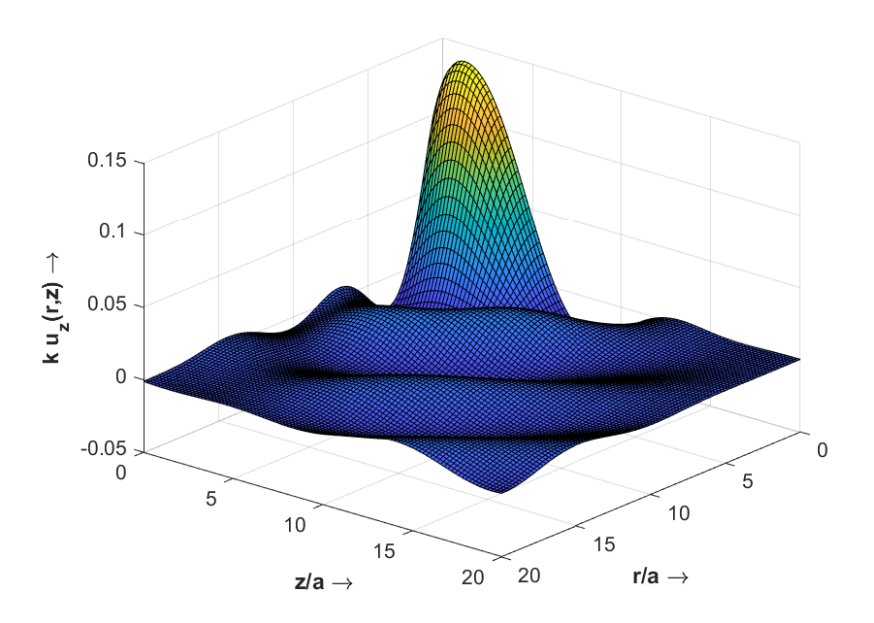


Figure 5.2.9: Surface plot showing the variation of normalized displacement components of Rayleigh wave fields with dimensionless r- and z-direction for case 2

#### 5.2.7 Conclusions

By employing the method of potentials, the coupled differential equations obtained as a consequence of the substitutions in equations of motions in a micropolar elastic media decouples, and as a result the wave equations becomes more simpler to solve. On further application of appropriate Hankel integral transformation techniques, the displacement solutions of Rayleigh wave fields produced in a micropolar elastic half-space due to the surface seismic loading in two different cases are studied. The first case involves the generation of Rayleigh wave fields due to a sudden impact and the other due to uniformly distributed vertical load occupying a circular region of radius r. The displacement solutions are obtained in the form of infinite integrals for both cases. These integrals are numerically evaluated for the singularities, and are computed using MATLAB to observe their variation along different directions. Based on the solution obtained for a single layer element, the methodology is extended to compute the displacement solutions to finite Nlayers. A global stiffness matrix is also derived, which helps in computing the real solutions to the displacement components of Rayleigh waves in a multi-layered micropolar media. The numerical calculations suggests a larger change in amplitudes at the begining, suggesting the origin of Rayleigh wave fields due to surface seismic loading. These amplitudes tends to decrease and finally reaches zero, thus verifying the well-known decay behaviour of Rayleigh wave fields.

## CHAPTER 6

Concluding Remarks and Future Directions

## 6.1 Summary and concluding remarks

This thesis significantly advanced the mathematical modeling of Rayleigh wave fields across three critical stages. Specifically, it focused on (a) incorporation of microstructural effects for refining boundary and/or interface conditions in traditional well-known nonlocal micropolar models, (b) incorporation of resonating structures, like spring-mass systems for controlling vibrations and frequency bandgap formation, and (c) modelling of external seismic pulse through initial and boundary conditions for generation of Rayleigh wave fields. These findings provide a strong framework for future studies and applications involving Rayleigh wave propagation and control.

The accurate representation of Rayleigh wave behavior in real materials demands the consideration of microstructures, as traditional models often overlook their significant impact on wave propagation. At micro- and nano-scales, the influence of long-range intermolecular forces and microstructures becomes increasingly important, requiring the consideration of nonlocal, micropolar, or nonlocal micropolar elasticity theories to adequately describe these small-scale interactions.

Asymptotic analysis of nonlocal boundary value problems highlights the critical role of near-surface behavior. Previous research has shown that boundary layer effects in a non-local semi-infinite medium can be incorporated by refining classical elasticity boundary conditions, yielding effective corrections. However, existing literature lacks a comparable analysis for nonlocal micropolar media, both in semi-infinite structure and in layered structures. This thesis addresses this gap by deriving nonlocal micropolar corrected dispersion relations, incorporating refinements in both boundary and interface conditions obtained through asymptotic analysis, thus extending the understanding of boundary layer effects in nonlocal micropolar systems.

By integrating resonant structures, specifically nonlinear spring-mass systems, onto a surface of the medium, the research in this thesis demonstrated the ability to manipulate Rayleigh waves, effectively creating metasurfaces. Novel designs are developed to control wave behavior and achieve mode conversion, with a detailed study of hardening and softening effects. Through the analysis of dual spring-mass metasurfaces, we identified cut-off frequencies and tunable frequency bandgaps, highlighting the critical role of non-linearity, input amplitude, and substrate characteristics. Notably, the multiple scattering

formulation proved essential for accurately capturing inter-resonator interactions, revealing that deeper source locations significantly enhance ground-borne vibration attenuation. Furthermore, the demonstrated tunability of metasurfaces through hardening nonlinearities and mass adjustments offers a powerful approach for optimizing vibration mitigation and mode conversion. These findings collectively establish a comprehensive framework for designing effective seismic metasurfaces, with potential applications in diverse fields requiring precise control of Rayleigh wave propagation. The optimization of frequency bandgaps and wave control achieved through the parametric tuning of these innovative metasurface designs are demonstrated in this thesis, which has proven to have potential applications in geophysics for seismic protection or vibration control.

This thesis introduced a novel approach to modeling Rayleigh wave generation through initial conditions or boundary conditions. A novel problem is tackled that involved transitioning from an initial value problem to a boundary value formulation, providing new insights into wave excitation mechanisms in elastic media. The study investigated wave field generation due to prescribed initial displacements and velocities, employing transformation techniques to derive solutions. While asymptotic methods effectively captured Rayleigh wave behavior, they exhibited limitations in representing bulk waves, as evidenced by discrepancies with exact solutions. Further, the research extended to micropolar elastic media, utilizing potential methods and Hankel transforms to analyze Rayleigh wave generation from surface seismic loading introduced through boundary conditions. The research demonstrated the effectiveness of the developed methodologies in capturing complex wave propagation dynamics.

In summary, this thesis has made significant contributions in advancing the theoretical understanding of Rayleigh wave propagation across diverse media, including nonlocal micropolar continuum and engineered metasurfaces. By effectively bridging classical and modern elasticity frameworks, this research addressed crucial gaps in boundary conditions and explored novel wave control strategies. These findings offer valuable insights into complex wave dynamics, with direct implications for seismic hazard mitigation and the development of advanced technologies, thus establishing a robust foundation for future explorations in wave propagation and control.

The following are the chapterwise conclusions of the thesis:

- Chapter 2.1: The equivalence between nonlocal integral and differential formulations for Rayleigh waves breaks down in a nonlocal micropolar semi-infinite medium, necessitating refined boundary conditions to account for boundary layer effects and reveal distinct Rayleigh wave modes, particularly highlighting the significance of micropolar effects in materials with high Poisson's ratios.
- Chapter 2.2: In viscoelastic micropolar nonlocal solids, Rayleigh wave propagation exhibits multiple modes with distinct particle motions, where the number of propagating modes depends on the interplay between nonlocal and material parameters, and refined models are needed to accurately capture boundary layer effects.
- Chapter 3.1: Refined boundary and interface conditions for nonlocal Rayleigh waves in layered media, derived through asymptotic analysis, are essential for accurately capturing nonlocal effects, particularly within the interface.
- Chapter 3.2: Through asymptotic analysis, the reduction of double integral formulations of nonlocal stresses to single integrals, combined with refined boundary and interface conditions, reveals the distinct dispersive behaviors of Rayleigh waves in micropolar and purely elastic materials, emphasizing the influence of nonlocal parameters and material stiffness.
- Chapter 4.1: The control of Rayleigh wave propagation and bandgap formation in metasurfaces is significantly influenced by resonator design, nonlinearities, input amplitude, and substrate material properties, demonstrating the existence of cut-off frequencies and the tunability of bandgap characteristics.
- Chapter 4.2: The multiple scattering formulation proves crucial for analyzing seismic metasurfaces, effectively capturing inter-resonator interactions and near-field effects, and demonstrating that design parameters like source depth, resonator non-linearity, and the number of resonators significantly impact ground-borne vibration attenuation.
- Chapter 5.1: While the asymptotic hyperbolic-elliptic model effectively captures Rayleigh wave behavior generated from initial conditions in an elastic half-space, it exhibits limitations in representing bulk wave contributions, leading to discrepancies compared to exact solutions.

• Chapter 5.2: The application of the method of potentials and Hankel integral transformations to analyze Rayleigh wave fields generated by surface seismic loading in a micropolar elastic half-space reveals the decay behavior of these waves and provides a methodology extensible to multi-layered media.

#### 6.2 Future directions

The asymptotic formulations used in this thesis can provide a foundation for further exploration using alternative kernels beyond the Bessel kernel. A comparative study of different kernel choices would assess their impact on the accuracy and efficiency of the solutions. Furthermore, the refinement techniques introduced can be extended to coupled theories, such as nonlocal thermoelasticity and piezoelectricity, to analyze wave propagation in more complex material systems.

This thesis further lays the groundwork for the investigation into the vibration control capabilities of metasurfaces, exploring diverse resonator structures, including elastic beams, plates, and shells. The tunability of these resonators, achieved through variations in arrangement, spatial organization, and material properties, can be analyzed to optimize frequency bandgap formation. Additionally, optimization strategies can be developed, and simulation capabilities enhanced, based on the theoretical foundations established herein.

The influence of small-scale effects on the performance of nonlocal devices remains a critical area for future investigation. Analysis of how factors such as size-dependent material properties and surface effects impact device behavior is warranted. This work opens the possibility of developing a continuum representation for small-scale metasurfaces, moving beyond discrete systems and enabling the application of homogenization techniques.

Finally, the initial value problem approach introduced in this thesis can be applied to model real-world explosions and blasts. This will enable the prediction of Rayleigh wave fields and their propagation characteristics, providing valuable insights for seismic hazard assessment and mitigation. This research suggests the possibility of designing adaptive metasurfaces, tailored to the intensity of blasts modelled via initial conditions, for effective vibration control. Additionally, space-time modulated metasurfaces could be designed, providing advanced modeling capabilities in these scenarios. Further development of complex initial conditions modelling, to better simulate real world events, is encouraged.

#### **APPENDICES**

## Appendix A

The refined boundary conditions are applied on the stresses to give a linear homogeneous system of equations in  $\mathcal{X}, \mathcal{Y}_1$  and  $\mathcal{Y}_2$ . The co-efficient matrix takes the form,

$$A = [a_{ij}]_{3\times3},$$

where,

$$\begin{array}{lll} a_{11} & = & \frac{1}{2}a^2s\omega^2\left(q_{10}^3\omega^2(\alpha-\beta+2) + q_{10}s^2\omega^2(\alpha-2\beta+4)\right) + \frac{1}{2}as\omega^2\left(iq_{10}^2\omega(\alpha+\beta-2) + i\alpha s^2\omega\right) + (\beta-2)q_{10}s\omega^2, \\ a_{12} & = & -\frac{1}{2}a^2\omega^2\left((\beta+2)q_{20}^2s^2\omega^2 + 2q_{20}^4\omega^2 + 2(\beta-1)s^4\omega^2\right) + \frac{1}{2}ia(\beta-2)q_{20}s^2\omega^3 + \omega^2\left(q_{20}^2 + (\beta-1)s^2\right), \\ a_{13} & = & \frac{1}{2}a^2\left(q_{30}^2\omega^2\left(2\beta\zeta + (\beta+2)s^2\right) - 2q_{30}^4 + 2s^2\omega^2\left(\beta\zeta - (\beta-1)s^2\omega^2\right)\right) - \frac{1}{2}a(\beta-2)q_{30}s^2\omega^2 \\ & \quad - \left(2q_{30}^2 + \left(\beta\zeta - (\beta-1)s^2\omega^2\right)\right), \\ a_{21} & = & \frac{1}{2}a^2\omega^2\left(2\alpha q_{10}^4\omega^2 + q_{10}^2s^2\omega^2(3\alpha+\beta-2) + s^4\omega^2(\alpha+2\beta-4)\right) - \omega^2\left(2\alpha q_{10}^2 + 2s^2(\alpha+\beta-2)\right), \\ a_{22} & = & \left(\beta-2\right)q_{20}s\omega^2 - \frac{1}{2}a^2(\beta-2)q_{20}s\omega^2\left(2q_{20}^2\omega^2 + 3s^2\omega^2\right), \\ a_{23} & = & i(\beta-2)q_{30}s\omega - \frac{1}{2}ia^2(\beta-2)q_{30}s\omega\left(3s^2\omega^2 - 2q_{30}^2\right), \\ a_{31} & = & 0, \\ a_{32} & = & 0, \\ a_{33} & = & \frac{1}{2}\zeta\eta J\omega\left(-a^2\left(3iq_{30}s^2\omega^2 + 2iq_{30}^3\omega^2\right) + as^2\omega + 2iq_{30}\right). \end{array}$$

## Appendix B

The expressions of  $T_{ij}$  (i, j = 1, 2, 3) in Eq. (3.1.46) are defined as

$$\begin{split} \xi_1 &= \Upsilon_2 \left( \alpha_1^{(0)} \beta_2^{(0)} W \cosh \left( \eta \, \beta_2^{(0)} \right) + Z \sinh \left( \eta \, \beta_2^{(0)} \right) \right) - 2 \beta_2^{(0)} \left( \alpha_1^{(0)} X \cosh \left( \eta \, \alpha_2^{(0)} \right) + \alpha_2^{(0)} Y \sinh \left( \eta \, \alpha_2^{(0)} \right) \right) \\ \xi_2 &= \Upsilon_2 \left( \beta_1^{(0)} X \sinh \left( \eta \, \beta_2^{(0)} \right) + \beta_2^{(0)} Y \cosh \left( \eta \, \beta_2^{(0)} \right) \right) - 2 \beta_2^{(0)} \left( \alpha_2^{(0)} \beta_1^{(0)} W \sinh \left( \eta \, \alpha_2^{(0)} \right) + Z \cosh \left( \eta \, \alpha_2^{(0)} \right) \right) \\ \xi_3 &= \Upsilon_2 \cosh \left( \eta \, \beta_2^{(0)} \right) - 2 \cosh \left( \eta \, \alpha_2^{(0)} \right) \\ \xi_4 &= \alpha_2^{(0)} \cosh \left( \eta \, \alpha_2^{(0)} \right) \left( (-\gamma_2) \, Y - 2 U \right) + \alpha_2^{(0)} \cosh \left( \eta \, \beta_2^{(0)} \right) \left( \Upsilon_2 U + Z \right) \\ &+ \alpha_1^{(0)} \left( \alpha_2^{(0)} \beta_2^{(0)} W \sinh \left( \eta \, \beta_2^{(0)} \right) - \gamma_2 X \sinh \left( \eta \, \alpha_2^{(0)} \right) \right) \\ \xi_5 &= -\alpha_2^{(0)} \cosh \left( \eta \, \alpha_2^{(0)} \right) \left( 2 V - \beta_1^{(0)} \gamma_2 W \right) + \alpha_2^{(0)} \cosh \left( \eta \, \beta_2^{(0)} \right) \left( \Upsilon_2 V - \beta_1^{(0)} X \right) \\ &- \alpha_2^{(0)} \beta_2^{(0)} Y \sinh \left( \eta \, \beta_2^{(0)} \right) + \gamma_2 Z \sinh \left( \eta \, \alpha_2^{(0)} \right) \\ \eta_1 &= \Upsilon_2 \left( \alpha_1^{(0)} X \sinh \left( \eta \, \alpha_2^{(0)} \right) + \alpha_2^{(0)} Y \cosh \left( \eta \, \alpha_2^{(0)} \right) \right) - 2 \alpha_2^{(0)} \left( \alpha_1^{(0)} \beta_2^{(0)} W \sinh \left( \eta \, \beta_2^{(0)} \right) + Z \cosh \left( \eta \, \beta_2^{(0)} \right) \right) \\ \eta_2 &= \Upsilon_2 \left( \alpha_2^{(0)} \beta_1^{(0)} W \cosh \left( \eta \, \alpha_2^{(0)} \right) + Z \sinh \left( \eta \, \alpha_2^{(0)} \right) \right) - 2 \alpha_2^{(0)} \left( \beta_1^{(0)} X \cosh \left( \eta \, \beta_2^{(0)} \right) + \beta_2^{(0)} Y \sinh \left( \eta \, \beta_2^{(0)} \right) \right) \\ \eta_3 &= \Upsilon_2 \sinh \left( \eta \, \alpha_2^{(0)} \right) - 2 \alpha_2^{(0)} \beta_2^{(0)} \sinh \left( \eta \, \beta_2^{(0)} \right) \right) \end{split}$$

The coefficients  $Q_{21}^{(n,0)},~Q_{23}^{(n,0)}$  and  $\overline{Q}_{21}^{(2,0)},~\overline{Q}_{23}^{(2,0)}$  are given by,

$$\begin{split} Q_{21}^{(1,0)} &= -\frac{1}{2} \left. \sigma_{21}^{(1,0)} \right|_{\varkappa_s = 0}, \; Q_{23}^{(1,0)} &= \frac{1}{2} \left. \frac{\partial}{\partial \chi} \left( \sigma_{21}^{(1,0)} \right) \right|_{\varkappa_s = 0}, \\ Q_{21}^{(2,0)} &= -\frac{1}{2} \left. \sigma_{21}^{(2,0)} \right|_{\varkappa_s = 1} e^{-\frac{1}{\epsilon_2}}, \; Q_{23}^{(2,0)} &= \frac{\eta}{2} \left. \frac{\partial}{\partial \chi} \left( \sigma_{21}^{(2,0)} \right) \right|_{\varkappa_s = 1} e^{-\frac{1}{\epsilon_2}}, \\ \overline{Q}_{21}^{(2,0)} &= -\frac{1}{2} \left. \sigma_{21}^{(2,0)} \right|_{\varkappa_s = 0}, \; \overline{Q}_{23}^{(2,0)} &= -\frac{\eta}{2} \left. \frac{\partial}{\partial \chi} \left( \sigma_{21}^{(2,0)} \right) \right|_{\varkappa_s = 0} \end{split}$$

The coefficients  $Q_{21}^{(n,1)},~Q_{23}^{(n,1)}$  and  $\overline{Q}_{21}^{(2,1)},~\overline{Q}_{23}^{(2,1)}$  are given by,

$$\begin{split} Q_{21}^{(1,1)} &= -\frac{1}{2} \left[ \sigma_{21}^{(1,1)} + \frac{1}{\eta} \frac{\partial}{\partial \varkappa_s} \left( \sigma_{11}^{(1,0)} \right) \right] \bigg|_{\varkappa_s = 0}, \\ Q_{23}^{(1,1)} &= \frac{1}{2} \left[ \frac{\partial}{\partial \chi} \left( \sigma_{21}^{(1,1)} \right) + \frac{1}{\eta} \frac{\partial^2}{\partial \chi \partial \varkappa_s} \left( \sigma_{21}^{(1,0)} \right) \right] \bigg|_{\varkappa_s = 0}, \\ Q_{21}^{(2,1)} &= -\frac{1}{2} \left[ \sigma_{21}^{(2,1)} + \frac{\partial}{\partial \varkappa_s} \left( \sigma_{21}^{(2,0)} \right) \right] \bigg|_{\varkappa_s = 1} e^{-\frac{1}{\epsilon_2}}, \ \overline{Q}_{21}^{(2,1)} &= -\frac{1}{2} \left[ \sigma_{21}^{(2,1)} - \frac{\partial}{\partial \varkappa_s} \left( \sigma_{21}^{(2,0)} \right) \right] \bigg|_{\varkappa_s = 0} \\ Q_{23}^{(2,1)} &= \frac{\eta}{2} \left[ \frac{\partial}{\partial \chi} \left( \sigma_{21}^{(2,1)} \right) + \frac{\partial^2}{\partial \chi \partial \varkappa_s} \left( \sigma_{21}^{(2,0)} \right) \right] \bigg|_{\varkappa_s = 1} e^{-\frac{1}{\epsilon_2}}, \ \overline{Q}_{23}^{(2,1)} &= \frac{-\eta}{2} \left[ \frac{\partial}{\partial \chi} \left( \sigma_{11}^{(2,1)} \right) - \frac{\partial^2}{\partial \chi \partial \varkappa_s} \left( \sigma_{11}^{(2,0)} \right) \right] \bigg|_{\varkappa_s = 0} \end{split}$$

## Appendix C

The expressions for the terms defined in the dispersion relations are given as follows:

$$\begin{split} \prod_{1}^{(i)} &= \left(\Theta_{2}^{(i)}\right)^{2} - 2, \\ \prod_{2}^{(i)} &= -\frac{1}{2} \left[ \left(\Theta_{1}^{(i)}\right)^{2} \left( \left(\mathbf{v}_{10}^{(i)}\right)^{2} - 1 \right) + \left(\mathbf{v}_{10}^{(i)}\right)^{2} - 2 \right) \right] \\ \prod_{3}^{(i)} &= -\left[ \left(\Theta_{2}^{(i)}\right)^{2} - \left(\mathbf{v}_{20}^{(i)}\right)^{2} - 1 \right] \\ G_{1} &= \prod_{1}^{(1)} \left( \prod_{1}^{(2)} + \prod_{3}^{(2)} \right) \chi, \\ G_{2} &= \prod_{2}^{(1)} \left( \prod_{1}^{(2)} + \prod_{3}^{(2)} \right) \chi \\ X &= -\left( \prod_{1}^{(1)} \chi + \prod_{3}^{(2)} \right), \\ Y &= -\left( \prod_{3}^{(1)} \chi + \prod_{1}^{(2)} \right) \\ Z &= -\left( \prod_{3}^{(1)} \chi - \prod_{3}^{(2)} \right) \\ U &= -\left( 2 \prod_{2}^{(2)} Y + \prod_{1}^{(2)} Z \right), \\ V &= 2 \prod_{2}^{(2)} W + \prod_{1}^{(2)} X \\ W &= -\left( \prod_{1}^{(1)} \chi - \prod_{1}^{(2)} \right) \\ \text{where } \Theta_{1}^{(i)} &= \frac{c_{1}^{(i)}}{c_{2}^{(i)}}, \; \Theta_{3}^{(i)} &= \frac{c_{1}^{(i)}}{c_{2}^{(i)}}, \; \chi = \frac{\mu^{(1)} + \kappa^{(1)}}{\mu^{(2)} + \kappa^{(2)}}. \end{split}$$

## Appendix D

The elements of the matrix P are given by,

$$\begin{aligned} p_{11} &= -\xi; \quad p_{12} = -\xi; \quad p_{13} = \beta \xi; \quad p_{14} = \zeta \xi; \quad p_{15} = -\beta \xi; \quad p_{16} = -\zeta \xi; \\ p_{21} &= -\alpha; \quad p_{22} = \alpha; \quad p_{23} = \xi^2; \quad p_{24} = \xi^2; \quad p_{25} = \xi^2; \quad p_{26} = \xi^2 \\ p_{31} &= 0; \quad p_{32} = 0; \quad p_{33} = \xi s_1; \quad p_{34} = \xi s_2; \quad p_{35} = \xi s_1; \quad p_{36} = \xi s_2; \\ p_{41} &= -\xi e^{-\alpha z}; \quad p_{42} = -\xi e^{\alpha z}; \quad p_{43} = \beta \xi e^{-\beta z}; \quad p_{44} = \zeta \xi e^{\beta z}; \quad p_{45} = -\beta \xi e^{-\zeta z}; \quad p_{46} = -\zeta \xi e^{\zeta z}; \\ p_{51} &= -\alpha e^{-\alpha z}; \quad p_{52} = \alpha e^{\alpha z}; \quad p_{53} = \xi^2 e^{-\beta z}; \quad p_{54} = \xi^2 e^{\beta z}; \quad p_{55} = \xi^2 e^{-\zeta z}; \quad p_{56} = \xi^2 e^{\zeta z}; \\ p_{61} &= 0; \quad p_{62} = 0; \quad p_{63} = \xi s_1 e^{-\beta z}; \quad p_{64} = \xi s_2 e^{\beta z}; \quad p_{65} = \xi s_1 e^{-\zeta z}; \quad p_{66} = \xi s_2 e^{\zeta z}. \end{aligned}$$

The elements of the matrix Q are given by,

$$q_{11} = -b_{11}; \quad q_{12} = -b_{11}; \quad q_{13} = -b_{12}; \quad q_{14} = -b_{13}; \quad q_{15} = b_{12}; \quad q_{16} = b_{13};$$

$$q_{21} = -b_{21}; \quad q_{22} = b_{21}; \quad q_{23} = -b_{22}; \quad q_{24} = -b_{22}; \quad q_{25} = -b_{22}; \quad q_{26} = -b_{22};$$

$$q_{31} = 0; \quad q_{32} = 0; \quad q_{33} = \xi b_{32}; \quad q_{34} = \xi b_{33}; \quad q_{35} = -\xi b_{32}; \quad q_{36} = -\xi b_{33};$$

$$q_{41} = b_{11}e^{-\alpha z}; \quad q_{42} = b_{11}e^{\alpha z}; \quad q_{43} = b_{12}e^{-\beta z}; \quad q_{44} = b_{13}e^{\beta z}; \quad q_{45} = -b_{12}e^{-\zeta z}; \quad q_{46} = -b_{13}e^{\zeta z};$$

$$q_{51} = b_{21}e^{-\alpha z}; \quad q_{52} = -b_{21}e^{\alpha z}; \quad q_{53} = b_{22}e^{-\beta z}; \quad q_{54} = b_{22}e^{\beta z}; \quad q_{55} = b_{22}e^{-\zeta z}; \quad q_{56} = b_{22}e^{\zeta z};$$

$$q_{61} = 0; \quad q_{53} = 0; \quad q_{62} = \xi b_{32}e^{-\beta z}; \quad q_{63} = \xi b_{33}e^{\beta z}; \quad q_{64} = -\xi b_{65}e^{-\zeta z}; \quad q_{66} = -\xi b_{33}e^{\zeta z}.$$

### REFERENCES

- [1] Achenbach, J. (2012). Wave propagation in elastic solids. Elsevier.
- [2] Graff, K. F. (2012). Wave motion in elastic solids. Courier Corporation.
- [3] Zeroug, S., & Bose, S. (2018, April). Recent advances in the use of acoustics across the frequency spectrum in the oil and gas industry. In AIP Conference Proceedings (Vol. 1949, No. 1). AIP Publishing.
- [4] Klimentos, T. (1995). Attenuation of P-and S-waves as a method of distinguishing gas and condensate from oil and water. *Geophysics*, 60(2), 447-458.
- [5] Djuraev, U., Jufar, S. R., & Vasant, P. (2017). A review on conceptual and practical oil and gas reservoir monitoring methods. *Journal of Petroleum Science and Engineering*, 152, 586-601.
- [6] Zhang, J., Lian, Z., Zhou, Z., Song, Z., Liu, M., & Yang, K. (2022). Leakage detection in a buried gas pipeline based on distributed optical fiber time-domain acoustic wave signal. *Engineering Failure Analysis*, 141, 106594.
- [7] Stein, S., & Wysession, M. (2009). An introduction to seismology, earthquakes, and earth structure. John Wiley & Sons.
- [8] Seredkina, A. I. (2021). The state of the art in studying the deep structure of the Earth's crust and upper mantle beneath the Baikal rift from seismological data. *Izvestiya*, *Physics of the Solid Earth*, 57(2), 180-202.
- [9] Tromp, J. (2020). Seismic wavefield imaging of Earth's interior across scales. Nature Reviews Earth & Environment, 1(1), 40-53.
- [10] Sarvazyan, A. P., Rudenko, O. V., Swanson, S. D., Fowlkes, J. B., & Emelianov, S. Y. (1998). Shear wave elasticity imaging: a new ultrasonic technology of medical diagnostics. *Ultrasound in medicine & biology*, 24(9), 1419-1435.
- [11] Sarvazyan, A. P., Urban, M. W., & Greenleaf, J. F. (2013). Acoustic waves in medical imaging and diagnostics. *Ultrasound in medicine & biology*, 39(7), 1133-1146.
- [12] Wang, C. J. (2003). An overview of shock wave therapy in musculoskeletal disorders. *Chang Gung medical journal*, 26(4), 220-232.
- [13] Cleveland, R. O., & Sapozhnikov, O. A. (2005). Modeling elastic wave propagation in kidney stones with application to shock wave lithotripsy. *The Journal of the Acoustical Society of America*, 118(4), 2667-2676.
- [14] Rayleigh, L. (1885). On waves propagated along the plane surface of an elastic solid. *Proceedings of the London mathematical Society*, 1(1), 4-11.
- [15] Aggelis, D. G., Shiotani, T., & Polyzos, D. (2009). Characterization of surface crack depth and repair evaluation using Rayleigh waves. *Cement and Concrete Composites*, 31(1), 77-83.
- [16] Hevin, G., Abraham, O., Pedersen, H. A., & Campillo, M. (1998). Characterization of surface cracks with Rayleigh waves: a numerical model. *Nat & E International*, 31(4), 289-297.

- [17] Xu, L., Su, Y., Yang, J., & Su, Z. (2023). Frequency-dependent scattering of wideband laser-generated Rayleigh waves for vertical surface crack characterization. *Smart Materials and Structures*, 32(4), 045001.
- [18] Kazemirad, S., & Mongeau, L. (2013). Rayleigh wave propagation method for the characterization of a thin layer of biomaterials. *The Journal of the Acoustical Society of America*, 133(6), 4332-4342.
- [19] Matthews, M. C., Hope, V. S., Clayton, C. R. I., & Rayleigh. (1996). The use of surface waves in the determination of ground stiffness profiles. *Proceedings of the Institution of Civil Engineers-Geotechnical* Engineering, 119(2), 84-95.
- [20] Zhang, Z. D., Saygin, E., He, L., & Alkhalifah, T. (2021). Rayleigh wave dispersion spectrum inversion across scales. *Surveys in Geophysics*, 1-23.
- [21] Xia, J., Miller, R. D., Park, C. B., Ivanov, J., Tian, G., & Chen, C. (2004). Utilization of high-frequency Rayleigh waves in near-surface geophysics. *The Leading Edge*, 23(8), 753-759.
- [22] Briggs, A., & Kolosov, O. (2010). Acoustic microscopy (Vol. 67). Oxford University Press.
- [23] Korkh, Y. V., Perov, D. V., & Rinkevich, A. B. (2015). Detection of subsurface microflaws using the high-frequency acoustic microscopy method. *Russian Journal of Nondestructive Testing*, 51, 198-209.
- [24] Kozic, E., Hammer, R., Rosc, J., Sartory, B., Siegert, J., Schrank, F., & Brunner, R. (2018). Metallization defect detection in 3D integrated components using scanning acoustic microscopy and acoustic simulations. *Microelectronics Reliability*, 88, 262-266.
- [25] Laux, D., De Weerd, W., Papaioannou, D., Kitajima, S., Rondinella, V. V., & Despaux, G. (2014). Scanning acoustic microscope for mechanical characterization and density estimation of irradiated nuclear fuel. *Progress in Nuclear Energy*, 72, 63-66.
- [26] Chakrapani, S. K., Bond, L. J., & Edwards, R. S. (2018). Rayleigh wave nondestructive evaluation for defect detection and materials characterization. *Nondestructive Evaluation of Materials*. ASM International, 266-282.
- [27] Chen, D., Lv, G., Guo, S., Zuo, R., Liu, Y., Zhang, K., & Feng, W. (2020). Subsurface defect detection using phase evolution of line laser-generated Rayleigh waves. *Optics & Laser Technology*, 131, 106410.
- [28] Herrmann, J., Kim, J. Y., Jacobs, L. J., Qu, J., Littles, J. W., & Savage, M. F. (2006). Assessment of material damage in a nickel-base superalloy using nonlinear Rayleigh surface waves. *Journal of applied physics*, 99(12).
- [29] Walker, S. V., Kim, J. Y., Qu, J., & Jacobs, L. J. (2012). Fatigue damage evaluation in A36 steel using nonlinear Rayleigh surface waves. *Ndt & E International*, 48, 10-15.
- [30] Baghani, M., Mohammadi, M., & Farajpour, A. (2016). Dynamic and stability analysis of the rotating nanobeam in a nonuniform magnetic field considering the surface energy. *International Journal of Applied Mechanics*, 8(04), 1650048.
- [31] Qiao, Q., Xia, J., Lee, C., & Zhou, G. (2018). Applications of photonic crystal nanobeam cavities for sensing. *Micromachines*, 9(11), 541.
- [32] Garcia-Sanchez, D., San Paulo, A., Esplandiu, M. J., Perez-Murano, F., Forró, L., Aguasca, A., & Bachtold, A. (2007). Mechanical detection of carbon nanotube resonator vibrations. *Physical review letters*, 99(8), 085501.
- [33] Babaei Gavan, K., Westra, H. J., van der Drift, E. W., Venstra, W. J., & van der Zant, H. S. (2009). Size-dependent effective Young's modulus of silicon nitride cantilevers. *Applied Physics Letters*, 94(23).

- [34] Chen, S., & Carroll, D. L. (2002). Synthesis and characterization of truncated triangular silver nanoplates. Nano letters, 2(9), 1003-1007.
- [35] Geim, A. K., & Novoselov, K. S. (2007). The rise of graphene. Nature materials, 6(3), 183-191.
- [36] Bunch, J. S., Van Der Zande, A. M., Verbridge, S. S., Frank, I. W., Tanenbaum, D. M., Parpia, J. M., & McEuen, P. L. (2007). Electromechanical resonators from graphene sheets. Science, 315(5811), 490-493.
- [37] Farajpour, M. R., Rastgoo, A., Farajpour, A., & Mohammadi, M. (2016). Vibration of piezoelectric nanofilm-based electromechanical sensors via higher-order non-local strain gradient theory. *Micro & Nano Letters*, 11(6), 302-307.
- [38] Murmu, T., & Adhikari, S. (2013). Nonlocal mass nanosensors based on vibrating monolayer graphene sheets. Sensors and Actuators B: Chemical, 188, 1319-1327.
- [39] Faleh, N. M., Ahmed, R. A., & Fenjan, R. M. (2018). On vibrations of porous FG nanoshells. *International Journal of Engineering Science*, 133, 1-14.
- [40] Wang, Q., & Varadan, V. K. (2007). Application of nonlocal elastic shell theory in wave propagation analysis of carbon nanotubes. *Smart Materials and Structures*, 16(1), 178.
- [41] Arani, A. G., Amir, S., Shajari, A. R., & Mozdianfard, M. R. (2012). Electro-thermo-mechanical buckling of DWBNNTs embedded in bundle of CNTs using nonlocal piezoelasticity cylindrical shell theory. *Composites Part B: Engineering*, 43(2), 195-203.
- [42] Ke, L. L., Wang, Y. S., Yang, J., & Kitipornchai, S. (2014). The size-dependent vibration of embedded magneto-electro-elastic cylindrical nanoshells. Smart Materials and Structures, 23(12), 125036.
- [43] Haile, J. M. (1992). Molecular dynamics simulation: elementary methods. John Wiley & Sons, Inc..
- [44] Lurie, A. I. (2010). Theory of elasticity. Springer Science & Business Media.
- [45] Truesdell, C., & Toupin, R. (1960). The classical field theories. Springer Berlin Heidelberg.
- [46] Mindlin, R. D., & Tiersten, H. (1962). Effects of couple-stresses in linear elasticity. Archive for Rational Mechanics and analysis, 11, 415-448.
- [47] Mindlin, R. D. (1964). Micro-structure in linear elasticity. Archive for rational mechanics and analysis, 16, 51-78.
- [48] Hadjesfandiari, A. R., & Dargush, G. F. (2011). Couple stress theory for solids. International Journal of Solids and Structures, 48(18), 2496-2510.
- [49] Eringen, A. C., & Suhubi, E. (1964). Nonlinear theory of simple micro-elastic solids—I. *International Journal of Engineering Science*, 2(2), 189-203.
- [50] Eringen, A. C., & Kafadar, C. B. (1971). Part I. Polar field theories. Continuum Physics, 1-73.
- [51] Eringen, A. C. (1966). Linear theory of micropolar elasticity. Journal of Mathematics and Mechanics, 909-923.
- [52] Nowacki, W. (1974). The linear theory of micropolar elasticity. In Micropolar Elasticity: Symposium Organized by the Department of Mechanics of Solids, June 1972. Vienna: Springer Vienna, 1-43.
- [53] Eringen, A. C., & Wegner, J. L. (2003). Nonlocal continuum field theories. Appl. Mech. Rev., 56(2), B20-B22.
- [54] Salehipour, H., Shahidi, A. R., & Nahvi, H. (2015). Modified nonlocal elasticity theory for functionally graded materials. *International Journal of Engineering Science*, 90, 44-57.
- [55] Mindlin, R. D., & Eshel, N. (1968). On first strain-gradient theories in linear elasticity. *International Journal of Solids and Structures*, 4(1), 109-124.

- [56] Askes, H., & Aifantis, E. C. (2011). Gradient elasticity in statics and dynamics: an overview of formulations, length scale identification procedures, finite element implementations and new results. *International Journal of Solids and Structures*, 48(13), 1962-1990.
- [57] Lim, C. W., Zhang, G., & Reddy, J. (2015). A higher-order nonlocal elasticity and strain gradient theory and its applications in wave propagation. *Journal of the Mechanics and Physics of Solids*, 78, 298-313.
- [58] Shenoy, V. B., Miller, R., Tadmor, E. B., Rodney, D., Phillips, R., & Ortiz, M. (1999). An adaptive finite element approach to atomic-scale mechanics—the quasicontinuum method. *Journal of the Mechanics and Physics of Solids*, 47(3), 611-642.
- [59] Eringen, A. C., & Edelen, D. (1972). On nonlocal elasticity. *International journal of engineering science*, 10(3), 233-248.
- [60] Eringen, A. C. (1983). On differential equations of nonlocal elasticity and solutions of screw dislocation and surface waves. *Journal of applied physics*, 54(9), 4703-4710.
- [61] Eringen, A. C. (1984). Plane waves in nonlocal micropolar elasticity. International Journal of Engineering Science, 22(8-10), 1113-1121.
- [62] Abdollahi, R., & Boroomand, B. (2014). Nonlocal elasticity defined by Eringen's integral model: introduction of a boundary layer method. *International journal of solids and structures*, 51(9), 1758-1780.
- [63] Maznev, A. A., & Gusev, V. E. (2015). Waveguiding by a locally resonant metasurface. *Physical Review B*, 92(11), 115422.
- [64] Amer, A. A. G., Sapuan, S. Z., Nasimuddin, N., Alphones, A., & Zinal, N. B. (2020). A comprehensive review of metasurface structures suitable for RF energy harvesting. *IEEE Access*, 8, 76433-76452.
- [65] De Ponti, J. M., Colombi, A., Ardito, R., Braghin, F., Corigliano, A., & Craster, R. V. (2020). Graded elastic metasurface for enhanced energy harvesting. New Journal of Physics, 22(1), 013013.
- [66] Zhou, J., Zhang, P., Han, J., Li, L., & Huang, Y. (2021). Metamaterials and metasurfaces for wireless power transfer and energy harvesting. *Proceedings of the IEEE*, 110(1), 31-55.
- [67] Walser, R. M. (2001, July). Electromagnetic metamaterials. In Complex Mediums II: beyond linear isotropic dielectrics (Vol. 4467, pp. 1-15). SPIE.
- [68] Cui, T. J., Smith, D. R., & Liu, R. (2010). Metamaterials (p. 1). New York: springer.
- [69] Watts, C. M., Liu, X., & Padilla, W. J. (2012). Metamaterial electromagnetic wave absorbers. Advanced materials, 24(23), OP98-OP120.
- [70] Palermo, A., Krödel, S., Marzani, A., & Daraio, C. (2016). Engineered metabarrier as shield from seismic surface waves. *Scientific reports*, 6(1), 1-10.
- [71] Colombi, A., Zaccherini, R., Aguzzi, G., Palermo, A., & Chatzi, E. (2020). Mitigation of seismic waves: Metabarriers and metafoundations bench tested. *Journal of Sound and Vibration*, 485, 115537.
- [72] Zhang, X., & Liu, Z. (2004). Negative refraction of acoustic waves in two-dimensional phononic crystals.

  Applied Physics Letters, 85(2), 341-343.
- [73] Sukhovich, A., Jing, L., & Page, J. H. (2008). Negative refraction and focusing of ultrasound in twodimensional phononic crystals. Physical Review B—Condensed Matter and Materials Physics, 77(1), 014301.
- [74] Kan, W., & Shen, Z. (2017). Ultra-transparent media with anisotropic mass density for broadband acoustic invisibility. Applied Physics Letters, 111(22).

- [75] Zhu, J., Chen, T., Song, X., Chen, C., Liu, Z., & Zhang, J. (2019). Three-dimensional large-scale acoustic invisibility cloak with layered metamaterials for underwater operation. *Physica Scripta*, 94(11), 115003.
- [76] Ben-Menahem, A., & Singh, S. J. (2012). Seismic waves and sources. Springer Science & Business Media.
- [77] Doyle, P. A., & Scala, C. M. (1996). Near-field ultrasonic Rayleigh waves from a laser line source. *Ultrasonics*, 34(1), 1-8.
- [78] Pekeris, C. L. (1955). The seismic surface pulse. Proceedings of the national academy of sciences, 41(7), 469-480.
- [79] Maruyama, T., Tsugawa, T., Kato, H., Ishii, M., & Nishioka, M. (2012). Rayleigh wave signature in ionograms induced by strong earthquakes. *Journal of Geophysical Research: Space Physics*, 117(A8).
- [80] Dobrin, M. B., Simon, R. F., & Lawrence, P. L. (1951). Rayleigh waves from small explosions. Eos, Transactions American Geophysical Union, 32(6), 822-832.
- [81] Murphy, J. R. (1981). Near-field Rayleigh waves from surface explosions. Bulletin of the Seismological Society of America, 71(1), 223-248.
- [82] Zhou, R. M., & Stump, B. W. (2004). Rayleigh waves generated by mining explosions and upper crustal structure around the Powder River Basin, Wyoming. *Bulletin of the Seismological Society of America*, 94(4), 1410-1429.
- [83] Heckman, W. S., & Hagerty, D. J. (1978). Vibrations associated with pile driving. Journal of the Construction Division, 104(4), 385-394.
- [84] Massarsch, K. R., & Fellenius, B. H. (2008). Ground vibrations induced by impact pile driving.
- [85] Kaplunov, Y. D. and Kossovich, L. Y. (2004). Asymptotic model of Rayleigh waves in the far-field zone in an elastic half-plane. *Doklady Physics*, 49(4), 234–236.
- [86] Kaplunov, J., Zakharov, A. and Prikazchikov, D. (2006). Explicit models for elastic and piezoelastic surface waves. IMA Journal of Applied Mathematics, 71(5), 768–782.
- [87] Kaplunov, J. and Prikazchikov, D. A. (2017). Asymptotic theory for Rayleigh and Rayleigh-type waves. Advances in Applied Mechanics, 1–106.
- [88] Khajiyeva, L. A., Prikazchikov, D. A. and Prikazchikova, L. A. (2018). Hyperbolic-elliptic model for surface wave in a pre-stressed incompressible elastic half-space. *Mechanics Research Communications*, 92, 49–53.
- [89] Prikazchikov, D. (2020). Explicit model for surface waves in a pre-stressed, compressible elastic half-space. International Journal of Mathematics and Physics, 11, 13-19.
- [90] Nobili, A. and Prikazchikov, D. A. (2018). Explicit formulation for the Rayleigh wave field induced by surface stresses in an orthorhombic half-plane. European Journal of Mechanics - A/Solids, 70, 86–94.
- [91] Şahin, Onur. (2021). Mixed boundary value problems for Rayleigh wave in a half-plane with cubic anisotropy. ZAMM - Journal of Applied Mathematics and Mechanics, 101.
- [92] Wootton, P. T., Kaplunov, J. and Prikazchikov, D. (2020). A second-order asymptotic model for Rayleigh waves on a linearly elastic half plane. *IMA Journal of Applied Mathematics*, 85(1), 113–131.
- [93] Erbas, B., Kaplunov, J. and Prikazchikov, D. A. (2012). The Rayleigh wave field in mixed problems for a half-plane. *IMA Journal of Applied Mathematics*, 78(5), 1078–1086.
- [94] Kaplunov, J. (1986). Transient dynamic of an elastic half plane subject to a moving load. *Institute for Problems in Mechanics, Moscow, Preprint No. 277.*

- [95] Kaplunov, J., Nolde, E., & Prikazchikov, D. A. (2010). A revisit to the moving load problem using an asymptotic model for the Rayleigh wave. *Wave Motion*, 47(7), 440–451.
- [96] Gupta, S., Dwivedi, R., & Dutta, R. (2021). Rayleigh wave propagation at the boundary surface of dry sandy  $(SiO_2)$  thermoelastic solids. *Engineering Computations*, 38(8), 3368-3387.
- [97] Gupta, S., & Ahmed, M. (2017). On Rayleigh waves in self-reinforced layer embedded over an incompressible half-space with varying rigidity and density. *Procedia Engineering*, 173, 1021-1028.
- [98] Gupta, S., Smita, Pramanik, S., & Verma, A. K. (2021). Secular equation of Rayleigh surface wave in a dry sandy half-space coated by a thin self-reinforced layer. *Arabian Journal of Geosciences*, 14, 1-8.
- [99] Brockhouse, B. N., Arase, T., Caglioti, G., Rao, K. R., & Woods, A. D. B. (1962). Crystal dynamics of lead. I. Dispersion curves at 100 K. *Physical Review*, 128(3), 1099.
- [100] Harrison, W. A. (1963). Electronic structure and the properties of metals. i. formulation. *Physical Review*, 129(6), 2503.
- [101] Wallis, R. F. (1965). Lattice dynamics. Oxford, Pergamon Press.
- [102] Voigt, W. (1887). Theoretische studien über die elastizitätsverhältnisse der krystalle. Abhandlungen der Mathematischen Classe der Königlichen Gesellschaft der Wissenschaften zu Göttingen, 34, 3–51.
- [103] Cosserat, EMP, & Cosserat, F. (1909). Theory of deformable bodies. A. Hermann et fils.
- [104] Günther, W. (1958). Zur statik und kinematik des cosseratschen kontinuums. Abh. Braunschweig. wiss. ges, 10(213), 1.
- [105] Schaefer, H. (1967). Das cosserat kontinuum. ZAMM-Journal of Applied Mathematics and Mechanics/Zeitschrift f
  ür Angewandte Mathematik und Mechanik, 47(8), 485-498.
- [106] Suhubi, E. S., & Eringen, A. C. (1964). Nonlinear theory of micro-elastic solids—II. International Journal of Engineering Science, 2(4), 389-404.
- [107] Grioli, G. (1960). Elasticita asimmetrica. Annali di matematica pura ed applicata, 50, 389-417.
- [108] Aero, E. L., & Kuvshinskii, E. V. (1961). Fundamental equations of the theory of elastic media with rotationally interacting particles. Soviet Physics-Solid State, 2(7), 1272-1281.
- [109] Toupin, R. (1962). Elastic materials with couple-stresses. Archive for rational mechanics and analysis, 11(1), 385-414.
- [110] Kröner, E. (1963). On the physical reality of torque stresses in continuum mechanics. *International Journal of Engineering Science*, 1(2), 261-278.
- [111] Koiter, W. T. (1964). Couple-stresses in the theory of elasticity, I and II, Prec. Roy. Netherlands Acad. Sci. B, 67, 0964.
- [112] Mindlin, R. D. (1965). Second gradient of strain and surface-tension in linear elasticity. *International journal of solids and structures*, 1(4), 417-438.
- [113] Yang, F. A. C. M., Chong, A. C. M., Lam, D. C. C., & Tong, P. (2002). Couple stress based strain gradient theory for elasticity. *International journal of solids and structures*, 39(10), 2731-2743.
- [114] Lam, D. C., Yang, F., Chong, A. C. M., Wang, J., & Tong, P. (2003). Experiments and theory in strain gradient elasticity. *Journal of the Mechanics and Physics of Solids*, 51(8), 1477-1508.
- [115] Eringen, A. C. (2012). Microcontinuum field theories: I. Foundations and solids. Springer Science & Business Media.

- [116] Lazar, M., & Maugin, G. A. (2007). On microcontinuum field theories: the Eshelby stress tensor and incompatibility conditions. *Philosophical Magazine*, 87(25), 3853-3870.
- [117] Eringen, A. C., & Eringen, A. C. (1999). Theory of micropolar elasticity (pp. 101-248). Springer New York.
- [118] Eringen, A. C. (1990). Theory of thermo-microstretch elastic solids. International journal of engineering science, 28(12), 1291-1301.
- [119] Kuvshinskii, E. V., & Aero, E. L. (1963). Continuum theory of asymmetric elasticity. Fizika tverdogo tela, 5, 2592.
- [120] Palmov, V. (1964). Fundamental equations of the theory of asymmetric elasticity. Journal of Applied Mathematics and Mechanics, 28(3), 496-505.
- [121] Mindlin, R. D. (1965). Stress functions for a Cosserat continuum. *International Journal of Solids and Structures*, 1(3), 265-271.
- [122] Nowacki, W., & International centre for mechanical sciences. courses and lectures; no. 25. (1972). Theory of micropolar elasticity (Vol. 494). Berlin: Springer.
- [123] Dyszlewicz, J. (2012). Micropolar theory of elasticity (Vol. 15). Springer Science & Business Media.
- [124] Nowacki, W., & Olszak, W. (Eds.). (1974). *Micropolar Elasticity*. CISM International Centre for Mechanical Sciences.
- [125] Hassanpour, S., & Heppler, G. R. (2017). Linear theory of micropolar elasticity: A Survey of the representative notations and experimental investigations of the micropolar elastic moduli. *Math. Mech. Solid*, 22(2), 224-242.
- [126] Eringen, A. C. (1964). Simple microfluids. International Journal of Engineering Science, 2(2), 205-217.
- [127] Eringen, A. C. (1966). Mechanics of micromorphic materials. In Applied Mechanics: Proceedings of the Eleventh International Congress of Applied Mechanics Munich (Germany) 1964 (pp. 131-138). Springer Berlin Heidelberg.
- [128] Eringen, A. C. (1968). Mechanics of micromorphic continua. In Mechanics of Generalized Continua: Proceedings of the IUTAM-Symposium on The Generalized Cosserat Continuum and the Continuum Theory of Dislocations with Applications, Freudenstadt and Stuttgart (Germany) 1967 (pp. 18-35). Berlin, Heidelberg: Springer Berlin Heidelberg.
- [129] Shaat, M. (2018). A reduced micromorphic model for multiscale materials and its applications in wave propagation. *Composite Structures*, 201, 446-454.
- [130] Barbagallo, G., Madeo, A., d'Agostino, M. V., Abreu, R., Ghiba, I. D., & Neff, P. (2017). Transparent anisotropy for the relaxed micromorphic model: macroscopic consistency conditions and long wave length asymptotics. *International Journal of Solids and Structures*, 120, 7-30.
- [131] Romano, G., Barretta, R., & Diaco, M. (2016). Micromorphic continua: non-redundant formulations. *Continuum Mechanics and Thermodynamics*, 28, 1659-1670.
- [132] Neff, P., Ghiba, I. D., Madeo, A., Placidi, L., & Rosi, G. (2014). A unifying perspective: the relaxed linear micromorphic continuum. Continuum Mechanics and Thermodynamics, 26, 639-681.
- [133] Kunin, I. A. (1968). The theory of elastic media with microstructure and the theory of dislocations. In Mechanics of Generalized Continua: Proceedings of the IUTAM-Symposium on The Generalized Conservat Continuum and the Continuum Theory of Dislocations with Applications, Freudenstadt and Stuttgart (Germany) 1967 (pp. 321-329). Berlin, Heidelberg: Springer Berlin Heidelberg.

- [134] Kunin, I. A. (1984). On foundations of the theory of elastic media with microstructure. *International Journal of Engineering Science*, 22(8-10), 969-978.
- [135] Kunin, I. A. (2012). Elastic media with microstructure I: one-dimensional models (Vol. 26). Springer Science & Business Media.
- [136] Trovalusci, P., & Pau, A. (2014). Derivation of microstructured continua from lattice systems via principle of virtual works: the case of masonry-like materials as micropolar, second gradient and classical continua.

  Acta Mechanica, 225(1), 157-177.
- [137] Shaat, M. (2019). Size-dependence of Young's modulus and Poisson's ratio: Effects of material dispersion. Mechanics of Materials, 133, 111-119.
- [138] Trovalusci, P. (2014). Molecular approaches for multifield continua: origins and current developments. In Multiscale modeling of complex materials: phenomenological, theoretical and computational aspects (pp. 211-278). Vienna: Springer Vienna.
- [139] Capriz, G. (2013). Continua with microstructure (Vol. 35). Springer Science & Business Media.
- [140] Gurtin, M. E., & Podio-Guidugli, P. (1992). On the formulation of mechanical balance laws for structured continua. Zeitschrift für angewandte Mathematik und Physik ZAMP, 43, 181-190.
- [141] Maugin, G. A. (2017). Non-classical continuum mechanics. Springer Verlag, Singapor.
- [142] Tuna, M., & Trovalusci, P. (2020). Scale dependent continuum approaches for discontinuous assemblies: Explicit'and 'implicit'non-local models. *Mechanics Research Communications*, 103, 103461.
- [143] Maugin, G. A. (2020). Material inhomogeneities in elasticity. CRC Press.
- [144] Ghavanloo, E., & Fazelzadeh, S. A. (2016). Evaluation of nonlocal parameter for single-walled carbon nanotubes with arbitrary chirality. *Meccanica*, 51, 41-54.
- [145] Kröner, E. (1967). Elasticity theory of materials with long range cohesive forces. International Journal of Solids and Structures, 3(5), 731-742.
- [146] Edelen, D. G. B., Green, A. E., & Laws, N. (1971). Nonlocal continuum mechanics. Archive for Rational Mechanics and Analysis, 43, 36-44.
- [147] Edelen, D. G., & Laws, N. (1971). On the thermodynamics of systems with nonlocality. Archive for Rational Mechanics and Analysis, 43, 24-35.
- [148] Eringen, A. C. (1972). Nonlocal polar elastic continua. International journal of engineering science, 10(1), 1-16.
- [149] Eringen, A. C. (1972). Linear theory of nonlocal elasticity and dispersion of plane waves. *International Journal of Engineering Science*, 10(5), 425-435.
- [150] Eringen, A. C., Speziale, C. G., & Kim, B. S. (1977). Crack-tip problem in non-local elasticity. Journal of the Mechanics and Physics of Solids, 25(5), 339-355.
- [151] Eringen, A. C. (1987). Theory of nonlocal elasticity and some applications. Res Mech., 21(4), 313-342.
- [152] Pisano, A. A., & Fuschi, P. (2003). Closed form solution for a nonlocal elastic bar in tension. *International journal of Solids and Structures*, 40(1), 13-23.
- [153] Polizzotto, C., Fuschi, P., & Pisano, A. A. (2006). A nonhomogeneous nonlocal elasticity model. *European Journal of Mechanics-A/Solids*, 25(2), 308-333.
- [154] Pisano, A. A., Sofi, A., & Fuschi, P. (2009). Finite element solutions for nonhomogeneous nonlocal elastic problems. *Mechanics Research Communications*, 36(7), 755-761.

- [155] Atanackovic, T. M., & Stankovic, B. (2009). Generalized wave equation in nonlocal elasticity. Acta Mechanica, 208(1), 1-10.
- [156] Di Paola, M., Failla, G., & Zingales, M. (2009). Physically-based approach to the mechanics of strong non-local linear elasticity theory. *Journal of Elasticity*, 97, 103-130.
- [157] Di Paola, M., Failla, G., Pirrotta, A., Sofi, A., & Zingales, M. (2013). The mechanically based non-local elasticity: an overview of main results and future challenges. *Philosophical Transactions of the Royal Society A: Mathematical, Physical and Engineering Sciences*, 371(1993), 20120433.
- [158] Chakraborty, A. (2007). Wave propagation in anisotropic media with non-local elasticity. *International journal of solids and structures*, 44(17), 5723-5741.
- [159] Roy, I., Acharya, D. P., & Acharya, S. (2015). Rayleigh wave in a rotating nonlocal magnetoelastic halfplane. *Journal of Theoretical and Applied Mechanics*, 45(4), 61.
- [160] Singh, D., Kaur, G., & Tomar, S. (2017). Waves in nonlocal elastic solid with voids. *Journal of Elasticity*, 128(1), 85-114.
- [161] Kaur, G., Singh, D., & Tomar, S. (2018). Rayleigh-type wave in a nonlocal elastic solid with voids. European Journal of Mechanics-A/Solids, 71, 134-150.
- [162] Tung, D. X. (2019). Dispersion equation of Rayleigh waves in transversely isotropic nonlocal piezoelastic solids half-space. Vietnam Journal of Mechanics, 41(4), 363-371.
- [163] Sarkar, N., De, S., & Sarkar, N. (2019). Waves in nonlocal thermoelastic solids of type II. *Journal of Thermal Stresses*, 42(9), 1153-1170.
- [164] Biswas, S. (2020). Rayleigh waves in a nonlocal thermoelastic layer lying over a nonlocal thermoelastic half-space. *Acta Mechanica*, 231(10), 4129-4144.
- [165] Pramanik, D., & Manna, S. (2023). Love-like wave dispersion in a highly non-homogeneous viscoelastic orthotropic layer under the effect of non-local elasticity. *Mathematical Methods in the Applied Sciences*, 46(14), 15048-15072.
- [166] Pramanik, D., & Manna, S. (2024). Love-like wave fields at the interface of sliding contact with non-local elastic heterogeneous fluid-saturated fractured poro-viscoelastic layer. European Journal of Mechanics-A/Solids, 105350.
- [167] Lu, P., Lee, H. P., Lu, C., & Zhang, P. (2007). Application of nonlocal beam models for carbon nanotubes. International journal of Solids and Structures, 44(16), 5289-5300.
- [168] Aydogdu, M. (2009). A general nonlocal beam theory: its application to nanobeam bending, buckling and vibration. *Physica E: Low-dimensional Systems and Nanostructures*, 41(9), 1651-1655.
- [169] Thai, H. T. (2012). A nonlocal beam theory for bending, buckling, and vibration of nanobeams. *International Journal of Engineering Science*, 52, 56-64.
- [170] Ghannadpour, S. A. M., Mohammadi, B., & Fazilati, J. (2013). Bending, buckling and vibration problems of nonlocal Euler beams using Ritz method. *Composite Structures*, 96, 584-589.
- [171] Li, C., Yao, L., Chen, W., & Li, S. (2015). Comments on nonlocal effects in nano-cantilever beams. International Journal of Engineering Science, 87, 47-57.
- [172] Ebrahimi, F., & Nasirzadeh, P. (2015). A nonlocal Timoshenko beam theory for vibration analysis of thick nanobeams using differential transform method. *Journal of Theoretical and Applied Mechanics*, 53(4), 1041-1052.

- [173] Lu, P., Zhang, P. Q., Lee, H. P., Wang, C. M., & Reddy, J. (2007). Non-local elastic plate theories. Proceedings of the Royal Society A: Mathematical, Physical and Engineering Sciences, 463(2088), 3225-3240.
- [174] Duan, W. H., & Wang, C. M. (2007). Exact solutions for axisymmetric bending of micro/nanoscale circular plates based on nonlocal plate theory. *Nanotechnology*, 18(38), 385704.
- [175] Pradhan, S. C., & Phadikar, J. K. (2009). Nonlocal elasticity theory for vibration of nanoplates. *Journal of Sound and Vibration*, 325(1-2), 206-223.
- [176] Ansari, R., Sahmani, S., & Arash, B. (2010). Nonlocal plate model for free vibrations of single-layered graphene sheets. *Physics Letters A*, 375(1), 53-62.
- [177] Srividhya, S., Raghu, P., Rajagopal, A., & Reddy, J. (2018). Nonlocal nonlinear analysis of functionally graded plates using third-order shear deformation theory. *International Journal of Engineering Science*, 125, 1-22.
- [178] Manna, S., & Som, R. (2024). Flexural waves at the edge of nonlocal elastic plate associated with the Pasternak foundation. *Journal of Vibration and Control*, 30(1-2), 130-139.
- [179] Hu, Y. G., Liew, K. M., Wang, Q., He, X. Q., & Yakobson, B. I. (2008). Nonlocal shell model for elastic wave propagation in single-and double-walled carbon nanotubes. *Journal of the Mechanics and Physics of Solids*, 56(12), 3475-3485.
- [180] Khademolhosseini, F., Rajapakse, R. K. N. D., & Nojeh, A. (2010). Torsional buckling of carbon nanotubes based on nonlocal elasticity shell models. *Computational materials science*, 48(4), 736-742.
- [181] Ghavanloo, E., & Fazelzadeh, S. A. (2013). Nonlocal elasticity theory for radial vibration of nanoscale spherical shells. *European Journal of Mechanics-A/Solids*, 41, 37-42.
- [182] Avramov, K. V. (2018). Nonlinear vibrations characteristics of single-walled carbon nanotubes by nonlocal elastic shell model. *International Journal of Non-Linear Mechanics*, 107, 149-160.
- [183] Timesli, A. (2020). An efficient approach for prediction of the nonlocal critical buckling load of double-walled carbon nanotubes using the nonlocal Donnell shell theory. SN Applied Sciences, 2(3), 407.
- [184] Arash, B., & Wang, Q. (2014). A review on the application of nonlocal elastic models in modeling of carbon nanotubes and graphenes. *Modeling of carbon nanotubes, graphene and their composites*, 57-82.
- [185] Rafii-Tabar, H., Ghavanloo, E., & Fazelzadeh, S. A. (2016). Nonlocal continuum-based modeling of mechanical characteristics of nanoscopic structures. *Physics Reports*, 638, 1-97.
- [186] Askari, H., Younesian, D., Esmailzadeh, E., & Cveticanin, L. (2017). Nonlocal effect in carbon nanotube resonators: A comprehensive review. *Advances in Mechanical Engineering*, 9(2), 1687814016686925.
- [187] Srinivasa, A. R., & Reddy, J. N. (2017). An overview of theories of continuum mechanics with nonlocal elastic response and a general framework for conservative and dissipative systems. *Applied Mechanics Reviews*, 69(3), 030802.
- [188] Behera, L., & Chakraverty, S. (2017). Recent researches on nonlocal elasticity theory in the vibration of carbon nanotubes using beam models: a review. Archives of Computational Methods in Engineering, 24, 481-494.
- [189] Shaat, M., Ghavanloo, E., & Fazelzadeh, S. A. (2020). Review on nonlocal continuum mechanics: physics, material applicability, and mathematics. *Mechanics of Materials*, 150, 103587.

- [190] Gopalakrishnan, S., & Narendar, S. (2013). Wave propagation in nanostructures: nonlocal continuum mechanics formulations. Springer Science & Business Media.
- [191] Eringen, A. C. (1974). Theory of nonlocal thermoelasticity. International Journal of Engineering Science, 12(12), 1063-1077.
- [192] Eringen, A. C. (1984). Theory of nonlocal piezoelectricity. Journal of mathematical physics, 25(3), 717-727.
- [193] Eringen, A. C. (1973). Theory of nonlocal electromagnetic elastic solids. *Journal of Mathematical Physics*, 14(6), 733-740.
- [194] Xu, X. J., Deng, Z. C., Zhang, K., & Xu, W. (2016). Observations of the softening phenomena in the nonlocal cantilever beams. *Composite Structures*, 145, 43-57.
- [195] Murmu, T., & Pradhan, S. C. (2009). Buckling analysis of a single-walled carbon nanotube embedded in an elastic medium based on nonlocal elasticity and Timoshenko beam theory and using DQM. Physica E: Low-dimensional Systems and Nanostructures, 41(7), 1232-1239.
- [196] Murmu, T., & Pradhan, S. C. (2009). Small-scale effect on the vibration of nonuniform nanocantilever based on nonlocal elasticity theory. *Physica E: Low-dimensional Systems and Nanostructures*, 41(8), 1451-1456.
- [197] Khodabakhshi, P., & Reddy, J. (2015). A unified integro-differential nonlocal model. *International Journal of Engineering Science*, 95, 60-75.
- [198] Peddieson, J., Buchanan, G. R., & McNitt, R. P. (2003). Application of nonlocal continuum models to nanotechnology. *International journal of engineering science*, 41(3-5), 305-312.
- [199] Tuna, M., & Kirca, M. (2016). Exact solution of Eringen's nonlocal integral model for vibration and buckling of Euler-Bernoulli beam. *International Journal of Engineering Science*, 107, 54-67.
- [200] Shaat, M., Faroughi, S., & Abasiniyan, L. (2017). Paradoxes of differential nonlocal cantilever beams: Reasons and a novel solution. arXiv preprint arXiv:1802.01494.
- [201] Koutsoumaris, C. C., Eptaimeros, K. G., & Tsamasphyros, G. J. (2017). A different approach to Eringen's nonlocal integral stress model with applications for beams. *International Journal of Solids and Structures*, 112, 222-238.
- [202] Chebakov, R., Kaplunov, J., & Rogerson, G. A. (2016). Refined boundary conditions on the free surface of an elastic half-space taking into account non-local effects. Proceedings of the Royal Society A: Mathematical, Physical and Engineering Sciences, 472(2186), 20150800.
- [203] Chebakov, R., Kaplunov, J., & Rogerson, G. A. (2017). A nonlocal asymptotic theory for thin elastic plates.

  Proceedings of the Royal Society A: Mathematical, Physical and Engineering Sciences, 473(2203), 20170249.
- [204] Kaplunov, J., Prikazchikov, D. A., & Prikazchikova, L. (2022). On nonlocally elastic Rayleigh wave. Philosophical Transactions of the Royal Society A, 380(2231), 20210387.
- [205] Kaplunov, J., Prikazchikov, D. A., & Prikazchikova, L. (2023). On integral and differential formulations in nonlocal elasticity. European Journal of Mechanics-A/Solids, 100, 104497.
- [206] Şahin, O., Erbaş, B., & Ege, N. (2023). Nonlocal antiplane shear interfacial waves. Mechanics Research Communications, 128, 104074.
- [207] Şahin, O. (2024). An asymptotic formulation for boundary value problems in a nonlocal elastic half-space. *Acta Mechanica*, 235(4), 2061-2075.
- [208] Wu, M. L., Wu, L. Y., Yang, W. P., & Chen, L. W. (2009). Elastic wave band gaps of one-dimensional phononic crystals with functionally graded materials. *Smart Materials and Structures*, 18(11), 115013.

- [209] Hussein, M. I., Leamy, M. J., & Ruzzene, M. (2014). Dynamics of phononic materials and structures: Historical origins, recent progress, and future outlook. *Applied Mechanics Reviews*, 66(4), 040802.
- [210] Zhu, R., Liu, X. N., Hu, G. K., Yuan, F. G., & Huang, G. L. (2015). Microstructural designs of plate-type elastic metamaterial and their potential applications: a review. *International Journal of Smart and Nano Materials*, 6(1), 14-40.
- [211] Al Ba'Ba'A, H., & Nouh, M. (2017). An investigation of vibrational power flow in one-dimensional dissipative phononic structures. *Journal of Vibration and Acoustics*, 139(2), 021003.
- [212] Aladwani, A., Almandeel, A., & Nouh, M. (2019). Fluid-structural coupling in metamaterial plates for vibration and noise mitigation in acoustic cavities. *International Journal of Mechanical Sciences*, 152, 151-166.
- [213] Liu, Z., Zhang, X., Mao, Y., Zhu, Y. Y., Yang, Z., Chan, C. T., & Sheng, P. (2000). Locally resonant sonic materials. science, 289(5485), 1734-1736.
- [214] Huang, H. H., Sun, C. T., & Huang, G. L. (2009). On the negative effective mass density in acoustic metamaterials. *International Journal of Engineering Science*, 47(4), 610-617.
- [215] Huang, G. L., & Sun, C. T. (2010). Band Gaps in a Multiresonator Acoustic Metamaterial. Journal of Vibration and Acoustics, 132(3).
- [216] Wang, K., Zhou, J., Wang, Q., Ouyang, H., & Xu, D. (2019). Low-frequency band gaps in a metamaterial rod by negative-stiffness mechanisms: design and experimental validation. *Applied Physics Letters*, 114(25).
- [217] Nobrega, E. D., Gautier, F., Pelat, A., & Dos Santos, J. M. C. (2016). Vibration band gaps for elastic metamaterial rods using wave finite element method. *Mechanical Systems and Signal Processing*, 79, 192-202.
- [218] Nouh, M., Aldraihem, O., & Baz, A. (2014). Vibration characteristics of metamaterial beams with periodic local resonances. *Journal of Vibration and Acoustics*, 136(6), 061012.
- [219] Lou, J., He, L., Du, J., & Wu, H. (2020). Revealing the linear and nonlinear dynamic behaviors of metabeams with a dynamic homogenization model. *Journal of Vibration and Acoustics*, 142(3), 031011.
- [220] Cheng, Y., Xu, J. Y., & Liu, X. J. (2008). One-dimensional structured ultrasonic metamaterials with simultaneously negative dynamic density and modulus. *Physical Review B—Condensed Matter and Materials Physics*, 77(4), 045134.
- [221] Chen, J. S., Huang, Y. J., & Chien, I. T. (2017). Flexural wave propagation in metamaterial beams containing membrane-mass structures. *International Journal of Mechanical Sciences*, 131, 500-506.
- [222] Nouh, M. A., Aldraihem, O. J., & Baz, A. (2016). Periodic metamaterial plates with smart tunable local resonators. *Journal of Intelligent Material Systems and Structures*, 27(13), 1829-1845.
- [223] Fang, X., Chuang, K. C., Jin, X. L., Wang, D. F., & Huang, Z. L. (2021). An inertant elastic metamaterial plate with extra wide low-frequency flexural band gaps. *Journal of Applied Mechanics*, 88(2), 021002.
- [224] Peng, H., & Pai, P. F. (2014). Acoustic metamaterial plates for elastic wave absorption and structural vibration suppression. *International Journal of Mechanical Sciences*, 89, 350-361.
- [225] Brûlé, S., Enoch, S., & Guenneau, S. (2020). Emergence of seismic metamaterials: Current state and future perspectives. *Physics Letters A*, 384(1), 126034.
- [226] Achaoui, Y., Antonakakis, T., Brûlé, S., Craster, R. V., Enoch, S., & Guenneau, S. (2017). Clamped seismic metamaterials: ultra-low frequency stop bands. *New Journal of Physics*, 19(6), 063022.

- [227] Brulé, S., Javelaud, E. H., Enoch, S., & Guenneau, S. (2014). Experiments on seismic metamaterials: molding surface waves. *Physical review letters*, 112(13), 133901.
- [228] Miniaci, M., Krushynska, A., Bosia, F., & Pugno, N. M. (2016). Large scale mechanical metamaterials as seismic shields. *New Journal of Physics*, 18(8), 083041.
- [229] Krödel, S., Thomé, N., & Daraio, C. (2015). Wide band-gap seismic metastructures. Extreme Mechanics Letters, 4, 111-117.
- [230] Achaoui, Y., Ungureanu, B., Enoch, S., Brûlé, S., & Guenneau, S. (2016). Seismic waves damping with arrays of inertial resonators. *Extreme Mechanics Letters*, 8, 30-37.
- [231] Colombi, A., Roux, P., Guenneau, S., Gueguen, P., & Craster, R. V. (2016). Forests as a natural seismic metamaterial: Rayleigh wave bandgaps induced by local resonances. *Scientific reports*, 6(1), 19238.
- [232] Colombi, A., Colquitt, D., Roux, P., Guenneau, S., & Craster, R. V. (2016). A seismic metamaterial: The resonant metawedge. *Scientific reports*, 6(1), 27717.
- [233] Palermo, A., & Marzani, A. (2018). Control of Love waves by resonant metasurfaces. *Scientific reports*, 8(1), 7234.
- [234] Colquitt, D. J., Colombi, A., Craster, R. V., Roux, P., & Guenneau, S. R. L. (2017). Seismic metasurfaces: Sub-wavelength resonators and Rayleigh wave interaction. *Journal of the Mechanics and Physics of Solids*, 99, 379-393.
- [235] Ren, X., Das, R., Tran, P., Ngo, T. D., & Xie, Y. M. (2018). Auxetic metamaterials and structures: a review. Smart materials and structures, 27(2), 023001.
- [236] Carta, G., Jones, I. S., Movchan, N. V., Movchan, A. B., & Nieves, M. J. (2017). Gyro-elastic beams for the vibration reduction of long flexural systems. Proceedings of the Royal Society A: Mathematical, Physical and Engineering Sciences, 473(2203), 20170136.
- [237] Liu, W., Yoon, G. H., Yi, B., Yang, Y., & Chen, Y. (2020). Ultra-wide band gap metasurfaces for controlling seismic surface waves. *Extreme Mechanics Letters*, 41, 101018.
- [238] Lou, J., Fang, X., Du, J., & Wu, H. (2022). Propagation of fundamental and third harmonics along a nonlinear seismic metasurface. *International Journal of Mechanical Sciences*, 221, 107189.
- [239] Lou, J., Fang, X., Fan, H., & Du, J. (2022). A nonlinear seismic metamaterial lying on layered soils. Engineering Structures, 272, 115032.
- [240] Lou, J., Fan, H., Fang, X., & Du, J. (2023). Rayleigh wave attenuation by a nonlinear metasurface with both vertical and horizontal resonators. *International Journal of Applied Mechanics*, 15(07), 2350055.
- [241] Palermo, A., Yousefzadeh, B., Daraio, C., & Marzani, A. (2022). Rayleigh wave propagation in nonlinear metasurfaces. *Journal of Sound and Vibration*, 520, 116599.
- [242] Carneiro, D., Reumers, P., Lombaert, G., & Degrande, G. (2024). Seismic metasurfaces for broadband vibration mitigation in layered soil. *Soil Dynamics and Earthquake Engineering*, 181, 108689.
- [243] Pu, X., Palermo, A., Cheng, Z., Shi, Z., & Marzani, A. (2020). Seismic metasurfaces on porous layered media: Surface resonators and fluid-solid interaction effects on the propagation of Rayleigh waves. *International Journal of Engineering Science*, 154, 103347.
- [244] Zeighami, F., Palermo, A., & Marzani, A. (2019). Inertial amplified resonators for tunable metasurfaces. Meccanica, 54, 2053-2065.

- [245] Zeng, Y., Cao, L., Wan, S., Guo, T., Wang, Y. F., Du, Q. J., & Wang, Y. S. (2022). Seismic metamaterials: Generating low-frequency bandgaps induced by inertial amplification. *International Journal of Mechanical Sciences*, 221, 107224.
- [246] Fang, X., Lou, J., Chen, Y. M., Wang, J., Xu, M., & Chuang, K. C. (2023). Broadband Rayleigh wave attenuation utilizing an inertant seismic metamaterial. *International Journal of Mechanical Sciences*, 247, 108182.
- [247] Xu, Y., Cao, Z., Cui, K., Cai, Y., & Pu, X. (2023). Tunable metasurfaces for seismic Love wave manipulation: A theoretical study. *International Journal of Mechanical Sciences*, 251, 108327.
- [248] Zeng, C., Zhao, C., & Zeighami, F. (2022). Seismic surface wave attenuation by resonant metasurfaces on stratified soil. *Earthquake Engineering & Structural Dynamics*, 51(5), 1201-1223.
- [249] Chandrasekharaiah, D. S., & Debnath, L. (2014). Continuum mechanics. Elsevier.
- [250] Heinbockel, J. H. (2001). Introduction to tensor calculus and continuum mechanics (Vol. 52). Victoria, British Columbia: Trafford.
- [251] Sobolev, S. L., Frank, P., & von Mises, R. (1937). Some problems in wave propagation. Differential and integral equations of mathematical physics, 468-617.
- [252] Babich, V., & Kiselev, A. (2018). Elastic waves: high frequency theory. CRC Press.
- [253] Barnett, D. M., & Lothe, J. (1974). Consideration of the existence of surface wave (Rayleigh wave) solutions in anisotropic elastic crystals. *Journal of physics F: Metal physics*, 4(5), 671.
- [254] Kamotskii, I. V., & Kiselev, A. P. (2009). An energy approach to the proof of the existence of Rayleigh waves in an anisotropic elastic half-space. *Journal of applied mathematics and mechanics*, 73(4), 464-470.
- [255] Friedlander, F. G. (1948). On the total reflection of plane waves. The Quarterly Journal of Mechanics and Applied Mathematics, 1(1), 376-384.
- [256] Chadwick, P. (1976). Surface and interfacial waves of arbitrary form in isotropic elastic media. *Journal of Elasticity*, 6(1), 73-80.
- [257] Gurtin, M. E., & Sternberg, E. (1962). On the linear theory of viscoelasticity. Archive for rational mechanics and analysis, 11(1), 291-356.
- [258] Christensen, R. M. (2013). Theory of viscoelasticity. Courier Corporation.
- [259] Rogula, D. (1965). Influence of spatial acoustic dispersion on dynamical properties of dislocations. Bulletin de l'Académie Polonaise des Sciences, Séries des Sciences Techniques, 13, 337-343.
- [260] Kundu, P., Mondal, D., & Sarkar, S. (2021). Effect of the movement across a finite fault in visco-elastic half-space of Burger's Rheology for different types of crack surface. *Geomechanics and Geophysics for Geo-Energy and Geo-Resources*, 7(2), 42.
- [261] Mahato, P., Mondal, D., & Sarkar, S. (2022). Determination of effect of the movement of an infinite fault in viscoelastic half space of standard linear solid using fractional calculus. *Physica Scripta*, 97(12), 125015.
- [262] Rogula, D. (1982). Introduction to nonlocal theory of material media. In Nonlocal theory of material media. Vienna: Springer Vienna, 123-222.
- [263] Krumhansl, J. A. (1968). Some considerations of the relation between solid state physics and generalized continuum mechanics. In Mechanics of Generalized Continua: Proceedings of the IUTAM-Symposium on The Generalized Cosserat Continuum and the Continuum Theory of Dislocations with Applications, Freudenstadt and Stuttgart (Germany), 298-311. Berlin, Heidelberg: Springer Berlin Heidelberg.

- [264] Povstenko, Y. Z. (1999). The nonlocal theory of elasticity and its applications to the description of defects in solid bodies. *Journal of Mathematical Sciences*, 97, 3840-3845.
- [265] Gradshteyn, I. S., & Ryzhik, I. M. (2014). Table of integrals, series, and products. Academic press.
- [266] Goda, I., Assidi, M., & Ganghoffer, J. F. (2014). A 3D elastic micropolar model of vertebral trabecular bone from lattice homogenization of the bone microstructure. *Biomechanics and modeling in mechanobiology*, 13, 53-83.
- [267] Carcione, J. M. (1992). Rayleigh waves in isotropic viscoelastic media. Geophysical Journal International, 108(2), 453-464.
- [268] Okereke, O. E., Iwueze, I. S., & Ohakwe, J. (2014). Some contributions to the solution of cubic equations.

  British Journal of Mathematics & Computer Science, 4(20), 2929.
- [269] Bender, C. M., & Orszag, S. A. (2013). Advanced mathematical methods for scientists and engineers I:

  Asymptotic methods and perturbation theory. Springer Science & Business Media.
- [270] Love, A. E. H. (1911). Some Problems of Geodynamics. Some Problems of Geodynamics Publisher: Cambridge University Press.
- [271] Fu, C. E. Y. (1946). Studies on seismic waves: II. Rayleigh waves in a superficial layer. *Geophysics*, 11(1), 10-23.
- [272] Maznev, A. A. (2022). On the effective medium model of the interaction of rayleigh waves with mass–spring oscillators on the surface. *Wave Motion*, 115, 103074.
- [273] Lamb, H. (1904). I. On the propagation of tremors over the surface of an elastic solid. *Philosophical Transactions of the Royal Society of London*. Series A, Containing papers of a mathematical or physical character, 203(359-371), 1-42.
- [274] Debnath, L., & Bhatta, D. (2016). Integral transforms and their applications. Chapman and Hall/CRC.
- [275] Pham, C. V., & Vu, T. N. A. (2024). On the well-posedness of Eringen's non-local elasticity for harmonic plane wave problems. Proceedings of the Royal Society A, 480(2293), 20230814.
- [276] Anh, V. T. N., Vinh, P. C., Tuan, T. T., & Hue, L. T. (2023). Weakly nonlocal Rayleigh waves with impedance boundary conditions. Continuum Mechanics and Thermodynamics, 35(5), 2081-2094.
- [277] Lapwood, E. R. (1949). The disturbance due to a line source in a semi-infinite elastic medium. Philosophical Transactions of the Royal Society of London. Series A, Mathematical and Physical Sciences, 242(841), 63-100.
- [278] Mondal, A. K., & Acharya, D. P. (2006). Surface waves in a micropolar elastic solid containing voids. Acta Geophysica, 54, 430-452.